REFERENCE ONLY

UNIVERSITY OF LONDON THESIS

Degree PhD Year 2006 Name of Author ABOU NEEL EA-C

Collagen-Phosphate Glass Fibres for Biomedical and Tissue Engineering Applications

Thesis submitted by

Ensanya Ali El-Saed Abou Neel

For the degree of
DOCTOR OF PHILOSOPHY

Division of Biomaterials and Tissue Engineering
University College London
Eastman Dental Institute
256 Gray's Inn Road
London
WC1X 8LD

-2006-

ProQuest LLC
789 East Eisenhower Parkway
P.O. Box 1346
Ann Arbor, MI 48106-1346

In Memory of My Brother

Acknowledgements

I would like to start by expressing my appreciation to Dr. Showan Nazhat for his supervision, guidance, and academic support, without which this work would not have been possible. I would also like to express my gratitude to my second supervisor, and Head of Division, Professor Jonathan Knowles for his helpful assistance during my Ph.D. I would also like to acknowledge Professor Robert Brown and Dr. Mike Wiseman (Tissue Regeneration & Engineering Centre, Institute of Orthopaedics) for their valuable time, advice, and guidance. In addition I would also like to thank Dr. Vehid Salih and Dr. Mark Lewis for their advice regarding the biological section of this thesis. I would also like to thank Dr. Chris Hope for his help with the confocal, Aviva Petri for her assistance with the statistics, and Mr. Mike Kyser, and Nicky Mordan for their help with SEM. I am indebted to Prof. Peter Lee and Matt Kershaw for the XMT work, Dr. Jonathan Pratten for the antibacterial study, and Dr. Ifthkar Ahmed for XRD analysis.

This research would not have been possible without the financial and academic support provided by the Ministry of Higher Education in Egypt, the Egyptian Education and Cultural Bureau in UK, to which I am very grateful. My special appreciation goes to Prof. Alaa Elgindy, Dr. Amr Elatraby, Dr. Nader Matar, and Dr. Mahmoud El-Khouly for their invaluable support.

Most importantly, this research could not have been possible without the endless support of my husband, grandmother, dearest parents, my brothers and sisters, and my lovely and patient children.

Abstract

The aim of this project was to develop three-dimensional (3-D) constructs of phosphate-based glass fibres (PGF) incorporated dense collagen matrices for biomedical and tissue engineering applications. For this, a novel method of "plastic compression" (PC) was used which rapidly removes fluid from hyper-hydrated collagen gels through the application of unconfined compressive load. The project objectives were: the understanding of structure-property relationship of PGF; the understanding of the mechanisms of PC to produce dense collagenous matrices, and the application of PC to produce cellular 3-D constructs of PGF reinforced collagen matrices.

PGF are unique glasses as they are degradable and biocompatible, and their degradation can be controlled through their chemistry. Two different quaternary glass systems incorporating CuO and Fe_2O_3 into the ternary glass system (in molar percentage) 50 P_2O_5-30 CaO-20 Na_2O were developed for either antibacterial or tissue engineering applications. These additional oxides were incorporated into the glass structure by partially substituting Na_2O. The rate of degradation was significantly decreased by the incorporation of both oxides possibly due to increased cross-link density, which correlated with an increase in the density and glass transition temperature. There was a further decrease in degradation with increasing fibre diameter. The amount of Cu^{2+} release increased with increasing CuO content, and 10 mol % was the most effective in killing *Staphylococcus epidermidis*. Fe_2O_3 had a much more significant effect on rate of degradation, and the rate of Fe^{3+} release decreased with increasing Fe_2O_3 content. From the compositions and fibre diameters investigated, fibres containing 3-5 mol % Fe_2O_3 with a diameter of ~ 30 μm were more durable, and therefore suitable for use as scaffolds. Furthermore, upon long term degradation, the iron containing glass systems showed the potential for tube formation.

PC depends mainly on the ability of collagen to undergo creep deformation and no recovery upon load removal. Using this principle, a dense collagen matrix with improved mechanical properties was produced. PC was also successful in producing PGF-PC collagen constructs with different compositions. It was anticipated that PGF would initially further enhance the mechanical properties of the constructs. Moreover, PGF also provided the intriguing possibility of capillary-like channels within the collagen for cell and nutrient transportations. The effect of PGF incorporation was assessed morphologically, mechanically, and biologically using live/dead staining. Increasing the proportion of PGF yielded significantly stiffer, stronger constructs while compromising their compliance. At greatest, only 20 % cell death due to either PC or PGF incorporation occurred, however, a significant increase in cell viability after 24 hours was observed. The findings suggested that PC is effective for engineering composite, biomimetic collagen matrices with controllable properties.

TABLE OF CONTENTS

		Page
Acknowledgments		iii
Abstract		iv
Table of Contents		v
List of Tables		xiii
List of Figures		xvi
Chapter 1	**Introduction**	**1**
Chapter 2	**Literature Review**	**7**
2.1.	Strategies of Tissue Engineering	7
2.1.1.	Cell Therapy	7
2.1.2.	Drug/Gene Therapy	8
2.1.3.	Cells Placed on or within Matrices	9
2.2.	Scaffolds for Tissue Engineering	12
2.3.	Glasses for Biomedical Applications	14
2.4.	Phosphate-Based Glasses	16
2.4.1.	Chemistry of Phosphate-Based Glasses	17
2.4.2.	Properties of Phosphate-Based Glasses	21
2.4.3.	General Applications of Phosphate-Based Glasses	22
2.4.3.1.	Technological Applications	22
2.4.3.2.	Nuclear Waste Hosts	22
2.4.3.3.	Controlled Release Glasses	22
2.4.3.4.	Reinforcing Agents	24
2.5.	Potential Biomedical Applications of Phosphate-Based Glasses	25
2.5.1.	Phosphate-Based Glass Monoliths	25
2.5.1.1.	Ternary Glass Systems	26
2.5.1.2.	Quaternary Glass Systems	28
2.5.2.	Phosphate-Based Glass Fibres	32
2.5.2.1.	Ternary Glass Systems	34

2.5.2.2.	Quaternary Glass Systems	34
2.6.	Biomedical Applications of Collagen	34
2.6.1.	Delivery Vehicle	35
2.6.2.	Soft Tissue Repair	37
2.6.2.1.	Skin or Mucosal Substitute	37
2.6.2.2.	Cartilage Repair	39
2.6.2.3.	Other Soft Tissue Applications	40
2.6.3.	Hard Tissue Repair	41
2.7.	Sequential and Higher Structure of Type I Collagen	42
2.8.	Mechanical Properties of Reconstituted Collagen Gels	47
2.8.1.	Methods to improve the mechanical Properties of Reconstituted Collagen Gels	48
2.8.1.1.	Cell Seeding	48
2.8.1.2.	Chemical Cross-Linking	51
2.8.1.3.	Dynamic Mechanical Conditioning	52
2.8.1.4.	Plastic Compression	52
2.9.	Collagen/Inorganic Hybrids or Composites as Biomaterials	53
Chapter 3	**Copper Containing Phosphate Glass Fibres**	**57**
3.1.	Introduction	57
3.2.	Experimental	58
3.2.1.	Materials	58
3.2.1.1.	Raw Materials	58
3.2.1.1.1.	Chemical Equations and Compositional Calculations	58
3.2.1.2.	Methods of Preparation	60
3.2.1.2.1.	Bulk Glass Preparation	60
3.2.1.2.2.	Glass Fibre Production	61
3.2.2.	Methods of Characterisation	62
3.2.2.1.	Bulk Glass	62
3.2.2.1.1.	Density Measurements	62
3.2.2.1.2.	X-Ray Diffraction Analysis	63

3.2.2.2.	Glass Fibres	63
3.2.2.2.1.	Fibre Diameter Measurements	63
3.2.2.2.2.	Determination of Thermal Properties	64
a)	Differential Scanning Calorimetry	64
I.	Technique	64
II.	Method	67
b)	Differential Thermal Analysis	67
I.	Technique	67
II.	Method	69
3.2.2.2.3.	Determination of Fibre Degradation	69
a)	Long Term Degradation Study	69
b)	Short Term Degradation Study	70
3.2.2.2.4.	Determination of Surface Area to Volume Ratio of the Glass Fibres	70
3.2.2.2.5.	Ion Chromatography	70
a)	Technique	70
b)	Method	72
I.	Cation Release	73
II.	Copper Ion Release	74
III.	Anion Release	75
3.2.2.2.6.	Antibacterial Assessment	76
3.2.2.2.7.	Statistical Analysis	77
3.3.	Results	77
3.3.1.	Bulk Glass	77
3.3.1.1.	Density Measurements	77
3.3.1.2.	X-Ray Diffraction Analysis	78
3.3.2.	Glass Fibres	79
3.3.2.1.	Fibre Diameter Measurements	79
3.3.2.2.	Thermal Properties	80
3.3.2.2.1.	Differential Scanning Calorimetry	80
3.3.2.2.2.	Differential Thermal Analysis	81
3.3.2.3.	Fibre Degradation	84

3.3.2.3.1.	Long Term Degradation Study	84
3.3.2.3.2.	Short Term Degradation Study	85
3.3.2.4.	Determination of Surface Area to Volume Ratio of the Glass Fibres	87
3.3.2.5.	Ion Chromatography	88
3.3.2.5.1.	Cation Release	88
3.3.2.5.2.	Copper Ion Release	91
3.3.2.5.3.	Anion Release	93
3.3.2.6.	Antibacterial Assessment	98
3.4.	Discussion	100
Chapter 4	**Iron Containing Phosphate Glass Fibres**	**110**
4.1.	Introduction	110
4.2.	Experimental	110
4.2.1.	Materials	110
4.2.1.1.	Raw Materials	110
4.2.1.1.1.	Chemical Equations and Compositional Calculations	110
4.2.1.2.	Methods of Preparation	111
4.2.1.2.1.	Bulk Glass Preparation	111
4.2.1.2.2.	Glass Fibre Production	112
4.2.2.	Methods of Characterisation	112
4.2.2.1.	Bulk Glass	112
4.2.2.1.1.	Density Measurements	112
4.2.2.2.	Glass Fibres	112
4.2.2.2.1.	Fibre Diameter Measurements	112
4.2.2.2.2.	Determination of Thermal Properties	113
a)	Differential Scanning Calorimetry	113
b)	Differential Thermal Analysis	113
4.2.2.2.3.	Determination of Fibre Degradation	114
a)	Long Term Degradation Study	114
b)	Short Term Degradation Study	114
4.2.2.2.4.	Determination of Surface Area to Volume Ratio of	

	the Glass Fibres	115
4.2.2.2.5.	Ion Chromatography	115
a)	Cation Release	115
b)	Iron Ion Release	115
c)	Anion Release	116
4.2.2.2.6.	pH change	116
4.2.2.2.7.	Scanning Electron Microscopy	116
a)	Technique	116
b)	Method	117
4.2.2.2.8.	Statistical Analysis	117
4.3.	Results	118
4.3.1.	Bulk Glass	118
4.3.1.1.	Density Measurements	118
4.3.2.	Glass Fibres	118
4.3.2.1.	Fibre Diameter Measurements	118
4.3.2.2.	Thermal Properties	119
4.3.2.2.1.	Differential Scanning Calorimetry	119
4.3.2.2.2.	Differential Thermal Analysis	121
4.3.2.3.	Fibre Degradation	125
4.3.2.3.1.	Long Term Degradation Study	125
4.3.2.3.2.	Short Term Degradation Study	126
4.3.2.4.	Determination of Surface Area to Volume Ratio of the Glass Fibres	128
4.3.2.5.	Ion Chromatography	129
4.3.2.5.1.	Cation Release	129
4.3.2.5.2.	Iron Ion Release	132
4.3.2.5.3.	Anion Release	133
4.3.2.6.	pH Change	137
4.3.2.7.	Scanning Electron Microscopy	138
4.3.2.7.1.	Short Term Degradation	138
4.3.2.7.2.	Long Term Degradation	139
4.4.	Discussion	141

4.5.	Overall Discussion for the Phosphate-Based Glass Fibres	153
Chapter 5	**The Investigation of Plastic Compression of Collagen Gels for the Production of Dense Scaffold**	**158**
5.1	Introduction	158
5.2	Experimental	158
5.2.1.	Materials	158
5.2.1.1	Raw Materials	158
5.2.1.2.	Method of Gel Preparation	159
5.2.2.	Methods of Characterisations	159
5.2.2.1.	Investigation into Unconfined Compression of Collagen Gels	159
5.2.2.1.1	Technique	159
a)	Theory of Dynamic Mechanical Analysis	161
b)	Theory of Creep and Recovery Analysis	163
5.2.2.1.2	Methods	164
a)	Quasi-Static Mechanical Analysis	164
b)	Dynamic Mechanical Analysis	165
c)	Creep and Recovery Analysis	166
5.2.2.1.3	Statistical Analysis	167
5.2.2.2.	Plastic Compression to Produce Dense Collagen Constructs	167
5.2.2.2.1.	Analysis of Plastic Compression of Collagen Gels	167
5.2.2.2.2.	Application of the Plastic Compression Technique	168
5.2.2.2.3.	Characterisation of the Properties of Compressed Collagen Gels	169
a)	Scanning Electron Microscopy	169
b)	Thermo-Gravimetric Analysis	170
I.	Technique	170
II.	Method of Analysis	171
c)	Mechanical Properties under Quasi-Static Uniaxial	

	Tensile Testing	172
5.3.	Results	173
5.3.1	Investigation into Unconfined Compression of Collagen Gels	173
5.3.1.1.	Quasi-Static Mechanical Analysis	173
5.3.1.2.	Dynamic Mechanical Analysis	174
5.3.1.3.	Creep and Recovery Analysis	176
5.3.2.	Plastic Compression to Produce Dense Collagen Constructs	179
5.3.2.1.	Analysis of Plastic Compression of Collagen Gels	179
5.3.2.2.	Properties of Collagen Constructs Produced through Plastic Compression	182
5.3.2.2.1.	Weight Loss due to Plastic Compression	182
5.3.2.2.2.	Scanning Electron Microscopy	183
5.3.2.2.3.	Thermo-Gravimetric Analysis	184
5.3.2.2.4.	Mechanical Properties under Quasi-Static Uniaxial Tensile Testing	185
5.4.	Discussion	186
Chapter 6	**Development and Characterisation of 3-D Phosphate Glass Fibre Incorporated PC Collagen Constructs**	**193**
6.1.	Introduction	193
6.2.	Experimental	193
6.2.1.	Materials	193
6.2.1.1.	Raw Materials	193
6.2.1.1.1.	Phosphate Glass Fibres	193
6.2.1.1.2.	Collagen	194
6.2.1.2.	Method of Preparation	194
6.2.1.2.1.	Production of Unidirectional Phosphate Glass Fibres	194
6.2.1.2.2.	Preparation of Acellular PGF-PC Collagen Constructs	197
6.2.1.2.3.	Preparation of Cellular PGF-PC Collagen Constructs	199

a)	Cell Culture	199
I)	Maintenance of Primary Human Oral Fibroblasts	199
II)	Cell Subculture	200
III)	Cell Counting	200
IV)	Cryopreservation of Cells	201
b)	Sterilization of Glass Fibres	201
c)	Sterilization of the Casting Mould Setup	201
d)	Formation of Constructs	202
6.2.2.	Methods of Characterisation	202
6.2.2.1.	Characterisation of Acellular PGF-PC Collagen Constructs	202
6.2.2.1.1.	Morphological Characterisations	202
a)	Scanning electron microscopy	202
b)	X-Ray Microtomography	203
6.2.2.1.2.	Quantification of PGF-PC Collagen Components	203
a)	Thermo-Gravimetric Analysis	203
b)	Ashing	204
6.2.2.1.3.	Quasi-Static Uniaxial Tensile Testing	204
6.2.2.2.	Characterisation of Cellular PGF-PC Collagen Constructs	205
6.2.2.2.1.	Cell Viability using Live/Dead Staining and Confocal Microscopy	205
a)	Technique	205
b)	Methods	206
I)	Preliminary Experiment	206
II)	Cell Viability up to 24 h	207
6.2.2.3.	Statistical Analysis	208
6.3.	Results	208
6.3.1.	Acellular PGF-PC Collagen Constructs	208
6.3.1.1.	Morphological Characterisation	208
6.3.1.1.1.	Scanning Electron Microscopy	208
6.3.1.1.2.	X-Ray Microtomography	210

6.3.1.2.	Quantification of PGF-PC Collagen Components	212
6.3.1.2.1.	Thermo-Gravimetric Analysis	212
6.3.1.2.2.	Ashing	215
6.3.1.3.	Quasi-Static Uniaxial Tensile Testing	215
6.3.2.	Cellular PGF-PC Collagen Constructs	219
6.3.2.1.	Preliminary Experiment	219
6.3.2.2.	Cell Viability up to 24 h	220
6.4.	Discussion	223
Chapter 7	**Summary, Conclusions, and Further Work**	**229**
7.1.	Summary and Conclusions	229
7.2.	Recommendation for Further Work	233
7.2.1.	Copper Containing Phosphate Glass Fibres	233
7.2.2.	Iron Containing Phosphate Glass Fibres	233
7.2.3.	PC Collagen	234
7.2.4.	PGF-PC Collagen	234
References		**236**
Appendices		**267**
Appendix I:	List of Conference Proceedings and Abstracts	267
Appendix II:	List of Publications	268

List of Tables

Chapter 2

2.1	Commercially available collagen-based medical devices (Pachence, 1996).	35
2.2	Various collagen types and the major collagen families (adapted from Gelse *et al.*, 2003).	43
2.3	Summary of mechanical properties of cell seeded collagen	

constructs as reported in the literature. 50

Chapter 3

3.1 Glass codes and composition of glasses investigated. 57
3.2 Raw materials used in glass preparation. 58
3.3 Melt temperatures used for pulling fibres for different copper containing glass compositions. 62
3.4 T_g (°C) of copper containing glasses as measured by DSC 81
3.5 Fibre diameters, surface area to volume ratio, and degradation rate of fibres pulled at 400 and 1200 m.min^{-1} for copper containing glass compositions. 87
3.6 Cation release data (ppm.mg^{-1} h^{-1}) of copper containing glass fibres pulled at 400 and 1200 m.min^{-1}. 91
3.7 Anion release data (ppm.mg^{-1} h^{-1}) of copper containing glass fibres pulled at 400 and 1200 m.min^{-1}. 98

Chapter 4

4.1 Glass codes and composition of glasses investigated. 110
4.2 Raw materials used in glass preparation. 111
4.3 Melt temperatures used for pulling fibres for different iron containing glass compositions. 112
4.4 T_g (°C) of iron containing glasses as measured by DSC. 121
4.5 Fibre diameters, surface area to volume ratio, and degradation rate of fibres pulled at 400 and 1600 m.min^{-1} for iron containing glass compositions. 129
4.6 Cation release data (ppm. mg^{-1} h^{-1}) of iron containing glass fibres pulled at 400 and 1600 m.min^{-1}. 132
4.7 Anion release data (ppm. mg^{-1} h^{-1}) for iron containing glass fibres pulled at 400 and 1600 m.min^{-1}. 137

Chapter 5

5.1 Raw materials used in collagen gel preparation. 158

5.2 Strain and modulus for collagen gel under different unconfined compressive stresses. 174

5.3 Percentage weight loss through fluid expulsion, final height, and the percentage height reduction for the two stress levels compared to self compression. 182

5.4 Percentage weight loss through fluid expulsion by combination of compression and blotting actions. 182

Chapter 6

6.1 Theoretical time (t), number of fibres (n), and spacing between fibres (S_f), at different stepper motor frequencies and RPM of 400 m.min^{-1}, used to cover the surface area the mould used for casting of collagen. 197

6.2 Summary of the average weight loss % of PGF-PC collagen with three different amounts of PGF and its individual components from TGA, and the % construct components calculated at 200 °C and from ashing. 213

6.3 Summary of the mechanical properties in terms of Young's Modulus, tensile break strength and strain failure, presented as Mean ± Standard Deviation of PGF-PC collagen with three different PGF contents and PC collagen as a control. 219

6.4 % Cell viability in immediately (1 h) and 24h seeded PC produced constructs at each step of PC (sheet & spiral form) compared to non-compressed gel control. 223

List of Figures

Chapter 2

2.1 Diagrammatic representation of cell-matrix tissue engineering strategy (Rose and Oreffo, 2002). 10

2.2 Nomenclature and representation of PO_4 tetrahedra with different polymerizations (adapted from Kirkpatrick and Brow, 1995). 19

2.3 Conception of collagen-mediated gene delivery (Sano *et al.*, 2003). 37

2.4 Supramolecular structure of type I collagen (a) primary amino acid sequence (α chain) (Friess, 1998), (b) secondary and tertiary structure, and (c) quaternary structure (Gelse *et al.*, 2003). 46

2.5 Schematic illustration of collagen/mineral composite formation resulting from thermally triggered self assembly of collagen fibrils and liposomal mineralization (Pederson *et al.*, 2003). 54

2.6 Alkaline phosphatase catalyzed mineralization onto a collagen material (Yamauchi *et al.*, 2004). 56

Chapter 3

3.1 Fibre drawing machine (a) Lenton furnace, (b) drum and (c) motor. 61

3.2 Diagrammatic representation of differential scanning calorimetry. 65

3.3 Diagrammatic representation of T_g obtained from DSC. T_a is the equivalent value to T_o on the liquid side of the transition, and T_{inf} is the point of inflection (Richardson, 1976). 66

3.4 Diagrammatic representation of DTA. 68

3.5 Diagrammatic representation of T_g, exothermic, and endothermic peaks as measured by DTA. 68
3.6 Schematic diagram of ion chromatography (from IC manual). 71
3.7 Example of a chromatogram obtained for anion release (Ahmed *et al.*, 2005). 72
3.8 Different anion species detected by ion chromatography (Ahmed *et al.*, 2005). 76
3.9 Bulk density as a function of copper oxide content. 78
3.10 Light microscope image of glass fibres embedded in resin and pulled at (a) 400 and (b) 1600 $m.min^{-1}$. 79
3.11 Fibre diameter as a function of pulling speed for copper containing compositions. 80
3.12 DSC trace of glass fibres pulled at 400 $m.min^{-1}$ for the different CuO compositions. 81
3.13 DTA graphs of 0 mol % CuO bulk glass and fibres pulled at different speeds. 82
3.14 DTA graphs for 1 mol % CuO bulk glass and fibres pulled at different speeds. 83
3.15 DTA graphs for 5 mol % CuO bulk glass and fibres pulled at different speeds. 83
3.16 DTA graphs for 10 mol % CuO bulk glass and fibres pulled at different speeds. 84
3.17 Percentage weight $loss.h^{-1}$ as a function of both CuO content and fibre pulling speeds. 85
3.18 Percentage weight loss versus time for fibres pulled at 400 $m.min^{-1}$ for copper containing glass compositions. 86
3.19 Percentage weight loss versus time for fibres pulled at 1200 $m.min^{-1}$ for copper containing glass compositions. 86
3.20 Na^+ release for fibres pulled at 400 $m.min^{-1}$ for copper containing glass compositions. 89
3.21 Na^+ release for fibres pulled at 1200 $m.min^{-1}$ for copper containing glass compositions. 89

3.22 Ca^{2+} release for fibres pulled at 400 $m.min^{-1}$ for copper containing glass compositions. 90

3.23 Ca^{2+} release for fibres pulled at 1200 $m.min^{-1}$ for copper containing glass compositions. 90

3.24 Cu^{2+} release for fibres pulled at 400 $m.min^{-1}$ for copper containing glass compositions. 92

3.25 Cu^{2+} release for fibres pulled at 1200$m.min^{-1}$ for copper containing glass compositions. 92

3.26 $(PO_4)^{3-}$ release from fibres pulled at 400 $m.min^{-1}$ for copper containing glass compositions. 94

3.27 $(PO_4)^{3-}$ release from fibres pulled at 1200$m.min^{-1}$ for copper containing glass compositions. 94

3.28 $(P_2O_7)^{4-}$ release from fibres pulled at 400 $m.min^{-1}$ for copper containing glass compositions. 95

3.29 $(P_2O_7)^{4-}$ release from fibres pulled at 1200 $m.min^{-1}$ for copper containing glass compositions. 95

3.30 $(P_3O_9)^{3-}$ release from fibres pulled at 400 $m.min^{-1}$ for copper containing glass compositions. 96

3.31 $(P_3O_9)^{3-}$ release from fibres pulled at 1200$m.min^{-1}$ for copper containing glass compositions. 96

3.32 $(P_3O_{10})^{5-}$ release from fibres pulled at 400 $m.min^{-1}$ for copper containing glass compositions. 97

3.33 $(P_3O_{10})^{5-}$ release from fibres pulled at 1200 $m.min^{-1}$ for copper containing glass compositions. 97

3.34 Number of attached *S. epidermidis* to glass fibres pulled at 400 and 1200 $m.min^{-1}$ for control and copper containing glass compositions. Error bars represent standard deviations, data normalised to weight of fibres. 99

3.35 Number of viable *S. epidermidis* in solution after contact with control and copper containing glass fibres pulled at 400 and 1200 $m.min^{-1}$. Error bars represent standard deviations, data normalised to weight of fibres. 99

3.36 Effect of CuO content and pulling speed on glass transition temperature measured through DSC and DTA. 101

3.37 Schematic structure of sodium-copper metaphosphate glasses. (a) binary sodium metaphosphate (50 P_2O_5-50 Na_2O) linear chain structure, (b) Na^+ are partially replaced by Cu^{2+}, and (c) binary copper metaphosphate (50 P_2O_5-50 CuO) as all the Na^+ in (a) are replaced by Cu^{2+} (Shih *et al.*, 1998). 106

3.38 Percentage weight loss.h^{-1} against CuO content. 106

Chapter 4

4.1 Heating rate versus T_g as measured by onset and ½ ΔCp. 114

4.2 Bulk glass density as a function on iron oxide content. 118

4.3 Fibre diameter as a function of rig-pulling speed for iron containing glass compositions. 119

4.4 Example 1 of a DSC trace of glass fibres pulled at 1600 m.min^{-1} for different glass compositions investigated. 120

4.5 Example 2 of a DSC trace of the 2 mol % Fe_2O_3 containing glass. 120

4.6 DTA graphs of 0 mol % Fe_2O_3 bulk glass and fibres pulled at different speeds. 121

4.7 DTA graphs of 1 mol % Fe_2O_3 bulk glass and fibres pulled at different speeds. 122

4.8 DTA graphs of 2 mol % Fe_2O_3 bulk glass and fibres pulled at different speeds. 123

4.9 DTA graphs of 3 mol % Fe_2O_3 bulk glass and fibres pulled at different speeds. 123

4.10 DTA graphs of 4 mol % Fe_2O_3 bulk glass and fibres pulled at different speeds. 124

4.11 DTA graphs of 5 mol % Fe_2O_3 bulk glass and fibres pulled at different speeds. 124

4.12 Percentage weight loss versus time for glass fibres with 3 mol % Fe_2O_3 pulled at different speeds. 125

4.13 Percentage weight loss versus time for glass fibres with 4 mol % Fe_2O_3 pulled at different speeds. 126

4.14 Percentage weight loss versus time for glass fibres with 5 mol % Fe_2O_3 pulled at different speeds. 126

4.15 Percentage weight loss versus time for fibres pulled at 400 $m.min^{-1}$ of iron containing glass compositions. 128

4.16 Percentage weight loss versus time for fibres pulled at 1600 $m.min^{-1}$ of iron containing glass compositions. 128

4.17 Na^+ release from fibres pulled at 400 $mmin^{-1}$ of iron containing glass compositions. 130

4.18 Na^+ release from fibres pulled at 1600 $mmin^{-1}$ of iron containing glass compositions. 130

4.19 Ca^{2+} release from fibres pulled at 400 $mmin^{-1}$ of iron containing glass compositions. 131

4.20 Ca^{2+} release from fibres pulled at 1600 $mmin^{-1}$ of iron containing glass compositions. 131

4.21 Fe^{3+} release from fibres pulled at 400 $mmin^{-1}$ of iron containing glass compositions. 133

4.22 Fe^{3+} release from fibres pulled at 1600 $mmin^{-1}$ of iron containing glass compositions. 133

4.23 $(PO_4)^{3-}$ release from fibres pulled at 400 $mmin^{-1}$ of iron containing glass compositions. 134

4.24 $(PO_4)^{3-}$ release from fibres pulled at 1600 $mmin^{-1}$ of iron containing glass compositions. 134

4.25 $(P_3O_9)^{3-}$ release from fibres pulled at 400 $mmin^{-1}$ of iron containing glass compositions. 135

4.26 $(P_3O_9)^{3-}$ release from fibres pulled at 1600$mmin^{-1}$ of iron containing glass compositions. 135

4.27 $(P_3O_{10})^{5-}$ release from fibres pulled at 400 $mmin^{-1}$ of iron containing glass compositions. 136

4.28 $(P_3O_{10})^{5-}$ release from fibres pulled at 1600 $mmin^{-1}$ of iron containing glass compositions. 136

4.29 pH changes of fibres pulled at 400 $mmin^{-1}$ in deionised water. 138
4.30 pH changes of fibres pulled at 1600 $m.min^{-1}$ in deionised water. 138
4.31 SEM of 2 mol % Fe_2O_3 glass fibres pulled at 400 $m.min^{-1}$ (a) 0 day, (b) after being incubated in deionised water at 37°C for 6 h, (c) after 96 h, SEM of 5 mol % Fe_2O_3 glass fibres pulled at 400 $m.min^{-1}$. (d) 0 day, (e) after 6 h, and (f) after 96 h. 139
4.32 SEM of 2 mol % Fe_2O_3 glass fibres pulled at 400 $m.min^{-1}$ (a) 0 day, (b) after being incubated in deionised water for 7 days, (c) after 1 year, (d) 1 year at high magnification. 140
4.33 SEM of 5 mol % Fe_2O_3 glass fibres pulled at 400 $m.min^{-1}$ (a) 0 day, (b) after being incubated in deionised water for 3 months, (c) after 6 months, (d) after 1.5 year. 141
4.34 Effect of Fe_2O_3 content and rig-pulling speed on glass transition temperature measured through DSC and DTA. 142
4.35 Schematic representation of phosphate glass structure: (a) chain structure, (b) cross link formation by Ca^{2+} (adapted from Uo *et al.*, 1998). 144
4.36 Idealized structure for iron pyrophosphate glass showing the position of Fe^{2+} and Fe^{3+} (adapted from Yu *et al.*, 1997b). 146
4.37 Log % weight $loss.h^{-1}$ against iron oxide content. 148
4.38 Degradation rate against bulk density of copper containing phosphate glass fibres. 155
4.39 Degradation rate against bulk density of iron containing phosphate glass fibres. 155

Chapter 5

5.1 Cross section of dynamic mechanical analyzer (from DMA-7e, Perkin-Elmer manual). 160
5.2 (a) The parallel plate and (b) extension analysis measuring system (from DMA-7e, Perkin-Elmer manual). 160
5.3 Material response (strain) following application of an

	oscillatory stress for (a) an ideal solid, (b) an ideal liquid, and (c) viscoelastic materials (from Jones, 1999).	162
5.4	Typical creep response of viscoelastic solids (from Jones, 1999).	164
5.5	Diagrammatic model of the dynamic scan used for analysis of the dynamic properties of collagen gel. Where the total force is the sum of the static and dynamic force ($F_T=F_S+F_D$).	165
5.6	Stress regime applied during creep and recovery analysis.	166
5.7	Diagrammatic representation of plastic compression technique for preparing collagen. (a) non-compressed gel (b) compressed gel, and (c) a spiral construct (adapted from Brown *et al.*, 2005).	169
5.8	Diagrammatic representation of (a) weight loss and (b) weight gain during thermogravimetric run. Point A is the start of weight variation, B is the end of weight variation, and C is the inflexion point. mi is the initial while mf is the final weight (adapted from the DTA / TGA manual).	171
5.9	Photograph of the spirally assembled PC collagen being clamped for mechanical testing.	172
5.10	Unconfined compressive stress and modulus-strain curves for collagen gels.	174
5.11	Storage modulus, loss modulus, and tan δ as a function of time obtained through unconfined compressive DMA of collagen gels.	175
5.12	Static and dynamic strain as a function of time obtained through unconfined compressive DMA of collagen gels.	175
5.13	Raw creep and recovery data for collagen gel in response to different unconfined compressive stresses.	176
5.14	Normalised creep and recovery data for collagen gel in response to different unconfined compressive stresses.	177
5.15	Strain rate as a function of the applied stress during the creep phase.	178

5.16 Expanded region of the creep and recovery data under creep stress of 1723.3 $N.m^{-2}$. 178

5.17 Percentage recovery under different unconfined compressive stresses after 10 min. 179

5.18 Sample height as a function of time comparing two stress levels of 0.14 and 1.4 $kN.m^{-2}$ applied for 5 minutes, illustrating the nature of the plastic compression/compaction (PC) of collagen gels. 180

5.19 Sample height related to the theoretical height of 6.2 mm as a function of time comparing two stress levels of 0.14 and 1.4 $kN.m^{-2}$ applied for 5 minutes. 181

5.20 SEM of collagen through processing by PC technique (a) non-compressed collagen gel, (b) collagen sheet after plastic compression, (c, d) cross section of spirally assembled PC collagen, and (e) longitudinal section of spiral collagen construct. The white arrows refer to the presence of micro-spaces between different layers of the spiral construct. 184

5.21 TGA thermogram of the spirally assembled PC collagen. 185

5.22 Tensile stress and modulus-strain curve for the spirally assembled PC collagen. 186

5.23 Diagrammatic representation of collagen fibrils under tensile loading (a) random orientation of collagen fibrils, (b)stretching of collagen fibrils, and (c) sliding of the collagen fibrils. 191

Chapter 6

6.1 The relationship between the stepper motor frequency and the drum cross-head speed. The arrows showed the chosen frequencies for producing PGF with different quantities. 195

6.2 Diagrammatic representation of fibre spacing at 25 Hz frequency considering the fibre diameter of 35 μm. 196

6.3 (a) Diagrammatic representation of glass fibres aligned at a drum SMF of 25 Hz showing the theoretical fibre number and spacing between two adjacent fibres, (b) diagram showing the routine PC processing used for producing PGF-PC collagen with a standard stress of 1.4 $kN.m^{-2}$ for 5 minutes at 37 °C, (c) PGF-PC collagen sheet (~ 50 μm thick), and (d) PGF-PC spiral assembly (1.75 ± 0.25 mm diameter). 198

6.4 Photograph showing the different steps in preparation of the spirally assembled PGF-PC collagen (a) aligned PGF attached to the bottom of the mould, (b) collagen gel casted on the top on pre-aligned PGF, (c) PGF-collagen gel, and (d) PGF-PC collagen spiral. 198

6.5 The principle of the confocal laser scanning microscope (Brigitte, 1998). 205

6.6 Scanning electron micrograph of cross-sectional view of the spirally assembled PGF- PC collagen with (a) Low PGF generated at 50 Hz SMF, (b) medium PGF generated at 25 Hz SMF, (c) high PGF generated at 12.5 Hz SMF, and (d) high magnification of (c). The circle refers to the clustering of a group of fibres seen after processing, (e) lateral view of the spirally assembled PGF-PC collagen, and (f) PC collagen spiral. 209

6.7 XMT of cross-sectional (a-c) and three dimensional views (d-f) of PGF-PC collagen with low (a & d), medium (b & e), and high PGF (c & e) respectively. The circle refers to the clustering seen after processing. 211

6.8 Thermo-gravimetric plot of PC collagen and PGF-PC collagen at three weight percentages. Three regions of weight variation were identified as I, II, and III. (a) PC collagen, (b) 8 % PGF-PC collagen, (c) 21 % PGF-PC collagen, (d) 30 % PGF-PC collagen spiral assemblies, and (e) PGF. 212

6.9 Thermo-gravimetric plot of phosphate glass fibres. 214

6.10 Stress-strain curves obtained from quasi-static tensile testing of (a) PC collagen, (b) 8 % PGF-PC collagen, (c) 21 % PGF-PC collagen, and (d) 30 % PGF-PC collagen spiral assemblies. 216

6.11 Stress-strain curve revealing the characteristic mechanical properties of 30 weight % PGF-PC collagen under tensile mode. 216

6.12 Effect of weight % of PGF on modulus of elasticity of PGF-PC collagen spiral assemblies. 217

6.13 Toe-in region and maximum strain for PGF-PC collagen spiral assemblies and PC collagen as a control. ** Highly significant to PC collagen. 218

6.14 Maximum strength for PGF-PC collagen spiral assemblies and PC as a control. ** Highly significant to PC collagen. 219

6.15 Confocal laser scanning micrographs of HOF immediately cultured (1 h) and entrapped within PC collagen sheet seeded with (a) 100 % dead cells, and (b) 50/50 % live/dead cells. 220

6.16 Confocal laser scanning micrographs of HOF immediately cultured (1 h) and entrapped within (a) non-compressed collagen, (b) PC collagen sheet, and (c) 21 wt % PGF-PC collagen sheet. The arrows indicate the edges of a glass fibre. Live cells are green and dead cells are red. 221

6.17 Confocal laser scanning micrograph after 24 h culture of HOF entrapped within (a) non-compressed collagen, (b) PC collagen sheet, (c) PC collagen spiral, (d) 21 wt % PGF-PC collagen sheet, and (e) 21 wt % PGF-PC collagen spiral construct. The arrows indicate the edges of a glass fibre. 222

6.18 Closer view of HOF seeded in 21 wt % PGF-PC collagen sheet demonstrating the attachment of cells showed no preference to either collagen or glass fibres (as indicated by the dashed lines). 222

Chapter 1

Introduction

Tissue loss resulting from congenital abnormalities, traumatic injury, or disease is a major health care problem worldwide. When this occurs in the craniofacial region, it can also be highly emotive with serious physiological and psychological consequences. In the United States, for example, about 7 %, or 227,500 of the children born each year are affected by birth defects of the head and face. According to the American Society of Plastic Surgeons, in 2001, 37,732 surgeries were performed to repair these defects, an increase of 2 % over those recorded in 2000. Traumatic injuries to the craniofacial region can include blunt trauma, lacerations, and burns. According to the American Burn Institute, there are 1.1 million burn injuries each year that are serious enough to require medical treatment. In 2001, 16,879 adults needed plastic surgery to repair burn injuries, while 24,298 required maxillofacial surgery for injuries. Cancers of the head and neck on the other hand, including the skin of the face, the esophagus, the larynx, the mouth, and the nasal passages, also affect about 55,000 Americans each year[•].

Current methods of restoring tissues include transplantation or surgical transfer of relevant tissue from healthy parts of the same patient (autogenic transplantation) or from a donor (allogenic transplantation). Autogenic transplantation is considered the gold standard demonstrating the best clinical outcome. However, there are several drawbacks of this approach including donor site infection, morbidity, pain, and additional cost of operation. On the other hand, allogenic transplantation is severely limited by the availability of donor

[•] Encyclopedia of surgery: A guide for patients and Caregivers. http://www.surgeryencyclopedia.com/Ce-Fi/Craniofacial-Reconstruction.html. 2005-Thomson Gale.

supply, and many patients may die before the transplanted organs become available. Furthermore, even when the organ is available, immunological rejection of the transplant due to imperfect match can be a common problem, and lifelong immunosuppression in the recipient will cause additional morbidity and mortality (Marler *et al.*, 1998).

The most widely used alternative for transplantation involves replacing sophisticated tissues and organs with biomaterials which can be mechanical devices or artificial prosthesis such as prosthetic valves, and joints. A biomaterial has been defined as "any material, natural or man-made, that should comprise whole or part of a living structure or a biomedical device which performs, augments, or replaces a natural function" (Enderle *et al.*, 2000). Such materials will be in contact with the living biological systems for a significant period of time. An interaction between the material and host will take place, which must not have any undesirable effect on both the host and the biomaterials (Williams, 1987). Although many of these devices have a positive impact by replacing the function that has been lost through disease or injury, they will not restore the defective part to the biological function of the living structure. Upon long-term implantation, these devices may undergo failure due to wear, and the wear debris could induce an inflammatory response in the host tissues. In order to deal with these problems, within the last two decades, a new field in healthcare technology known as "tissue engineering" has emerged to offer a biological substitute to the lost tissue or organ.

The first use of the term "tissue engineering" was to refer to the observation of an organization of endothelium-like structure on the surface of poly (methyl methacrylates) ophthalmic prosthesis (Wolter and Meyer, 1984). More recently, tissue engineering has been defined as "the application of the principles and methods of engineering and the life

sciences toward the fundamental understanding of the structure-function relationships in normal and pathologic mammalian tissues and the development of biological substitutes that restore, maintain, or improve tissue functions" (Chapekar, 2000, Walgenbach *et al.*, 2001). It has also been defined as "the application of scientific principles to the design, construction, modification and growth of living tissues using biomaterials, cells, and factors, alone or in combination" (Rose *et al.*, 2002).

Research interest in the tissue engineering field has grown tremendously since its beginning, with approximately over 5000 articles with "tissue engineering" as a keyword having been published since the year 2000. The potential applications have become more widespread to now include most of the body tissues. At the beginning, attempts to engineer skin for severely burned patients (Minuth *et al.*, 1997) and cartilage for repair of joint disease such as osteoarthritis (Yu *et al.*, 1997a, Hutmacher, 2000, Ochi *et al.*, 2001, Hardingham *et al.*, 2002) were made. Recently, biological substitutes have been developed to include oral tissues (Saadeh *et al.*, 2001, Ueda *et al.*, 2001, Young *et al.*, 2002, Schmelzeisen *et al.*, 2003), liver (Harimoto *et al.*, 2002, Dvir-Ginzberg *et al.*, 2003), kidney (Steer and Nigam, 2004), cardiovascular tissues as heart valves (Shinoka, 2002) and blood vessels (Berglund *et al.*, 2003, Nasseri *et al.*, 2003, Berglund *et al.*, 2004), nerve (Itoh *et al.*, 2002a), bone (Shin *et al.*, 2004, Zhang and Ma, 2004), and urinary bladder (Gabouev *et al.*, 2003, Chung *et al.*, 2005).

Currently there are two main approaches to tissue engineering which are substitutive and histoconductive, or histoinductive approaches. The former approach involves *in vitro* construction of living tissue or organ that is transplanted into the body, while the latter approach involves *in vivo* construction of the living tissue or organ by optimizing the

structure and composition of the matrix, selection of appropriate cells for optimal proliferation, and use of highly specific growth factors or gene therapy transfection for such cytokines. This second approach is practically useful for many connective tissues, as it is advantageous to engineer these tissues *in vivo* rather than *in vitro* (Walgenbach *et al.*, 2001). Each approach depends mainly on seeding appropriate cells into or onto a scaffold required to support the cells during their growth.

Generally, materials used as scaffolds fall into three categories: ceramics or polymers or composites. Ceramic materials such as porous hydroxyapatite, Bioglass®, and calcium phosphate are bioactive, but they have low biodegradability which is often associated with inflammation and immunological reaction. Synthetic polymers such as the Food and Drug Administration (FDA) approved α-hydroxy-polyesters e.g. polyglycolic acid (PGA), polylactic acid (PLA), and polycaprolactone (PCL) have controllable degradation and mechanical properties. However, one of the major limitations with these polymers is lack of biological components that will enhance cell behaviour. Natural polymers such as collagen, alginate, and agarose can be processed at mild conditions that allow for incorporation of cells and sensitive agents or drugs. However, the lack of mechanical properties is an important issue to be considered. Recently, polymer/ceramic composite scaffolds have been used to combine the properties of the phases for bone tissue engineering applications (Kikuchi *et al.*, 2001, Yamauchi *et al.*, 2004, Kikuchi *et al.*, 2004). However, scaffolds should provide both biomimetic architecture and mechanical support for cells.

This project developed and characterised phosphate-based glass fibres (PGF) for potential biomedical applications, and three dimensional constructs of PGF-incorporated dense

collagen matrices for tissue engineering applications. Collagen is the major protein in connective tissues, and is one of the most widely used natural polymers. However, the weakness of mechanical properties of *in vitro* reconstituted collagen gels makes their handling very difficult. For this, a novel method of "Plastic Compression" (PC) was used which rapidly removes fluid from the hyper-hydrated reconstituted collagen gels through the application of unconfined compressive load to develop either acellular or cellular scaffolds (Brown *et al.*, 2005). Common methods of improving the mechanical properties of collagen include the use of cells and cross-linking. However, cell seeding is quite a lengthy and expensive procedure often requiring culture in tissue bioreactors, and the cross-linking could compromise the collagen biocompatibility.

Phosphate glasses are a unique class of materials that are degradable and biocompatible, and their degradation can be controlled by changing the glass chemistry. The main idea of introducing phosphate glass fibres was to develop a degradable matrix with enhanced mechanical properties required to support cell growth without compromising the biological properties of collagen. Phosphate glasses contain elements that are natural constituents of the human body. Moreover, these fibres were also anticipated to have the potential for providing an intriguing possibility of capillary-like channels (Knowles, 2003) within the collagen for cell and nutrient transportations. Initially, a study was performed by doping the highly degradable ternary glass based on 50 P_2O_5 -30 CaO-20 Na_2O with modifying metal oxides such as copper oxides and iron oxides, by partially substituting sodium oxide. The 50 mol % P_2O_5 ternary glass composition was chosen as it has been demonstrated to easily form fibres. Copper oxide was also incorporated for its potential antibacterial effect (Mulligan *et al.*, 2003a) which was anticipated for wound healing applications. On the other hand, iron oxide was incorporated as it has demonstrated

biocompatibility with a number of cell types including myoblasts (Ahmed *et al.*, 2004c), and osteoblasts (Bitar *et al.*, 2005).

This thesis is divided into a further six chapters. Chapter 2 gives a literature review of the different tissue engineering strategies, phosphate-based glasses, their potential medical applications, a review on collagen and its biomedical applications, and the approaches for enhancing its mechanical properties. In Chapter 3, the development and experimental methods used for characterisation of antibacterial copper containing glass fibres are described. Chapter 4 details the development and experimental methods for characterisation of PGF with different iron oxide contents. Chapter 5 focuses on the understanding of the mechanics behind the unconfined plastic compression that was used for preparation of tissue analogous implants based on collagen. This chapter also highlights the methods used for characterisation of collagen produced through plastic compression. Chapter 6 reports on the utilisation of plastic compression for the development of 3-D unidirectional-fibre incorporated collagen constructs with different compositions. Characterisation of these scaffolds in terms of morphological, mechanical properties, and biological assessment of the effect of PC and PGF content on primary human oral fibroblasts (HOF) viability up to 24 h is also included. Chapter 7 summarises the main findings of this work, and suggests further study to be considered in this area.

Chapter 2

Literature Review

2.1 Strategies of Tissue Engineering

Tissue engineering is a field that draws the attention of researchers from a variety of backgrounds including biologists, biochemists, materials scientists, genetic engineers, and clinicians. Tissue engineering focuses on biological substitutes of the damaged or diseased tissues. Generally, there are three strategies that have been adopted or evolved for the creation of new tissue which include the following:

2.1.1. Cell Therapy

Cell therapy or otherwise known as cell substitutes have been adopted in order to avoid the complications of surgery, and allow replacement of only those cells that supply the required function. This concept assumed that the cells are inherently intelligent. Langer (2000) named the strategy of cells transplantation as 'neomorphogenesis'. When isolated cells are injected randomly *in vivo*, they generally do not form tissues, but when they are placed close enough together; they tend to form a tissue-like structure. For example, isolated mammary epithelial cells form structures that make milk when placed close together even outside the body; whereas endothelial cells form capillary tubes when in close proximity to each other *in vitro*. However, the limitations with this approach are either immunological rejection or the cells may not be able to maintain their phenotype for long periods *in vivo* (Langer, 1997, Bonassar and Vacanti, 1998). To avoid the immunological rejection, cells can be isolated from the body by a membrane, which

prevents the direct contact of cell transplants with the immune cells or antibodies, but allows the transport of nutrients and waste products (Langer, 1997). This approach is called "cell encapsulation", and is used to treat most of the enzymes and hormonal deficiencies by sustained and controlled release of cells that express the deficient substance such as pancreatic islets, hepatocytes, adrenal cortical cells, and cells transfected to secrete specific enzymes. It also allows for transplantation of mammalian cells, genetically engineered or xenogenic cells without immunosuppression. This strategy can also be used as an alternative to conventional drug delivery (Drury and Mooney, 2003) since the release of cells would be in a manner that is responsive to the need of the body. The cells could also have an unlimited supply of the therapeutic agents without the expense and problem of protein or drug purification (Vallbacka *et al.*, 2001). These secretory cells are commonly encapsulated within hydrogel matrices such as alginates. The cells can be easily mixed with alginate before gelling, and its gelling under mild conditions will not affect the cells.

2.1.2. Drug/Gene Therapy

The success of this approach depends mainly on the discovery, purification, and large-scale production of appropriate signaling molecules, such as growth factors which induce cell migration, proliferation and differentiation. However, the development of appropriate carriers to deliver these molecules to their targets together with the problem and the expense of purification limit the scope of this approach (Langer, 1997). These problems could be obviated by gene therapy (Walgenbach, *et al.*, 2001) which offers the possibility of genetic modification of isolated and expanded cells to produce populations of

progenitor cells over expressing selected signalling molecules or growth factors (Rose and Oreffo, 2002).

2.1.3. Cells Placed on or within Matrices

This is the most widely used strategy where the specific cells are isolated from a biopsy specimen from the patient, expanded in culture until a sufficient number of cells have been reached for the intended application. The cells are then combined with a porous biodegradable synthetic or natural scaffold, which can be formed in the shape of the defect to be replaced as in Figure 2.1. The cells should adhere to the scaffold, proliferate, and over time form a new tissue. This new tissue can be grown *in vitro* in the scaffold, eventually reaching an "organoid" stage where it is suitable for implantation into the patient to replace the damaged or diseased tissue or to be allowed to grow *in situ* within the defect. A scaffold should carry out a number of functions such as (a) provide structural integrity and define a potential space for the engineered tissue, (b) act as a template for the three dimensional organisation of the new tissue, (c) maintain spaces for the diffusion of gas, nutrients and possibly for in-growth of blood vessels from the host tissue bed, and (d) transmit tissue-specific mechanical forces to cue the behaviour of cells within it (Marler *et al.*, 1998).

As previously mentioned, the concept of tissue engineering is based on the repair and regeneration of biological tissues and can be guided by application and control of three important elements: cells, materials, and/or chemically active proteins (cytokines) (Bonassar and Vacanti, 1998). These three elements are called the tissue engineering triad, and they will be considered in more details.

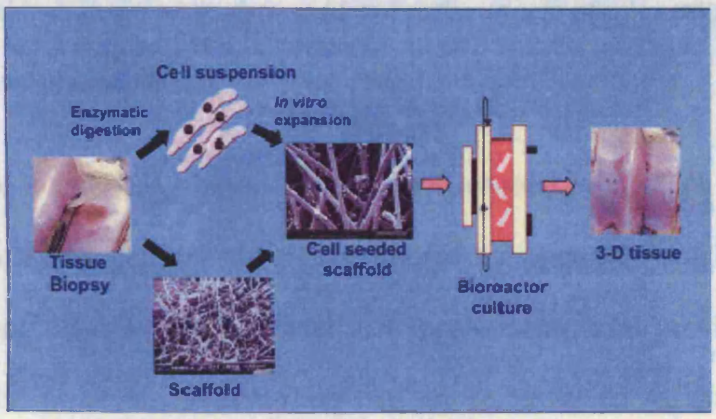

Figure 2.1: Diagrammatic representation of cell-matrix tissue engineering strategy (Rose and Oreffo, 2002).

For cell manipulations, three essential factors should be considered which include cell source, cell seeding, and culture conditions. Determination of the cell source is crucial for tissue engineering. Initially an animal source was used, but the problem of immunological rejection made the human source more favourable. Human cells can be either primary or cell lines. Primary cells may be autogenic, from the same individual; allogenic, from a different individual of the same species; xenogenic, from genetically different species; or syngenic, from a genetically identically individual. Both xenogenic and allogenic cells are not preferable due to the possibility of immunological rejection (Bonassar and Vacanti, 1998). Cell lines are genetically modified cells designed to proliferate indefinitely; they rapidly expand in culture, and they are most commonly used in gene therapy. However, the possibility of stimulating the immune response, or their tendency to lose differentiated function, and/or neoplastic transformation limit the use of these cells (Marler *et al.*, 1998). Some approaches have been attempted to make universal cell lines or immortal cells by removing or masking the protein on the cell surfaces that normally identify the cells as

"nonself". This strategy was also used to make types of pig cells acceptable for transplantation to a human being.

Currently, there is increasing interest in using human stem cells which can give a wide variety of tissues; these cells may be adult or embryonic stem cells. Adult stem cells such as mesenchymal, haematopoietic, neural and hepatic stem cells provide an unlimited supply of cells; however, understanding the factors involved in differentiation and regulation of lineage formation is critical for engineering a new tissue. These cells are usually present in bone marrow and in other tissues of the body even in fat removed from liposuction (Hardingham *et al.*, 2002). Embryonic stem cells are attractive as they have the potential to divide and form all tissue of the body in early embryonic development; however, they are still not easy to manipulate in culture medium in order to produce fully differentiated cells used to create or regenerate specific organs (Chapekar, 2000, Griffith and Naughton, 2002, Hardingham *et al.*, 2002).

The seeding of cells onto a scaffold can either be in a static form by the direct application of a cell suspension to a scaffold material, or by a dynamic form by the application of cell suspension to the scaffold under agitated conditions such as stirring, spinning flask, or rotating in two or three dimensions. Successful seeding of a thin polymer scaffold (<2 mm thick) can be achieved with static method, while thicker (>2 mm thick) scaffolds require a dynamic technique for optimal and uniform cell distribution (Marler *et al.*, 1998). A bioreactor is a more advanced procedure for growing cells in large quantities. It is a growth chamber that contains stirrers and sensors to regulate the diffusion of gas and nutrient to the scaffold as well as the waste product out of the scaffold. In a bioreactor, the new tissues remodel or change their shape in response to being mechanically loaded as

they are subjected to variation in fluid forces and this in turn produces an improvement in their mechanical properties (Nasseri *et al.*, 2003).

Growth factors are cytokines that are secreted by many cell types and function as signalling molecules. They may be added to the matrix as a simple addition or can be bound to the polymers, and the matrix itself can serve as a drug delivery vehicle. They modulate the cell behaviour by promotion or inhibition of cellular migration, proliferation, differentiation, adhesion and gene expression by up-regulating or down-regulating the synthesis of proteins, growth factors and receptors. An example of the growth factors are bone morphogenic proteins (BMPs) which are essential in bone morphogenesis (Rose and Oreffo, 2002).

2.2. Scaffolds for Tissue Engineering

The ideal scaffold should be (a) biocompatible, non-toxic, non-carcinogenic, and sterilizable, (b) three-dimensional and highly porous with interconnected pore network for cell growth and flow transport of nutrients and metabolic waste (Hutmacher, 2000), (c) of a suitable surface chemistry for cell attachment i.e. preferably contain binding sites for cells such as fibronectin or therapeutic molecules, including genes (Walgenbach *et al.*, 2001), (d) biodegradable with a controllable degradation rate to match tissue growth *in vitro* and/or *in vivo*, (e) mechanically comparable with the tissue being replaced (Bonassar and Vacanti, 1998), (f) of high surface area to volume ratio to get the desired cell density (Langer, 2000), and (g) of low weight to volume ratio so that small amounts of degradation products will minimally affect the tissue.

Generally, materials used as scaffolds fall into three categories: ceramic or polymeric or composite. Ceramic materials such as porous hydroxyapatite, bioactive glasses such as Bioglass®, calcium phosphate are most commonly used in bone tissue engineering as they form chemical bonds with the surrounding tissues. However, *in vivo,* these materials can resorb relatively slowly (e.g. of the order of years in the case of hydroxyapatite). This low biodegradability can be associated with inflammation and immunological reaction.

Polymeric materials can be synthetic or naturally based. The most widely used synthetic polymers include poly (α-hydroxy acids) of aliphatic polyesters such as polyglycolic acid (PGA), polylactic acid (PLA), or copolymers of PLGA, polycaprolactone (PCL), and polyethylene glycol (PEG). With these polymers, the mechanical properties (e.g. strength, stiffness and ductility), degradation rate, microstructure, and permeability can be easily controlled during their manufactures. Moreover, these polymers are FDA approved. However, one of the major limitations with these polymers is the lack of biological components that will enhance cell behaviour.

Alternate scaffold materials are natural polymers such as collagen, alginate, agarose, hyaluronic acid, chitosan, fibrin, fibronectin, and glycosaminoglycan. These polymers can be processed at mild conditions that allow for the incorporation of cells, sensitive agents, and drugs; they can be delivered in a minimally invasive manner, since they are usually injectable materials (Drury and Mooney, 2003). Being natural, they contain amino acid sequences which may facilitate cell attachment and differentiation (Langer, 1997). However the lack of mechanical properties of the materials and limitations in controlling their structure are important issues to be considered.

Recently, a strategy of combining natural and synthetic polymers to optimize the biomaterials for promoting specific cell-biomaterials interactions has evolved. For example, there has been a growing interest to generate a new class of synthetic biodegradable polymers containing integrin polypeptide sequence (RGD) region, which is a part of the extracellular protein fibronectin, to provide a more natural environment for growing cells i.e. to confer specific biological properties (Langer 1997, Bonassar and Vacanti 1998, Langer, 2000, Rose and Oreffo 2002). RGD is an abbreviation of the amino acid sequence in fibronectin; arginine, glycine, and aspargines respectively. These polymers are synthesized with the RGD either in the backbone, the branches, or constructed entirely of polypeptide sequences. This can be important for the tissues in load bearing areas as it allows for the physical stimuli to be sensed by cells in the new tissue in a more physiological manner. These polymers can then be bioactive polymers, as they play an active role in guiding tissue development (Langer 1997).

Composite scaffolds have also been attempted, which are a combination of two or more physically distinct and mechanically separable phases usually a matrix and filler. Polymer/ceramic composites are the most commonly used as scaffold materials especially for bone tissue engineering (Kikuchi *et al.*, 2001, Rother *et al.,* 2002, Blaker *et al.,* 2003 Boccaccini *et al.,* 2003, Yamauchi *et al.*, 2004, and Kikuchi *et al.*, 2004).

2.3. Glasses for Biomedical Applications

The word glass is derived from a late-Latin term *glaesum* used to refer to a lustrous and transparent substance. Also, the word *vitreous* originating from the Latin word *vitrum* often was used to describe glassy substances. Glazed stone beads appeared as far back as 12,000 BC in Egypt and several of the artefacts unearthed from the tombs of pharaohs

exhibit excellent glass inlay work in various colours. Purely glass objects appeared around 4000 BC, but were merely decorative (Varshnya, 1994). However, it was around 1500 BC when there were significant developments in both the art and the technology of glasses, and this was followed by further developments in glass science by Faraday, Zeiss, Abbe and Scott. The primary interest of these scientists was in glasses for optical use. Nowadays, glasses are widely used both for everyday applications; the idea of using a soluble glass as a biomaterial is a relatively new (Franks, 2000).

Glasses are either described as supercooled liquids from the chemistry point of view or as solids from the theory of elasticity. They are amorphous inorganic polymers where the atoms are arranged in an extended three dimensional network as in a crystal, but without periodicity and symmetry; however, the network is not entirely random. Lack of periodicity is responsible for the gradual breakdown of the glass network on heating, and the lack of symmetry is responsible for the isotropic properties of the glass (Zachariasen, 1932).

The trend in biomaterials is to develop and employ materials that undergo reactions in living tissue without compromising the natural biological process. These materials include glasses and glass-ceramics, and are called bioactive materials. Hench (1993) defined a bioactive material as "a material that elicits a specific biological response at the interface of the material, which results in the formation of a bond between the tissues and the material." For a given material to be bioactive with bone, for example, it should be able to form a biologically active apatite layer on its surface in the presence of physiological environment. This layer resembles the mineral part of bone tissue in its composition. Therefore, it preferentially attracts the surrounding osteoblasts to attach,

proliferate, differentiate, and lay down a new matrix of collagen fibrils and the mineral component of bone that will directly be bonded to original bone tissue (Kokubo *et al.*, 2004). The interaction between the material and its surrounding environment involves several processes such as partial dissolution of the material surface, ion exchange, changes in the surrounding pH, and ion re-precipitation (Ferraz *et al.*, 2000).

Silica-based glasses are an interesting class of bioactive materials developed by Hench *et al.* (1971) for biomedical applications (Saravanapavan *et al.*, 2003, Gough *et al.*, 2004a & b, Day and Boccaccini 2005, Bosetti and Cannas 2005, Cerruti *et al.*, 2005). They are commercially available under the name of Bioglass®. They are based on 45S5 composition that corresponds to (in weight %) 45 SiO_2-24.5 CaO-24.5 Na_2O-6 P_2O_5, and the $(SiO_4)^{4-}$ tetrahedra are the basic building block. These glasses have shown great success in many clinical applications in both dental and orthopaedic fields, but still some questions has been raised related to the long term effect of silica (Salih *et al.*, 2000), mostly because these glasses are essentially non-biodegradable.

2.4. Phosphate-Based Glasses

Phosphate compositions exhibit a pronounced tendency to form glasses upon the cooling of their melts. The first reported phosphate glass composition was a binary glass composed of Na_2O-P_2O_5, which was discovered over a century ago under the name of Graham's salt or sodium hexametaphosphate. This glass found potential use in widespread industrial applications due to its ability to form complexes with either alkali or alkali earth metals and exhibiting a colloidal activity in solutions (Van Wazer, 1950 a and b). In recent decades, numerous phosphate-based glass formulations ranging among binary, ternary and quaternary compositions have been developed.

2.4.1. Chemistry of Phosphate-Based Glasses

In studying the phosphate glass structure, three important elements that should be considered are glass formers, glass modifiers, intermediate oxides and the interaction between them.

Glass or network formers can be either primary or conditional glass formers. Primary network formers include SiO_2, B_2O_3, and P_2O_5 and are able to form glasses by themselves. Conditional glass formers however, are not able to form glasses under normal conditions, but under certain circumstances they can replace the network forming oxides. These oxides include GeO_2, Bi_2O_3, As_2O_3, Sb_2O_3, TeO_2, Al_2O_3, Ga_2O_3 and V_2O_5 (Knowles *et al.*, 2003).

Glass modifiers are not part of the glass network, but they act to balance the glass network. They are generally alkali and alkali earth metal oxides such as Na_2O, K_2O, MgO, CaO (Zachariasen, 1932, Greaves *et al.*, 1997, Knowles *et al.*, 2003). For example, pure phosphate (P_2O_5) glass is chemically unstable due to its hygroscopic nature, and the addition of metal oxides improves its stability (Lockyer *et al.*, 1995, Sales *et al.*, 2000). The interaction between the network former and modifier affects the organization of the glass network and therefore its properties (Schneider *et al.*, 2005). Before studying the interaction between the network former and modifier, the structure of phosphate glass should be considered in more detail.

Intermediate oxides are oxides such as Al_2O_3, Fe_2O_3, MgO, and BeO, which can not form glasses under their own, but to some extent they can substitute for the network former.

These oxides when they incorporated into the glass, they produce changes in colour and conductivity.

Generally, phosphate glasses are inorganic polymers composed entirely of $(PO_4)^{3-}$ tetrahedra that is regarded as the backbone of the glass as shown in Figure 2.2. Each tetrahedron composed of one phosphorus ion (P^{5+}) that is charge balanced with four O^{2-} ions. For charge compensation, one oxygen atom will share its two electrons with P^{5+}, and it is called terminal double bonded oxygen (DBO). The other three oxygens share only one of their two electrons; they are still free to combine with other P^{5+}, in this case they can form bridging oxygens (BO)* or with metal ions, where they can form non-bridging oxygen (NBO). The bridging oxygen is covalently bonded to two glass former atoms while the non-bridging oxygens are ionically bonded only on one side; therefore, the binding energy of a BO is higher than that of a NBO (Khattak *et al.*, 2004).

The structure of the tetrahedra is classified according to the number of BO per tetrahedra, and denoted by Q^i terminology, where Q refers to the phosphorus atom bonded to four oxygen atoms forming tetrahedra, and i refers to the number of bridging oxygens per tetrahedron starting from zero to a maximum of three atoms. For example, Q^3 tetrahedra (PO_4) posses three covalent bridging oxygen bonds to the neighbouring tetrahedra as in vitreous P_2O_5; accordingly, it is a neutral unit, and is known as a branching unit. Q^2 tetrahedra $(PO_4)^-$ possess two covalent bridging oxygen bonds with the neighbouring tetrahedra; therefore, it carries one negative charge, and is known as a middle unit. Q^1 tetrahedra $(PO_4)^{2-}$ unit possess one covalent bridging oxygen bond with the neighbouring

* Bridging oxygens: are oxygen ions taking part in P-O-P bonds (by which the P tetrahedra join to other tetrahedra) while the non-bridging oxygens are that assigned to –P=O or M-O-P bonds (where M is cation). Marasinghe *et al.*, 2000.

tetrahedra, and it carries two negative charges, and is known as an end unit. $Q^0 (PO_4)^{3-}$ is an isolated tetrahedron unit with no bridging oxygen to the neighbouring tetrahedron; therefore, it carries three negative charges and known as an orthophosphate unit (Kirkpatrick and Brow, 1995, Brow 2000, Walter *et al.*, 2001, Cacaina and Simon, 2003). The number of negative charges each unit carries depends on the number of NBO it has as in Figure 2.2.

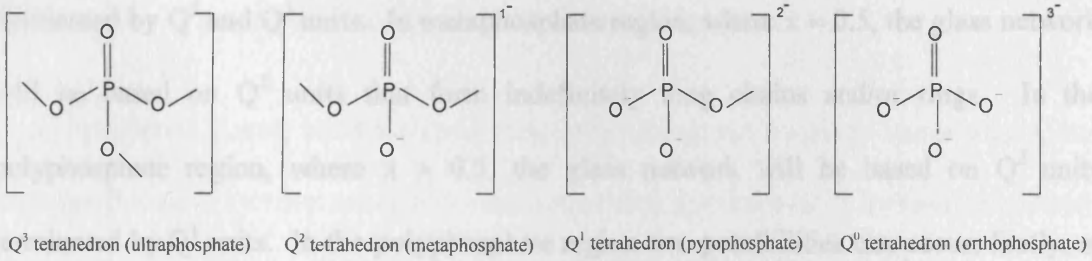

Figure 2.2: Nomenclature and representation of PO_4 tetrahedra with different polymerizations (adapted from Kirkpatrick and Brow, 1995).

One model that was proposed for the interaction between the glass network and the modifying oxides is a depolymerisation model. According to this model, the addition of modifying oxides leads to the cleavage of P-O-P links i.e. depolymerisation of the glass network, which starts from vitreous P_2O_5, with the creation of negatively charged NBO at the expense of BO. The negatively charged NBO will coordinate with the modifier cations, for optimisation of the coordination number of metal ions (Hoppe, 1996, Walter *et al.*, 1997, Brow 2000 & Hoppe *et al.*, 2000). The depolymerisation scheme according to Kirkpatrick and Brow (1995) passes from $Q^3 \rightarrow Q^2 \rightarrow Q^1 \rightarrow Q^0$ as the amount of modifier oxide (e.g. monovalent metal oxides) increases as follow:

$$2\,Q^3 + R_2O \rightarrow 2\,Q^2$$

$$2\,Q^2 + R_2O \rightarrow 2\,Q^1$$

$$2\,Q^1 + R_2O \rightarrow 2\,Q^0$$

Accordingly, the amount of metal oxides in the glass (x) and hence the oxygen to phosphorus ratio sets the number of linkage of each tetrahedron via bridging oxygen to other tetrahedra. In the ultraphosphate region, where $0 \leq x \leq 0.5$, the glass network will be dominated by Q^2 and Q^3 units. In metaphosphate region, where $x = 0.5$, the glass network will be based on Q^2 units that form indefinitely long chains and/or rings. In the polyphosphate region, where $x > 0.5$, the glass network will be based on Q^2 units terminated by Q^1 units. In the polyphosphate region two possibilities can occur; firstly, at $x = 0.67$ the network is based on phosphate dimer, two Q^1 tetrahedra units linked by one bridging oxygen, and is called a pyrophosphate unit; secondly, at $x = 0.75$, the network is based on isolated Q^0 unit (Brow 2000 & Walter *et al.*, 2001).

Another proposed model that was considered for the interaction between modifying oxides and the glass network is repolymerisation (Hoppe, 1996). This model is applied for the glass in the ultraphosphate region, and is used to explain the packing density and M-O coordination number, where M refers to metal. In this model, it was assumed that all terminal oxygen atoms including not only NBO in Q^2 middle unit but also DBO in Q^3 branching units tend to coordinate with the metal oxides. This coordination leads to reorganisation of the network structure so that each PO_4 unit is finally connected to four phosphorus or metal atoms with the metal atoms included in M-O-P bridges. At the point where all terminal oxygen atoms are involved in M-O-P bridges the structure is stabilised. For this model, it was supposed that the double bonded oxygens (DBOs) carry a slightly

negative charge that should be compensated by the opposite charge of P atoms. While the P atoms are not the first inter-tetrahedral neighbour of DBO, because the direction of P=O bonds tend to approach the centre of adjacent rings in P_4O_{10} or P_2O_5; therefore, a defect in the glass structure will result. This defect is eliminated by the presence of a real neighbour of modifying oxides. Hoppe (1996) concluded that depolymerisation is the predominating model affecting phosphate glass structure.

2.4.2. Properties of Phosphate-Based Glasses

Phosphate-based glasses are characterised by low melting and transition temperatures, and high coefficient of thermal expansion that extend their applications in technological fields (Kirkpatrick and Brow, 1995, Shih *et al.*, 1998 & 1999). They also have a unique property of degradation which can be readily and predictably manipulated by changing glass composition (Knowles, 1994 and 2003, Cartmell *et al.*, 1998a & b, Salih *et al.*, 2000, Franks *et al.*, 2000, 2001, 2002, Knowles *et al.*, 2001, Mulligan *et al.*, 2003a & b, Ahmed *et al.*, 2004a, b & c, Parsons *et al.*, 2004a, Gao *et al.*, 2004a and Alam *et al.*, 2005). The glass composition can be adjusted to obtain degradation times ranging from hours to several months (Clement *et al.*, 1999a). The degradation can be reduced by the incorporation of cations with high electrostatic field strength (Zn^{2+}, Pb^{2+}) to increase the covalency of M-O-P bonds, or cations with high valence (Al^{3+} and Fe^{3+}), or substitution of some of the oxygen atoms by nitrogen (Delahaye *et al.*, 1998).

2.4.3. General Applications of Phosphate-Based Glasses

2.4.3.1. Technological Applications

Phosphate-based glasses have been used in a wide range of technological applications such as sensors, solid-state batteries, laser devices, and air tight seals for metals with high coefficient of thermal expansion (Schneider *et al.*, 2005). These glasses were also developed for achromatic optical elements due to their low dispersion and relatively high refractive indices. However, the poor chemical durability of these glasses compared to silicate or borosilicate glasses can limit their applications.

2.4.3.2. Nuclear Waste Hosts

Iron phosphate glasses have found uses as matrices for vitrifying nuclear waste products (Marasinghe *et al.*, 2000, Mesko and Day 1999, Fang *et al.*, 2000) due to their high waste loading ability, low processing temperature, and high chemical durability which are comparable to most silicate and borosilicate glasses. They can also maintain their high chemical durability even after devitrification of wasteforms (Ray *et al.*, 1999).

2.4.3.3. Controlled Release Glasses

Controlled release glasses are a class of materials that completely dissolve in water, leaving no solid residue. Their degradation is an erosion controlled process that follows zero order release over the life of the material (Gao *et al.*, 2004a). They can be produced in different forms such as powder, granules, fibre, cloth, tubes, and cast blocks of various shapes (Gilchrist *et al.*, 1991).

Polyphosphate glass provides a source of phosphate that support the growth of recombinant *Escherichia Coli* to a density 40 % higher than that obtained with typical fermentation media. The high solubility of polyphosphate together with the absence of precipitate formation when mixed with the fermentation media supports its use for this purpose (Curless *et al.*, 1996).

Soluble glasses containing trace elements such as copper, cobalt, and selenium were manufactured under the trade name of Cosecure®. They were designed for oral administration in form of a rumen bolus to ruminant animals for the treatment of trace element deficiencies (Telfer *et al.*, 1985).

Copper releasing phosphate glasses were also used as molluscicides to control the snail hosts of schistosomiasis. The glass composition and the physical form can be changed in a reproducible manner to suit the chemistry of the water body being treated. Moreover, most of the released Cu is in non-toxic or weakly toxic form as copper polyphosphate complex that acts as secondary releasing complexes (O'Sullivan *et al.*, 1991).

Silver releasing phosphate glasses were used clinically to control long term infection in indwelling catheters. A cartridge with silver containing glass was inserted in line between the catheter and urine collection bag. When it is in position, this insert bathed with urine as it flowed from the bladder into the collection bag. The silver ions released inhibit bacterial proliferation (Gilchrist *et al.*, 1991). Also they can be potentially used for treatment of vesicoureteral flux and urinary incontinence (Cartmell *et al.*, 1998b).

2.4.3.4. Reinforcing Agents

Phosphate-based glasses have been used as reinforcing agents for many degradable polymers such as tyrosine based polymers (Choueka *et al.*, 1995), acrylic acid based drug delivery systems (Fernandez *et al.*, 2002), polycaprolactone (PCL) (Corden *et al.*, 2000, Prabhakar *et al.*, 2005), and polylactic acid (PLA) (Navarro *et al.*, 2004) for potential biomedical application in hard tissue repair and reconstruction. The rationale for using such a combination is to produce a completely degradable composite with improved mechanical properties, and to improve the biological response of the material by incorporation of these bioactive glasses that release ions which are favourable for cell attachment and proliferation. By developing a totally degradable composite, the problems associated with the conventional metallic implants of stress shielding, the need for secondary surgical intervention for implant removal and the long term foreign body reaction should then be eliminated.

Phosphate-based glasses have also been used for the reinforcement of hydroxyapatite (HA) to improve its mechanical properties to be used as bone implant materials in load bearing applications or as coatings to metallic implant materials for orthopaedic and dental applications (Lopes *et al.*, 2000, Knowles *et al.*, 1993, Ferraz *et al.*, 1999a & b, 2000). The glass acts as a sintering aid by providing a phase that can be easily sintered without grain coarsening as occurs with small particles of HA. The observed improvement in mechanical properties was attributed to the development of this secondary phase together with the reduction in the solid state reaction, which occurs at the grain boundaries. For this application, phosphate glass was incorporated in small amounts (2 to 5 weight %) which are sufficient for sintering purposes.

2.5. Potential Biomedical Applications of Phosphate-Based Glasses

Phosphate-based glasses have shown to have potential applications as soft, hard tissue implant materials. Gough *et al.* (2002 and 2003) demonstrated that sodium phosphate glasses have been shown to have a minimal level of macrophage activation evident from low amounts of peroxide and interleukin-1β release. Moreover, early primary craniofacial osteoblasts attachment and spreading was also obtained. Upon long term culture up to 28 days, the craniofacial osteoblasts exhibited cytoskeletal characteristics and the level of collagen synthesis similar to those of the positive control. It has also been shown that the biocompatibility was related to the glass degradation and the ions released, as it was difficult for cells to attach to a labile surface, and to form a physical anchorage. Low cytotoxicity (Uo *et al.*, 1998), and high number of adherent and viable cells, indicated by DNA content and maintenance of cellular function (Bitar *et al.*, 2004) were obtained for glasses with lower degradation rates.

2.5.1. Phosphate-Based Glass Monoliths

A number of glass systems have been developed, which may be either ternary or quaternary, for potential use as hard tissue substitutes or antimicrobial delivery systems. All these systems have a common feature of containing $P_2O_5 \geq 45$ mol %. Comprehensive studies have been carried out to give an overview of the physical properties of the glass such as thermal properties, degradation, ion release, and the basic glass structure and their biocompatibility.

2.5.1.1. Ternary Glass Systems

Franks *et al.* (2000) developed a ternary glass system based on the composition of 45 P_2O_5-x CaO-(55-x) Na_2O, where x was between 8 and 40 mol %. Initial work investigated the dissolution and ion release of these glasses. It was observed that as an inverse relationship between calcium oxide (CaO) content and the degradation rate existed. Moreover, this relationship was linear over time for glasses containing up to 20 mol % CaO. However, at 20 mol % CaO, a slight exponential degradation behaviour appeared, which became prominent at 32 mol % CaO. The linearity of the degradation was explained by an ion exchange process, where sodium ion (Na^+) is exchanged with hydroxonium ion (H_3O^+). This ion exchange was more severe at low CaO content, and this was correlated with the sharp increase in pH of the medium. The calcium ion (Ca^{2+}) release data correlated better with the degradation process than Na^+. This indicated that Ca^{2+} and its interaction with the glass network were suggested to be the dominant factors on glass degradation. Two processes were suggested to be responsible for the degradation of high CaO glasses; an ion exchange process, followed by a gradual breakdown of the glass network.

A thermal and structural study on the same glass system was also carried out by Franks *et al.* (2001) using differential thermal analysis (DTA) and x-ray diffraction analysis (XRD). The results showed that only one crystallisation and melting peak was obtained at both low (less than 20 mol %) and high CaO content (32 mol %). However, in the middle compositional region (20 mol %CaO), two crystalline and two melting peaks were detected.

The biological response to this glass system was analysed by Salih *et al.* (2000) to assess their potential application for bone regeneration. Two human osteoblast cell lines, MG63 and HOS (TE85) were incubated in the glass extracts with different concentrations (neat, 1:4, 1:16, 1:64 dilution) for two and five days. The MTT assay was used to study cell growth, and the ELISA assay was used to measure the expression of antigens such as bone sialoprotein, osteonectin, and fibronectin which play a vital role in bone metabolism and integrity. The results showed that low soluble glasses enhanced bone cell growth and antigen expression at all tested dilutions. On the other hand, the highly soluble glasses significantly reduced cell proliferation, and down-regulated antigen expression especially with neat and 1:4 dilutions at five days. The authors suggested that these results were related to ions released from the glass during degradation and the resultant pH changes. They suggested that with low dissolution rate glass, greater amounts of Ca^{2+} is released that is known to have an essential role in cell activation mechanisms affecting both cell growth and function. However, with highly soluble glasses, a sharp increase in pH associated with high release rates of Na^{+} and phosphorus ions $(PO_4)^{2-}$ may have a deleterious effect on cells.

Due to the higher degradation and unfavourable cellular response associated with high sodium content, Franks (2000) also developed another ternary system by complete replacement of Na_2O in the above mentioned system with potassium oxide (K_2O). This new system was based on 45 P_2O_5- x CaO-(55-x) K_2O composition, where x was between 16 and 32 mol %. Glass with CaO outside the above mentioned range was difficult to prepare due to its crystallisation on casting. It was observed that the P_2O_5-CaO-K_2O system dissolved at higher rate than P_2O_5-CaO-Na_2O system.

Ternary glass systems based on (45, 50 & 55) P_2O_5-(30, 35 & 40) CaO-Na_2O was developed by Ahmed *et al.* (2004a). A linear increase in glass transition temperature (T_g) and crystallisation temperature (T_c) was obtained with increasing CaO. A similar increase was observed with increasing P_2O_5 from 45 to 50 mol %; however, at 55 mol % a decrease in both properties was obtained. The same trend was also observed for the glass degradation behaviour. For understanding the effect of composition on physical and chemical properties, a structural study was also carried out using XRD and nuclear magnetic resonance (^{31}P NMR). NMR revealed the presence of Q^1 and Q^2 species at 45 mol % P_2O_5; however, only Q^2 species was detected for 50 and 55 mol % P_2O_5. The nonlinearity in T_g and degradation that was obtained with varying P_2O_5 was explained by the presence of Q^1 species at 45 mol % P_2O_5 that may have an effect on packing density* that accounted for such behaviour.

2.5.1.2. Quaternary Glass Systems

Moving from ternary to quaternary glass, Franks *et al.* (2002) developed a quaternary system based on 45 P_2O_5-(32-x) CaO-23 Na_2O-x MgO, where x was between 0 and 22 mol %. This system was formed by the partial substitution of Ca^{2+} in the ternary glass with magnesium ion (Mg^{2+}) that has the same valence, but a different ionic radius. This study looked at the overall degradation characteristics and the effect of released ions on cell proliferation. The results showed that the trend of the degradation process lost its exponential nature and became more linear with time with decreasing CaO content. This emphasised the influential role of CaO on the degradation process. Generally, the degradation rate was decreased by substitution of CaO with MgO although Mg^{2+} has the

* Packing density is related to the mass density and gives the fraction of the space which is filled by spheres of ionic radii Hoppe, 1996.

same valence as Ca^{2+}. The MTT assay was used to asses the effect of glass extracts at different dilutions as mentioned previously on proliferation of human osteoblasts cell line (MG63) for two and five days. The results were normalised to the control cells incubated in normal medium. The result showed that glasses with little or no MgO showed a slight decrease in cell proliferation only after two days; however, after five days all tested glass compositions showed equal or greater cell proliferation than control cells.

Another quaternary glass system based on 45 P_2O_5-(20, 24, 28 & 32) CaO-(35-x) Na_2O-x K_2O system, where x was between 0 and 25 mol %, was developed by Knowles *et al.* (2001). This system was synthesised by the partial substitution of K_2O for Na_2O to study the effect of substitution of a monovalent ion with another of different ionic radius. The degradation of this system was affected by CaO as well as K_2O content. It was observed that at 20 mol % CaO, K_2O initially reduced the degradation which then increased with further addition of K_2O. The same trend was also observed at 24 and 28 mol % CaO with the degradation reaching the same value for the ternary glass (P_2O_5-K_2O-CaO) at maximum substitution of Na_2O. At 32 mol % CaO, an anomaly in degradation was observed, where weight gain was observed prior to weight loss. The degradation behaviour at 24 and 28 mol % was explained by the mixed alkali effect that occurs when one alkali ion is gradually replaced with another alkali ion while maintaining the total alkali content. This effect is responsible for some anomalies in the glass, as it affects the linearity of some of the physical properties, especially those associated with the diffusion of ions such as electrical conductivity, dielectric relaxation, and internal friction (Chakradhar *et al.*, 2003). It was prominent in this quaternary system for two reasons: firstly, the larger ionic radius of potassium ion (K^+) than Na^+ was expected to produce more disruption to the glass network, and to slow down the diffusion of K^+ in and out of

the glass; secondly, the K^+ is heavier than Na^+; therefore, the total weight loss associated with complete leaching of K^+ is larger than that with Na^+. The MTT assay showed that the K^+ had a positive effect on cell proliferation only at high amounts of 20 mol % K_2O regardless of the associated increase in degradation.

Fluoride containing quaternary glass system based on P_2O_5-CaO-Na_2O-CaF_2 composition was also developed by Franks (2000). It was thought that fluoride may play an active role in stabilising the apatite layer, which can be essential for bone applications. It was observed that the incorporation of fluoride ions (F^-) into glass was difficult in the presence of high level of hydrogen ions (H^+) that easily reacted with F^- at the melting of the glass leading to the formation of highly volatile hydrofluoric acid (HF). This high level of H^+ is possible when using P_2O_5 and sodium dihydrogen orthophosphate (NaH_2PO_4) as precursors due to the hygroscopic nature of the first and the decomposition of the second precursor giving rise to H_2O, which acts as a source of H^+ ions. This was avoided by using $Na(PO_3)x$ precursor that did not decompose. The author reported that this glass system was a promising material for biomedical applications because it was possible to produce a high calcium/phosphorus (Ca/P) ratio close to 1.67 as with hydroxyapatite (HA). However, this high Ca/P ratio was difficult to obtain with a ternary glass, where the CaO content can not be increased over 40 mol %.

Antimicrobial quaternary glass systems incorporating either Cu^{2+} or Ag^+ ions were successfully developed for potential application in treatment of oral infections (Mulligan *et al.* 2003 a and b). These glasses could be placed at the site of infection, for example, in periodontal pockets to treat the infection with ions being released as the glass degrades. They had common features of containing a P_2O_5 fixed at 45 mol %, and the two

antibacterial ions, Cu^{2+} or Ag^{+}, fixed at 0, 1, 5, 10 and 15 mol %. For each glass system, the calcium to sodium oxide (Ca/Na_2O) ratio was varied to normalise the degradation over compositions to give nominally the same release profile for the starting materials. Consequently, the overall effect on bacteria would be reflected by the presence or absence of antibacterial ions and their amounts. The effect of both glass systems on the viability of a *Streptococcus Sanguis* biofilm* using constant depth film fermenter (CDFF) was evaluated under simulated oral environment and compared to antimicrobial ions free glass and HA discs as controls. It was observed that by 24 h, there was a significant reduction in viable counts compared to the controls which was attributed to the release of antimicrobial ions, and the reduction was high for glasses containing more antimicrobial ions. However, a recovery of the cell counts was observed by 48 h which were still significantly lower than that of the controls and remained relatively constant between 48 h and eight days. The recovery was attributed to two reasons: firstly, the formation of a sacrificial layer formed by the dead bacterial cells that acted as a barrier against further penetration of antimicrobial ions into the biofilm; secondly, the differentiation of bacteria into another phenotype that was resistant. The results also showed that Ag^{+} are more potent antimicrobial ions than Cu^{2+} ions.

Iron oxide (Fe_2O_3) has also been incorporated to provide more flexibility in degradation rate by partial substitution of Na_2O, and this leads to the evolution of 50 P_2O_5-(30, 40 & 45) CaO-Na_2O-x Fe_2O_3 system, where x was between 1 and 5 mol % (Ahmed *et al.*, 2004c). Addition of Fe_2O_3 up to 5 mol % produced a decrease in degradation rate by one order of magnitude together with an increase in T_g as measured through DTA.

* Biofilm (dental plaque) can be described as a diverse microbial community attached to the tooth surface and encased in a matrix comprising of bacterial and host products (Mulligan et al., 2003).

2.5.2. Phosphate-Based Glass Fibres

Fibres have potential applications in the engineering of soft tissue such as muscle and ligament due to their chemistry and the fibre morphology which could mimic the fibrous form of these tissues (Knowles 2003). It has been suggested that the glass fibres can orient the muscle cells along their long axis to grow and form myotubes (Ahmed *et al.*, 2005, Shah *et al.*, 2005) particularly, the three dimensional mesh arrangements that provided the best configuration supporting cell attachment and proliferation. Generally, glass fibrous meshes with open mesh morphology allow for diffusion of nutrient and waste products in and out of the scaffolds, and would allow for ingrowth of vasculatures and hence the tissue. They would also provide the necessary structural support without compromising the porosity (Mooney *et al.*, 1996, De Diego *et al.*, 2000, Domingues *et al.*, 2001, Mahmood, *et al.*, 2001, Orefice *et al.*, 2001, Hatcher *et al.*, 2003, Clupper *et al.*, 2003 & 2004, Li *et al.*, 2005). Recently, it was also suggested that the fibres could also act as a nerve conduit, since they act as contact guidance for cell to orient, proliferate and grow (Lee *et al.*, 1999a, Hatcher *et al.*, 2003).

Phosphate glasses within certain compositions, i.e. those with more than 45 mol % P_2O_5, can be easily drawn into fibres due to their polymeric nature. The fibre drawing ability or spinnability is related to the ability of the longer chains to entangle with other chains. Entanglements of these chains allow for continuous filaments to be formed instead of clusters or droplets. Milberg and Daly (1963) assumed that the metaphosphate chains are composed of long chain molecules with the chain axes having a preference to be parallel to the long axis of the fibre, and that all chains have a random orientation around their respective axes. In perfectly oriented fibres, all chain axes are parallel to the fibre axis,

and the rotational disorder of the chains around their axes corresponds to the cylindrical symmetry of the fibre. Other authors have suggested that the drawing operation preferentially selects the strong bonds to be pulled because they are able to withstand the pulling stress. The continuity of fibres is related to the ability of these bonds to be aligned along the long axis of the fibre. Whereas, weak bonds can be extended for a short distance along the strong bonds, and are not able to form continuous fibres (Murgatroyd, 1948).

It has been reported that the glass fibres have higher strength properties and higher reactivity than the bulk glass. Choueka *et al.* (1995) attributed this improvement in mechanical properties to inherent stresses developed during fibre production and rapid cooling, which forces some bonds to be frozen at angles and lengths in a non-equilibrium position and some other bonds to be broken. However, De Diego *et al.* (2000) revealed the high strength properties of fibres to be due to the enhancement of the chemical bonding at the surface, and to the decreased possibility of phase separation during fibre production.

High heat was the conventional route used for fibre drawing where fragments of the starting glass are remelted, and fibres are drawn onto a rotating collection drum (Lin *et al.*, 1994, Choueka *et al.*, 1995, Marcolongo *et al.*, 1997& 1998, De-Diego *et al.*, 2000, Clupper *et al.*, 2003 and 2004). Adjustment of the melt temperature is necessary for obtaining a suitable viscosity for fibre drawing, as it was not feasible for glass with low melt viscosity to be drawn into fibres (Ahmed *et al.*, 2004a). Additionally, this temperature should be above the glass crystallisation temperature; otherwise, the fibre

drawing will be difficult (Clupper *et al.*, 2003), or the bioactivity will be reduced (Orifice *et al.*, 2001).

2.5.2.1. Ternary Glass Systems

Iron containing phosphate glass fibres [(56-73) P_2O_5-CaO-(5-22.5 wt %) Fe_2O_3] were used as reinforcing agents for the potential development of bioabsorbable composites for potential orthopaedic applications. A cortical plug method was used to test the biocompatibility; the results showed that no inflammation was observed up to five weeks. Also, incorporation of iron oxide into the fibres enhanced their tensile strength (Lin *et al.*, 1994). Glass fibres with 62.9 P_2O_5-21.9 Al_2O_3-15.2 ZnO supported proliferation and differentiation of human masseter muscle derived cells (Shah, 2005).

2.5.2.2. Quaternary Glass Systems

Glass fibres with 50 P_2O_5-30 CaO-(20-x) Na_2O-x Fe_2O_3, where x was between 1 and 5 mol % were produced. A dramatic improvement in immortal muscle precursor cell line attachment with the highest cell density was observed for fibres with 4 and 5 mol % Fe_2O_3 (Ahmed *et al.*, 2004c). Also, it was observed that glass fibres with 3 mol % Fe_2O_3 have demonstrated significant biocompatibility with both primary human osteoblasts and fibroblasts, supporting a clear proliferation pattern, and permitting a well spread morphology (Bitar *et al.*, 2005).

2.6. Biomedical Applications of Collagen

The biomedical use of collagen has dated back to 3750 BC when the Egyptian surgeons used it as catgut sutures (O'Grady and Bordon, 2003). Currently, collagen-based

biomaterials have found many therapeutic uses such as; a haemostatic agent, drug and gene delivery, soft tissue and hard tissue repair. Collagen based biomaterials have been shown to be biodegradable and biocompatible where the degradation can be controlled by cross-linking, easily purified from living organisms and have been manufactured into many formulations including sponges, membranes, fibres, and gels. Some of these biomaterials are commercially available as medical devices as given in Table 2.1.

Table 2.1: Commercially available collagen-based medical devices (Pachence, 1996).

Medical speciality	Application
General surgery	Haemostasis
Dermatology	Soft tissue augmentation
Dentistry	Oral wounds
	Periodontal ligament attachment
Ophthalmology	Corneal shields
Cardiovascular	Anti-infectious catheter cuffs
	Arterial puncture repair
Plastic and reconstructive surgery	Wound dressings
	Artificial skin
Orthopaedics	Bone repair
Urology	Bulking agent for incontinence
Drug delivery	Cancer therapeutic; growth factors

2.6.1. Delivery Vehicle

Systemic routs via oral or parental administration have been the conventional way for delivery of a drug into the body. However, due to the possible enzymatic degradation and the non-specific uptake of the drug, large doses are required to produce the desired local effect. The non-specific release of the drugs could be beneficial to some tissues, but toxic to the others. The use of a vehicle for controlled and sustained release of the drug to the specific tissue can be an alternative route (Drury and Mooney, 2003). Being biodegradable, collagen was tried for delivery of a wide variety of therapeutic agents such

as antibiotics (Ruszczak and Friess, 2003), carcinostatics (Lee *et al.*, 2001a), bone morphogenic protein (Geiger *et al.*, 2003), proteins (Fujioka *et al.*, 1998, Sano *et al.*, 2003) and chlorhexidine for the treatment of deep periodontal pockets (Vinholis *et al.*, 2001). The release of drug is affected by the gel concentration, preparation method, and the degree of cross-linking of the matrix.

Biodegradable collagen/PLGA microparticles for parenteral application were developed by Schlapp and Friess (2003) for the release of gentamicin. The microparticles provided a fast initial burst of antibiotic followed by a sustained controlled release for approximately 10 days. Collagen modified hyaluronan microparticles were also developed for potential delivery of sulfadiazine (Lee, *et al.*, 2001b).

Collagen has also been used in gene therapy to treat congenital or acquired diseases caused by the presence of abnormal protein produced from incorrect sequence of nucleic acid bases present in the nuclei of cells. A solution of collagen, gene vector and plasmid DNA, used to introduce the therapeutic gene into the nucleus of the host cells, can be formed into different formulations such as beads, sponges, membranes, and minipellets without heat processing or using solvent that may cause the deactivation of the gene vectors. After implantation into the body, the collagen solution becomes fibrous, and then a solid matrix that retains the gene vector and the plasmid DNA from immunological reaction and enzymatic degradation. This can provide a sustained release of gene vector as shown in Figure 2.3 (Sano *et al.*, 2003).

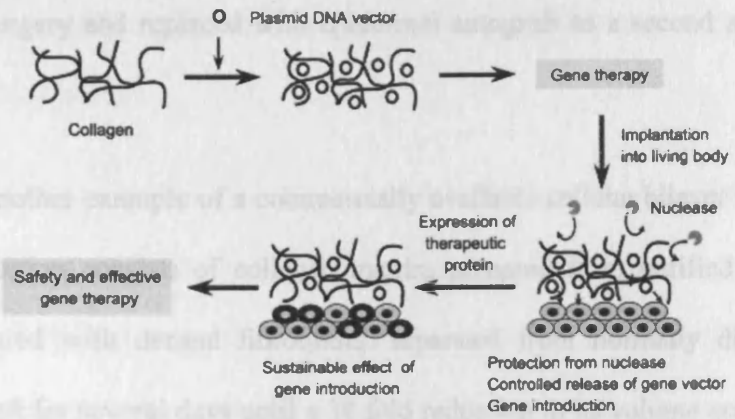

Figure 2.3: Conception of collagen-mediated gene delivery (Sano *et al.*, 2003).

2.6.2. Soft Tissue Repair

Collagen based biomaterials have found an increasing interest in tissue engineering applications for soft tissue repairs such as skin, cartilage, nerve, ligament, and vascular constructs.

2.6.2.1. Skin or Mucosal Substitute

Collagen has been widely used as an injectable material for cosmetic purposes to treat dermal defects (Ho *et al.*, 2003). A collagen-glycosaminoglycan sponge which is dense and mechanically strong was used as a dermal substitute, and it was commercially produced under the name of Integra™ (Sethi *et al.*, 2002, O'brien *et al.*, 2005). Integra™ is an acellular bilayer skin substitute; it consists of a porous lattice of collagen-glycosaminoglycan sponge, which constitutes the dermal layer and a superficial silicone polymer as pseudo-epidermis. The dermal layer serves as a biodegradable template to induce reorganization and formation of neodermis while the pseudo-epidermis acts as a barrier against mechanical action and infection during healing; therefore it requires to be

removed by surgery and replaced with epidermal autograft as a second step (Ruszczak, 2003).

Apligraft® is another example of a commercially available cellular bilayer skin substitute. The dermal portion consists of collagen matrix, prepared from purified bovine type I collagen, cultured with dermal fibroblasts, separated from normally discarded infant foreskin, and left for several days until a 30 fold reduction in its volume occurs, providing a dense collagen matrix that serve as a dermis. In the second step, this condensed collagen matrix is seeded with human dermal keratinocytes forming epidermal-like structure (Ruszczak, 2003).

Collagen sponges reinforced with polyglycolic acid (PGA) fibres (20 μm in diameter) was used by Itoch *et al.* (2004) as scaffolds for hair reconstitution assay to overcome the ectopic hair growth commonly associated with the silicon chamber frequently used for this purpose. This assay is a useful system to study cell-cell and epithelial-mesenchymal interactions involved in reconstruction of hair appendages such as hair follicles, sweat and sebaceous glands. The results showed that conventional collagen sponges disturbed normal hair growth, and was commonly associated with the development of the epidermal cysts and ectopic hairs. Nevertheless, PGA fibre reinforced collagen sponge supported proper restructuring of skin and hair follicles that was maintained for 6 months. The authors explained these findings by the role of PGA in reducing collagen sponge shrinkage, maintaining the pore size, hence accepting and maintaining high cell density, and finally limiting the leaking of cells which resulted in ectopic hair growth. The inclusion of PGA fibres also provided greater resistance to deformation, so it could be modified into various shapes suitable to fill an irregular defect. The authors recommended

the usefulness of the PGA reinforced collagen sponges for hair reconstitution in research and in clinical applications.

Imaizumi *et al* (2004) developed a collagen membrane as a matrix for either keratinocytes (monolayer cultured sheet) or for both keratinocytes and fibroblasts (double-layered cultured sheet) for potential application in mucosal defect in the oral cavity. The findings suggested that the double-layered cultured mucosal sheet could facilitate epithelial healing and prevent wound contraction.

2.6.2.2. Cartilage Repair

Isolated chondral lesions are a disease of young individuals who commonly subjected to traumatic injuries, and it has been known that chondral lesions have limited capacity for self repair due to the limited blood supply and lack of cells capable of entering the defect. Several different methods are currently in clinical use to replace the diseased cartilage, such as bone drilling and microfracturing, osteochondroplasty, and autologous chondrocyte transplantation. Drilling and microfracturing uses bone marrow or periosteum-derived mesenchymal progenitor cells to fill the chondral defect; however, the repair tissue formed as a result of this method is always fibrous not cartilagenous tissue. In osteochondroplasty, cylindrical osteochondral plugs mostly derived from non load bearing areas in the knee are used to fill the chondral defects. This method is considered the gold standard; however, the lack of suitable donor tissue and donor site morbidity, and the imperfect filling of the defect limit the scope of this approach (Ochi *et al.*, 2001, Aigner and Stove, 2003). Transplantation of autologous expanded cells in suspension has also been attempted. The defect is sutured closed with a periosteal flap to prevent cells from escaping. However, the possibility that the chondrocytes lose their phenotype due to

their dedifferentiation when they are cultured for long periods in a monolayer culture for expansion, and leakage of chondrocytes out of the defect under joint movement are the common limitations with this approach.

A new approach depends on the immobilization and transplantation of chondrocytes in a carrier scaffold which has been evolved to avoid the previous limitations. These cells can either be seeded directly onto scaffolds or be proliferated *in vitro* prior to their seeding; the latter case being practical due to the limited number of chondrocytes that can be harvested from tissue biopsies. Ochi *et al.,* 2001 cultivated the chondrocytes for 3 weeks in type I collagen before transplantation, and good clinical results suggested that this technique was promising for the management of chondral defect. Collagen was also used for cartilage repair by Hunter *et al.* (2002) and Veilleux *et al.* (2004). PLGA-collagen hybrid sponges had been used for *in vivo* and *in vitro* culture of chondrocytes. The PLGA sponge formed the external framework with the collagen micro-sponges occupying its porosity. This hybrid combined the good wettability of collagen allowing for easy seeding of chondrocytes with the high mechanical properties of PLGA sponge (Chen *et al.*, 2004). Moreover, Lee *et al.* (2003) developed collagen-glycosaminoglycan matrices for potential application for cartilage repair.

2.6.2.3. Other Soft Tissue Applications

Collagen was used as haemostatic agents in oral surgery, splenic repair, gynaecology and laparoscopy. The inherent ability of platelets to bind to collagen, and to stimulate the clotting cascade, together with the ability of collagen sponge to be sutured to the surrounding tissues, and to act as a template for new tissue ingrowth facilitate its success in this application (Pachence, 1996).

Collagen inserts as a shield was used to promote the wound healing after corneal transplantation. After being degraded it leaves a collagen solution that acts as a lubricant against the rubbing action of the eyelids (Friess, 1998).

A bioresorbable composite prepared by Dunn *et al.* (1997) by embedding collagen fibres within a matrix of PLA was developed as a scaffold for potential use in anterior cruciate ligament reconstruction.

O'Connor *et al.* (2001) used collagen gel to provide a three dimensional environment for the growth and extension of neurons from dissociated or damaged nerve and suppress apoptosis. While Berglund *et al.* (2003) prepared a blood vessel-like construct that consisted of an inner acellular supporting sleeve of cross-linked type I collagen to provide a temporary support during the cell mediated remodeling of the construct, and a second layer of endothelial cells incorporated uncross-linked collagen.

2.6.3. Hard Tissue Repair

A Bio-Gide® Collagen membrane has been used as a guided bone regeneration membrane for the treatment of periodontal disease, pre-implant dehiscence, and bone defects of numerous origins (Schlegel, 1997). Bio-Gide® is a bilayer membrane, consists of an outer compact smooth layer that is covered by a particularly dense film designed to prevent the invasion of soft tissue in a membrane protected defect, but allow for the cells to attach to the membrane. The inner layer is a rough porous side which is placed towards the bone defect in order to make bone ingrowth possible. Therefore, this membrane allows for preferential invasion of slow growing osseo-progenitor cells to migrate to, and hence reossify the bone defect, while preventing the invasion of fibroblasts. This membrane has

been shown to resorb within 6 months by enzymatic degradation via collagenases, gelatinases and proteinases (Schlegel *et al.*, 1997, Hillmann *et al.*, 2002).

Collagraft® was approved by the FDA as an alternative to autologous implant for bone tissue substitute. It is a porous collagen-calcium phosphate ceramic strip that is blended with patient's bone marrow before implantation (Geiger and Friess, 2003).

2.7. Sequential and Higher Structure of Type I Collagen

Collagen is the structural building block of the body; it forms the three dimensional matrix of all tissues that surround the cells and gives each tissue its characteristic structure, texture and shape. In the tendon, it confers the high strength; in the cornea, it is transparent; in the heart valve, it is fatigue resistant; and in the renal glomeruli, it is an excellent filtration system (O' Grady and Bordon, 2003). The term 'collagen' is a common name for proteins forming a characteristic triple helix structure of three polypeptide chains, and all members of the collagen family form this superstructure in extracellular matrix. There are 25 identified collagen types which differ in size, function, and distribution within tissues (Gelse, 2003). According to the structure and supramolecular organisation, collagens can be categorised into the different groups presented in Table 2.2. The most abundant and widespread family of collagens with approximately 90 % of the total collagen is represented by the fibril forming type. It is characterised by self assembly to form staggered fibrils that are strengthened by natural interchain cross-links. Non fibrillar collagen is thought to be associated with the surface of the fibrils which may be important in controlling their diameter (Sittinger *et al.*, 1996).

Table 2.2: Various collagen types and the major collagen families (adapted from Gelse *et al.*, 2003).

Collagen	Type
Fibril-forming collagens	I, II, III, V, XI
Fibril-associated collagens (FACIT)	IX, XII, XIV, XIX, XX, XXI.
Network forming collagens	VIII, X.
Anchoring fibrils	VII
Transmembrane collagens	XIII, XVII
Basement membrane collagens	IV.
Mutiplexins	XV, XVI, XVIII.

Type I collagen is the major fibrillar collagen and the most abundant among the different types. It accounts for 25 % of the dry protein in mammals; constituting more than 90 % (by weight) of the organic matrix of bone, and is also the major collagen component of tendons, skin, ligaments, cornea and many other interstitial tissues (Fujioka *et al.*, 1998, Gelse *et al.*, 2003, Friess, 1998). Type I collagen molecules are composed of three different polypeptide chains (heterotrimer), 2 identical α1 (I)-chains and one distinct α 2 (I)-chain. Each chain is made up of 1300-1700 free amino acid residues. These amino acids are formed by the ribosome of rough endoplasmic reticulum inside cells, mostly fibroblasts and osteoblasts. They are arranged in (G-X-Y) triplet where collagen type I consists of 388 triplets (Ho *et al.*, 2002, Friess, 1998, Gage and Francis, 1989). G is a glycine that occupies about 33 % of amino acid positions, while X and Y are often occupied by proline and 4-hydroxyproline respectively, which together occupy about 35 % of the amino acid positions in the chain. 4-hydroxyproline produced by the enzymatic post-translational hydroxylation of proline, catalyzed by propyl 3-hydroxylase and propyl 4-hydroxylase enzymes, and it occupies 10 % of amino acid position in collagen.

Collagen also contains an unusual amino acid hydroxylysine which is also produced by the post-translational modification of lysine via lysyl hydroxylase enzyme. Hydroxylysine allows for the attachment of sugar components, which are essential for formation of triple helix structure. This level of collagen structure is called the "primary structure" which is unique for type I collagen as shown in Figure 2.4 (a).

The presence of glycine representing the smallest amino acid in every third position in the triplet is essential for the triple helix formation. It forces each α chain to be assembled into left handed helical structure around a central axis with all glycine residues located in the core of the helix; however, the other amino acids (X-Y) are located on the outer positions. This level of ordering represents the "secondary structure". Then the three left handed helices are twined together to form right handed triple helix structure similar to a triple-stranded rope called "tertiary structure" as shown in Figure 2.4 (b). In each chain, the majority the amino acids, more than 1000, are organised into a central triple helix configuration called a "triple helix" or "collagenous domain". This triple helix representing the major part in fibril forming collagen is at the order of 300 nm long and 1.5 nm diameter. It is also surrounded by non-helical or non collagenous domains called "telopeptides" which contain 9-26 amino acids, and are involved in the covalent cross-linking between collagen molecules, as well as with other molecules of the surrounding matrix (Gelse *et al.*, 2003). The carboxyl (C-terminal) is thought to be essential for initiation of the triple helix formation, whilst the N-terminal is thought to be involved in primary fibril diameter regulation. At the junction of the triple helix and the N-terminal, there is a short triplet sequence. The non triplet sequence contains high levels of acidic and hydrophobic residues while the triple helix is basic (Gage and Francis, 1989). The triple helix structures are packaged in Golgi apparatus into secretory vesicles and released

into the extracellular spaces (Friess, 1998, Gelse *et al.*, 2003). In extracellular space, this soluble precursor of collagen, called "procollagen", is modified by specific peptidase (procollagen N-proteinase and procollagen C-proteinase) for the cleavage of N-terminal and C-terminal respectively. On the fourth level of order, "quaternary structure", the triple helix molecules stagger longitudinally and bilaterally into fibrils with a characteristic 70 nm periodicity with an additional gap of 40 nm between the adjacent molecules, each microfibrilis formed by quarter-staggered assemblies of 4-5 molecules as shown in Figure 2.4 (c). This process of self assembling of collagen molecules into microfibrilis called fibrilogenesis.

Fibrilogenesis forms fibrils with diameters ranging between 10 and 500 nm depending on the type and stage of development of the tissue; collected fibrils form a fibre, and intertwined fibres form a fibre bundle. Electrostatic and hydrophobic interactions of collagen molecules are involved in the quarter-staggered arrangement. It was suggested that the hydrophobic forces contribute to the stability more than the electrostatic interactions since there are 268 positive sites but only 249 negative charges available for bonding. Electrostatic attractive forces occur between pairs of oppositely charged amino acids; however, repulsive forces are formed between pairs of amino acids having the same charge (Rosenblatt *et al.*, 1994). Self assembly of collagen and its enzymatic cleavage are responsible for collagen insolubility (Usha and Ramasami, 1999, Ho *et al.*, 2002, Gelse *et al.*, 2003, O'Grady and Bordon 2003).

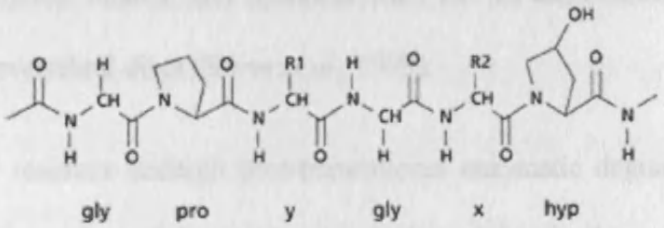

(a)

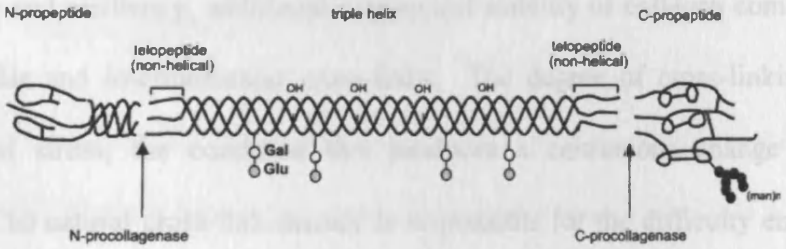

(b)

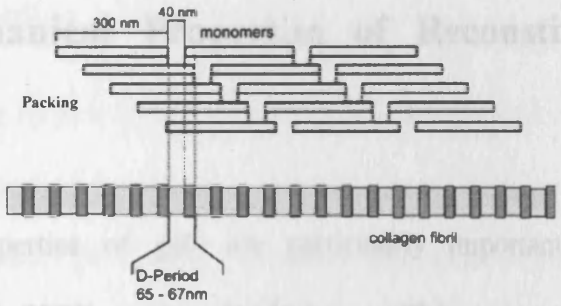

(c)

Figure 2.4: Supramolecular structure of type I collagen (a) primary amino acid sequence (α chain) (Friess, 1998), (b) secondary and tertiary structure, and (c) quaternary structure (Gelse *et al.*, 2003).

Type I collagen fibrils oriented differently in a variety of forms such as parallel aligned fibrillar structure in tissues such as tendon, ligament, dura mater and pericardium; aligned

networks in skin, blood vessels, and intestinal wall; and as combinations of the above networks as in intervertebral discs (Silver *et al.*, 1979).

Proline and lysine residues undergo post-translational enzymatic degradation; which is essential for the formation of intramolecular hydrogen bonds that contribute to the stability of the triple helix. Packing of the triple helix structure provides collagen fibres with strength and resiliency; additional mechanical stability of collagen comes from both interamolecular and intermolecular cross-links. The degree of cross-linking increased with age and stress, the condition that produces a continuous change in collagen properties. The natural cross-link density is responsible for the difficulty encountered in solubilising collagen under mild conditions (Friess, 1998).

2.8. Mechanical Properties of Reconstituted Collagen Gels

The mechanical properties of gels are particularly important when proposed as biomaterials (Gu *et al.*, 2003), as they should have sufficient strength to withstand forces and motions exerted by the host tissues (Lee *et al.*, 2001a). Type I collagen fibrils can be reconstituted in vitro by neutralisation of collagen solution. At the physiological conditions of pH and temperature, the monomers initially pack into small fibrillar segments with weak interactions which are subsequently enhanced by covalent cross-linking. Then these small segments grow by end to end fusion to form a highly interconnected random network of long continuous fibrils. The fact that this fibrillar assembly is highly hydrated with huge excess of fluids greater than 99 % occupying the interstitial spaces accounted for the inherent weakness together with the difficulty in

manipulation of these gels (Chandran and Barocas, 2004). This high fluid content is a result of the casting rather than any inherent property of the collagen gels, and the mechanical properties of collagen gels depend mainly on the integrity of its fibrillar structure and the fluid in-between.

2.8.1. Methods to Improve the Mechanical Properties of Reconstituted Collagen Gels

There are several approaches for improving the mechanical properties of collagen gels *in vitro* such as: cell seeding, chemical cross-linking, preloading or mechanical conditioning of the construct, and plastic compression.

2.8.1.1. Cell Seeding

The most widely used approach for producing collagen gels with improved mechanical properties is by entrapping cells within pre-set collagen solutions. After neutralisation and formation of the hydrated gel network, a mutual interaction between cells and the gel network takes place. The improved mechanical properties have been suggested to be due to gel compaction, and fibril orientation that the cells produce (Tuan *et al.*, 1996, Moriyama *et al.*, 2001, Seliketar *et al.*, 2003, Shi and Vesely, 2003, Garvin *et al.*, 2003). Gel compaction occurs mainly due to the cell contractile forces, which are able to expel the interstitial fluid and to generate a dense network structure. The fibril orientation or alignment results from the anisotropic strain developed when the network becomes mechanically strained by the cell traction forces (Sawhney and Howard, 2002, Girton *et al.*, 2002). In turn, these aligned collagen fibrils act as contact guidance for cells to align themselves, move, and finally exert further tractional forces that are parallel to the aligned

fibrils producing additional compaction (Girton *et al.*, 2002) or induce a change in the nuclear morphology influencing the cell synthetic activity (Awad *et al.*, 2000). It has been shown that cell incorporating collagen gels resulted in higher strength and stiffness than acellular gels (Awed *et al.*, 2003, Feng *et al.*, 2003a). This improvement in mechanical properties depends on several factors such as: cell type (Feng *et al.*, 2003a, Moriyama *et al.*, 2001, Garvin *et al.*, 2003, and Shi and Vesely, 2003), cell density (Awad *et al.*, 2000, and Feng *et al.*, 2003 b), passage number (Veilleux *et al.*, 2004), collagen concentration, and the concentration of serum in the culture medium (Cacou *et al*, 2000, Shi and Vesely, 2003). Gel compaction differs according to the type of cells, for example, chondrocytes produced lower contraction compared to human dermal fibroblasts under identical conditions (Hunter *et al.*, 2002). However, cardiomyocytes are stronger in their action compared to fibroblasts (Feng *et al.*, 2003b). Furthermore, the higher the cell density, the faster the contraction (Shi and Vesely, 2003), but it has been suggested that there may be a threshold limit beyond which the compaction will be independent on cell density (Awad *et al.*, 2000). Also, Shi and Vesely (2003) showed that there was no compaction observed over 8 weeks in the absence of serum, and the initial collagen concentration had an effect on the initial not the magnitude of the final contraction. A summary of the mechanical properties reported in the literature for cell seeded collagen gels is given in Table 2.3.

Table 2.3: Summary of mechanical properties of cell seeded collagen constructs as reported in the literature.

Collagen Source (Type)	Collagen Concentration (mg/ml)	Cell Type	Density (Cells/ml)	Culture Time (Days)	Modulus ($MN.m^2$)	Tensile Strength ($MN.m^2$)	Breaking Strain (%)	Authors
Rat tail (I)	2	RASM*	1×10^6	4	0.04	0.01	-	Seliktar *et al.*, 2003
		HASM†		4	0.02	0.005	-	
		HDF+		4	0.03	0.007	-	
		RASM		8	0.07	0.02	-	
		HASM		8	0.01	0.003	-	
		HDF		8	0.03	0.01	-	
Rat tail (I)	2	HDF		8	<0.01	0.015	-	Berglund *et al.*, 2004
		RASM		8	<0.01	0.03	-	
		HDF		23	<0.01	0.02	-	
		RASM		23	<0.01	0.028	-	
-	2	NHDF*	0.5×10^6	14	0.4 ± 0.1	0.1 ± 0.02	0.7 ± 0.1	Neidert *et al.*, 2004
Rat tail (I)	2	NRASM▲	1×10^6	56	5.3 ± 0.4	1.1 ± 0.2	9.3 ± 2.6	Shi and Vessely, 2003
(I)	-	ATIFs✧	1.2×10^6	7	0.49 ± 0.24	0.1 ± 0.01	-	Garvin *et al*, 2003
Porcine (I)	1.67	HF	2.5×10^6	14	0.8	0.22	-	Feng *et al.*, 2003a
				28	0.9	0.23	-	
				70	0.7	0.16	-	

* Rat aortic smooth muscle cells
† Human aortic smooth muscle cells
+ Human dermal fibroblasts
* Neonatal human dermal fibroblasts
▲ Neonatal rat aortic smooth muscle cells
✧ Avian tendon internal fibroblasts
‡ Rat fibroblasts
* Rat cardiomyocytes

2.8.1.2. Chemical Cross-Linking

The second approach for improving the mechanical properties of collagen gels is cross-linking (Charulatha and Rajaram, 2001, Koob *et al.*, 2001a & b, Lee *et al.*, 2001c, Yamauchi *et al.*, 2001, Itoh, 2002a, Koob and Hernandez 2002, Park *et al.*, 2002, Berglund *et al.*, 2004). As mentioned above in Section 2.9.1., collagen solution is able to form fibres at neutral pH and 37 °C, but the natural cross-links are absent *in vitro*, and the collagen fibres are not able to withstand force. Chemical cross-linking agents such as; glutraldehyde and carbodiimide are commonly used to form covalent cross links between the amino acid groups in the neighbouring proteins to improve the mechanical properties of collagen. However, the chemical reaction involved in cross-linking and the reaction products have an important effect on the biodegradation and biocompatibility of the resultant gels. Both cross–linking agents do not prevent the proteolytic degradation, but glutraldehyde significantly slows down the degradation. Moreover, the possibility of cytotoxicity associated with either the unreacted material or the reaction products can be another limitation of this method. Di-catechol nordihydroguaiaretic acid (NDGA) derived from plants has also been used as an alternative cross-linking agent. It has been shown NDGA was more effective in enhancing the tensile strength and stiffness than both glutraldehyde and carbodiimide (Koob *et al.*, 2001a& b, Koob and Hernandez, 2002). Another mild cross-linking agent has been also attempted was 4-butyrothilactone forming disulfide bonds, which avoids the complications associated with glutraldehyde and carbodiimide (Yamauchi *et al.*, 2001).

2.8.1.3. Dynamic Mechanical Conditioning

The third approach used to improve the mechanical properties of collagen gels is dynamic mechanical conditioning or preloading the collagen constructs. As mentioned previously, collagen gels consist of randomly oriented network that can resist forces in all direction i.e. mechanical isotropy (Newman *et al.*, 1997). The preloading of collagen with either a compression or tensile load produce fibril orientation normal or parallel to the direction of the applied load respectively (Girton *et al.*, 2002). This orientation induced mechanical anisotropy i.e. improved mechanical properties in the direction of induced orientation.

2.8.1.4. Plastic Compression

Plastic compression (PC) of native collagen gels is a novel method developed by Brown *et al.* (2005) for the production of tissue analogous implants. It achieved most of the demands for cell-independent tissue engineering. The key to this was the management of the fluid component of this hyper-hydrated gel for controlling matrix density and mechanical properties. The fluid was expelled by application of unconfined compressive load giving strictly plastic compaction i.e. the gels did not return to their original dimension after compression. The fluid expulsion was associated with huge scale shrinkage of more than 100 fold which provided the ability to controllably produce nano and microscale biomimetic structures. The compression process also produced mesoscale lamellar structure (less than 10 μm dimension) parallel to the fluid leaving surfaces with microlayering and embossed interface topography. This form of tissue fabrication was used for producing cellular constructs incorporating human dermal fibroblasts (HDF) since PC did not significantly reduce the cell viability, and the cells could withstand a relatively high level of fluid shear. HDF appeared normal, active, spreading throughout

the construct within three hours. The cell viability of was only reduced by 20 % after compression, and the cells tended to align with the lamellae. Spiralling of this PC produced structure around the short edge was also attempted for easy handling. It was observed that the cells retained normal morphology and remained distributed throughout the constructs including the core for 5 weeks. This spirally assembled constructs was used as a ligament models after incorporation of hydroxyapatite granules at either end of the spiral. This method was rapid in producing matrix with tissue-like characteristics within minutes, and highly reproducible in providing a matrix with controllable functional mechanical properties which could be implanted directly or after a short culture.

2.9. Collagen/Inorganic Hybrids or Composites as Biomaterials

Composites of collagen and inorganic biomaterials, commonly hydroxyapatite and calcium phosphate, have been developed for potential application in bone regeneration. The incorporation of the inorganic phase was to induce bioactivity and improve the mechanical properties. Hydroxyapatite/collagen composites were synthesised to be used as bone graft materials (Kikuchi *et al.*, 2001, , Itoh *et al.*, 2002 b, Rodrigues *et al.*, 2003, Kikuchi *et al.*, 2004) or as delivery devices for rhBMP-2 (Itoh *et al.*, 2001a) or β (NGF β) nerve growth factor (Letic-Gavrilovic *et al.*, 2003). The authors showed that these composites, having a nanostructure similar to natural bone, were biocompatible and suitable as bone substitutes.

Collagen-brushite and collagen octa-calcium phosphate were also developed by Jayaraman and Subramanian (2002), and the mineral counterparts were grown onto

collagen by crystal growth to produce a composite for potential application as a bone substitute.

Pederson *et al.* (2003) combined thermally triggered liposome mineralization with a collagen gel formation in an attempt to develop a novel injectable mineral/collagen biomaterial. This used the self assembly principle of collagen at physiological temperatures. Also, these liposomes encapsulated aqueous solute of Ca^{2+} and P that released at the lipid melting transition which was adjusted between 24 and 37 °C. The released Ca^{2+} and P reacted together to form poorly crystalline calcium phosphate minerals; see Figure 2.5.

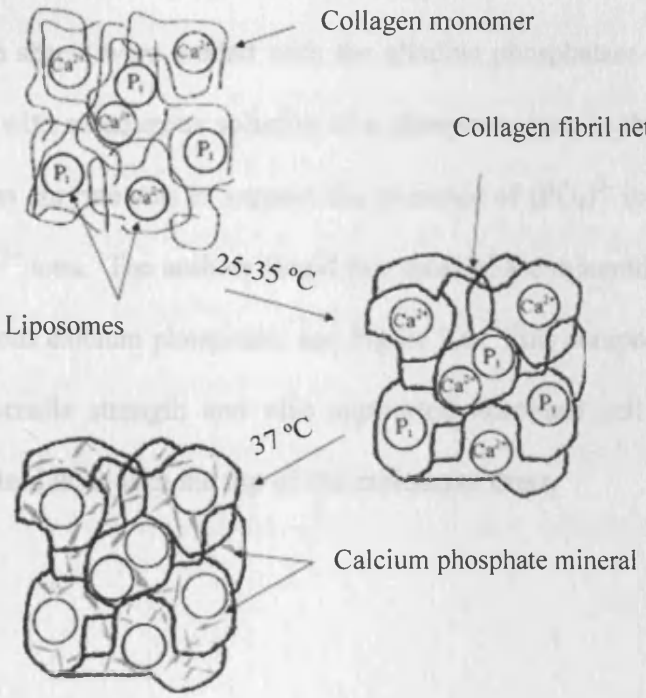

Figure 2.5: Schematic illustration of collagen/mineral composite formation resulting from thermally triggered self assembly of collagen fibrils and liposomal mineralization (Pederson *et al.*, 2003).

The formed mineral phases were highly pH dependant, for example, acidic pH favoured brushite formation; whilst neutral or basic pH favoured the formation of poorly crystalline hydroxyapatite. Collagen was used as a template for liposomal mineralisation, and the authors adjusted collagen concentration so that gelation of collagen occurred before mineral formation. The results suggested that in situ liposomal mineralisation of collagen gels may provide a route for formation of mineral/collagen composite biomaterials with significant interactions between the mineral and collagen phases.

Yamauchi *et al.*, 2004 developed a multilayer composite sheet consisting of alternate layers of both collagen and calcium phosphates on the micrometer scale (6-8 μm each layer thickness) was prepared by an enzymatic mineralisation process. In this method, collagen sheets were loaded with the alkaline phosphatase enzyme and allowed to be in contact with an aqueous solution of a phosphate ester in the presence of Ca^{2+} ions. The use of an enzyme was to support the presence of $(PO_4)^{3-}$ ions to form calcium phosphate with Ca^{2+} ions. The authors found that most of the mineralised phase was HA with some amorphous calcium phosphate; see Figure 2.6. This composite provided an improvement in the tensile strength and also supported fibroblast cell growth especially when the mineralised layer is at the top of the multilayer sheet.

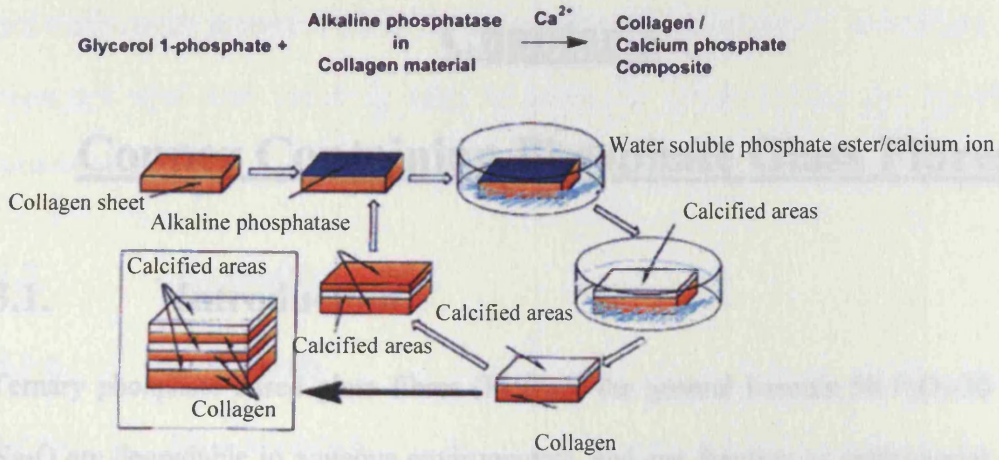

Figure 2.6: Alkaline phosphatase catalyzed mineralization onto a collagen material (Yamauchi *et al.*, 2004).

The aim of this project was to develop three-dimensional (3-D) constructs of phosphate-based glass fibres (PGF) incorporated dense collagen matrices for biomedical and tissue engineering applications. For this, a novel method of "plastic compression" (PC) was used which rapidly removes fluid from hyper-hydrated collagen gels through the application of unconfined compressive load. The project objectives were: the understanding of structure-property relationship of PGF; the understanding of the mechanisms of PC to produce dense collagenous matrices, and the application of PC to produce cellular 3-D constructs of PGF reinforced collagen matrices.

Chapter 3

Copper Containing Phosphate Glass Fibres

3.1. Introduction

Ternary phosphate-based glass fibres (PGF) of the general formula 50 P_2O_5-30 CaO-20 Na_2O are degradable in aqueous environments, and can function as antibacterial delivery systems via the inclusion of ions such as copper. As a result copper oxide (CuO) containing PGF were developed for their potential use in wound healing applications. The glass system developed was a quaternary 50 P_2O_5-30 CaO-(20-x) Na_2O-x CuO glass system where x is either 1, 5 or 10 mol % as given in Table 3.1.

Table 3.1: Glass codes and composition of glasses investigated.

Glass code	P_2O_5 content (mol %)	CaO content (mol %)	Na_2O content (mol %)	CuO content (mol %)
0 mol % CuO	50	30	20	0
1 mol % CuO	50	30	19	1
5 mol % CuO	50	30	15	5
10 mol % CuO	50	30	10	10

These glasses were produced by partial substitution of sodium oxide (Na_2O) in the ternary system with CuO. This substitution was carried out on a molar % basis rather than on weight % to study the effect of substituting one network modifying oxide with another (Wallace *et al.*, 1999). The effects of adding CuO on the thermal, structural, degradation

and antibacterial properties of PGF were investigated in this chapter. In addition, the fibre diameters were also varied in order to assess the effect of fibre size on the above mentioned properties.

3.2. Experimental

3.2.1. Materials

3.2.1.1. Raw Materials

3.2.1.1.1. Chemical Equations and Compositional Calculations

The precursors used in the preparation of this glass system are given in Table 3.2.

Table 3.2: Raw materials used in glass preparation.

Raw materials	**Supplier**
Sodium di-hydrogen orthophosphate anhydrous (NaH_2PO_4)	BDH, UK
Calcium carbonate ($CaCO_3$)	BDH, UK
Di-phosphorus pentoxide (P_2O_5)	BDH, UK
Copper sulphate ($CuSO_4$)	BDH, UK

The amounts of precursors required for the compositions investigated were calculated as follows:

Using NaH_2PO_4 to give Na_2O

	$2\,NaH_2PO_4$	$\rightarrow$ Na_2O +	P_2O_5 +	$2H_2O$
Molecular weight ($g.mol^{-1}$)	240	62	142	36
Relative molecular weight ($g.mol^{-1}$)		0.258	0.592	0.150

To obtain a glass composition containing 0.20 Na_2O, the required amount of NaH_2PO_4 would be $\left(\frac{0.20\times 62}{0.258}\right) = 48$ g. However, the breakdown of NaH_2PO_4 also produces P_2O_5 as one of its breakdown products. So to account for this, $(48\times 0.592) = 28.42$ g of P_2O_5 would also be present. This amount of P_2O_5 would then be subtracted from the required amount of P_2O_5. If the glass composition contained 0.50 P_2O_5, the required amount of P_2O_5 would equal to $(0.50\times 142) = 71$ g. Then, the amount of P_2O_5 to be added would be $(71 - 28.42) = 42.58$ g. Therefore, determination of the amount of P_2O_5 required should be considered after having calculated the amount of NaH_2PO_4 required.

Using $CaCO_3$ as a precursor to obtain CaO:

	$CaCO_3$	→	CaO	+	CO_2
Molecular weight ($g.mol^{-1}$)	100		56		44
Relative molecular weight ($g.mol^{-1}$)			0.56		0.44

To obtain a 0.30 CaO composition, the required amount of $CaCO_3$ would be 30 g; this was due to $CaCO_3$ having a molecular weight of 100. The mole fraction of CaO was kept constant for all the glass compositions investigated; therefore the amount of $CaCO_3$ used was the same.

Using $CuSO_4$ to give CuO:

It was unclear to predict the valence state of copper after it has been subjected to very high temperatures, i.e. whether it would be cuprous oxide (Cu_2O) or cupric oxide (CuO) or mixture of the two oxides (Mulligan, 2003). However, it is more likely that the copper would be present at the higher oxidation state due to having melted the glass at high temperature. The calculation for the CuO mol % was considered as follows:

	$CuSO_4$	→	CuO	+	SO_3
Molecular weight ($g.mol^{-1}$)	159.55		80		80
Relative molecular weight ($g.mol^{-1}$)			0.5		0.5

To obtain a 0.05 CuO composition, the required amount of $CuSO_4$ would be would be $\left(\frac{0.05 \times 80}{0.5}\right) = 8$ g. When the calculation was carried out for the amount of Cu in $CuSO_4$ to avoid the different possibilities of the valence state of copper at high temperature, the following was considered:

The molecular weight of Cu is 63.55 $g.mol^{-1}$, and the relative molecular weight of Cu is $\left(\frac{64}{159.55}\right) = 0.4$ $g.mol^{-1}$. Therefore, if the required glass contains 0.05 Cu, the required amount of $CuSO_4$ would be $\left(\frac{0.05 \times 64}{0.4}\right) = 8$ g. From these calculations, it was observed the same amount of $CuSO_4$ will be required to provide the same mol % of either Cu or CuO.

3.2.1.2. Methods of Preparation

3.2.1.2.1. Bulk Glass Preparation

The precursors used for the preparation of these phosphate-based glasses were weighed and thoroughly mixed, after which they were placed into a platinum/10 % rhodium (Pt/10 % Rh) crucible (Type 71040, Johnson Matthey, UK). The crucible was placed into a preheated furnace (Carbolite, model RHF 1500, UK) at 300 °C to allow for the removal of H_2O, CO_2, and SO_3 evolution, and to avoid excessive foaming of the glass melt. The glass was left at this temperature for 1 h, and then the temperature was increased by 200 $°C.h^{-1}$, until it reached the melting temperature of 1100 °C, and left for a further 1 h. Upon

removal of the crucible from the furnace, the melted glass was poured onto a stainless steel plate and left to cool to room temperature. Once cooled, the glass was placed into a sealed plastic bag and stored in a desiccator at room temperature.

3.2.1.2.2. Glass Fibre Production

Glass fibres were produced using a fibre drawing method from a custom built fibre-rig. The fibre-rig consisted of a top loading furnace (Lenton Furnace, UK) with a Pt/10 % Rh crucible containing a 15 mm long tip with a 1 mm diameter hole. Below the furnace, there was a pick up wheel (drum) connected to a servo motor which controlled the speed of fibre pulling as shown in Figure 3.1.

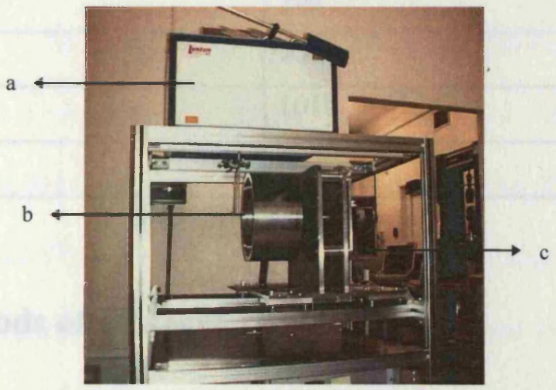

Figure 3.1: Fibre drawing machine (a) Lenton furnace, (b) drum and (c) motor.

The furnace temperature was adjusted to 1250 °C at a heating rate of 30 °C.min^{-1}. Once this temperature was reached, the glass was placed into the furnace crucible and left for 15 min to melt and homogenise. Once a meniscus of glass appeared at the bushing tip, the temperature was lowered to achieve a suitable viscosity from which the fibre could be drawn. The pulling temperatures were originally established by trial and error until the

glass fibres were obtained; see Table 3.3. An alumina rod was used to capture the melted glass and draw it onto the drum, which proceeded to pull the glass into a single continuous fibre at room temperature in an open air environment. The drum speed was changed to produce fibres with different diameters. The fibres were pulled at four different speeds of 400, 800, 1200 and 1600 $m.min^{-1}$ for each glass composition. Once pulled, the fibre bundles were stored in sealed plastic bags, and placed into a desiccator at room temperature.

Table 3.3: Melt temperatures used for pulling fibres for different copper containing glass compositions.

Glass composition	Melt temperature (°C)
0 mol % CuO	960
1 mol % CuO	980
5 mol % CuO	1010
10 mol % CuO	1020

3.2.2. Methods of Characterisation

3.2.2.1. Bulk Glass

3.2.2.1.1. Density Measurements

Density measurements were conducted on triplicate samples using Archimedes' Principle, on an analytical balance (Mettler Toledo, UK) with an attached density kit. Due to the soluble nature of the glass compositions investigated, ethanol was used as the submersion liquid for these measurements. The density kit was assembled onto the balance, and the

weight measurements of the samples in air, and submerged in ethanol were taken to calculate the density (ρ) using equation (3.1).

$$\rho = \left(\frac{M_{dry}}{M_{dry} - M_{wet}} \right) x \rho_{liquid} \quad (3.1)$$

Where: M_{dry} and M_{wet} are the masses of sample in air and liquid respectively, and ρ_{liquid} is density of ethanol at room temperature.

3.2.2.1.2. X-Ray Diffraction Analysis

This study was conducted in collaboration with Dr. I. Ahmed (Biomaterials and Tissue Engineering Division, UCL Eastman Dental Institute) to identify the crystalline phases present in the glass. The glass compositions were crystallised at the crystallisation temperatures obtained through the differential thermal analysis (section 3.2.2.2.2). The data was collected on a Phillips PW1780 Powder Diffractometer (Phillips, Holland) in flat plate geometry, using Ni filtered Cu Kα radiation. Data was collected from 10 to 100° 2 θ with a step size of 0.02° and a count time of 12 s. The phases were identified using the Crystallographica Search-Match (CSM) software (Oxford Cryosystems, UK) and the International Centre for Diffraction Data (ICDD) database (vols. 1-42).

3.2.2.2. Glass Fibres

3.2.2.2.1. Fibre Diameter Measurements

These measurements were carried out to identify the relationship between the drum pulling speed and fibre diameter. A bundle of fibres from each pulling speed was placed into a polytetrafluroethylene (PTFE) mould and embedded in an epoxy resin (Struers,

UK). The resin was left at room temperature to polymerise for 24 h, and the samples were removed from the mould. The samples were then subjected to a series of grinding and polishing steps using a Struers Rotopol-11 (Struers, UK). The polished samples were then observed under a light microscope that was attached to a Cool Snap Digital Image Analysis system (ISS Group Ltd, UK). The mean diameter of the fibres was calculated from measurements on 50 fibres. Image analysis software (Image Pro-Plus) was used to measure the diameter.

3.2.2.2.2. Determination of Thermal Properties

Differential scanning calorimetry (DSC) and differential thermal analysis (DTA) were used to obtain information about the thermal properties including glass transition (T_g), melting temperature (T_m), and crystallisation temperature (T_c) of glass fibres and bulk glass as a control.

a) Differential Scanning Calorimetry

I. Technique

The DSC was used for detection of T_g. It measures heat flow into or from a sample as it is heated, cooled or held under isothermal conditions to keep the specimen temperature exactly the same as the reference material. The temperatures of the sample and reference are controlled independently using separate, identical furnaces, and they are made identical by varying the power input to the two furnaces. The energy required to do this is a measure of the enthalpy or heat capacity changes in the sample relative to the reference; see Figure 3.2.

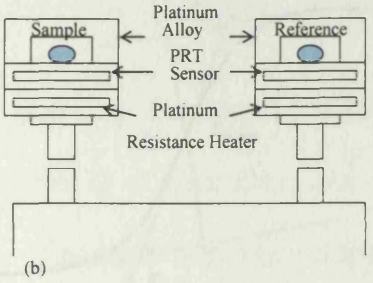

Figure 3.2: Diagrammatic representation of differential scanning calorimetry.

DSC is typically used in a full cycle of heating and cooling to ensure the validity of the results. This ensures that most events can be confirmed by their inverse signatures i.e., if the event is exothermic during heating, it should be endothermic on cooling, as the reverse process occurs unless they crystallise. DSC measures the true heat flow rather than a temperature differential which allows for more accurate calorimetric determinations. It uses platinum resistance thermometers rather than thermocouples that provides the most accurate and precise measurement of the sample temperature. Moreover, with DSC a small sample size can be applied to get information about the material properties mentioned above.

T_g is the main characteristic transformation temperature of the amorphous phase in non-crystalline or semi-crystalline materials. Glass transition events occur when a hard, solid, amorphous material or component undergoes transformation to a soft, rubbery, liquid phase during their heating. The reverse transformation also occurs during their cooling. The classic T_g is observed as an endothermic stepwise change in the DSC heat flow or heat capacity as shown in Figure 3.3.

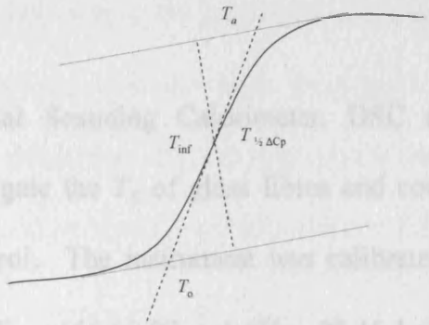

Figure 3.3: Diagrammatic representation of T_g obtained from DSC. T_a is the equivalent value to T_o on the liquid side of the transition, and T_{inf} is the point of inflection. (Richardson, 1976).

T_o can be used to represent T_g, it is normal to use the temperature at which evidence of the transition first appears (i.e. onset temperature, T_o), taken as the intersection between the extrapolated sloping portion and the baseline (Beckett, 1976) or by the temperature at which half the heat capacity increment is reached, $T_{½ \Delta Cp}$ which provides a reasonable and accurate representation of T_g (Richardson, 1976), but there is no reasonable agreement to the correct method.

T_g represents an upper (for a glass) or lower (for a rubber) end use temperature (Richardson, 1976) since it is a measure of the bulk properties; however, other thermal parameters such as T_c and T_m are temperatures for specific phases that may appears out of solutions. T_g is also a useful parameter during the glass fibre annealing process, which may be required to release inherent stresses developed during fibre production. This annealing is sometimes required to decrease the reactivity of the fibres without compromising their strength properties. Therefore, this treatment must be carried out below, and not close to the T_g otherwise a reduction in strength properties giving values close to that of the bulk glass (Choueka *et al.*, 1995).

II. Method

Pyris Diamond Differential Scanning Calorimeter, DSC (Perkin-Elmer Instruments, USA), was used to investigate the T_g of glass fibres and compared to that of the bulk, which was used as a control. The instrument was calibrated using the manufacturer's instructions, with indium (T_m = 156.60 °C and ΔH_f = 28.45 J.g^{-1}) and zinc (T_m = 419.47 °C , and ΔH_f = 108.37 J.g^{-1}) as standards. The following program was established for measuring T_g according to an initial study, which was carried out, and will be described in detail in section 4.2.2.2.2. Samples (n = 3) of 3 mg were heated, cooled and reheated at 100 °C.min^{-1} from 25 to 550 °C. The effect of the modifying oxide content and fibre pulling speed on T_g was investigated. All tests were carried out under nitrogen purge.

b) Differential Thermal Analysis

Differential thermal analysis (DTA) was used as a complementary approach to confirm T_g and to provide a more comprehensive thermal analysis in determining T_c, and T_m since DSC provided a narrow temperature range for glasses, from -50 to 600 °C.

I. Technique

The DTA is a technique based on measuring the temperature difference (ΔT) between sample and reference, heated under identical conditions in a controlled environment, as a function of time or temperature. This measurement is performed via a thermocouple fitted under the crucible containing the sample i.e., near the sample; see Figure 3.4. The thermocouples are not in direct contact with the sample to avoid contamination and degradation. The sample is contained in a small crucible designed with an indentation on the base to ensure a snug fit over the thermocouple. The main difference between DSC

and DTA is that DSC always keeps the specimen and reference at exactly the same temperature, while DTA always uses the same heat input rate to the two items and measures their temperature difference. DTA is also used to detect phase transitions during heating only and usually at a slow heating rate compared to DSC.

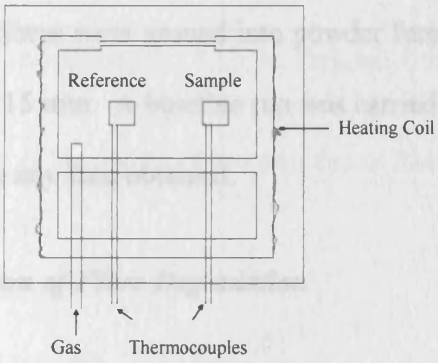

Figure 3.4: Diagrammatic representation of DTA.

Three types of transformations can be distinguished from a DTA data; T_g, endothermic transformation such as melting, and exothermic transformation such as crystallisation. T_g is obtained via the intersection of the curve and the centre line between the two base lines. While the melting and crystallisation temperatures are measured at the onset temperature for pure crystalline substances; however, for semi-crystalline substances such as polymers, it is measured at the peak top as shown in Figure 3.5.

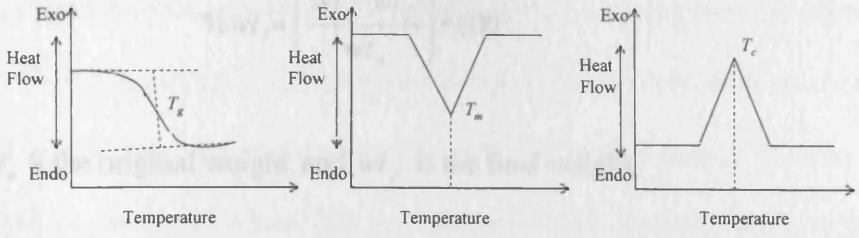

Figure 3.5: Diagrammatic representation of T_g, exothermic, and endothermic peaks as measured by DTA.

II. Method

Setaram Differential Thermal Analyser, DTA (Setaram, France) was used to determine T_g, T_c, and T_m. A heating rate of 20 °C.min^{-1} from 20 to 1000 °C was carried out under nitrogen purge. Two repeats of powdered samples (58 ± 2 mg) were used for each test. Both bulk glass and glass fibres were ground into powder form in an agate vibratory mill (Analysette 3, Spartan) for 15 min. A baseline run was carried out with an empty crucible and this was used to correct any data obtained.

3.2.2.2.3. Determination of Fibre Degradation

a) Long Term Degradation Study

The fibre degradation rates in deionised water at 37 ± 1 °C were obtained using a weight loss method. A glass fibre bundle of approximately 300 mg, with a length of 35 mm were placed into 13 ml of deionised water. The measurement was carried out in triplicate. At various time points, the medium was removed and the glass bottles were placed in an incubator at 37 °C for 24 h to dry before the final weight was recorded. The weight loss was plotted as percentage weight loss against time. The % weight loss ($\%wt_l$) was calculated using equation (3.2).

$$\%wt_l = \left(\frac{wt_o - wt_f}{wt_o} \right) * 100 \qquad (3.2)$$

Where: wt_o is the original weight, and wt_f is the final weight.

a) Short Term Degradation Study

A degradation study up to 6 h was conducted on three repeats of two of the glass fibres pulled at two speeds, 400 and 1200 m.min^{-1}. The degradation rate, expressed in % weight loss.h^{-1}, was taken from slope of % weight loss against time.

3.2.2.2.4. Determination of Surface Area to Volume Ratio of the Glass Fibres

The total surface area (*SA*) of the fibres, assuming that a fibre is a perfect cylinder, was calculated from equation (3.3).

$$SA = \left(2\pi r^2 + 2\pi rl\right)\left(\frac{Wt}{\pi r^2 l\rho}\right) \tag{3.3}$$

where: $\left(2\pi r^2 + 2\pi rl\right)$ was the surface area of a single fibre, r was the radius of a fibre, l was the length of a fibre used in the experiment (35 mm), Wt is the weight used in the experiment (300 mg), $Wt/\pi r2l\rho$ gave the number of fibres in a bundle, and ρ was the density of the glass. The total volume of fibres (V) was then calculated from Wt/ρ.

3.2.2.2.5. Ion Chromatography

a) Technique

Ion Chromatography (IC) performs ion analysis using either isocratic or gradient analysis. It consists of a liquid eluent, a high pressure pump, a sample injector, a separator column, a chemical suppressor, and a measurement cell. Before running a sample, the IC is calibrated with a standard solution. By comparing the data obtained from a sample to that obtained from the standard, sample ions can be identified and quantified. The basis of IC

analysis depends on four steps: eluent delivery, separation, detection, and data analysis as shown in Figure 3.6.

The eluent is a liquid that helps to separate the sample ions, and carries the sample through the ion chromatography system. The sample liquid is injected into the eluent stream by an auto-sampler injector. A pump forces both the eluent and sample through a separator column, which is a chemically inert tube packed with an active polymeric resin, where the sample ions are separated; the mode of separation is called ion exchange.

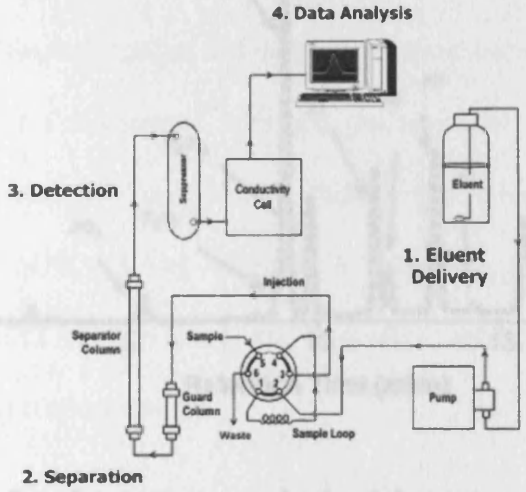

Figure 3.6: Schematic diagram of ion chromatography (from IC manual).

After the eluent and the sample ions leave the column, they flow to the detection cell which could be either conductivity or colorimetric cell. With the conductivity cells, the eluent and sample ions will flow through a suppressor which suppresses the conductivity of the eluent before it enters the detection cell to reduce the background signal and enhance the analyte signal. The detection cell measures either the conductivity or UV absorbance of the sample, and produces a signal based on the chemical and physical

property of the analyte. The detection cell then transmits the signal to the chromatography software (Chromeleon®) that analyses the data by comparing the data obtained from a sample to that of the standard. The sample ions can be identified by its retention time and is quantified by integrating the peak area, for example, for quantification of $(PO_4)^{3-}$, the peak area was considered as shown in Figure 3.7.

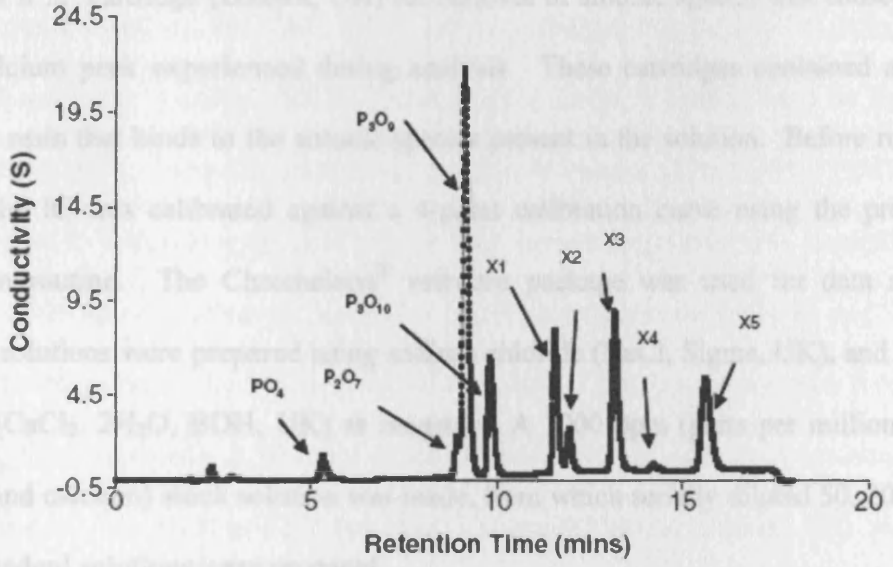

Figure 3.7: Example of a chromatogram obtained for anion release (Ahmed *et al.*, 2005).

b) Method

The post degradation medium after being diluted for fibres pulled at 400 and 1200 $m.min^{-1}$ for all compositions was simultaneously analysed for cations, anions and transition metal as copper, released during the degradation studies, through ion chromatography.

I. Cation Release

The analysis of Na^+ and Ca^{2+} release was carried out using a Dionex ICS-1000 ion chromatography system (Dionex, UK), consisting of a 25-µl sample loop. The separation was performed using a 20 mM MSA (Methanesulfonic acid, BDH, UK) eluent, and a 4x250 mm Ion Pac® CS12A separator column. The solution was first filtered through an 'OnGuard II A' cartridge (Dionex, UK) for removal of anionic species that caused a shift in the calcium peak experienced during analysis. These cartridges contained an anion exchange resin that binds to the anionic species present in the solution. Before running a sample, the IC was calibrated against a 4-point calibration curve using the predefined calibration routine. The Chromeleon® software package was used for data analysis. Standard solutions were prepared using sodium chloride (NaCl, Sigma, UK), and calcium chloride ($CaCl_2$. $2H_2O$, BDH, UK) as reagents. A 1000 ppm (parts per million) mixed (sodium and calcium) stock solution was made, from which serially diluted 50, 20, 10 and 1 ppm standard solutions were prepared.

The following calculations were carried out for preparation of a stock solution of 1000 ppm, taking into account that the relative atomic mass (RAM) of Na = 22.99, Ca = 40.08, and Cl = 35.45 $g.mol^{-1}$. The required mass of NaCl = relative molecular mass (RMM) of NaCl/RAM of Na = $\left(\frac{58.44}{22.99}\right)$ = 2.54 g. The required amount of $CaCl_2.2H_2O$ was calculated in the same way taking into consideration that RMM of $CaCl_2.2H_2O$ = 147 $g.mol^{-1}$. Then the required amounts of the two standards were dissolved in 1000 ml of deionised water in a volumetric flask to give 1000 ppm stock solution. A series of dilutions were carried out to obtain the required ppm standard solutions. For example, to

obtain a 50 ppm standard solution, 5 ml of the stock solution was accurately diluted with deionised water up to 100 ml in a volumetric flask.

II. Copper Ion Release

Transition metals ion release was conducted using a Dionex ICS-2500 ion chromatography system (Dionex, UK), consisting of a 25-µl sample loop. The separation was performed using an Ion Pac® CS5A cation-exchange column with attached CG5A guard column. The MetPac PDCA (Dionex, UK) eluent is readily used as the eluent concentrate to detect transition metals and lanthanide metals. The MetPac PDCA eluent uses pyridine-2, 6-dicarboxylic acid as a strong complexing agent that separates metal complexes via anion exchange, as most complexing agents are anionic and thus the resulting metal complex will have a negative charge. The metals are then detected by measuring the absorbance at 530 nm of the complex formed with the Postcolumn PAR reagent diluent. The MetPac PAR Postcolumn Reagent Diluent (Dionex, UK) uses 4 - 2-pyridylazo resorcinol (PAR) to form a light-absorbing complex, and is added through a mixing tee. The PAR diluent has a controlled pH and reacts with a wide range of metals, and offers detection limits in the low µg/L (ppb) range. The sample run time was set for 10 min. Prior to running the samples, the ICS-2500 was calibrated using cuprous chloride (CuCl, Sigma Aldrich, UK) and cupric chloride ($CuCl_2$, Sigma Aldrich, UK) as standards. A 1000 ppm stock solution incorporating both CuCl and $CuCl_2$ was prepared, from which serially diluted 50, 20, 10 and 1 ppm standard solutions were made. The calculations for the amount of CuCl and $CuCl_2$ standards for the preparation of the stock solution of 1000 ppm were performed after considering that the RAM of Cu = 63.55, Cl = 35.45 $g.mol^{-1}$, and the RMM of CuCl and $CuCl_2$ are 99 and 134.45 $g.mol^{-1}$ respectively.

III. Anion Release

The phosphate anion measurements were undertaken using a Dionex ICS-2500 ion chromatography system (Dionex, UK), consisting of a gradient pump with a 25-µl sample loop. In this method, polyphosphates were eluted using a 4x250 mm Ion Pac® AS16 anion-exchange column. A Dionex Anion Self-Regenerating Suppressor (ASRS®) was used at 223 mA. The Dionex EG40 eluent generator equipped with a potassium hydroxide (KOH) cartridge was used in conjunction with the ASRS®. The newly developed EG40 eluent generator system electrolytically produces high-purity KOH eluent using deionised water as the carrier stream at the point of use. The use of the EG40 hydroxide eluent generator gave negligible baseline shifts during the hydroxide gradients, along with greater retention time reproducibility. The sample run time was set for 20 min where the gradient program initiated from 30 mM KOH for 10 min, then increased from 30 to 60 mM KOH over 5 min, followed by remaining at 60 mM KOH for 3 min, and finally the KOH returned to 30 mM for 2 min. The Chromeleon® software package was used for data analysis. Standard solutions were prepared using sodium phosphate tribasic (Na_3PO_4), trisodium trimetaphosphate ($Na_3P_3O_9$), pentasodium tripolyphosphate ($Na_5P_3O_{10}$) (Sigma-Aldrich, UK) and tetrasodium pyrophosphate ($Na_4P_2O_7.10H_2O$) (BDH, UK). A 1000 ppm working solution containing all of the above 4 reagents was prepared, from which serially diluted 50, 20, 10 and 1 ppm standard solutions were prepared. The structures of the different anionic species investigated using ion chromatography are presented in Figure 3.8.

The following calculations were performed for preparation of stock solution of 1000 ppm, taking into account that the RAM of Na = 22.99, P = 30.97, O = 15.99, and H = 1.01

g.mol^{-1}. The required amount of Na_3PO_4 = RMM of Na_3PO_4/RAM of PO_4 = $\left(\frac{163.90}{94.93}\right)$ = 1.73 g. The calculations for $Na_3P_3O_9$, $Na_5P_3O_{10}$, and $Na_4P_2O_7.10H_2O$ standards were carried in the same way taking into accounts that the RMM of them are 305.79, 367.76, 445.93 g.mol^{-1} respectively, and the RMA of P_3O_9, P_3O_{10}, and P_2O_7 are 236.82, 252.81, and 173.87 g.mol^{-1} respectively.

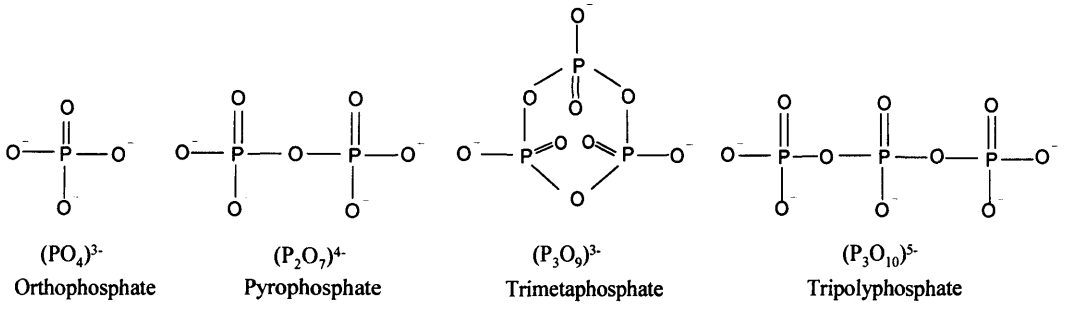

Figure 3.8: Different anion species detected by ion chromatography (Ahmed *et al.*, 2005).

3.2.2.2.6. Antibacterial Assessment

Antibacterial assessment was carried out on the copper containing glass fibres in collaboration with J. Pratten, Division of Microbial Diseases at UCL Eastman Dental Institute, to assess the effect of CuO content and fibre diameter on the number of bacteria adhered to glass fibres or present in the culture solution in which the fibres were placed.

Fibre bundles were produced from pulling speeds of 400 and 1200 m.min^{-1} for all the compositions investigated. Fibres of 30 mm in length and approximately 26 mg in weight were fixed to the lid of a sterile bijou bottle (Sarstedt Ltd, UK) using Araldite (Vantico Ltd, UK). An overnight culture of 5 ml of *Staphylococcus epidermidis* NCTC 11047 was

diluted to 1/1000 in phosphate buffered saline (PBS) (Oxoid, UK) and added to the bottle. In order to ensure the fibres were immersed in the culture solution, the bottle was inverted before being incubated at 37 °C for 3 h. After this time the lid with the attached fibres was removed and placed into a fresh bijou containing 5 ml of PBS and inserted for 5 min. Subsequently, fibres were placed into a third bijou bottle containing 1 ml of PBS and 3 glass beads of 2 mm diameter (Sigma, UK). This was then vortexed for 1 min to disrupt any adhered organisms and colony forming units (CFU) determined on tryptone soya agar plates (Oxoid, UK). Additionally, viable counts were determined for the overnight culture, in which the fibres were originally placed. This experimental procedure was carried out in triplicate for each of the parameters tested.

3.2.2.2.7. Statistical Analysis

One way analysis of variance (ANOVA) was carried out to assess the effect of pulling speeds on the different fibre diameters obtained. The Student's *t*-test was used to study the effect of both copper oxide and fibre diameter on antimicrobial properties. Significance was detected at a 0.05 level, and all statistical analysis was carried out using the SPSS system for Windows (SPSS 12.0.1).

3.3. Results

3.3.1. Bulk Glass

3.3.1.1. Density Measurements

Figure 3.9 shows the density of bulk glass against CuO content. It was observed that the bulk glass density increased linearly with increasing CuO content. The density increased

form 2.58 to 2.71 g.cm^{-3} by incorporation of 10 mol % CuO into the ternary glass formulation.

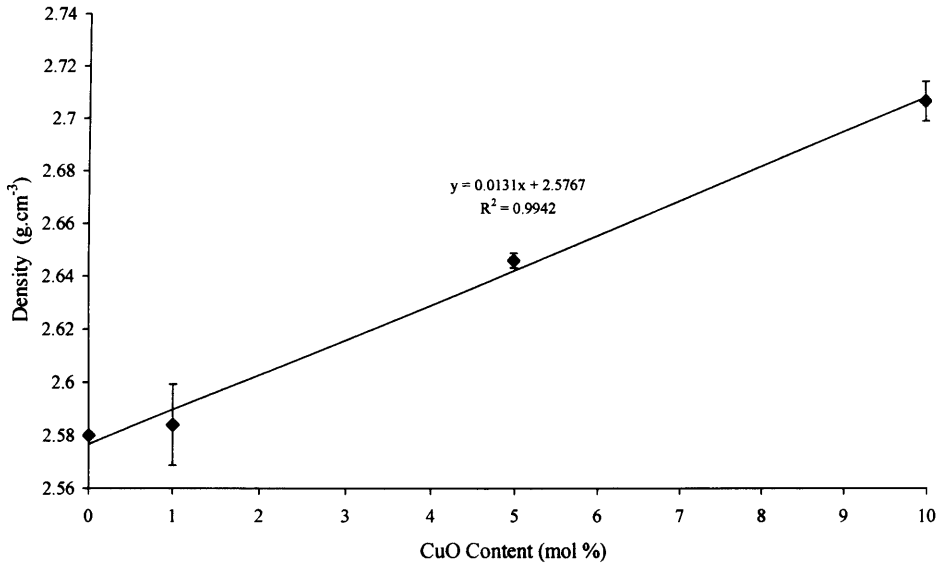

Figure 3.9: Bulk density as a function of copper oxide content.

3.3.1.2. X-Ray Diffraction Analysis

Results from the X-Ray diffraction analysis (XRD) showed that for the 0 mol % CuO glass, a $NaCa(PO_3)_3$ phase (ICDD no. 23-669) was identified using the Search Match software, along with the ICDD database. For the composition with 1 mol % CuO, the same $NaCa(PO_3)_3$ phase was also identified. However, there was also evidence for the presence of a small amount of a secondary phase, but it was not possible to identify this. For the composition containing 5 mol % CuO, two phases were identified, which were $NaCa(PO_3)_3$ (ICDD no. 23-669) and $NaCu(PO_4)$ (ICDD no. 32-1075). For the 10 mol % CuO glass, no direct match could be obtained from the database. Further investigation using Treor, showed a potential tetragonal phase and ICDD, and CSM indicated that this

phase could be isostructural or analogous with an ammonium calcium phosphate phase, $NH_4 Ca (PO_3)_3$.

3.3.2. Glass Fibres

3.3.2.1. Fibre Diameter Measurements

Fibres were pulled from each of the compositions investigated at the four different speeds of 400, 800, 1200, and 1600 $m.min^{-1}$. As expected, it was seen that the fibre diameter decreased with increasing pulling speed as can be seen from Figure 3.10 which shows the light microscope images of glass fibres pulled at 400 and 1600 $m.min^{-1}$ as an example.

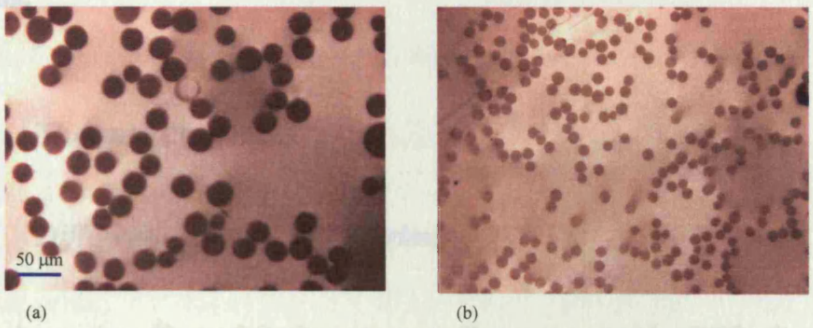

Figure 3.10: Light microscope images of glass fibres embedded in resin and pulled at (a) 400 and (b) 1600 $m.min^{-1}$.

Figure 3.11 shows the variation of the average fibre diameter as a function of the fibre pulling speed for the glass compositions investigated. As can be seen, there was a significant decrease ($p < 0.05$) in fibre diameter with an increase in drum pulling speed. The average fibre diameter for fibres pulled at 400 $m.min^{-1}$ was 32.0 ± 6.0 µm. However, an average of 12.1 ± 1.1 µm was observed for fibres pulled at 1600 $m.min^{-1}$.

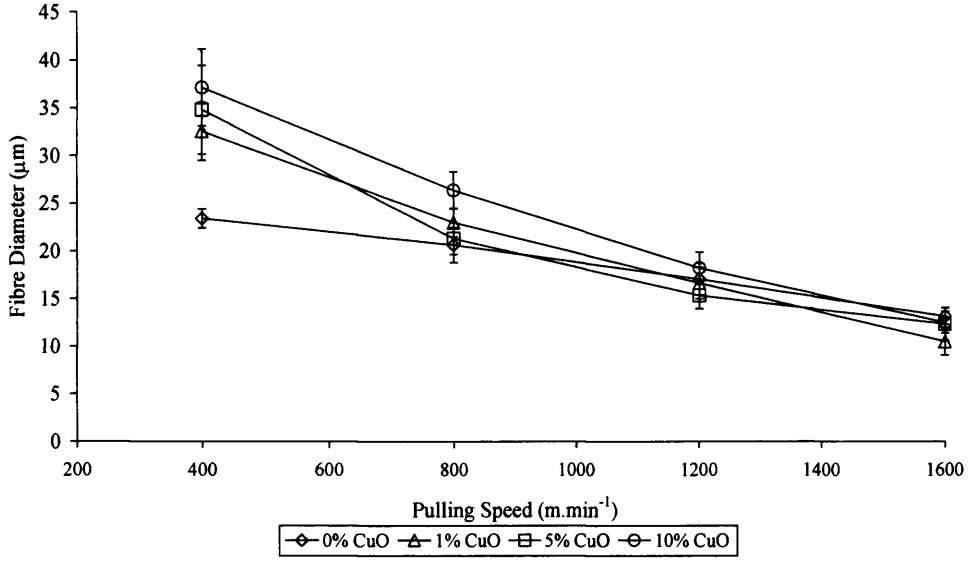

Figure 3.11: Fibre diameter as a function of pulling speed for copper containing compositions.

3.3.2.2. Thermal Properties

3.3.2.2.1. Differential Scanning Calorimetry

Figure 3.12 shows the effect of CuO content on T_g as measured by DSC. It was observed that the T_g of the glass containing 1 mol % CuO, was not significantly different as compared to the ternary (0 mol % CuO) composition. However, with the further addition of CuO to 5 and 10 mol %, the T_g values obtained increased significantly. It was also seen that the fibres pulled at different speeds from the same composition showed no difference in the T_g as given in Table 3.4, also the T_g of fibres were not different from that of the bulk glass that was used as a control.

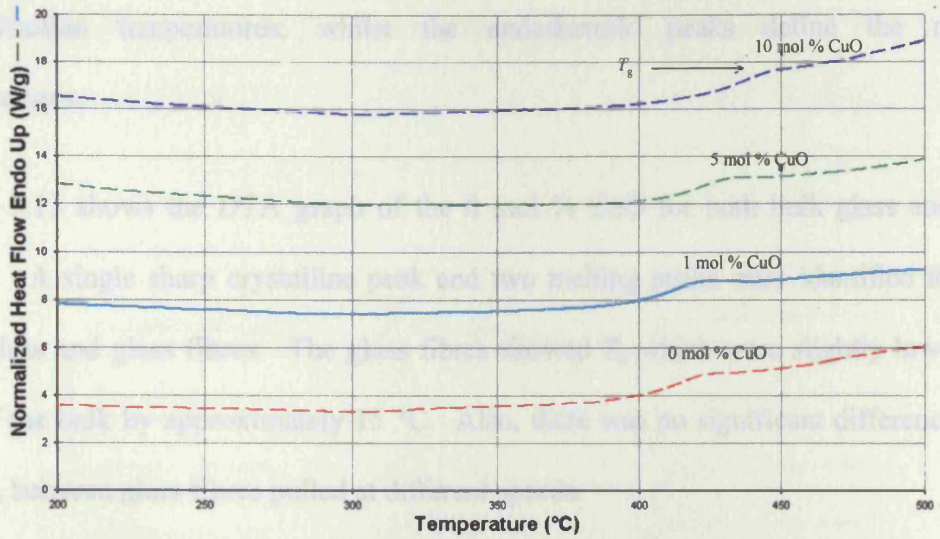

Figure 3.12: DSC trace of glass fibres pulled at 400 m.min^{-1} for the different CuO compositions.

Table 3.4: T_g (°C) of copper containing glasses as measured by DSC.

Pulling speed (m.min^{-1})	0 mol % CuO	1 mol % CuO	5 mol % CuO	10 mol % CuO
Control (bulk glass)	398 ± 1.1	391 ± 0.9	408 ± 1.5	418 ± 1.3
Fibres pulled at 400	399 ± 0.5	401 ± 0.9	407 ± 0.3	423 ± 1.4
Fibres pulled at 800	402 ± 0.6	402 ± 0.7	411 ± 2.7	424 ± 0.7
Fibres pulled at 1200	399 ± 1.9	403 ± 1.5	411 ± 1.0	424 ± 1.2
Fibres pulled at 1600	400 ± 1.5	407 ± 1.1	412 ± 2.6	425 ± 1.5

3.3.2.2.2. Differential Thermal Analysis

DTA was used to study the effect of both CuO content and fibres diameter on T_g, T_c, and T_m. From the DTA graphs obtained, the first observed shift in the base line defines the glass transition temperature, and the upward peaks are exothermic with the downward shifts or peaks being endothermic. The exothermic peaks are attributed to the

crystallisation temperatures, whilst the endothermic peaks define the melting temperatures.

Figure 3.13 shows the DTA graph of the 0 mol % CuO for both bulk glass and glass fibres. A single sharp crystalline peak and two melting peaks were identified for both bulk glass and glass fibres. The glass fibres showed T_c which were slightly lower than that of the bulk by approximately 15 °C. Also, there was no significant difference in T_c and T_m between glass fibres pulled at different speeds.

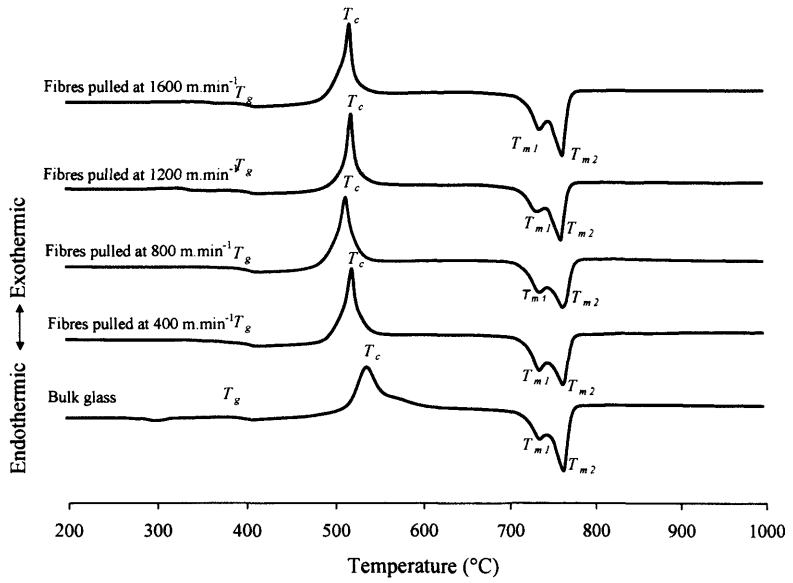

Figure 3.13: DTA graphs of 0 mol % CuO bulk glass and fibres pulled at different speeds.

The addition of CuO to the ternary composition resulted in a change in both the crystallisation peaks and melting peaks. The addition of 1 mol % CuO, shown in Figure 3.14, revealed the presence of a sharp T_c peak with a small shoulder region, and at higher temperatures, two T_m peaks were observed. The same was also observed, but with a small

shoulder appearing first followed by a sharp T_c peak with the addition of 5 mol % CuO composition as in Figure 3.15.

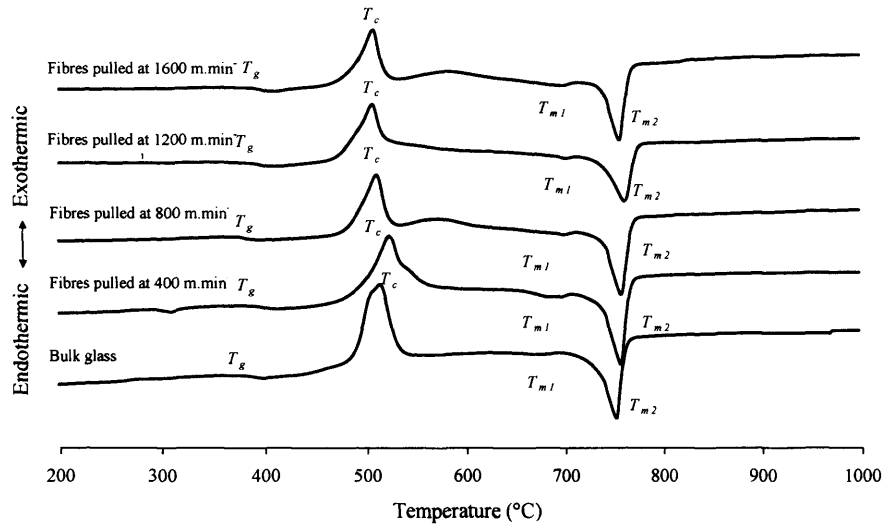

Figure 3.14: DTA graphs for 1 mol % CuO bulk glass and fibres pulled at different speeds.

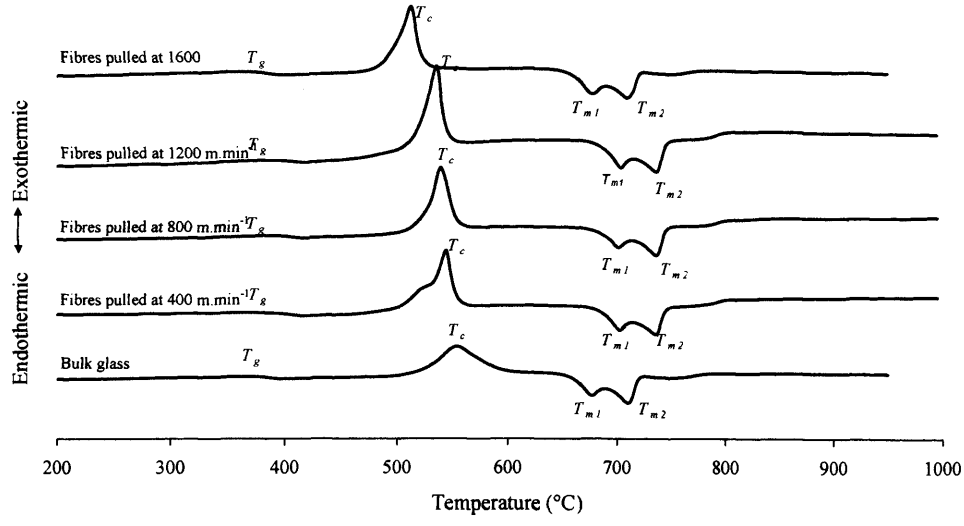

Figure 3.15: DTA graphs for 5 mol % CuO bulk glass and fibres pulled at different speeds.

A single sharp T_c peak was seen for the 10 mol % CuO composition, which was followed by two separate melting peaks as in Figure 3.16. Within each glass composition, similar thermal parameters were observed for the fibres obtained from the different pulling speeds.

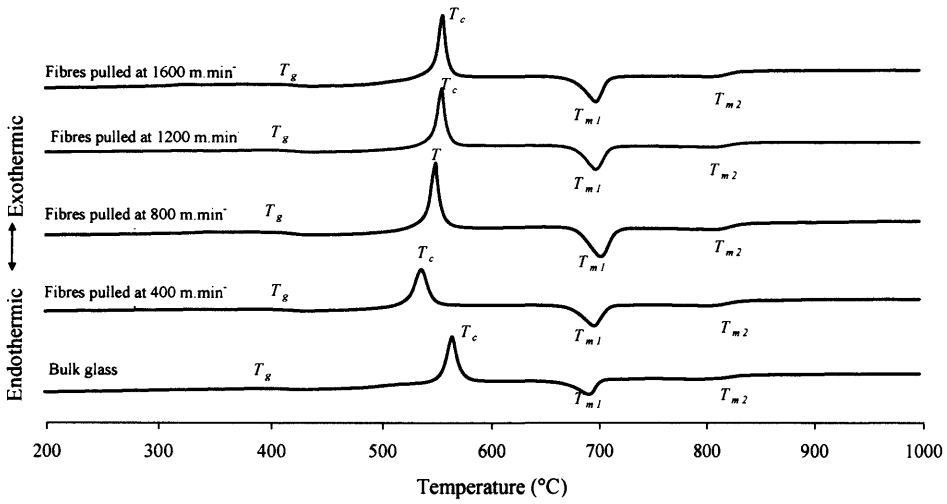

Figure 3.16: DTA graphs for 10 mol % CuO bulk glass and fibres pulled at different speeds.

3.3.2.3. Fibre Degradation

3.3.2.3.1. Long Term Degradation Study

Figure 3.17 shows the effect of both CuO content and fibre pulling speeds on the degradation rate which was presented as % weight loss.h^{-1}. It was apparent that the % weight loss.h^{-1} decreased with increasing CuO content, and with decreasing the pulling speed. Using this method (i.e. changing the drum speed), the lowest degradation rates

were observed for fibres pulled at 400 m.min^{-1} whilst the highest dissolution rates were observed for fibres pulled at 1600 m.min^{-1}.

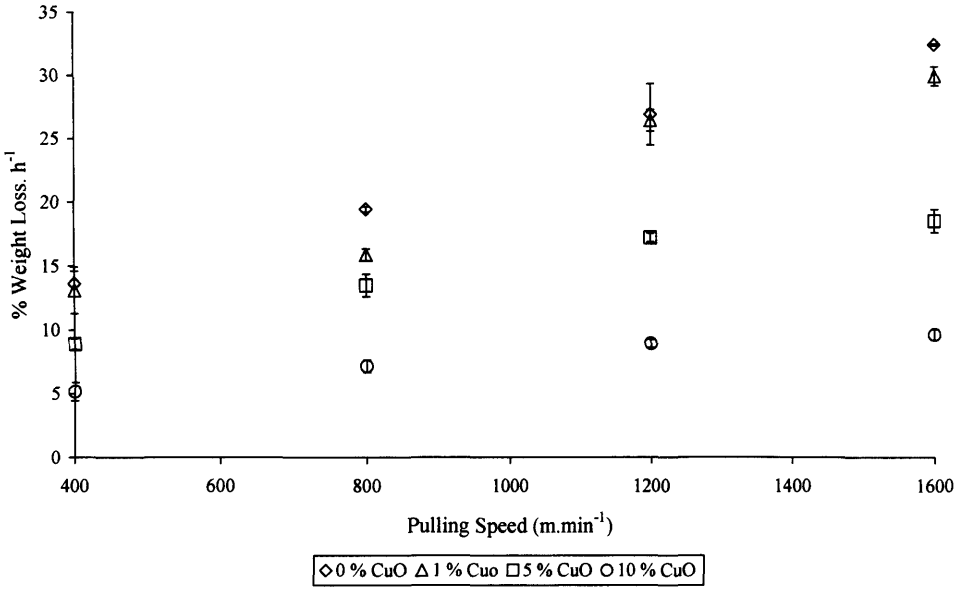

Figure 3.17: Percentage weight loss.h^{-1} as a function of both CuO content and fibre pulling speeds.

It was observed that this glass fibre system was highly degradable, and each glass composition degraded at a different time. For example, the ternary glass with 0 mol % CuO completely degraded within 6 h; however the glass composition with 10 mol % CuO completely degraded within 24 h. Therefore, another short term degradation study was carried out as outlined below to investigate the differences between the compositions and fibre diameter sizes.

3.3.2.3.2. Short Term Degradation Study

Figures 3.18 and 3.19 show the % weight loss against time for fibres pulled at 400 and 1200 m.min^{-1} respectively.

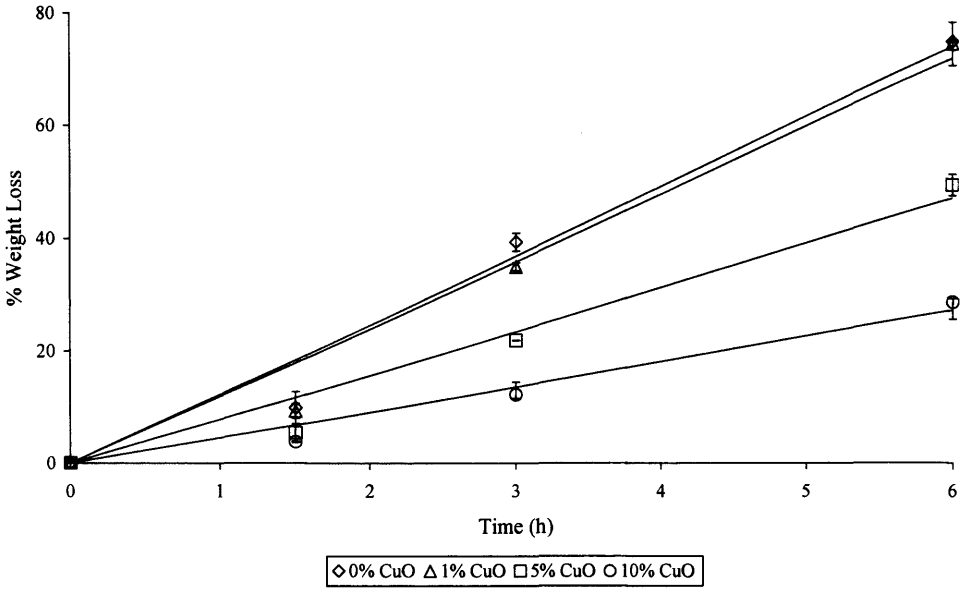

Figure 3.18: Percentage weight loss versus time for fibres pulled at 400 m.min^{-1} for copper containing glass compositions.

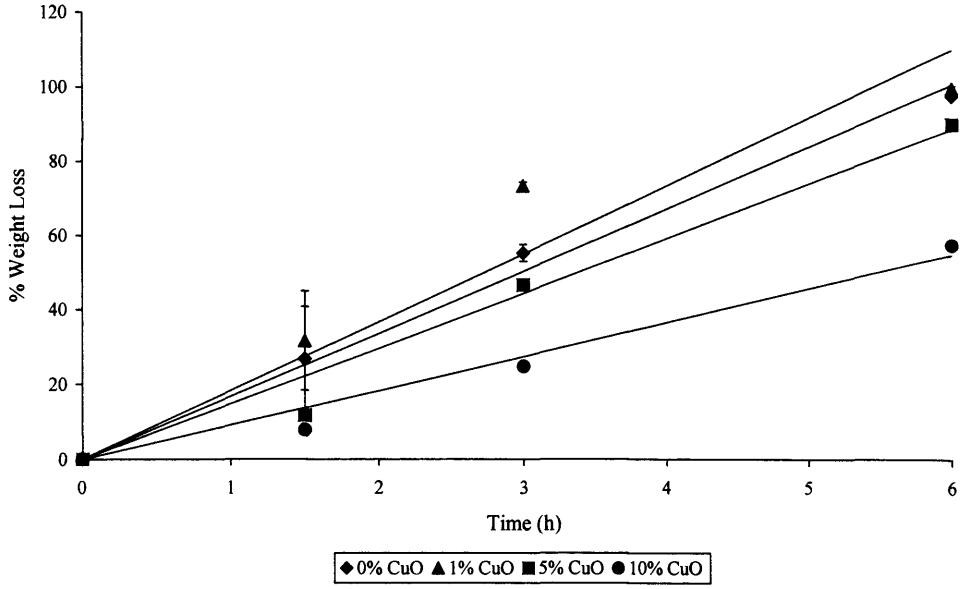

Figure 3.19: Percentage weight loss versus time for fibres pulled at 1200 m.min^{-1} for copper containing glass compositions.

As can be observed the degradation was linear over this time period, and the rate of degradation , calculated from the slope of the % weight loss against time, decreased with

increasing amounts of CuO with the lowest rate obtained for the composition containing 10 mol % CuO. However, 1 mol % CuO showed similar or slightly higher degradation rates than the 0 mol % CuO glass. Also, there was an increase in the rate of degradation with fibres pulled at 1200 $m.min^{-1}$ compared to the fibres pulled at 400 $m.min^{-1}$ as given in Table 3.5.

3.3.2.4. Determination of Surface Area to Volume Ratio of the Glass Fibres

A calculation of fibre surface area to volume ratio was carried out to determine if there was a relationship between this and the high degradation rate obtained for fibres pulled at 1200 $m.min^{-1}$ compared to fibres pulled at 400 $m.min^{-1}$. These values obtained are given in Table 3.5. It was apparent that fibres pulled at 1200 $m.min^{-1}$ showed a surface area to volume ratio that was approximately two fold higher than those for fibres pulled at 400 $m.min^{-1}$.

Table 3.5: Fibre diameters, surface area to volume ratio, and degradation rate of fibres pulled at 400 and 1200 $m.min^{-1}$ for copper containing glass compositions.

Composition (mol %)	Fibre diameter (μm)		Total surface area/ total volume ($x 10^5 m^{-1}$)		Degradation rate (% h^{-1})	
	400 $m.min^{-1}$	1200 $m.min^{-1}$	400 $m.min^{-1}$	1200 $m.min^{-1}$	400 $m.min^{-1}$	1200 $m.min^{-1}$
0 mol % CuO	23.4 ± 0.9	17.1 ± 1.7	1.71	2.34	12.31	16.74
1 mol % CuO	32.6 ± 3.0	16.7 ± 1.6	1.23	2.40	11.96	18.30
5 mol % CuO	34.8 ± 4.7	15.3 ± 1.4	1.15	2.61	7.83	14.75
10 mol % CuO	37.2 ± 4.0	18.2 ± 1.7	1.08	2.19	4.54	9.10

3.3.2.5. Ion Chromatography

3.3.2.5.1. Cation Release

Figures 3.20 and 3.21 show Na^+ release data, and Figures 3.22 and 3.23 show Ca^{2+} release data for glass fibres pulled at 400 and 1200 $m.min^{-1}$ respectively. As it can be seen, the cation release rate, calculated from the slope of the linear fit, showed a similar trend as observed for the degradation rate data. However, the Ca^{2+} release profile showed an identical trend with the weight loss data, where the rate of release for 1 mol % CuO showed a higher release rate than 0 mol % CuO for fibre pulled at 1200 $m.min^{-1}$. Also, both Na^+ and Ca^{2+} released at nearly the same level for both fibre formulations as given in Table 3.6.

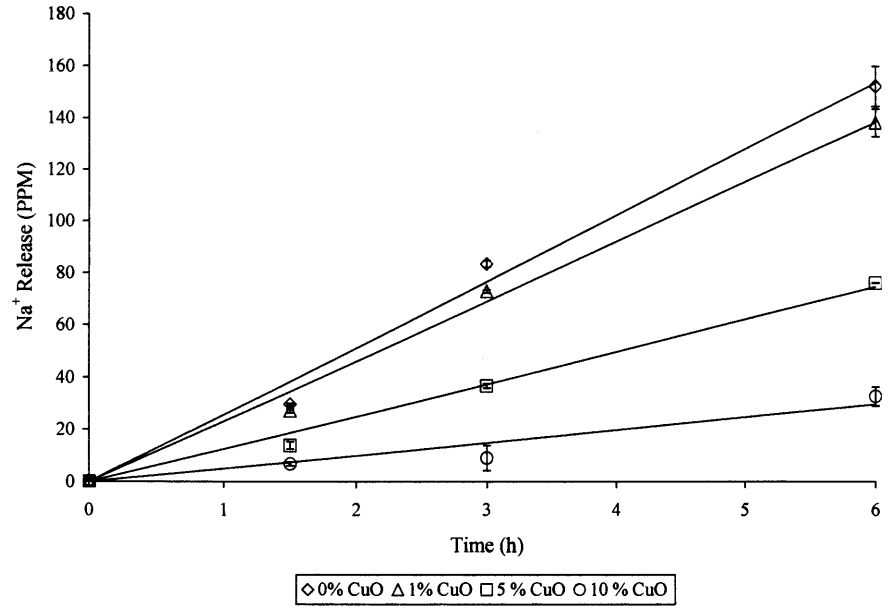

Figure 3.20: Na^+ release for fibres pulled at 400 $m.min^{-1}$ for copper containing glass compositions.

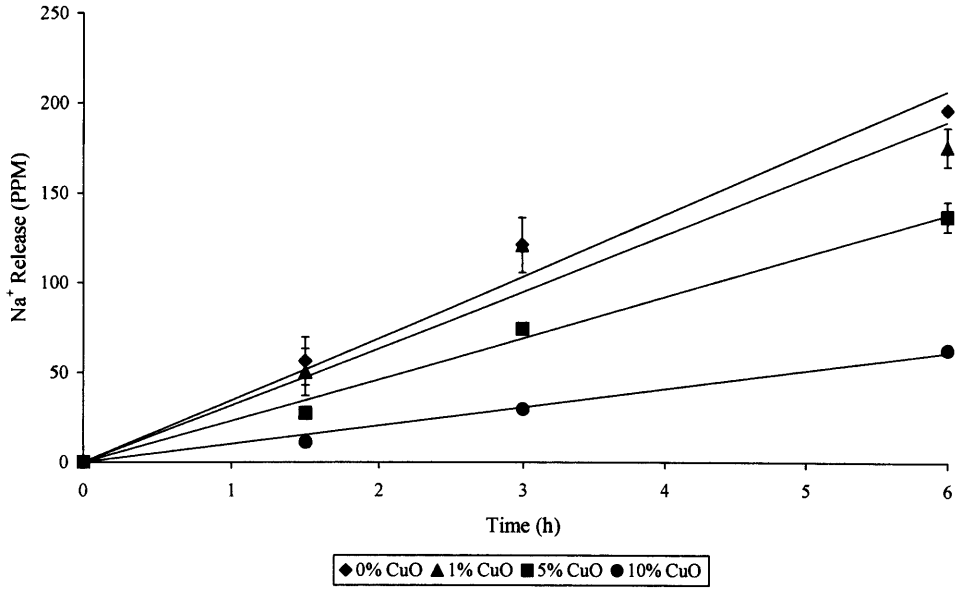

Figure 3.21: Na^+ release for fibres pulled at 1200 $m.min^{-1}$ for copper containing glass compositions.

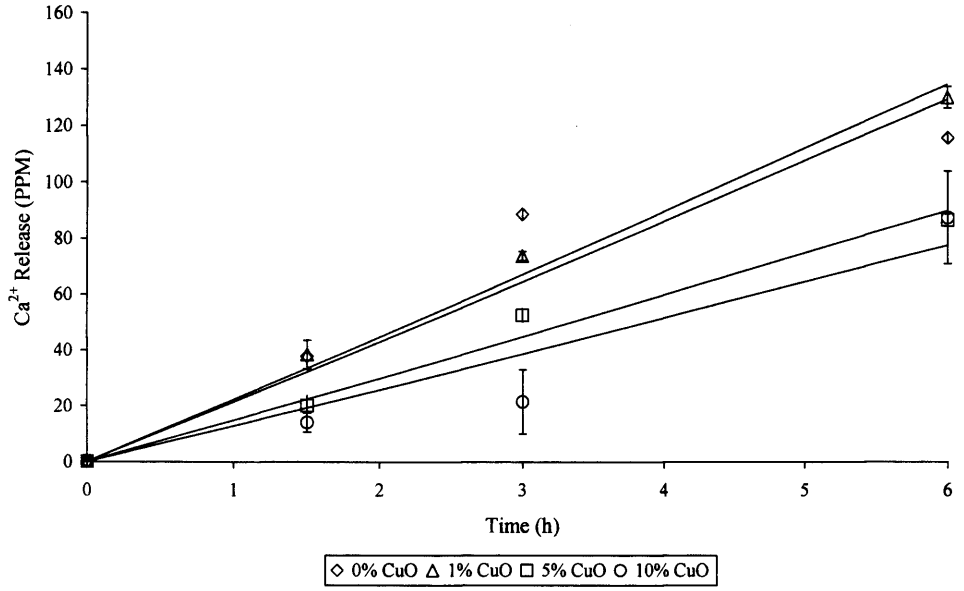

Figure 3.22: Ca^{2+} release for fibres pulled at 400 $m.min^{-1}$ for copper containing glass compositions.

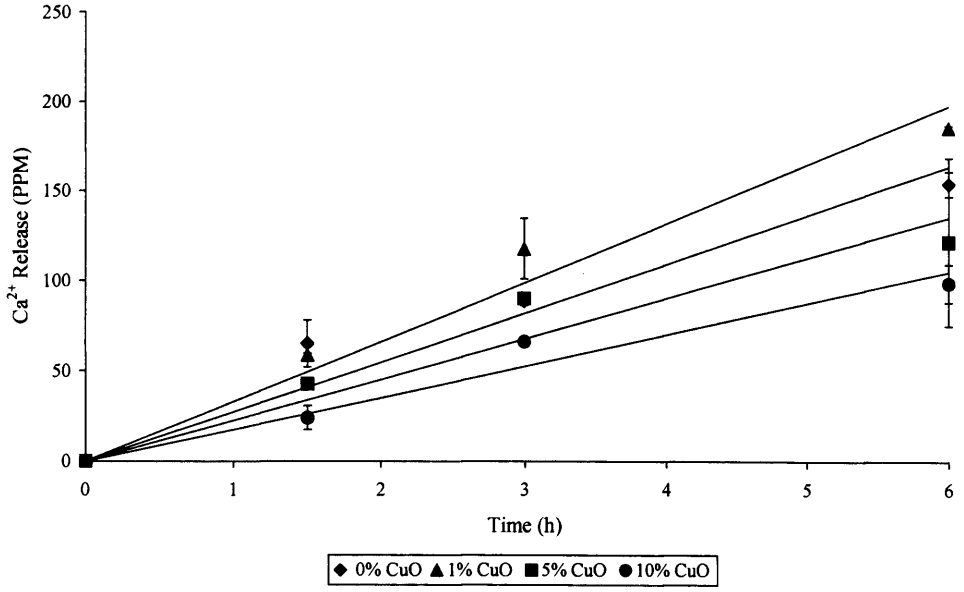

Figure 3.23: Ca^{2+} release for fibres pulled at 1200 $m.min^{-1}$ for copper containing glass compositions.

Table 3.6: Cation release data (ppm.mg^{-1} h^{-1}) of copper containing glass fibres pulled at 400 and 1200 m.min^{-1}.

CuO Content (mol%)	Fibre pulled at 400 m.min^{-1}			Fibre pulled at 1200 m.min^{-1}		
	Na^+	Ca^{2+}	Cu^{2+}	Na^+	Ca^{2+}	Cu^{2+}
0 mol % CuO	0.85	0.72	0	1.15	0.91	0
1 mol % CuO	0.77	0.75	0.06	1.05	1.10	0.12
5 mol % CuO	0.41	0.50	0.17	0.77	0.75	0.31
10 mol % CuO	0.16	0.43	0.22	0.34	0.58	0.44

3.3.2.5.2. Copper Ion Release

Cu^{2+} release data was obtained via ion chromatography and presented in (Figure 3.24 and 3.25) for both the fibre formulations investigated. As can be seen over the first six hours there was zero order release observed of the Cu^{2+} for all compositions containing CuO, as the release was linear with time. The amount of the Cu^{2+} released increased with increasing CuO content, and the rate of release increased with a reduction in fibre diameter as given in Table 3.6. Consequently, the glass fibres containing 10 mol % CuO had the lowest degradation rate, but released the highest levels of Cu^{2+} compared to the other compositions, and those pulled at 1200 m.min^{-1} showed higher release than those pulled at 400 m.min^{-1}.

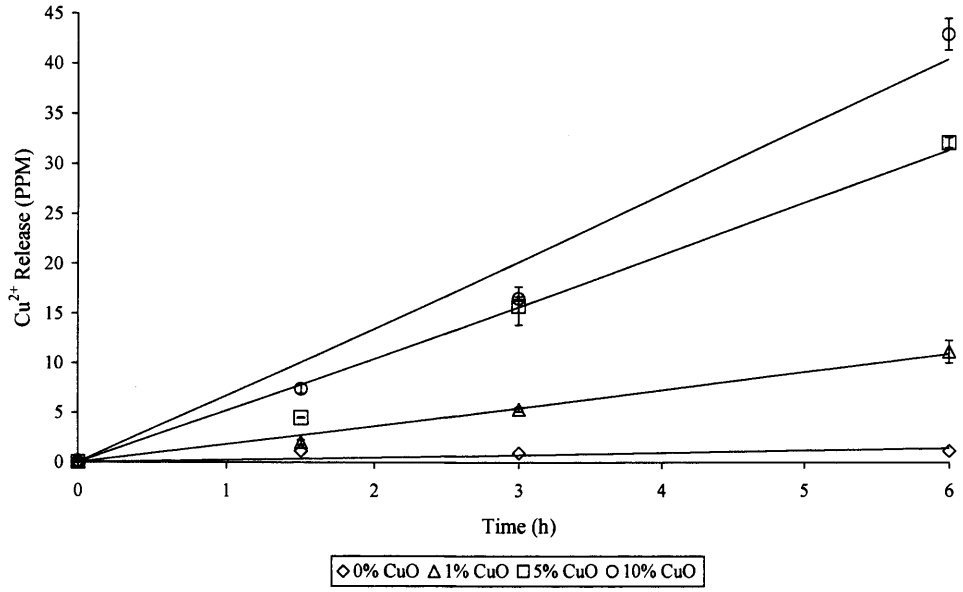

Figure 3.24: Cu^{2+} release for fibres pulled at 400 $m.min^{-1}$ for copper containing glass compositions.

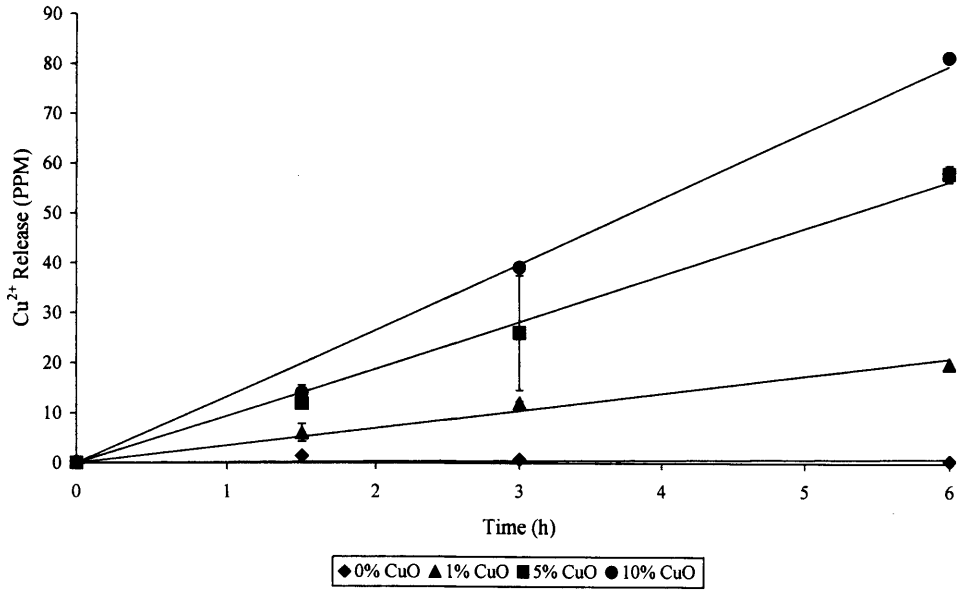

Figure 3.25: Cu^{2+} release for fibres pulled at 1200 $m.min^{-1}$ for copper containing glass compositions.

3.3.2.5.3. Anion Release

Four different anionic species were investigated in the post degradation solution which were; orthophosphate $(PO_4)^{3-}$ (Figures 3.26 and 3.27), pyrophosphate $(P_2O_7)^{4-}$ (Figures 3.28 and 3.29), cyclic trimetaphosphate $(P_3O_9)^{3-}$ (Figures 3.30 and 3.31) , and the linear tripolyphosphate $(P_3O_{10})^{5-}$ (Figures 3.32 and 3.33). The anion release curves showed similar trends to the degradation data where the release rate was higher for fibres pulled at 1200 $m.min^{-1}$ than those pulled at 400 $m.min^{-1}$ for all the anionic species investigated, and both fibre formulations showed identical trends for each anionic species. However, while the $(P_2O_7)^{4-}$, $(P_3O_9)^{3-}$ and $(P_3O_{10})^{5-}$ release decreased with increasing CuO content, there was no definite relationship with the amount of $(PO_4)^{3-}$ released. It was also seen that the cyclic metaphosphate $(P_3O_9)^{3-}$ species released the highest anionic levels in solution compared with the other anionic species. The release rate for $(P_3O_9)^{3-}$ compared well with the degradation rate data, where 1 mol % CuO released higher $(P_3O_9)^{3-}$ than 0 mol % CuO for fibres pulled at 1200 $m.min^{-1}$. The pyrophosphate $(P_2O_7)^{4-}$ species was the lowest released anion from the species investiagted. The results showing the release rate of the different anion species, calculated from the slope of the linear fit, are given in Table 3.7.

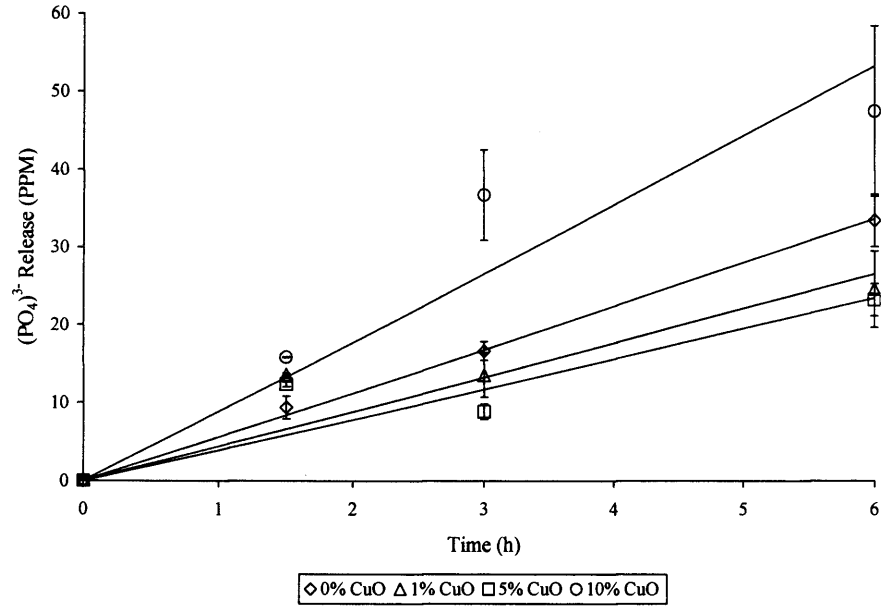

Figure 3.26: $(PO_4)^{3-}$ release from fibres pulled at 400 m.min^{-1} for copper containing glass compositions.

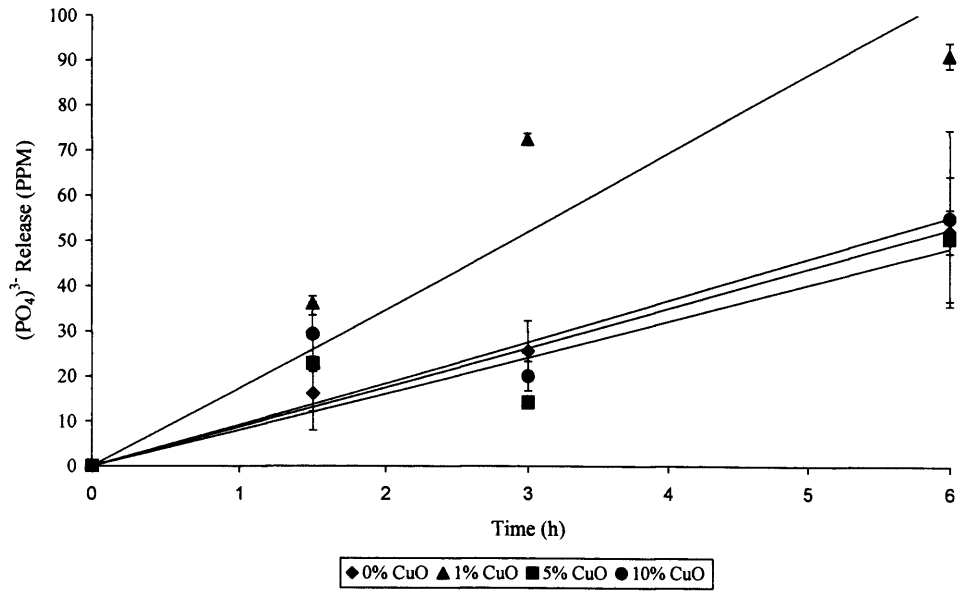

Figure 3.27: $(PO_4)^{3-}$ release from fibres pulled at 1200 m.min^{-1} for copper containing glass compositions.

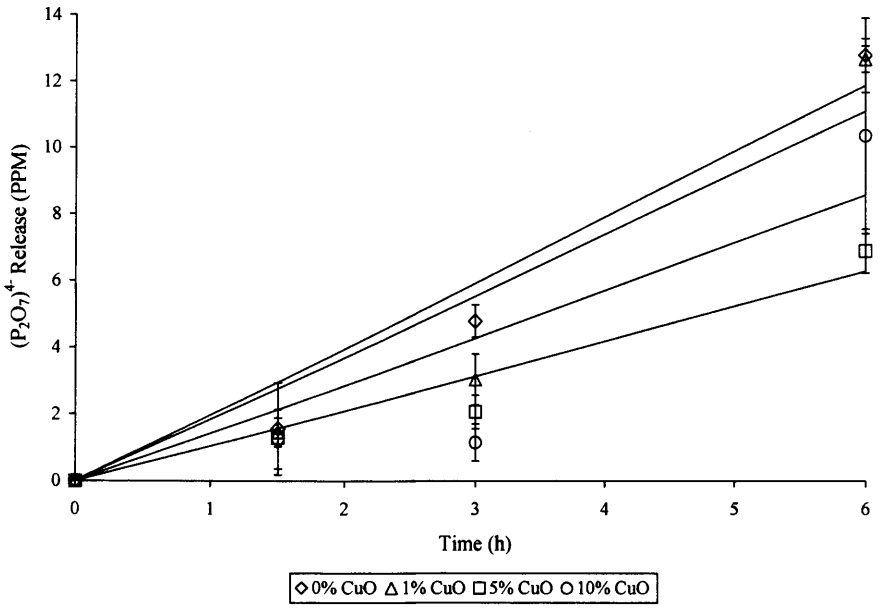

Figure 3.28: $(P_2O_7)^{4-}$ release from fibres pulled at 400 m.min^{-1} for copper containing glass compositions.

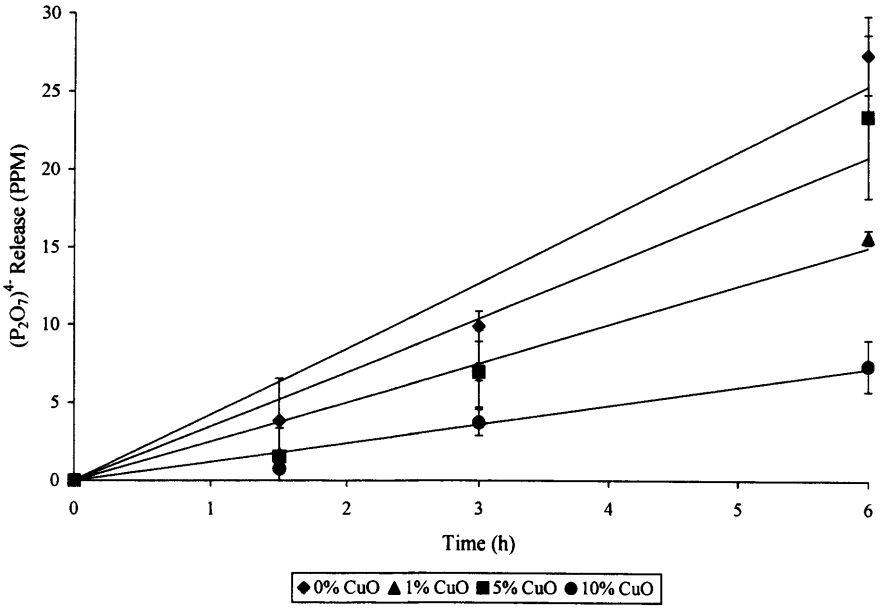

Figure 3.29: $(P_2O_7)^{4-}$ release from fibres pulled at 1200 m.min^{-1} for copper containing glass compositions.

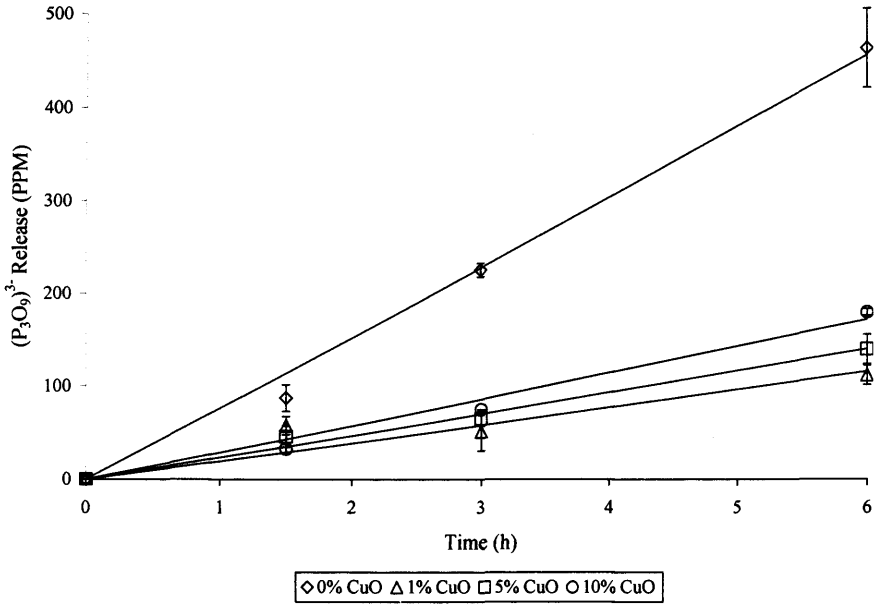

Figure 3.30: $(P_3O_9)^{3-}$ release from fibres pulled at 400 m.min^{-1} for copper containing glass compositions.

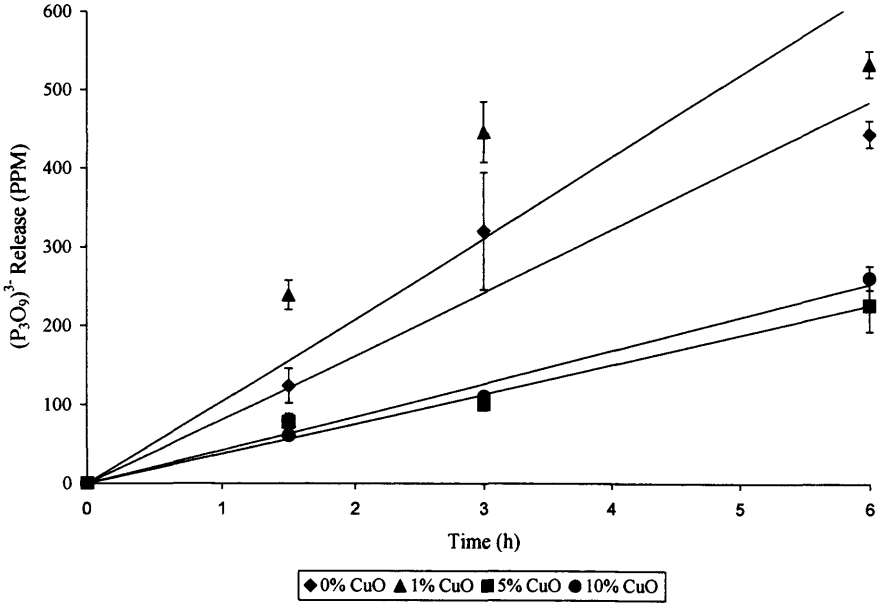

Figure 3.31: $(P_3O_9)^{3-}$ release from fibres pulled at 1200 m.min^{-1} for copper containing glass compositions.

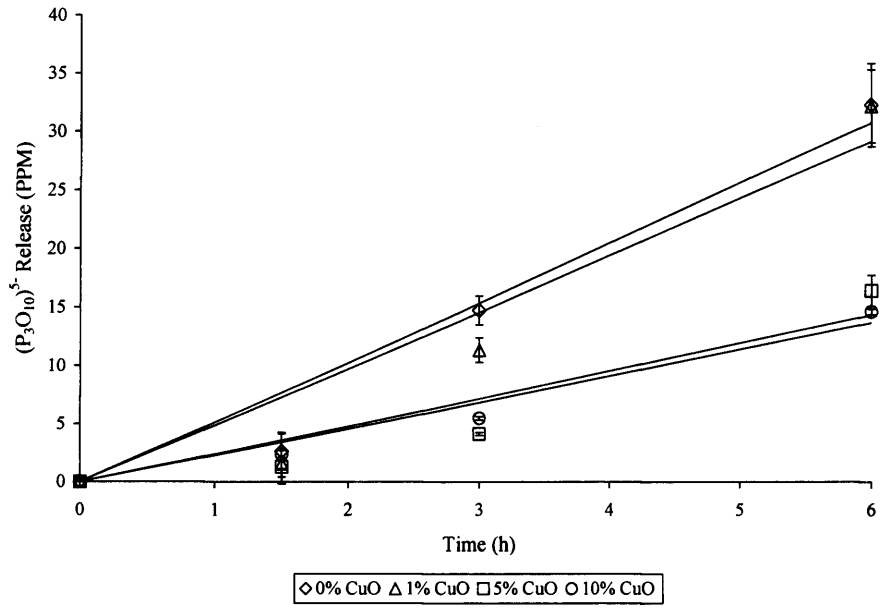

Figure 3.32: $(P_3O_{10})^{5-}$ release from fibres pulled at 400 m.min^{-1} for copper containing glass compositions.

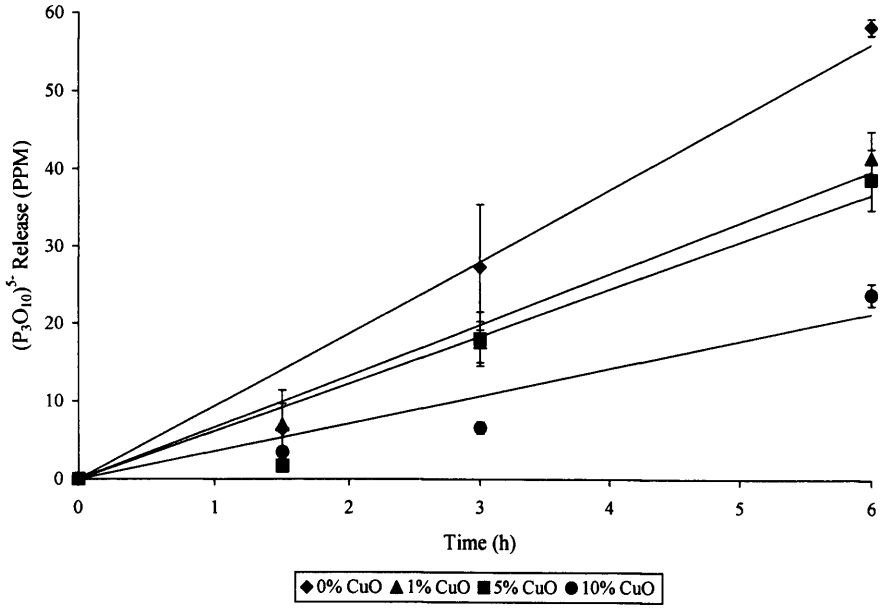

Figure 3.33: $(P_3O_{10})^{5-}$ release from fibres pulled at 1200 m.min^{-1} for copper containing glass compositions.

Table 3.7: Anion release data (ppm.mg^{-1} h^{-1}) of copper containing glass fibres pulled at 400 and 1200 m.min^{-1}.

CuO Content (mol%)	Fibre pulled at 400 m.min^{-1}				Fibre pulled at 1200 m.min^{-1}			
	$(PO_4)^{3-}$	$(P_2O_7)^{4-}$	$(P_3O_9)^{3-}$	$(P_3O_{10})^{5-}$	$(PO_4)^{3-}$	$(P_2O_7)^{4-}$	$(P_3O_9)^{3-}$	$(P_3O_{10})^{5-}$
0 mol % CuO	0.19	0.07	2.5	0.17	0.29	0.14	2.68	0.31
1 mol % CuO	0.15	0.06	0.64	0.16	0.58	0.08	3.45	0.22
5 mol % CuO	0.13	0.03	0.77	0.08	0.27	0.12	1.25	0.20
10 mol % CuO	0.30	0.05	0.95	0.08	0.31	0.04	1.40	0.12

3.3.2.6. Antibacterial Assessment

Viable counts were determined in order to assess the number of CFU adhered to the Cu-containing glass fibres as shown in Figure 3.34. A significantly higher ($p < 0.05$) number of *S. epidermidis* were attached to the control fibres (0 mol % CuO) which had been generated from a pulling speed of 1200 m.min^{-1} compared to 400 m.min^{-1}. However, this trend was not seen with any of the Cu-releasing fibres where there were no significant differences ($p \geq 0.05$) between the numbers of *S. epidermidis* attached to fibres pulled at 400 and 1200 m.min^{-1}. The attachment study showed that fibres containing 1 and 5 mol % CuO achieved greater than a 1 $\log_{10}$ CFU reduction, whilst fibres containing 10 mol % CuO reduced the number of bacteria attached by over 2 $\log_{10}$ CFU.

An average of 7.5 x 10^5 CFU per ml remained in the control inoculum after the removal of the fibres at 3 h as shown in Figure 3.35. There was no significant difference between the fibre diameters ($p \geq 0.05$) for a given composition.

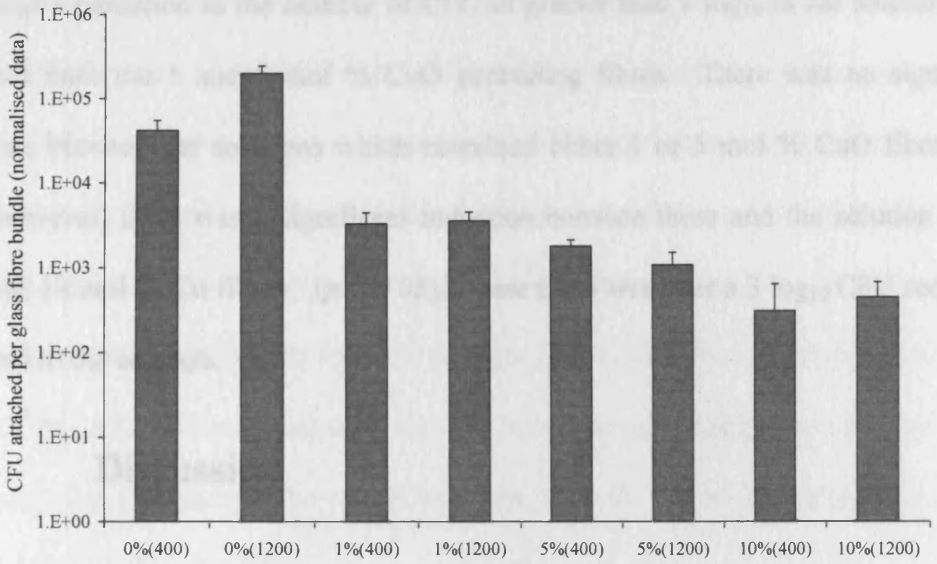

Figure 3.34: Number of attached *S. epidermidis* to glass fibres pulled at 400 and 1200 m.min^{-1} for control and copper containing glass compositions. Error bars represent standard deviations, data normalised to weight of fibres.

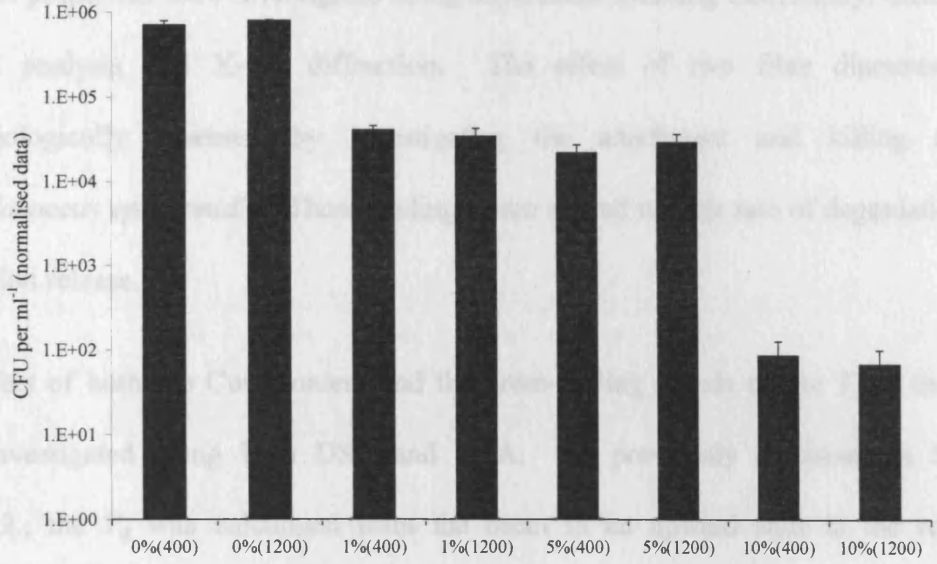

Figure 3.35: Number of viable *S. epidermidis* in solution after contact with control and copper containing glass fibres pulled at 400 and 1200 m.min^{-1}. Error bars represent standard deviations, data normalised to weight of fibres.

There was a reduction in the number of CFU of greater than 1 $\log_{10}$ in the solutions that contained both the 1 and 5 mol % CuO containing fibres. There was no significant difference between the solutions which contained either 1 or 5 mol % CuO fibres ($p \geq 0.05$); however, there was a significant reduction between these and the solution which contained 10 mol % Cu fibres ($p < 0.05$), where there was over a 3 $\log_{10}$ CFU reduction compared to the controls.

3.4. Discussion

In this chapter, CuO containing PGF were developed for potential uses in wound healing applications. These were produced with different diameters and characterised in terms of their structural and antibacterial properties. The effect of CuO and fibre pulling speed on the glass properties were investigated using differential scanning calorimetry, differential thermal analysis and X-ray diffraction. The effect of two fibre diameters was microbiologically assessed by investigating the attachment and killing against *Staphylococcus epidermidis*. These findings were related to their rate of degradation and copper ion release.

The effect of both the CuO content and the drum-pulling speeds on the T_g of the glass were investigated using both DSC and DTA. As previously discussed in Section 3.2.2.2.2., the T_g was calculated from the onset in an upward shift in the resultant thermogram during high speed calorimetry using DSC, while it was taken as the midpoint in the downward shift in the DTA graph. As it can be seen, both techniques showed similar trends in T_g values between 0 and 1 mol % CuO, and there was a significant increase in T_g for the compositions of 5 and 10 mol % CuO ($p < 0.05$) compared to 0 mol % CuO. However, there was no definite trend observed between the T_g of fibres obtained

from the different pulling speeds within each composition as shown in Figure 3.36. It was also observed that the T_g values obtained through DSC compared well to conventional DTA, therefore DSC offered a rapid and accurate technique in measuring the T_g of these glass formulations. Along with reducing the experimental time, DSC also offered the advantage of requiring a much smaller sample weight than that used for DTA (3 mg used for DSC while 58 mg when used for DTA), therefore rapid DSC was useful in assessing the T_g of the utilised small sample sizes. DTA, on the other hand, proved more useful when analysing the thermal properties at above 600 °C due to the temperature range limitation imposed by the DSC.

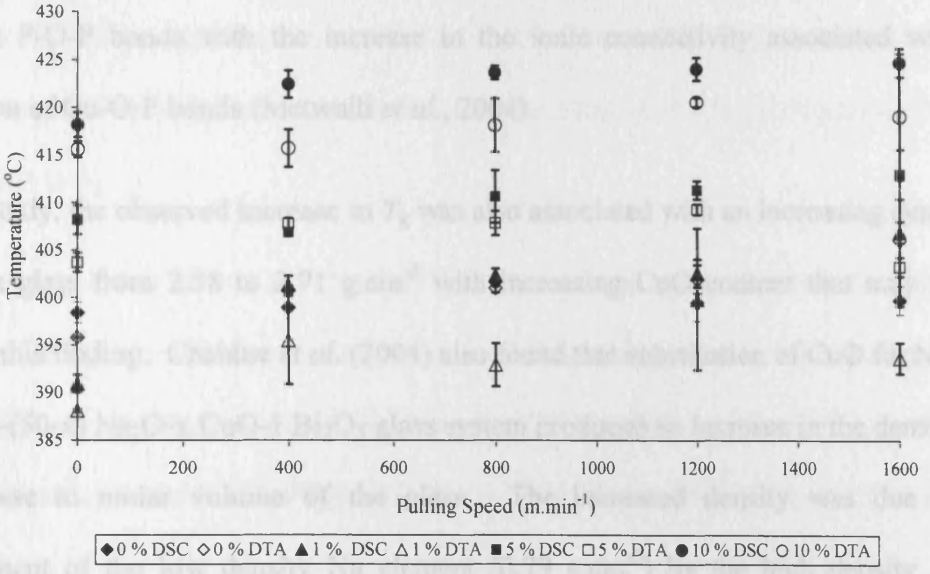

Figure 3.36: Effect of CuO content and pulling speed on glass transition temperature measured through DSC and DTA.

The observed increase in T_g with 5 and 10 mol % CuO could be explained by the findings of Shih *et al.* (1998, 1999) who previously investigated the ternary (40-70) P_2O_5-(0-60) Na_2O-(0-50) CuO glass system and revealed that with increasing CuO content, there was

an increase in T_g accompanied by an increase in hardness and chemical durability of the glasses. The authors also found that in the ultra and metaphosphate glass compositions, Cu-O-P bonds formed at the expense of the Na-O-P bonds while maintaining the P-O-P bond fraction. However, in polyphosphate glasses, the newly formed Cu-O-P bond substituted both Na-O-P and P-O-P bonds. They also stated that a copper cation with high electronegativity would substitute the sodium cation with lower electronegativity. As expected the Cu-O-P bonds increased the cross-link density between the phosphate chains resulting in an increase in the T_g. An increase in density and T_g was also observed for binary copper phosphate glasses in the ultraphosphate composition with increasing CuO content, and this was attributed to the simultaneous increase in the covalent characteristics of short P-O-P bonds with the increase in the ionic connectivity associated with the formation of Cu-O-P bonds (Metwalli *et al.*, 2004).

In this study, the observed increase in T_g was also associated with an increasing density of the bulk glass from 2.58 to 2.71 $g.cm^{-3}$ with increasing CuO content that may further support this finding. Chahine *et al.* (2004) also found that substitution of CuO for Na_2O in 40 P_2O_5-(50-x) Na_2O-x CuO-1 Bi_2O_3 glass system produced an increase in the density and a decrease in molar volume of the glass. The increased density was due to the replacement of the low density Na element (0.79 $g.cm^{-3}$) by the high density copper element (8.92 $g.cm^{-3}$). However, the reduction in molar volume was due to the fact that the Cu^{2+} had a lower relative ionic radius (0.073 nm) than the sum of two Na^+ radii (0.102 nm); therefore, the molar volume of Cu^{2+} (1.63×10^{-3} nm^3) was lower than that of two Na^+ (8.89×10^{-3} nm^3).

The DTA data obtained for the 0 mol % CuO composition showed a single sharp crystalline peak. The presence of a single T_c peak indicated the presence of a single crystalline phase. XRD data obtained confirmed that a single phase, $NaCa(PO_3)_3$ (ICDD no. 23-669), was present for this composition. A similar phase was also identified by Ahmed *et al.* (2004 a, b and c). For the 1 mol % CuO, a sharp T_c peak was seen with an attached small peak present as a small shoulder on the initial peak. However, only a single phase, $NaCa(PO_3)_3$ (ICDD no. 23-669), was identified from XRD analysis. The appearance of a shoulder suggested the presence of a second crystalline phase; however, if present, it could not be identified from XRD analysis. Consequently, there was no copper containing phase identified for this composition which may explain why there was no change in T_g with an addition of 1 mol % CuO. Another possible explanation is that 1 mol % CuO may not be sufficient for producing a cross-linked structure that would account for an increase in T_g.

For the composition with 5 mol % CuO content, a single sharp T_c peak was identified from the DTA graph. This peak also had a small shoulder protruding from it. Again, this was suggestive of the presence of two phases. XRD analysis verified this, and the two phases identified were $NaCa(PO_3)_3$ (ICDD no. 23-669) and $NaCu(PO_4)$ (ICDD no. 32-1075).

For the 10 mol % CuO composition a single sharp T_c peak was seen along with two separate and very distinct melting peaks. However, no match from the ICDD database was found for this composition. It is highly likely that this phase has not been commonly identified. A search of the Chemical Database Service (CDS) using Cu, Na, P and O as limiters gave 8 potential compounds, and a search using Cu, Ca, P and O only gave 5

compounds, none of which matched. However, using Treor to determine the crystalline phase, it was indicated that it could potentially be a tetragonal phase, and using this along with other search limiters, some evidence for the phase being isostructural with an ammonium calcium phosphate was shown.

The chemical durability of the glass fibres was assessed from their rate of degradation in deionised water. The results presented here suggested that there was no difference between the degradation rate of 0 and 1 mol % CuO for fibres pulled at 400 $m.min^{-1}$. However, there was an increase in the degradation rate of 1 mol % CuO relative to the 0 mol % CuO for fibres pulled at 1200 $m.min^{-1}$. This was consistent with the results obtained from thermal analysis, where there was no significant difference in T_g between both compositions. This can be further explained by the structural analysis employed using XRD, where similar phases were identified for both compositions suggesting similarity in properties. On the other hand, the addition of CuO at 5 and 10 mol % significantly reduced the rate of degradation ($p < 0.05$). An increase in the cross-link density would account for the observed decrease in degradation rates, since the Cu-O bonds are more covalent in nature than the Na-O bonds. Therefore the Cu-O-P bonds were more ionic in nature than Na-O-P bonds. It was more likely that the Cu^{2+} acted as network modifiers with their strengthening effect on the glass structure (Shih *et al.*, 1998, 1999, Chahine *et al.*, 2004).

Copper is one of the transition metals that can be present in more than one oxidation state in the glass structure (Bae and Weinberg, 1991, Cozar and Ardelean, 2003). It can also be present in three different valence states such as; metallic copper (Cu^{o}), cuprous (Cu^{+}) or cupric (Cu^{2+}). Each state has its own electronic configuration and coordination number;

therefore each would affect the glass structure in different ways. Cu° does not commonly exist in a glass melt in air. Cu^{2+} has a smaller ionic radius and greater field strength than Cu^{+}. Thus, it produces a glass structure with smaller P-O-P bond angles and greater Cu-O-P bond strength than Cu^{+}. Moreover, it produces a strong and dense glass structure (Shih and Chin, 1999). Khattak *et al.* (2004) measured the relative amounts of the different Cu valence state in telluride glass by using temperature-dependant magnetic susceptibility measurements combined with inductively coupled plasma spectroscopy. The results indicated the presence of Cu ions in the two valence states (Cu^{+}, Cu^{2+}) with Cu^{2+} predominating in the glass structure. Additionally, the ratio of non-bridging oxygen to the total oxygen (NBO/TO) increased with increasing CuO content that enter the glass network as a glass modifier suggesting the stronger effect of Cu^{2+} on depolymerising the glass structure.

Shih *et al.*, (1998) proposed a structural model for substitution of Na^{+} in metaphosphate glass either partly by Cu^{2+} to form ternary P_2O_5-Na_2O-CuO glass or completely to form a binary P_2O_5-CuO glass as shown in Figure 3.37. The authors concluded that in binary 50 P_2O_5-50 Na_2O, the ratio of BO/NBO was equals to 0.5. With partial or complete substitution of Na^{+} with Cu^{2+}, Cu-O-P bonds formed and replaced either partly or totally Na-O-P bonds without affecting P-O-P bonds.

The degradation rate was observed to be higher for fibres pulled at 1200 $m.min^{-1}$ than those pulled at 400 $m.min^{-1}$. This was attributed to the significant increase in surface area to volume ratio of these fibres. Percentage weight $loss.h^{-1}$ followed an inverse linear relationship against CuO content, and fibres pulled at 1200 $m.min^{-1}$ showed a higher

degradation rate (Figure 3.38), but if % weight loss.h^{-1} is normalised to the surface area, the opposite was observed indicating that the degradation was a complex process.

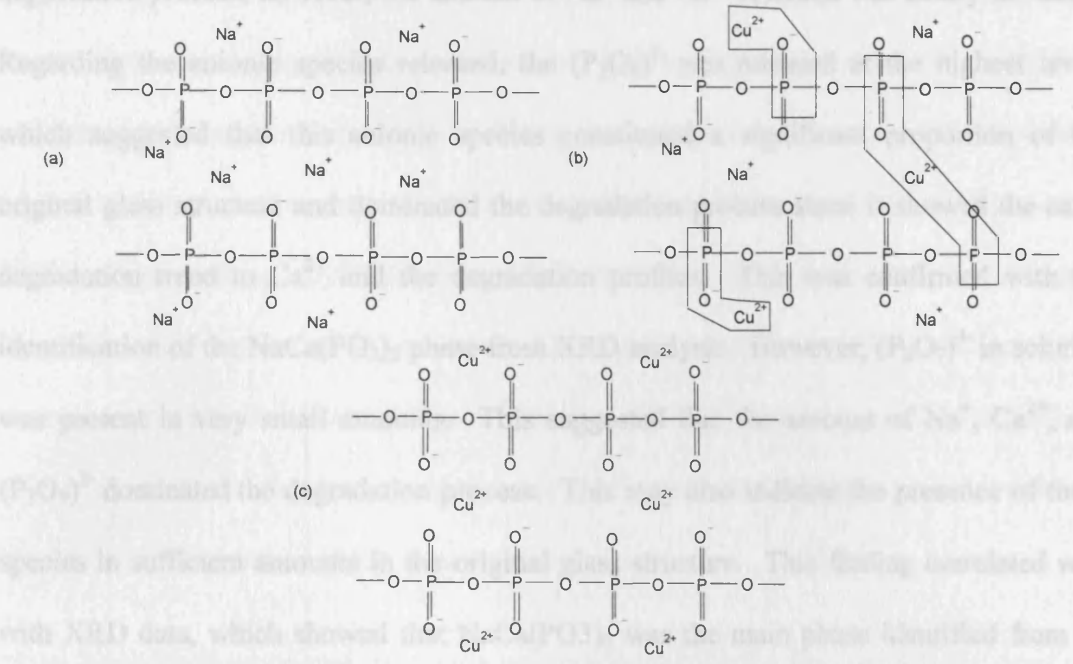

Figure 3.37: Schematic structure of sodium-copper metaphosphate glasses. (a) binary sodium metaphosphate (50 P_2O_5-50 Na_2O) linear chain structure, (b) Na^+ are partially replaced by Cu^{2+}, and (c) binary copper metaphosphate (50 P_2O_5-50 CuO) as all Na^+ in (a) are replaced by Cu^{2+} (Shih *et al.*, 1998).

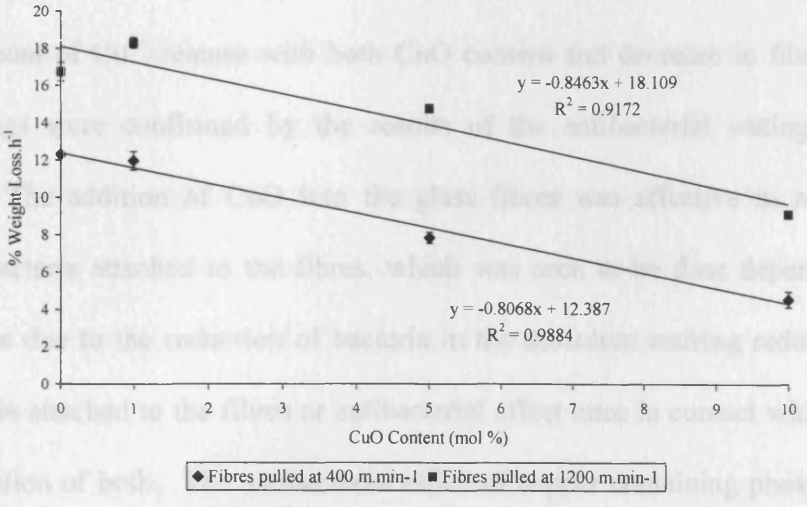

Figure 3.38: Percentage weight loss.h^{-1} against CuO content.

Ion release data mirrored the degradation profiles with the Ca^{2+} release showing an identical trend with the weight loss data which indicated the role of Ca^{2+} in the degradation process; however, the amount of Na^{+} and Ca^{2+} released was nearly the same. Regarding the anionic species released, the $(P_3O_9)^{3-}$ was released at the highest levels which suggested that this anionic species constituted a significant proportion of the original glass structure and dominated the degradation process since it showed the same degradation trend to Ca^{2+} and the degradation profiles. This was confirmed with the identification of the $NaCa(PO_3)_3$ phase from XRD analysis. However, $(P_2O_7)^{4-}$ in solution was present in very small amounts. This suggested that the amount of Na^{+}, Ca^{2+}, and $(P_3O_9)^{3-}$ dominated the degradation process. This may also indicate the presence of these species in sufficient amounts in the original glass structure. This finding correlated well with XRD data, which showed that $NaCa(PO3)_3$ was the main phase identified from all the glass compositions studied. Cu^{2+} release correlated with the amount of copper incorporated into the glass; therefore, it is suggested that it was possible to tailor the composition to obtain a slow rate of Cu release over a long period of time.

Ion release results mirrored the degradation results where there was an increase in both the rate and amount of Cu^{2+} release with both CuO content and decrease in fibre diameter. These findings were confirmed by the results of the antibacterial testing against *S. epidermidis*. The addition of CuO into the glass fibres was effective in reducing the number of bacteria attached to the fibres, which was seen to be dose dependent. This effect may be due to the reduction of bacteria in the inoculum causing reduction in the viable bacteria attached to the fibres or antibacterial effect once in contact with the fibres, or a combination of both. The antibacterial effect of copper containing phosphate-based glasses against *Streptococcus Sanguis* was demonstrated by Mulligan *et al.*, 2003a who

carried out the antibacterial study on glass discs with 45 mol % P_2O_5 using a Constant Depth Film Fermenter (CDFF). Copper is a metal ion known with its antibacterial activity (Mulligan *et al.*, 2003a, Barbucci *et al.*, 2002, and Wang *et al.*, 2005). The precise mechanism responsible for the antibacterial activity of copper has not been fully understood yet, but it is believed to be due to blockage of the enzyme system involved in bacterial respiration (Hassen *et al.*, 1998) or disruption of the cell envelope (Wang et al., 2005). There was no significant effect between fibre diameters in all CuO containing formulations in contrast to the controls. Therefore the dominant effect was due to the incorporation of CuO. However, fibres with 10 mol % CuO proved to be most effective in delivering sufficient amounts of antibacterial Cu^{2+} to prevent colonisation and reduce the number of viable bacteria in the local environment.

Many biomaterial-associated infections are composed of just a few species and nearly 80 % of the bacteria involved are *S. epidermidis*. This organism is an ever-present resident of human skin and mucous membranes that rarely causes infections in normal hosts. But as an opportunistic pathogen gains access through the skin via wounds and implants (Götz, 2002). Copper incorporated phosphate-based glass fibres, particularly those with 10 mol % CuO, could be prepared in a mesh form to be potentially used a wound dressing for the treatment of sever burns, leg ulcers, pressure sores, and infected surgical wounds providing both protection against ingress of micro organisms and when they dissolve they release copper ions which could help to combat the infection. The highly degradable nature of these fibres is beneficial for copper release, and these meshes would be used on temporary bases.

Copper incorporated phosphate glass fibres could also be potentially used as sutures which are probably the largest group of devices implanted in humans. Regardless of the composition, a suture is a foreign body to human tissue which may elicit a foreign body reaction to some degree. Being degradable, phosphate glass fibres will release copper as they degrade. The brittle nature of these materials, however, may be a potential problem and considering coating them with either synthetic or natural polymer may have an affect the copper ion release.

The incorporation of copper containing phosphate glass fibres into bone cement used for fixation of orthopaedic devices such as hip replacement devices could also be considered. The antibacterial ions released from the bone cement into the surrounding tissue around the replacement device help to reduce the number of bacteria left in the operative wound.

Chapter 4

Iron Containing Phosphate Glass Fibres

4.1. Introduction

In this chapter, fibres of the quaternary glass system based on 50 P_2O_5-30 CaO-(20-x) Na_2O-x Fe_2O_3 where x is either 1, 2, 3, 4, or 5 mol % as given in Table 4.1 were produced and characterised for potential tissue engineering applications. The thermal, degradation properties, pH change, ion release (cationic and anionic species), and the morphological changes of the degrading fibres were investigated to give an overall view of the relationship between Fe_2O_3 content, fibre diameter and these properties.

Table 4.1: Glass codes and composition of glasses investigated.

Glass code	P_2O_5 content (mol %)	CaO content (mol %)	Na_2O content (mol %)	Fe_2O_3 content (mol %)
0 mol % Fe_2O_3	50	30	20	0
1 mol % Fe_2O_3	50	30	19	1
2 mol % Fe_2O_3	50	30	18	2
3 mol % Fe_2O_3	50	30	17	3
4 mol % Fe_2O_3	50	30	16	4
5 mol % Fe_2O_3	50	30	15	5

4.2. Experimental

4.2.1. Materials

4.2.1.1. Raw Materials

4.2.1.1.1. Chemical Equations and Compositional Calculations

The precursors used in the preparation of this glass system are given in Table 4.2.

Table 4.2: Raw materials used in glass preparation.

Raw materials	Supplier
Sodium di-hydrogen orthophosphate anhydrous (NaH_2PO_4)	BDH, UK
Calcium carbonate ($CaCO_3$)	BDH, UK
Di-phosphorus pentoxide (P_2O_5)	BDH, UK
Iron III oxide (ferric oxide) (Fe_2O_3)	BDH, UK

The amounts of precursor materials were calculated using the same equations for copper containing quaternary glasses described in Section 3.2.1.1.1. For calculation of the required amount of Fe_2O_3, the molecular weight of Fe_2O_3 is 159.69 $g.mol^{-1}$. If the required glass composition contains 0.03 Fe_2O_3, the amount of Fe_2O_3 should be $(0.03 \times 159.69) = 4.78$ g. In general for all precursors used, only half of the weights calculated were used in order to avoid foaming of the glass over the crucible edge during melting.

4.2.1.2. Methods of Preparation

4.2.1.2.1. Bulk Glass Preparation

Preparation of iron containing bulk glasses was similar to copper containing glasses except that the melting started at 700 °C for half an hour to allow for the removal of H_2O and CO_2 evolution, and to avoid foaming of the glass melt. This was followed by melting at 1100 °C for 1 h. Upon removal of the crucible from the furnace, the melted glass was poured onto a stainless steel plate and left to cool to room temperature. Once cooled, the glass was placed into a sealed plastic bag and stored in a desiccator at room temperature.

4.2.1.2.2. Glass Fibre Production

The method used for the production of the glass fibres has been previously described in Section 3.2.1.2.2. The temperatures used for pulling the iron containing glass fibres are given in Table 4.3.

Table 4.3: Melt temperatures used for pulling fibres for different iron containing glass compositions.

Glass composition	Melt temperature (°C)
0 mol % Fe_2O_3	960
1 mol % Fe_2O_3	980
2 mol % Fe_2O_3	1010
3 mol % Fe_2O_3	1020
4 mol % Fe_2O_3	1025
5 mol % Fe_2O_3	1040

4.2.2. Methods of Characterisation

4.2.2.1. Bulk Glass

4.2.2.1.1. Density Measurements

Density measurements were carried out on three repeat specimens as previously described in Section 3.2.2.1.1.

4.2.2.2. Glass Fibres

4.2.2.2.1. Fibre Diameter Measurements

The mean fibre diameters were obtained from an average of 50 fibres of bundles embedded in resin using a digital image analysis system as described previously in Section 3.2.2.2.1.

4.2.2.2.2. Determination of Thermal Properties

a) Differential Scanning Calorimetry

An initial study was conducted on 3 mol % Fe_2O_3 and pulled at 1600 m.min^{-1} to determine a suitable heating rate and T_g measure that would be used for further studies. The samples were heated, cooled, and reheated from 25 °C to 550 °C at various heating rates of 10, 20, 50, 100, 150, 200 and 300 °C.min^{-1}. It was observed the baseline shift indicated the presence of T_g was clearly seen using a heating rate of 100 °C.min^{-1}. This heating rate was selected to calculate the T_g for the different glass compositions.

As previously stated in Section 3.2.2.2.2., T_g can be extrapolated either by the onset of the baseline shift or by the ½ ΔC_p. When the ½ ΔC_p and the onset of the baseline shift were plotted against the heating rate as shown in Figure 4.1, a straight line was observed from which the slope was calculated. By comparing the two slopes, the onset of the baseline shift showed a lower slope than ½ ΔC_p, which meant that the onset of the baseline was little affected by the changing of the heating rate, as compared to the ½ ΔC_p. Therefore, the onset of change in the endothermic direction (upwards) of the heat flow of the first heating run was used to calculate T_g.

The samples were heated/cooled/heated at 100 °C.min^{-1} between 25 and 550 °C. The effect of Fe_2O_3 content and the pulling speeds on T_g was conducted on three repeat specimens.

b) Differential Thermal Analysis

The effect of Fe_2O_3 content and the pulling speeds on T_g, T_c, *and* T_m was conducted on two repeat specimens as previously described in Section 3.2.2.2.2.

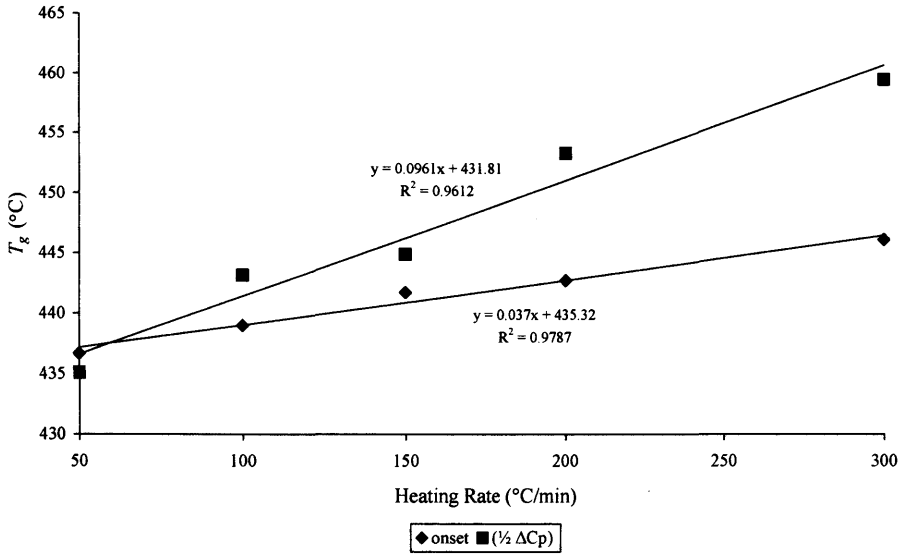

Figure 4.1: Heating rate versus T_g as measured by onset and ½ ΔCp.

4.2.2.2.3. Determination of Fibre Degradation

a) Long Term Degradation Study

Initial degradation tests were carried out in deionised water on fibres produced at the four different RPM for all compositions by ageing them up to 1 day, 1 week, 1 month and 3 months. At these time points, the solution was removed, and the glass bottles containing the fibres were placed in an incubator at 37 °C for 24 h to dry before the final weight was recorded. The % weight loss ($\%wt_l$) was calculated using equation described in Section 3.2.2.2.3.

b) Short Term Degradation Study

This study was carried out over 6, 24, 72 and 96 h for fibres pulled at 400 and 1600 $m.min^{-1}$ for all glass compositions which were used for an in depth study. The degradation rate, expressed in % weight $loss.h^{-1}$, was taken from slope of % weight loss against time.

4.2.2.2.4. Determination of Surface Area to Volume Ratio of the Glass Fibres

The method used to determine the total surface area to volume ratio of the glass fibres pulled at 400 and 1600 $m.min^{-1}$ for all compositions was previously described in Section 3.2.2.2.4.

4.2.2.2.5. Ion Chromatography

The post-degradation medium of the glass fibres pulled at 400 and 1600 $m.min^{-1}$ after being diluted were used for ion release study.

a) Cation Release

The method used to measure Na^+ and Ca^{2+} ion release was carried out as previously described in Section 3.2.2.2.4.

b) Iron Ion Release

The measurement of iron release was carried out using the Dionex ICS-2500 ion chromatography system (Dionex, UK). Prior to running the samples, the ICS-2500 was calibrated using mixed iron (II) chloride ($FeCl_2$) and iron (III) chloride ($FeCl_3$) (Sigma Aldrich, UK) as the reagents. 1000 ppm stock solution was made, from which serially diluted 50, 20, 10 and 1 ppm standard solutions were prepared. The calculations of the amounts of both $FeCl_2$ and $FeCl_3$ required for the preparation of the 1000 ppm stock solution was carried out as previously described in Section 3.2.2.2.5 taking into account that the RAM of Fe = 55.85, and Cl = 35.45 $g.mol^{-1}$; RMM of $FeCl_2$ and $FeCl_3$ were 126.75 and 162.20 $g.mol^{-1}$ respectively.

c) Anion Release

The method used to measure $(PO_4)^{3-}$, $(P_2O_7)^{4-}$, $(P_3O_9)^{3-}$, and $(P_3O_{10})^{5-}$ ion release was carried out as previously described in Section 3.2.2.2.4.

4.2.2.2.6. pH Change

The pH of the post degradation medium of fibres pulled at 400 and 1600 $m.min^{-1}$ was measured at each time point used in the degradation study. This measurement was conducted using an Orion pH meter (Orion, U.K) with a glass pH electrode (BDH, U.K). The meter was calibrated using colourkey standard solutions (BDH, UK).

4.2.2.2.7. Scanning Electron Microscopy

a) Technique

The scanning electron microscope (SEM) utilises electrons to create very detailed 3-dimensional images at much higher magnifications that are not possible with a light microscope. Because the SEM illuminates the samples with electrons, the samples are sputter coated to conduct electricity. The sample is then placed inside the microscope's vacuum column through an air-tight door. Once a vacuum has been created in the column, an electron gun emits a beam of high energy electrons, in the range of 0-40 kV: however, the beam diameter is too large to produce sharp images. Therefore, this beam travels downward through a series of magnetic lenses designed to reduce the diameter of the electron beam and focus the electrons to a very fine spot onto the surface of the specimen. Near the bottom, a set of scanning coils move the focused beam back and forth across the specimen, row by row. As the electron beam hits each spot on the sample, secondary electrons are knocked loose from its surface. A detector counts these electrons and sends the signals to an amplifier. The final image is built up

from the number of electrons emitted from each spot on the sample. The actual formation of the image requires a scanning system to construct the image point by point.

b) Method

Scanning electron microscopy was used to assess the morphological changes of the glass fibres pulled at 400 $m.min^{-1}$ with 2 and 5 mol % Fe_2O_3 during degradation in deionised water compared to as produced fibres. For SEM, the air dried glass fibres were cut with a sharp razor blade, and then mounted onto aluminium stubs with conducting sticky tabs. The samples were sputter coated with gold palladium alloy before being examined under the SEM (JEOL JSM-5500LV) operated at 10 kV.

4.2.2.2.8. Statistical Analysis

A one way analysis of variance (ANOVA) was carried out to assess the effect of pulling speeds on the different fibre diameters obtained. A two-way analysis of variance (ANOVA) was used to assess the effect of composition and fibre diameter on % weight loss, anion and cation release for all glass fibre compositions investigated. Significance was detected at a level of 0.05 for all tests conducted. When significant difference was found, a Dunnette *t* (2 sided) was carried out to set the significance of each composition against the base line control. All statistical analysis was carried out using the SPSS system for Windows (SPSS 12.0.1).

4.3. Results

4.3.1. Bulk Glass

4.3.1.1. Density Measurements

Figure 4.2 shows the mean density of the bulk glass as a function of composition. It was observed that the density increased linearly with increasing Fe_2O_3 content incorporated into the glass.

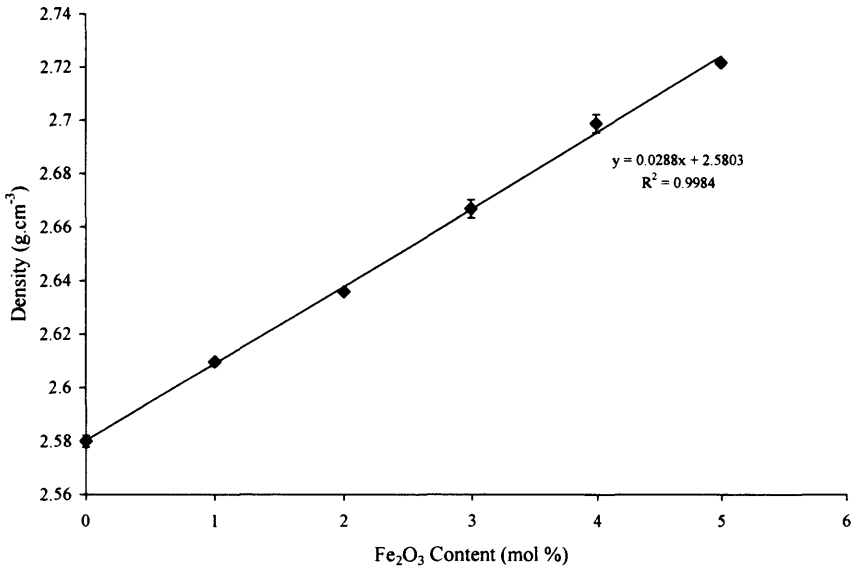

Figure 4.2: Bulk glass density as a function on iron oxide content.

4.3.2. Glass Fibres

4.3.2.1. Fibre Diameter Measurements

Figure 4.3 shows the fibre diameter measurements carried out for all the PGF compositions investigated, which were pulled from speeds of 400, 800, 1200, 1600 $m.min^{-1}$. A significant decrease ($p < 0.05$) in fibre diameters was seen with an increase

in drum pulling speed. An average fibre diameter of 31.6 ± 6.5 μm was observed for fibres pulled at 400 $m.min^{-1}$. However, an average of 13.1 ± 1.3 μm was observed for fibres pulled at 1600 $m.min^{-1}$.

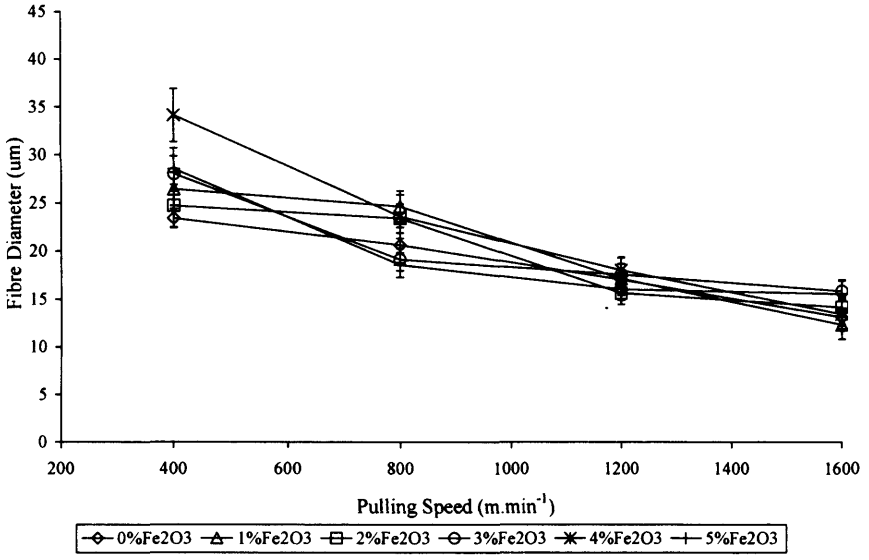

Figure 4.3: Fibre diameter as a function of rig-pulling speed for iron containing glass compositions.

4.3.2.2. Thermal Properties

4.3.2.2.1. Differential Scanning Calorimetry

Figure 4.4 shows DSC data of glass fibres pulled at 1600 $m.min^{-1}$ for different glass compositions as an example to show the effect of Fe_2O_3 content on T_g. There was a linear increase in T_g with increasing Fe_2O_3 content. The recorded T_g for the ternary glass composition (i.e. 0 mol % Fe_2O_3) was approximately 400 °C, and the addition of 5 mol % Fe_2O_3 increased the T_g to 450 °C. Figure 4.5 shows the DSC data of fibres pulled at the four different speeds for 2 mol % Fe_2O_3 composition as an example to show the effect of pulling speeds on T_g. There was no obvious effect of the rig-pulling

speeds, i.e., fibre diameters on T_g, as there was no clear difference in the T_g between the bulk glass and glass fibres and this was also confirmed for other composition as given in Table 4.4.

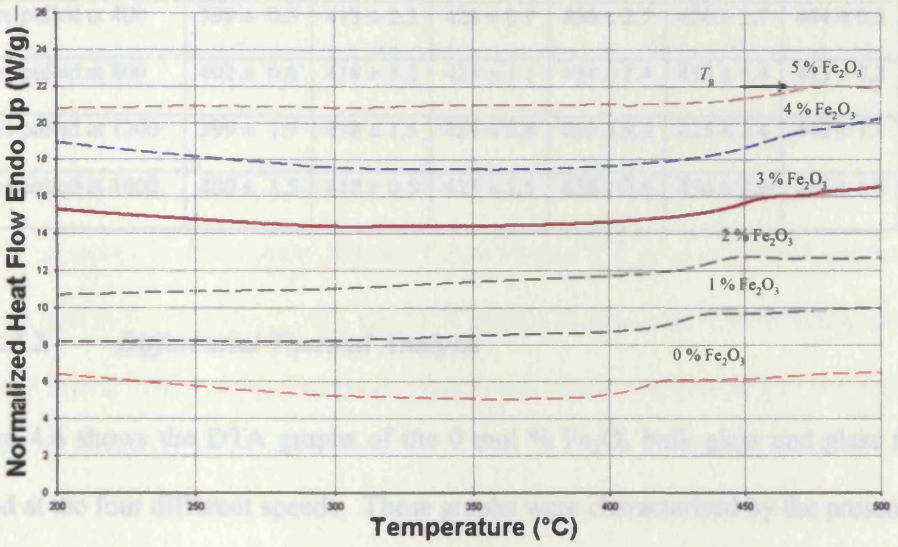

Figure 4.4: Example 1 of a DSC trace of glass fibres pulled at 1600 m.min^{-1} for the different glass compositions investigated.

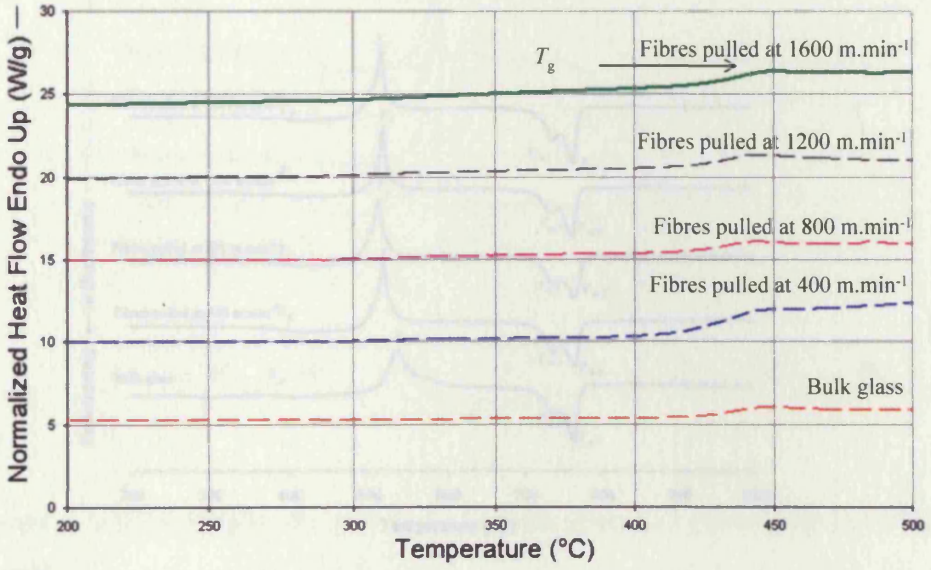

Figure 4.5: Example 2 of a DSC trace of the 2 mol % Fe_2O_3 containing glass.

Table 4.4: T_g (°c) of iron containing glasses as measured by DSC.

Bulk/fibres ($m.min^{-1}$)	0 mol % Fe_2O_3	1 mol % Fe_2O_3	2 mol % Fe_2O_3	3 mol % Fe_2O_3	4 mol % Fe_2O_3	5 mol % Fe_2O_3
Bulk glass	398 ± 1.1	416 ± 1.3	423 ± 1.5	433 ± 1.4	433 ± 1.4	439 ± 0.5
Fibers pulled at 400	399 ± 0.5	413 ± 2.3	426 ± 0.7	436 ± 2.7	436 ± 2.7	444 ± 0.5
Fibers pulled at 800	402 ± 0.6	418 ± 3.2	423 ± 1.1	434 ± 1.4	433 ± 1.4	443 ± 0.2
Fibers pulled at 1200	399 ± 1.9	418 ± 1.5	424 ± 0.8	435 ± 3.4	435 ± 3.4	445 ± 1.1
Fibers pulled at 1600	400 ± 1.5	418 ± 0.5	425 ± 1.5	436 ± 2.6	436 ± 2.6	434 ± 1.9

4.3.2.2.2. Differential Thermal Analysis

Figure 4.6 shows the DTA graphs of the 0 mol % Fe_2O_3 bulk glass and glass fibres pulled at the four different speeds. These graphs were characterised by the presence of a single sharp crystalline peak with two melting peaks. Glass fibres showed a slight shift of the T_c peak to a high temperature by approximately 15 °C as compared to the bulk glass.

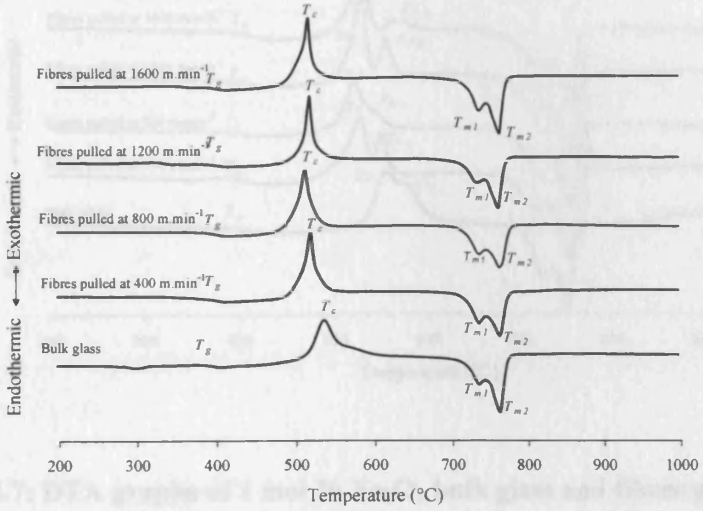

Figure 4.6: DTA graphs of 0 mol % Fe_2O_3 bulk glass and fibres pulled at different speeds.

Figure 4.7 shows the DTA graphs of 1 mol % Fe_2O_3 composition, the graphs showed two crystallisation and melting peaks. The crystallisation peaks of the glass fibres were shifted to lower temperatures than that of bulk glass. On the other hand, there was no obvious difference between glass transitions and melting temperatures of the bulk glass and fibres pulled at the four different speeds. Figure 4.8 shows the DTA graphs of 2 mol % Fe_2O_3 composition, the graph had two crystallisation peaks and a single broad melting peak, and upon magnification of the melting peak, it was easy to identify a second melting peak. Figures 4.9, 4.10, and 4.11 show the DTA graphs of 3, 4 and 5 mol % Fe_2O_3 respectively, the DTA graphs showed two crystallisation and two melting peaks, while a third melting peak could also be observed for the 5 mol % Fe_2O_3.

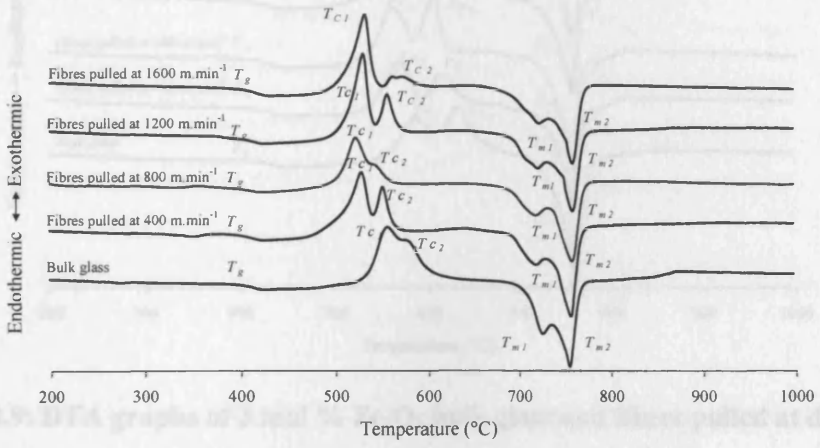

Figure 4.7: DTA graphs of 1 mol % Fe_2O_3 bulk glass and fibres pulled at different speeds.

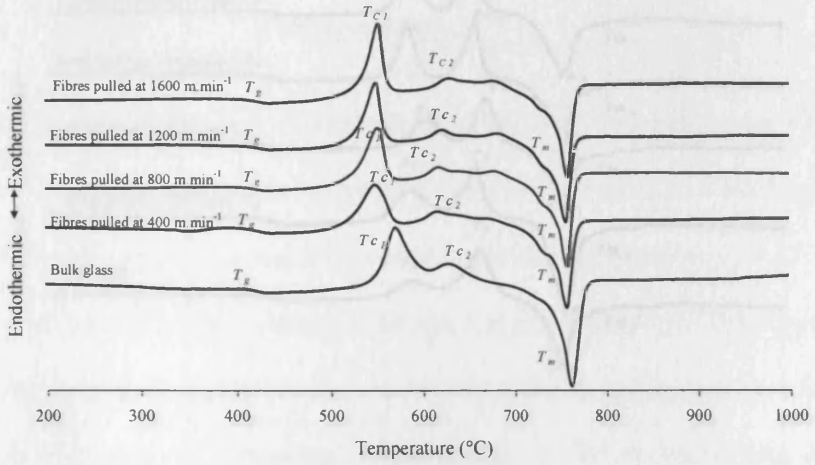

Figure 4.8: DTA graphs of 2 mol % Fe_2O_3 bulk glass and fibres pulled at different speeds.

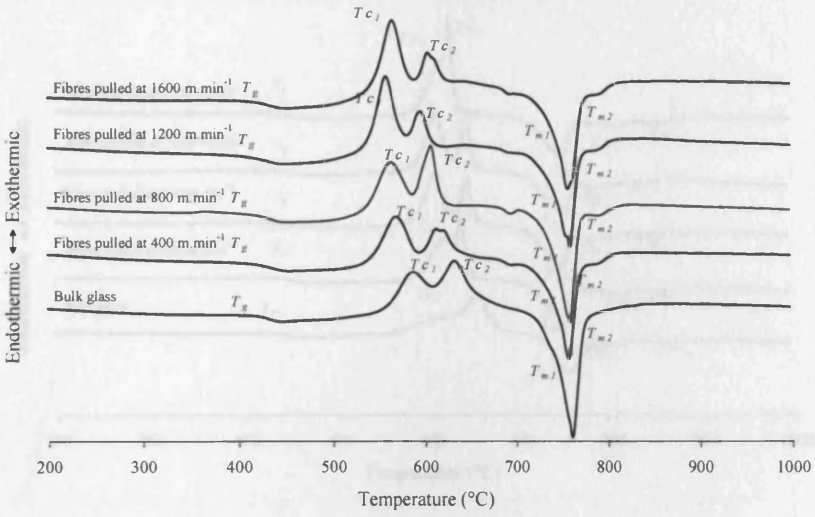

Figure 4.9: DTA graphs of 3 mol % Fe_2O_3 bulk glass and fibres pulled at different speeds.

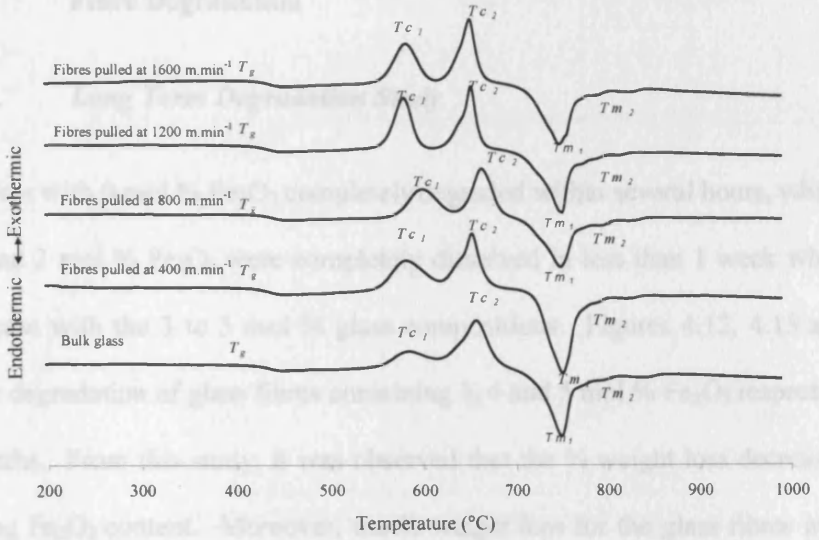

Figure 4.10: DTA graphs of 4 mol % Fe_2O_3 bulk glass and fibres pulled at different speeds.

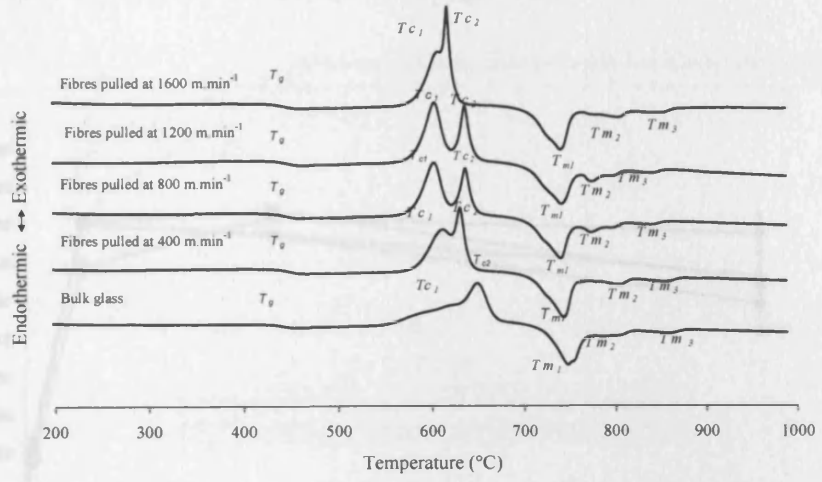

Figure 4.11: DTA graphs of 5 mol % Fe_2O_3 bulk glass and fibres pulled at different speeds.

It was also clear from the DTA data that an increase in T_g was obtained with increasing amounts of Fe_2O_3 incorporated into the glass; however, the crystallisation peaks shifted to lower temperatures with increasing amounts of iron oxide.

4.3.2.3. Fibre Degradation

4.3.2.3.1. Long Term Degradation Study

Glass fibres with 0 mol % Fe_2O_3 completely degraded within several hours, while those with 1 and 2 mol % Fe_2O_3 were completely dissolved in less than 1 week which was not the case with the 3 to 5 mol % glass compositions. Figures 4.12, 4.13 and 4.14 show the degradation of glass fibres containing 3, 4 and 5 mol % Fe_2O_3 respectively up to 3 months. From this study, it was observed that the % weight loss decreased with increasing Fe_2O_3 content. Moreover, the % weight loss for the glass fibres increased with increased pulling speeds i.e., decreasing fibre diameters. Fibres pulled at 400 $m.min^{-1}$ degraded slowly compared with those pulled at 1600 $m.min^{-1}$ for each of the glass compositions. The degradation process was not linear over time, and the degradation levelled off after a certain % of weight loss.

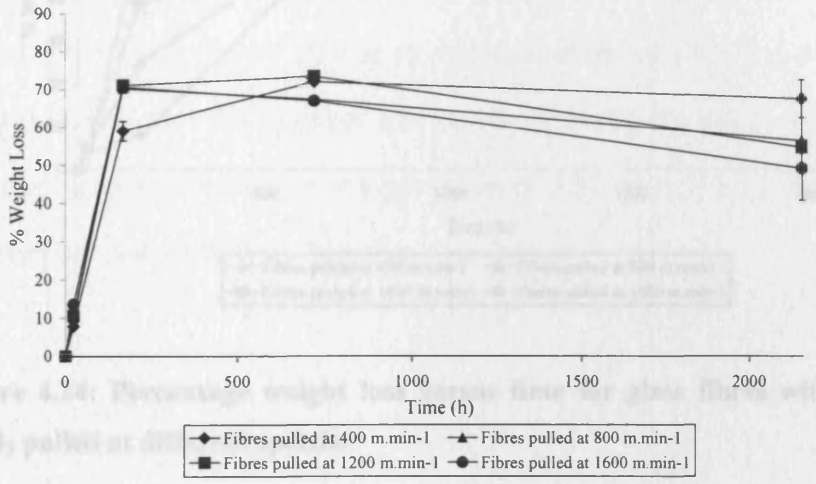

Figure 4.12: Percentage weight loss versus time for glass fibres with 3 mol % Fe_2O_3 pulled at different speeds.

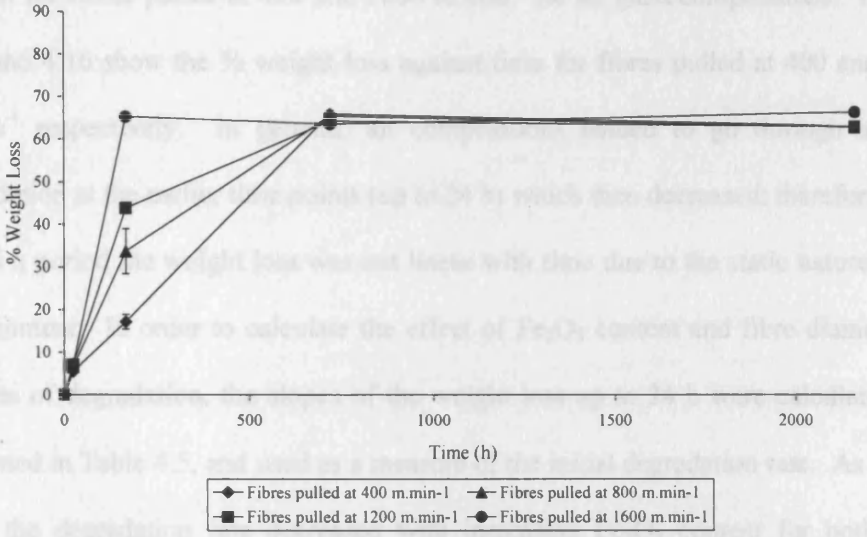

Figure 4.13: Percentage weight loss versus time for glass fibres with 4 mol % Fe_2O_3 pulled at different speeds.

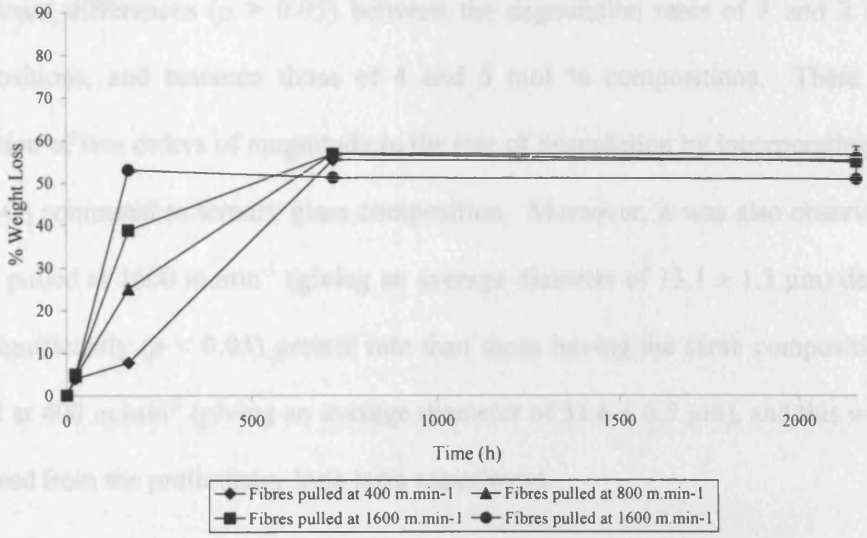

Figure 4.14: Percentage weight loss versus time for glass fibres with 5 mol % Fe_2O_3 pulled at different speeds.

4.3.2.3.2. Short Term Degradation Study

From the above experiment it was seen that each glass composition degraded at a different rate. For this reason, another short term degradation study was carried out up

to 96 h for fibres pulled at 400 and 1600 $m.min^{-1}$ for all glass compositions. Figures 4.15 and 4.16 show the % weight loss against time for fibres pulled at 400 and 1600 $m.min^{-1}$ respectively. In general, all compositions tended to go through a rapid degradation at the earlier time points (up to 24 h) which then decreased; therefore, over the 96 h period the weight loss was not linear with time due to the static nature of the environment. In order to calculate the effect of Fe_2O_3 content and fibre diameter on the rate of degradation, the slopes of the weight loss up to 24 h were calculated and presented in Table 4.5, and used as a measure of the initial degradation rate. As can be seen, the degradation rate decreased with increasing Fe_2O_3 content for both fibre diameters with all Fe_2O_3 containing glass fibres being significantly different ($p < 0.05$) compared to the control ternary formulation (0 mol % Fe_2O_3). However, there were no significant differences ($p > 0.05$) between the degradation rates of 1 and 2 mol % compositions, and between those of 4 and 5 mol % compositions. There was a reduction of two orders of magnitude in the rate of degradation by incorporating 5 mol % Fe_2O_3 compared to ternary glass composition. Moreover, it was also observed that fibres pulled at 1600 $m.min^{-1}$ (giving an average diameter of 13.1 ± 1.3 μm) degraded at a significantly ($p < 0.05$) greater rate than those having the same composition and pulled at 400 $m.min^{-1}$ (giving an average diameter of 31.6 ± 6.5 μm), and this was also observed from the preliminary long term experiment.

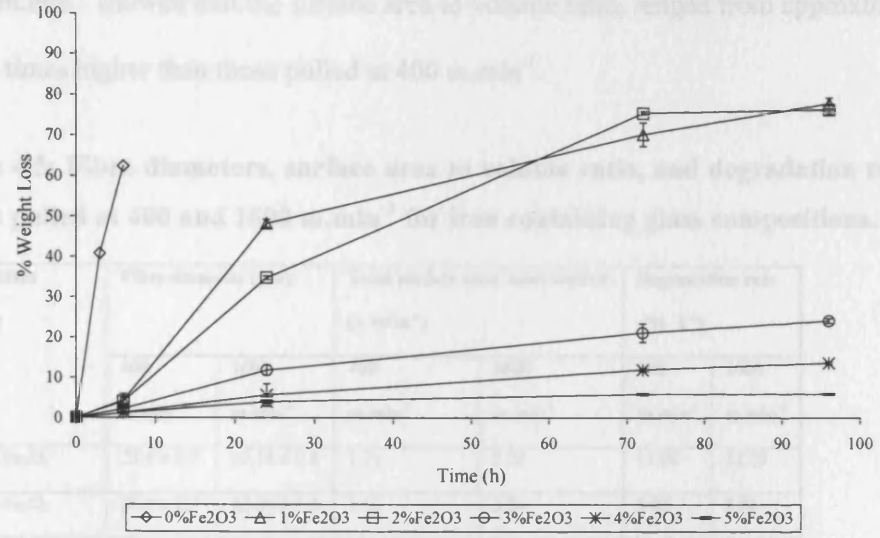

Figure 4.15: Percentage weight loss versus time for glass fibres pulled at 400 m.min^{-1} of iron containing glass compositions.

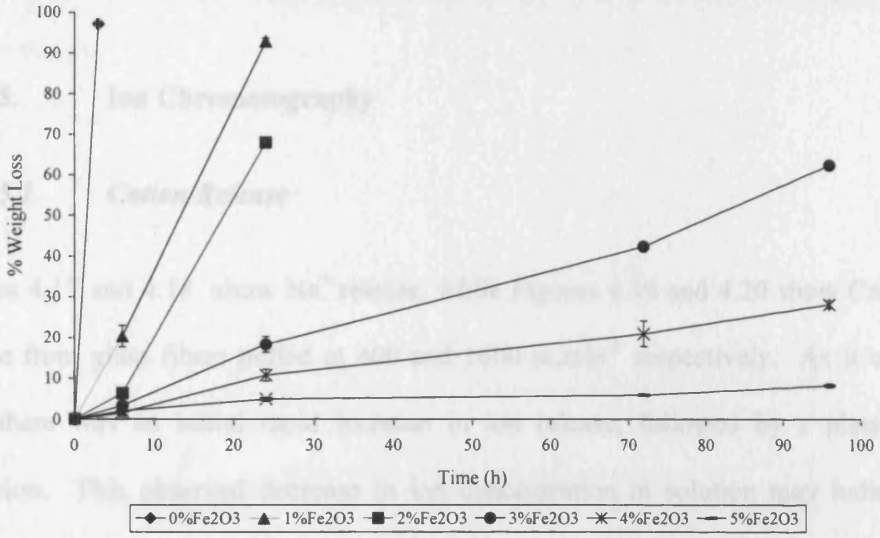

Figure 4.16: Percentage weight loss versus time for glass fibres pulled at 1600 m.min^{-1} of iron containing glass compositions.

4.3.2.4. Determination of Surface Area to Volume Ratio of the Glass Fibres

Table 4.5 gives the calculated surface area to volume ratios for glass fibres pulled at 400 and 1600 m.min^{-1} for all compositions. It was clearly apparent that fibres pulled at

1600 m.min^{-1} showed that the surface area to volume ratio, ranged from approximately 2 to 3 times higher than those pulled at 400 m.min^{-1}.

Table 4.5: Fibre diameters, surface area to volume ratio, and degradation rate of fibres pulled at 400 and 1600 m.min^{-1} for iron containing glass compositions.

Composition (mol %)	Fibre diameter (μm)		Total surface area/ total volume (x 10^5m^{-1})		Degradation rate (% h^{-1})	
	400 m.min^{-1}	1600 m.min^{-1}	400 m.min^{-1}	1600 m.min^{-1}	400 m.min^{-1}	1600 m.min^{-1}
0 mol % Fe_2O_3	23.4 ± 0.9	13.14 ± 0.8	1.71	3.05	11.04	32.29
1 mol % Fe_2O_3	26.5 ± 1.7	12.35 ± 1.5	1.51	3.24	1.94	3.84
2 mol % Fe_2O_3	35.9 ± 2.7	12.27 ± 1.7	1.12	3.26	1.41	2.73
3 mol % Fe_2O_3	34.2 ± 2.8	13.47 ± 1.5	1.17	2.97	0.49	0.75
4 mol % Fe_2O_3	40.8 ± 2.5	11.91 ± 1.5	0.98	3.36	0.23	0.44
5 mol % Fe_2O_3	28.6 ± 2.1	15.59 ± 1.5	1.40	2.57	0.17	0.21

4.3.2.5. Ion Chromatography

4.3.2.5.1. Cation Release

Figures 4.17 and 4.18 show Na^+ release, while Figures 4.19 and 4.20 show Ca^{2+} ion release from glass fibres pulled at 400 and 1600 m.min^{-1} respectively. As it can be seen there was an initial rapid increase in ion release, followed by a plateau or reduction. This observed decrease in ion concentration in solution may indicate a precipitation process taking place between 24 to 96 h within the static degradation medium. Due to this precipitation process the slopes of the initial part up to 24 h were used to calculate the apparent rates of ion release which are given in Table 4.6. Both Na^+ and Ca^{2+} were released at approximately the same levels. Glass fibres with low Fe_2O_3 released higher amounts of both cations than those with high Fe_2O_3 content. Intriguingly, however, although all glass compositions contained 30 mol % CaO, there was a decrease in the Ca^{2+} ion release with an increase in Fe_2O_3 content. In all

compositions, the rate of Na^+ and Ca^{2+} released were higher for fibres pulled at 1600 $m.min^{-1}$ than those pulled at 400 $m.min^{-1}$.

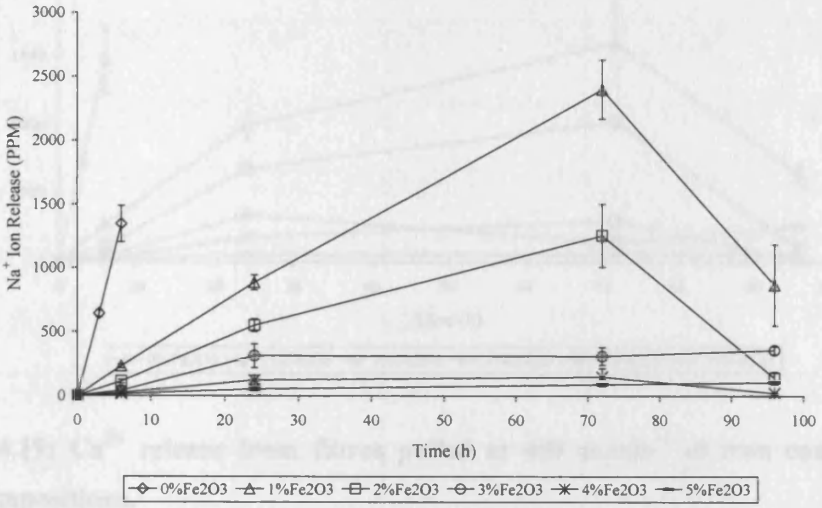

Figure 4.17: Na^+ release from fibres pulled at 400 $m.min^{-1}$ of iron containing glass compositions.

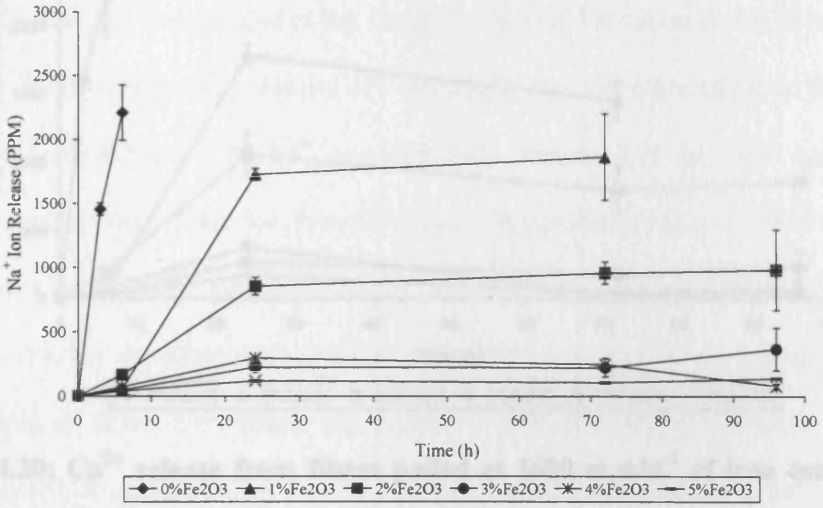

Figure 4.18: Na^+ release from fibres pulled at 1600 $m.min^{-1}$ of iron containing glass compositions.

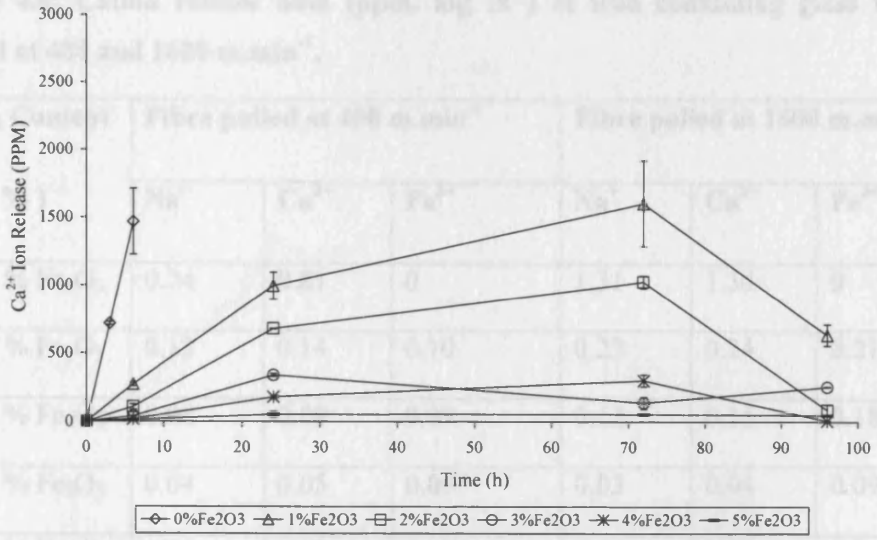

Figure 4.19: Ca^{2+} release from fibres pulled at 400 $m.min^{-1}$ of iron containing glass compositions.

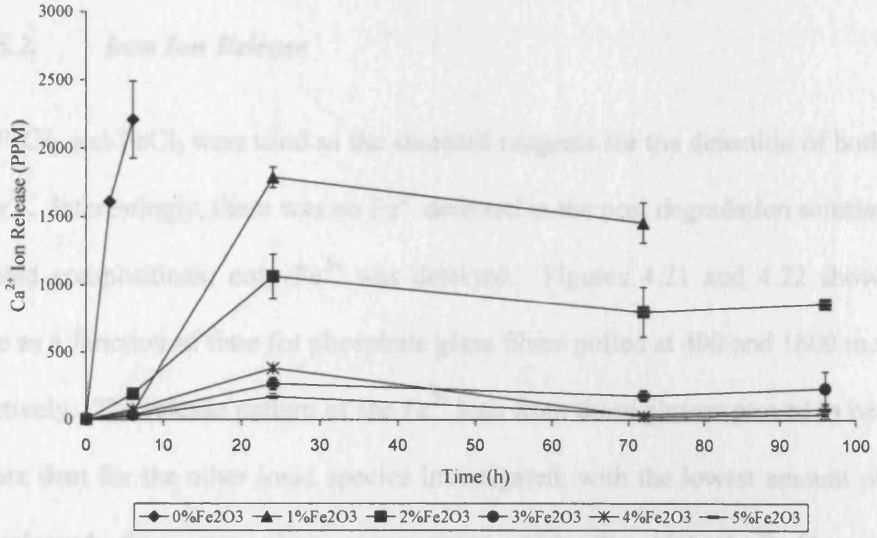

Figure 4.20: Ca^{2+} release from fibres pulled at 1600 $m.min^{-1}$ of iron containing glass compositions.

Table 4.6: Cation release data (ppm. $mg^{-1}.h^{-1}$) of iron containing glass fibres pulled at 400 and 1600 $m.min^{-1}$.

Fe_2O_3 Content (mol %)	Fibre pulled at 400 $m.min^{-1}$			Fibre pulled at 1600 $m.min^{-1}$		
	Na^+	Ca^{2+}	Fe^{3+}	Na^+	Ca^{2+}	Fe^{3+}
0 mol % Fe_2O_3	0.74	0.81	0	1.31	1.34	0
1 mol % Fe_2O_3	0.12	0.14	0.10	0.23	0.24	0.21
2 mol % Fe_2O_3	0.08	0.09	0.09	0.12	0.15	0.18
3 mol % Fe_2O_3	0.04	0.05	0.09	0.03	0.04	0.09
4 mol % Fe_2O_3	0.01	0.02	0.08	0.04	0.05	0.04
5 mol % Fe_2O_3	0.001	0.01	0.05	0.02	0.02	0.02

4.3.2.5.2. Iron Ion Release

Both $FeCl_2$ and $FeCl_3$ were used as the standard reagents for the detection of both Fe^{2+} and Fe^{3+}. Interestingly, there was no Fe^{2+} detected in the post degradation solutions for all tested compositions; only Fe^{3+} was detected. Figures 4.21 and 4.22 show Fe^{3+} release as a function of time for phosphate glass fibres pulled at 400 and 1600 $m.min^{-1}$, respectively. The release pattern of the Fe^{3+} ions from these glasses proved to be more complex than for the other ionic species investigated, with the lowest amount of Fe^{3+} ions released from the glass composition with the highest Fe_2O_3 content. Consequently, there was an inverse relationship between the amount of Fe^{3+} released and the amount of Fe_2O_3 in the glass. Fe^{3+} release was higher for fibres pulled at 1600 $m.min^{-1}$ than for those pulled at 400 $m.min^{-1}$ as given in Table 4.6.

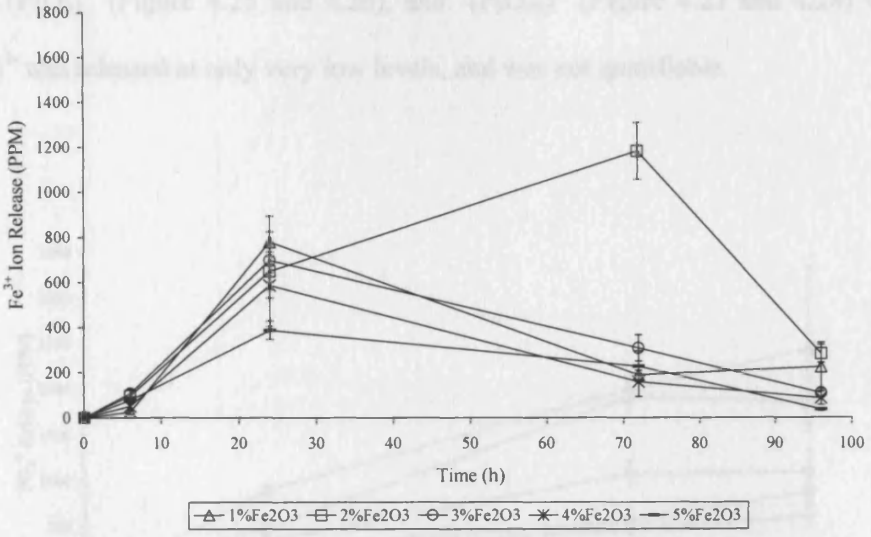

Figure 4.21: Fe^{3+} release from fibres pulled at 400 mmin^{-1} of iron containing glass compositions.

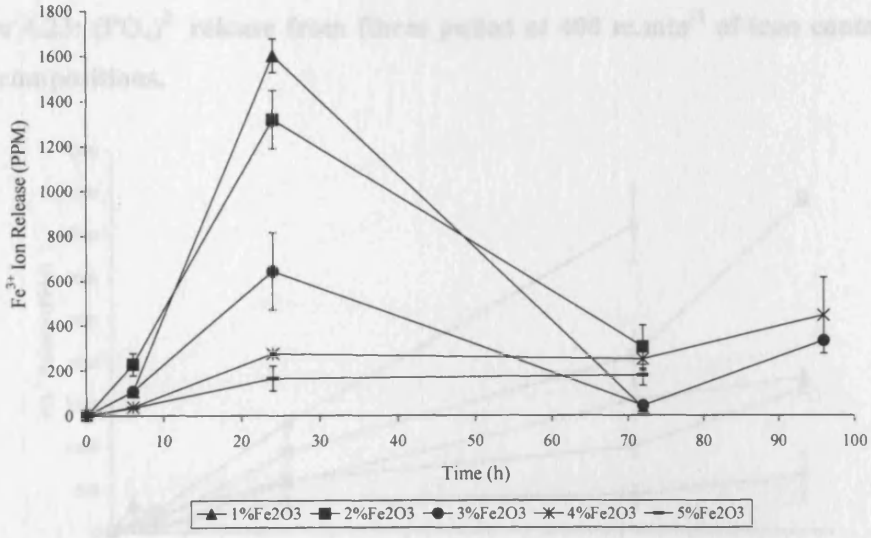

Figure 4.22: Fe^{3+} release from fibres pulled at 1600 mmin^{-1} of iron containing glass compositions.

4.3.2.5.3. Anion Release

Only three out of the four anionic species investigated were identified in the post degradation solution of the iron glass system. These were $(PO4)^{3-}$ (Figure 4.23 and

4.24), $(P_3O_9)^{3-}$ (Figure 4.25 and 4.26), and $(P_3O_{10})^{5-}$ (Figure 4.27 and 4.28) while, $(P_2O_7)^{4-}$ was released at only very low levels, and was not quatifiable.

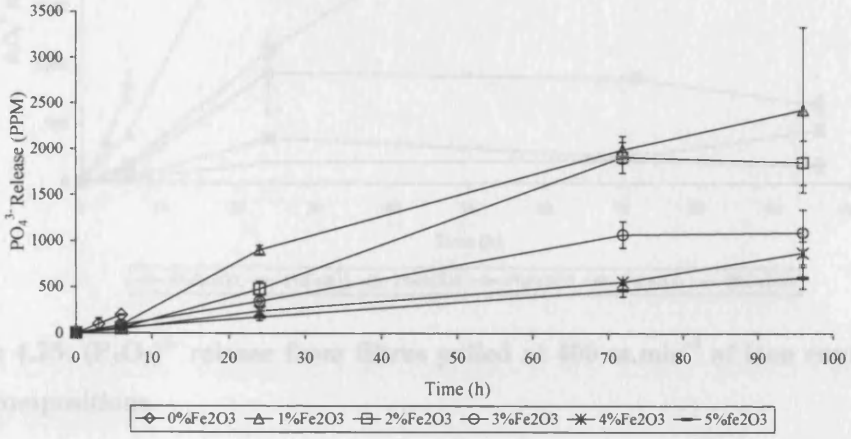

Figure 4.23: $(PO_4)^{3-}$ release from fibres pulled at 400 m.min^{-1} of iron containing glass compositions.

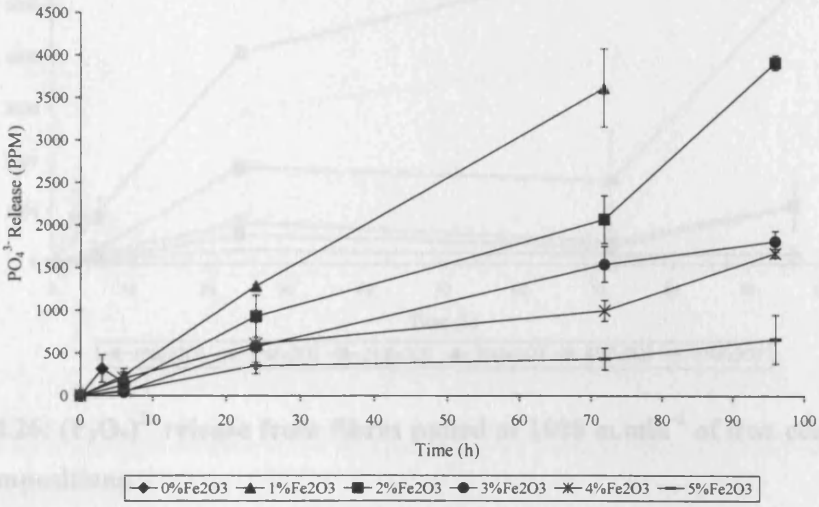

Figure 4.24: $(PO_4)^{3-}$ release from fibres pulled at 1600 m.min^{-1} of iron containing glass compositions.

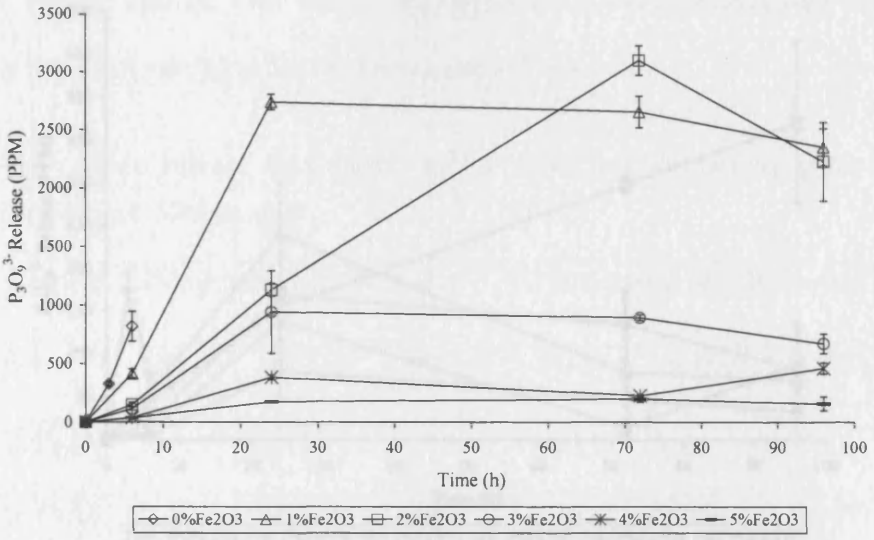

Figure 4.25: $(P_3O_9)^{3-}$ release from fibres pulled at 400 m.min^{-1} of iron containing glass compositions.

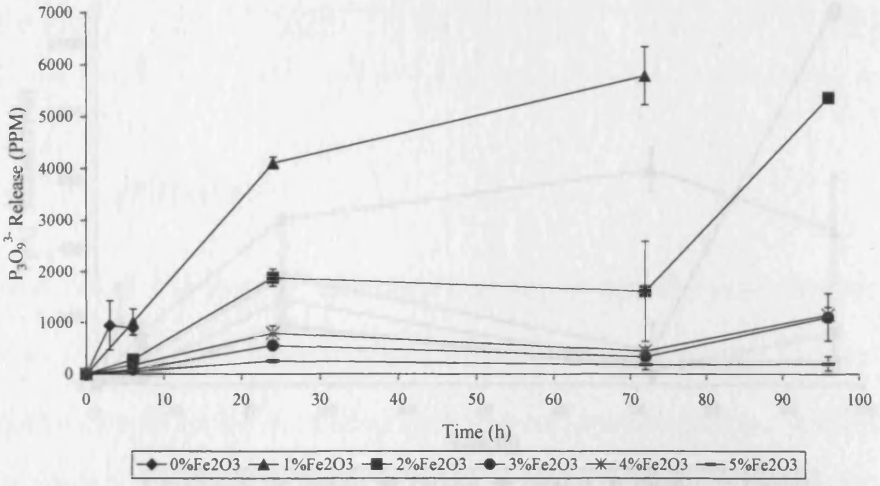

Figure 4.26: $(P_3O_9)^{3-}$ release from fibres pulled at 1600 m.min^{-1} of iron containing glass compositions.

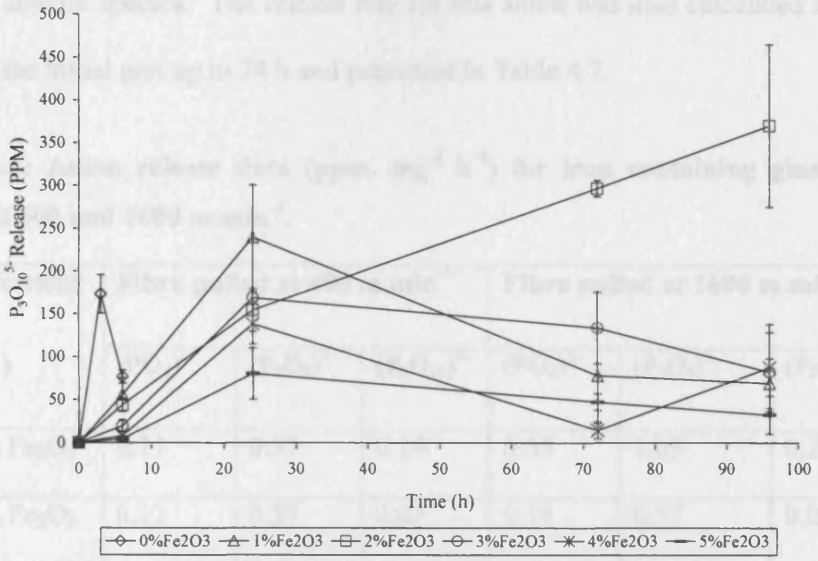

Figure 4.27: $(P_3O_{10})^{5-}$ release from fibres pulled at 400 m.min^{-1} of iron containing glass compositions.

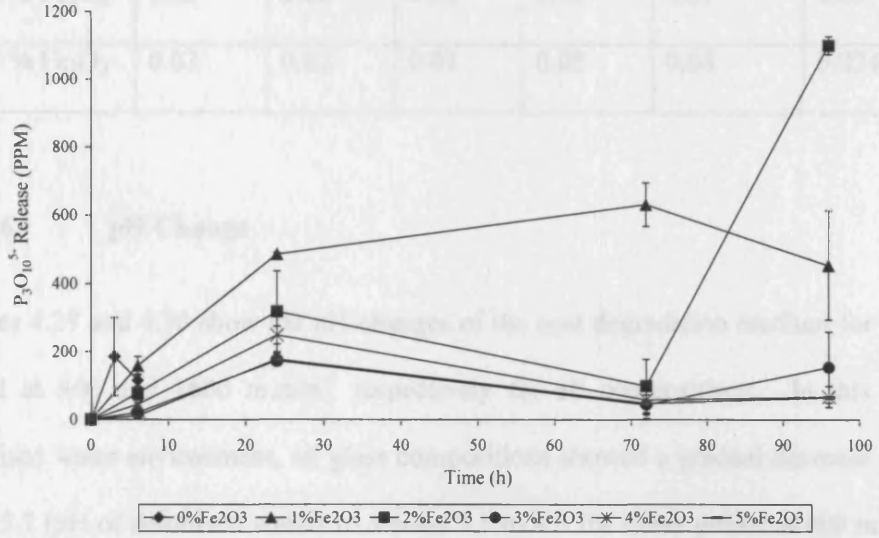

Figure 4.28: $(P_3O_{10})^{5-}$ release from fibres pulled at 1600 m.min^{-1} of iron containing glass compositions.

It was seen that the release profile for the different anionic species showed the same trends as those seen for the cations with the fibres having high surface area to volume ratio yielding higher rates of release. The highest level of release was observed for the

$(P_3O_9)^{3-}$ anionic species. The release rate for this anion was also calculated from the slope of the initial part up to 24 h and presented in Table 4.7.

Table 4.7: Anion release data (ppm. mg^{-1} h^{-1}) for iron containing glass fibres pulled at 400 and 1600 $m.min^{-1}$.

Fe_2O_3 Content (mol %)	Fibre pulled at 400 $m.min^{-1}$			Fibre pulled at 1600 $m.min^{-1}$		
	$(PO_4)^{3-}$	$(P_3O_9)^{3-}$	$(P_3O_{10})^{5-}$	$(PO_4)^{3-}$	$(P_3O_9)^{3-}$	$(P_3O_{10})^{5-}$
0 mol % Fe_2O_3	0.11	0.37	0.19	0.35	1.05	0.21
1 mol % Fe_2O_3	0.12	0.37	0.03	0.18	0.57	0.07
2 mol % Fe_2O_3	0.06	0.15	0.02	0.13	0.26	0.04
3 mol % Fe_2O_3	0.05	1.3	0.02	0.08	0.07	0.02
4 mol % Fe_2O_3	0.03	0.05	0.02	0.09	0.11	0.03
5 mol % Fe_2O_3	0.03	0.02	0.01	0.05	0.04	0.024

4.3.2.6. pH Change

Figures 4.29 and 4.30 show the pH changes of the post degradation medium for fibres pulled at 400 and 1600 $m.min^{-1}$ respectively for all compositions. In this static deionised water environment, all glass compositions showed a gradual decrease in pH from 5.7 (pH of deionised water) to around 3.5 to 4.5 for fibres pulled at 400 $m.min^{-1}$ and 3 to 4.5 for fibres pulled at 1600 $m.min^{-1}$ over the 96 h period. The highest Fe_2O_3 containing PGF showed the least pH changes.

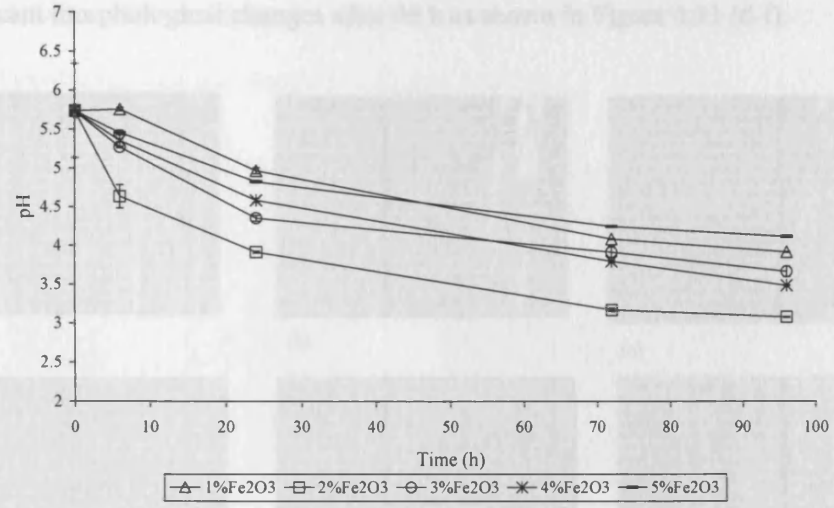

Figure 4.29: pH changes of fibres pulled at 400 mmin^{-1} in deionised water.

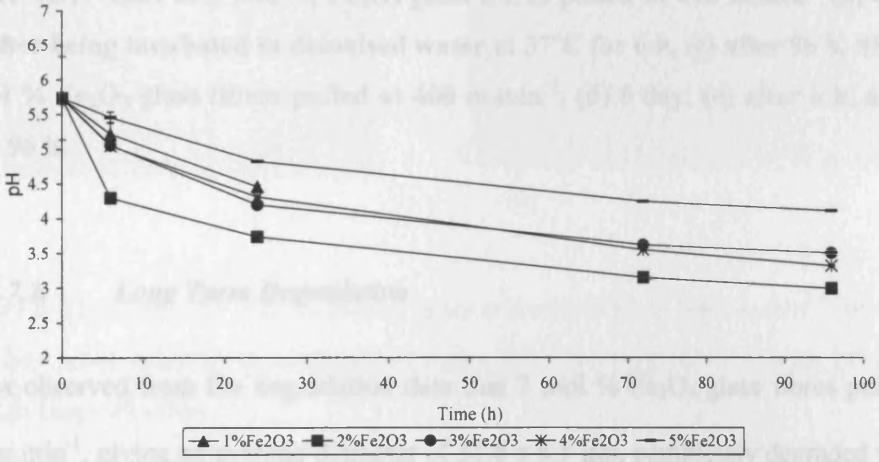

Figure 4.30: pH changes of fibres pulled at 1600 m.min^{-1} in deionised water.

4.3.2.7. Scanning Electron Microscopy

4.3.2.7.1. Short Term Degradation

Figure 4.31 (a-c) shows the SEM of the 2 mol % Fe_2O_3 containing PGF before and after incubation in deionised water. Cracks can be observed on the surface of the glass

fibres after 6 h. However, glass fibres with 5 mol % Fe_2O_3 did not demonstrate any significant morphological changes after 96 h as shown in Figure 4.31 (d-f).

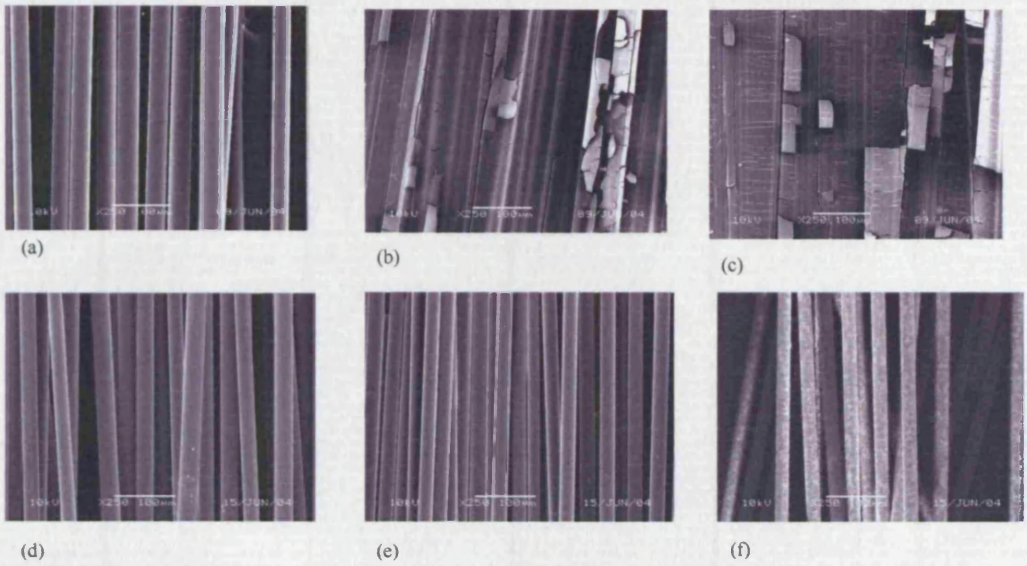

Figure 4.31: SEM of 2 mol % Fe_2O_3 glass fibres pulled at 400 m.min^{-1} (a) 0 day, (b) after being incubated in deionised water at 37°C for 6 h, (c) after 96 h, SEM of 5 mol % Fe_2O_3 glass fibres pulled at 400 m.min^{-1}. (d) 0 day, (e) after 6 h, and (f) after 96 h.

4.3.2.7.2. Long Term Degradation

It was observed from the degradation data that 2 mol % Fe_2O_3 glass fibres pulled at 400 m.min^{-1}, giving an average diameter of 31.6 ± 6.5 μm, completely degraded within week. Therefore, SEM of the precipitate of completely degraded fibres showed the presence of tube-like structures, which may have been formed out of this precipitate as seen in Figure 4.32 (b). This precipitate was delicate to handle for SEM processing, and some samples were left for a significant period of time to see if this structure was maintained. After a year of incubation, another SEM was taken of the precipitate. It can be seen that a well developed tube-like structure shown in Figure 4.32 (c, d) was

present. Under higher magnification, formation of large aggregates can be seen on the surface of this tube, and from these aggregates a small tube which represents a single glass fibre can also be seen (arrows in Figure 4.32 (d).

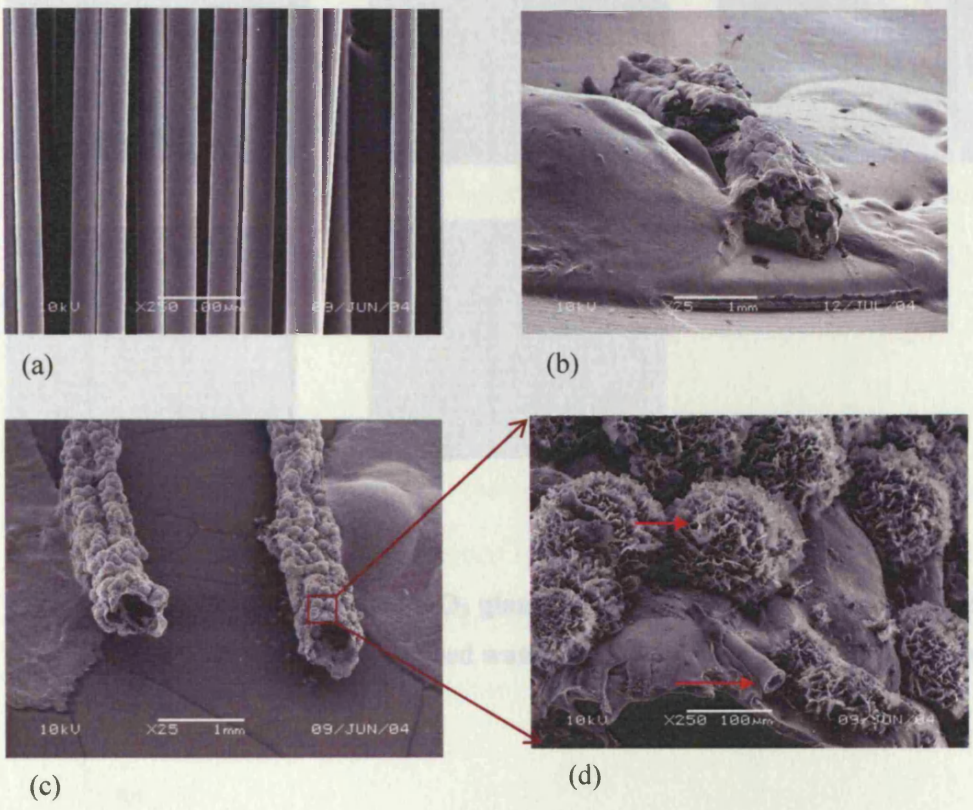

Figure 4.32: SEM of 2 mol % Fe_2O_3 glass fibres pulled at 400 m.min^{-1} (a) 0 day, (b) after being incubated in deionised water for 7 days, (c) after 1 year, (d) 1 year at high magnification.

Moving from PGF containing 2 mol % Fe_2O_3 to the relatively stable composition containing 5 mol % Fe_2O_3, a clear difference could be observed between the two compositions. Phosphate glass fibres with 5 mol % Fe_2O_3 did not demonstrate any morphological changes up to one week, when only a beginning of crack formation could be seen. However, after three months of incubation, the fibres became hollow and appeared as tubes [Figure 4.33(b)]. At six months and 1.5 year periods [Figure

4.33(c-e)], the tube, on higher magnification, appeared to consist of several layers but a further detailed study to determine the composition of these layers would be required.

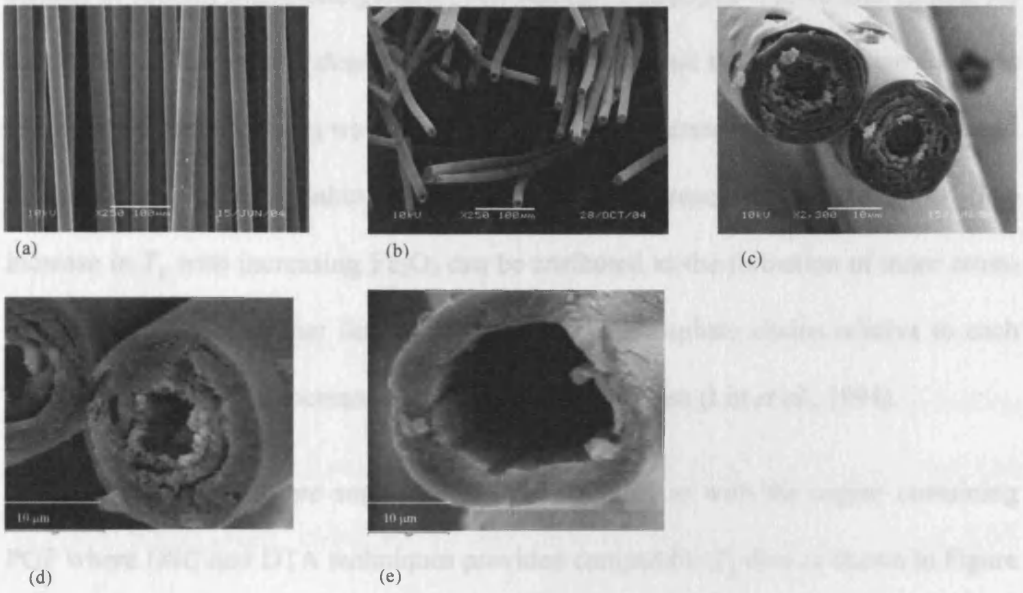

Figure 4.33: SEM of 5 mol % Fe_2O_3 glass fibres pulled at 400 m.min^{-1} (a) 0 day, (b) after being incubated in deionised water for 3 months, (c) after 6 months, (d & e) after 1.5 year.

4.4. Discussion

This chapter investigated the iron containing PGF composition developed for potential tissue engineering application. These were investigated to understand how the chemistry and surface area of the fibres affect the release of ions, which in turn may affect cell behaviour. The thermal properties of glasses are also important, as it provides an overview on the possible transformations through which the glass can go at different temperatures and give valuable information on the morphological structure.

It was observed that by increasing the Fe_2O_3 content in the glass a linear increase in T_g and density occurred. The density at room temperature increased from 2.58 to 2.72

g.cm^{-3}. This finding suggested that a more stable glass was produced by the addition of Fe_2O_3 as observed by Concas *et al.* (1995) who found that increasing the Fe_2O_3 content in sodium phosphate glasses (1-x) $NaPO_3$- x Fe_2O_3 (x = 5, 10 and 15 mol %) resulted in an increase in density. The authors found that the density value for glass containing 5 mol % Fe_2O_3 was 2.76 g.cm^{-3}, which was comparable to the 2.72 g.cm^{-3} obtained in this study, taking into account the difference in compositions. The increase in T_g with increasing Fe_2O_3 can be attributed to the formation of more cross-linked Fe-O-P chains, that limited the mobility of phosphate chains relative to each other, and produced an increases in the density of the glass (Lin *et al.*, 1994).

The results presented here suggested the same finding as with the copper containing PGF where DSC and DTA techniques provided comparable T_g data as shown in Figure 4.34. Moreover, there was no observed major difference in the thermal properties between bulk glass and fibres pulled at different speeds as confirmed by DTA. This finding may suggest that the thermal history had no major effect on these properties.

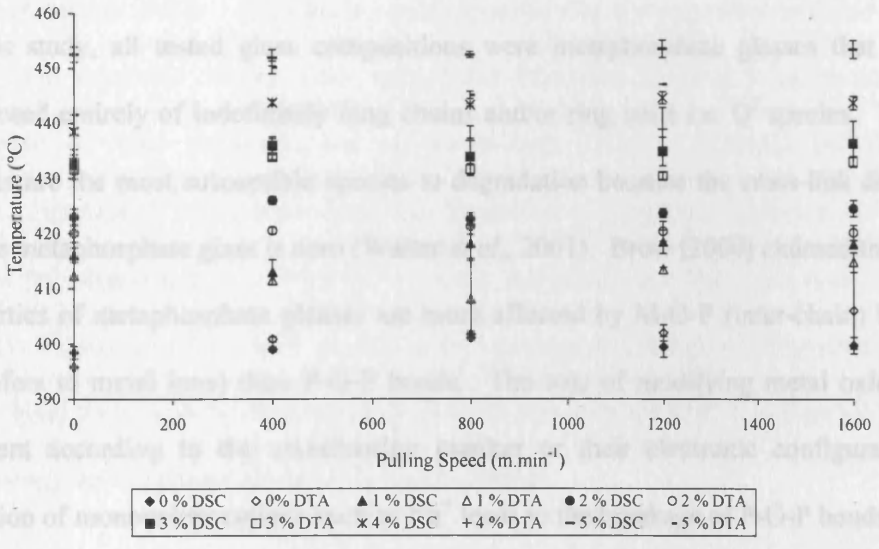

Figure 4.34: Effect of Fe_2O_3 content and rig-pulling speed on glass transition temperature measured through DSC and DTA.

DTA graphs showed the presence of a single crystalline peak for the ternary glass (0 mol % Fe_2O_3) along with two melting peaks as in Figure 4.6. This result suggested the presence of a single crystalline phase within this composition. At 2 mol % Fe_2O_3 two crystalline peaks with a single broad melting peak was identified, and upon magnification of this broad peak, another small peak appeared as a shoulder region. The presence of this second small peak was suggestive that a second crystalline phase was present in small amounts. For the 1, 3 4 and 5 mol % compositions, two crystalline and two melting peaks could be identified which suggested the presence of two separate crystalline phases within these compositions. However, a third melting peak could also be seen for 5 mol % composition. This finding is in agreement with the number of phases identified by Ahmed *et al.* (2004c) who carried out XRD analysis on these glass compositions revealed the presence of three phases sodium-calcium phosphate [$NaCa(PO_3)_3$] (which constituted the main phase), iron sodium phosphate [$NaFeP_2O_7$] (identified for all composition except 1 mol % Fe_2O_3); and a calcium phosphate [CaP_2O_6].

In this study, all tested glass compositions were metaphosphate glasses that were composed entirely of indefinitely long chains and/or ring units i.e. Q^2 species. These species are the most susceptible species to degradation because the cross-link density for the metaphosphate glass is zero (Walter *et al.*, 2001). Brow (2000) claimed that the properties of metaphosphate glasses are more affected by M-O-P (inter-chain) bonds (M refers to metal ions) than P-O-P bonds. The role of modifying metal oxides is different according to the coordination number or their electronic configurations. Addition of monovalent cations such as Na^+ leads to the breakage of P-O-P bonds with the creation of non-bridging oxygens that are charge balanced with one Na^+ as in Figure 4.35 (a).

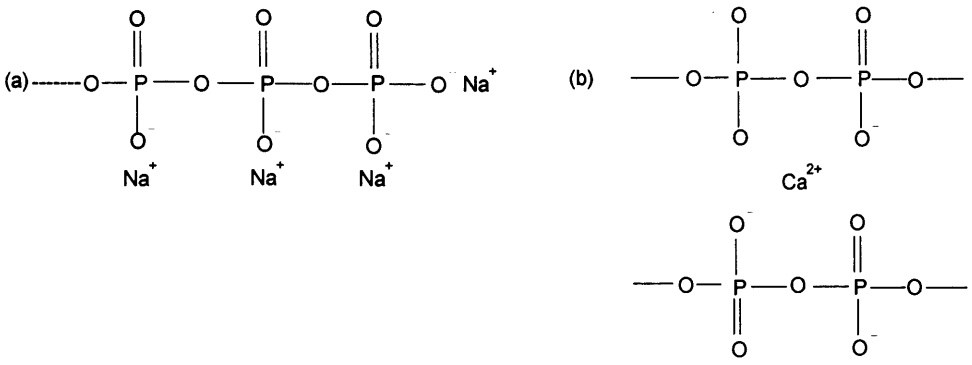

Figure 4.35: Schematic representation of phosphate glass structure: (a) chain structure, (b) cross link formation by Ca^{2+} ion (adapted from Uo *et al.*, 1998).

However, there were different mechanisms suggested for the role of divalent cation as Ca^{2+} in reducing the glass degradation. Firstly, Ca^{2+} with its two positive charges could form either a cross-linked structure by forming ionic bonds with two non-bridging oxygens (NBO) in between the glass chains as in Figure 4.35 (b) (Bunker *et al.*, 1984, Delahaye *et al.*, 1998, Uo *et al.*, 1998, Hoppe *et al.*, 2000, Franks, 2000). Secondly, it could form a more stable and stronge structure such as a ring instead of a chain (Kurkjian 2000). Thirdly, it could decrease the concentration of NBO sites, hence, the reactivity of the glass with water from the leaching solution and the diffusivity of water molecules and cations through the glass (Cacaina and Simon, 2003). Fourthly, it could slow down the formation of a hydrated layer on the glass surface by obstructing the diffusion of water molecules into the glass (Gao *et al.*, 2004a). Trivalent cations such as Al^{3+} or Fe^{3+} can act as network forming oxides and accordingly they enter the PO_4 tetrahedron backbone forming Al-O-P or Fe-O-P bonds that strengthen the glass network (Gao *et al.*, 2004a).

In this study, trivalent Fe^{3+} ions replaced the monovalent Na^{+}. Iron is one of the transition metals that can exist in more than one electronic configuration i.e., in more than one valence state where it can exist as Fe^{2+} or Fe^{3+}. The results in this study

showed that substitution of Fe_2O_3 for Na_2O greatly reduced the degradation of PGF. This was also found by Yu *et al.* (1997b), Marasinghe *et al.* (1997) and Ray *et al.* (1999) who explained the improvement in chemical durability of iron phosphate glass to the formation of Fe-O-P bonds which are more strong and hydration resistant at the expense of P-O-P bonds. However, it was unclear whether Fe existed as Fe^{2+} or Fe^{3+} since the valence state of iron in the glass would have a different effect on the glass properties. Fe^{3+} was more likely to act as a network former; however, Fe^{2+} would more likely act like a network modifier, and would improve the chemical durability to a lesser extent than would Fe^{3+} (Yu *et al.*, 1997b). Alternatively, Ray *et al.* (1999) reported that the chemical durability is improved regardless the concentration of Fe^{2+} and Fe^{3+} in the glass.

There are several factors which would affect the iron valence in the glass. Firstly, the iron content in the glass, where increasing the iron content leads to a decrease in Fe^{2+} and an improvement in the durability of the glass (Yu *et al.*, 1997b). Secondly, the processing temperature has a stronger effect on iron valence than time (Yu *et al.*, 1997b and Ray *et al.*, 1999). There would be an increase in Fe^{2+} concentration with increasing the melting temperature of glass preparation. Thirdly, the chemicals used for glass preparation; it was observed that the valence state of iron was more sensitive to the reducing ability of these chemicals. For example, glasses prepared with $NH_4H_2PO_4$ would be expected to contain considerably more Fe^{2+} than those prepared with P_2O_5. This was due to the release of NH_3 during degradation of $NH_4H_2PO_4$ that acts as a reducing agent (Marasinghe *et al.*, 1997 and Yu *et al.*, 1997b).

The valence state of iron would affect the glass structure and properties by its position within the glass (Yu *et al.*, 1997b, Melankovic *et al.*, 2001). Yu *et al.* (1997b)

proposed a model for the Fe in the iron-phosphate glass with a pyrophosphate composition as shown in Figure 4.36.

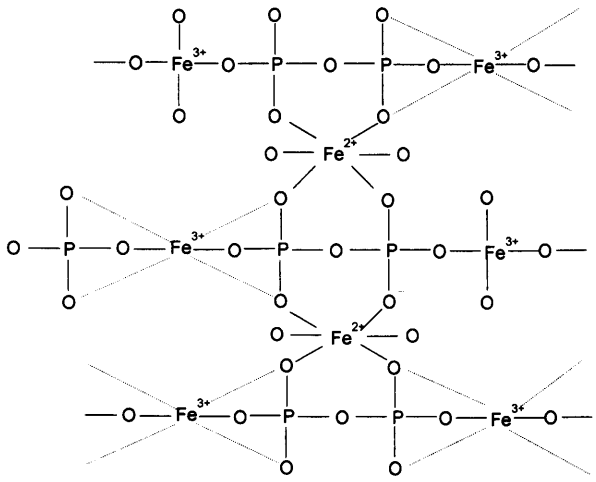

Figure 4.36: Idealized structure for iron pyrophosphate glass showing the position of Fe^{2+} and Fe^{3+} ions (adapted from Yu *et al.*, 1997b).

This model proposed that the smaller Fe^{3+} occupy tetrahedral or octahedral sites, or a highly distorted octahedral position within the backbone of the glass in place of P-O-P bonds with the exception of a P-O-P bond that was present in the P_2O_7 group. However, the larger Fe^{2+} occupied an octahedral position between the glass chains.

From the preliminary long term degradation study, the degradation presented as % weight loss was not linear over time, and the degradation levelled off after certain percentage of weight loss. This could be due to the static environment in which the study was carried out which favoured the precipitation. It was also observed that glass fibres with 0 to 2 mol % Fe_2O_3 were highly degradable compared to those with 3 to 5 mol %. Moreover, there was an inverse relationship between the fibre diameter and the degradation with fibres pulled at 1600 $m.min^{-1}$ showed the highest degradation. These findings were also confirmed by the short term study carried out over 96 h to

study the effect of both composition and fibre diameter using only fibres pulled at 400 and 1600 $m.min^{-1}$ on the degradation rate. From this short term degradation study, the degradation rate, calculated from the slope of the linear portion of the weight loss % against time curve up to 24 h, decreased with increasing Fe_2O_3 content for fibres pulled at 400 and 1600 $m.min^{-1}$. Compared to the control ternary composition, there was a reduction by two orders of magnitude in the degradation rate by incorporating 5 mol % Fe_2O_3.

The calculated degradation rate based on the values given in Table 4.5 was in the range of 2.7×10^{-6} to 4.5×10^{-8} $g.cm^{-2}min^{-1}$. This rate falls in the range reported by Bunker *et al.*, (1984) who stated that the rate of phosphate glass degradation ranged over four orders of magnitude from 10^{-4} to 10^{-9} $g.cm^{-2}min^{-1}$. It has also been reported that the iron modified phosphate glass can degrade as slowly as 10^{-8} $g.cm^{-2}.h^{-1}$ (Parsons *et al.*, 2004b). Conversely, the rate of degradation obtained in this study was one order of magnitude higher than that measured by Rinehart *et al.* (1999), which was quoted at 10.9×10^{-9} $g.cm^{-2}min^{-1}$. In Rinehart's study, the degradation was carried out on bundles of fibres with composition of (54 PO_4-27 CaO-12 ZnO- 2.5 Na_3PO_4-4.5 Fe_2O_3) in phosphate-buffered saline (PBS). A lower rate of degradation would be expected in PBS than in deionised water due to a higher ion concentration.

Theoretically, by using the calculated rate of degradation from the slopes of the % weight loss versus time over 24 h, it can be assumed that the fibres pulled at 400 $m.min^{-1}$ (giving rise to an average fibre diameter of 31.6 ± 6.5 μm) would completely degrade within 9, 52 and 92 h for fibres with 0, 1 and 2 mol % Fe_2O_3 respectively. However, in practice, due to the static environment in which the study was carried out, which may have lead to solution saturation followed by ion precipitation and/or reduced rates of degradation, the fibres took a longer time to completely degraded.

This could be due to the increase in the concentration of solution around the fibres by the dissolved phosphate chains and cations, which could in turn decrease the dissolution dynamic force (saturation effect) as reported previously by Reinhart *et al.*, (1999). The saturation effect can also be used to explain the observed non linear behaviour observed after 24 h. In a similar study carried out by Delahaye *et al.* (1998) on metaphosphate bulk glasses in an acidic solution [pH = 3] up to 300 minutes, the degradation was linear only up to 100 minutes, which then decreased showing non linear behaviour. The proposed explanation was the increase in the ionic strength of the solution leading to an increase in the electrostatic interaction in the hydrated layer, and this was responsible for the observed decrease in degradation and the non-linear behaviour obtained.

The fibre degradation behaviour of the iron containing glasses followed an exponential relationship against Fe_2O_3 content as shown in Figure 4.37, which closely mirrored the behaviour observed for the bulk glasses containing iron (Ahmed *et al.*, 2004, Parsons *et al.*, 2004b).

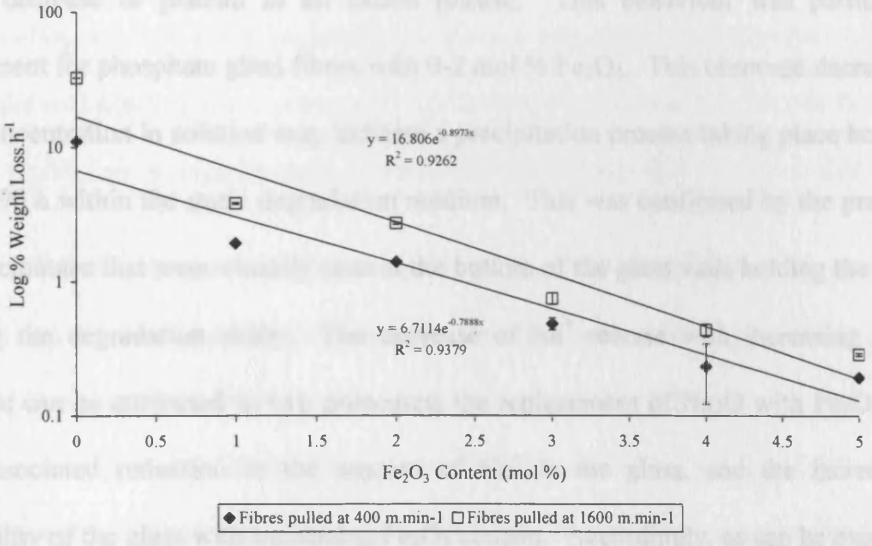

Figure 4.37: Log % weight loss.h^{-1} against iron oxide content.

From Figure 4.37, the degradation rate was higher for fibres with smaller diameters (pulled at 1600 $m.min^{-1}$) than those of higher diameter (pulled at 400 $m.min^{-1}$). This can be assumed to be due to a higher surface area to volume ratio. However, if the % weight $loss.h^{-1}$ was normalised to the surface area, and then plotted against Fe_2O_3 content the same exponential relationship could be obtained but in a reverse order. Hence, the fibres pulled at 1600 $m.min^{-1}$ showed lower values than that of fibres pulled at 400 $m.min^{-1}$. This suggested that the degradation process was more complex than expected.

The ion release study is important since the ions released from a biomaterial into the surrounding environment may affect cellular behaviour and function. Unlike silicate glass, dissolved phosphate chain and rings are quite stable in aqueous environment and only hydrolyse slowly, and under normal conditions, phosphates in aqueous solution never polymerise, as a result the application of chromatographic technique is useful (Sales *et al.*, 2000).

As it can be observed from the release data, there was an initial rapid increase followed by a decrease or plateau in all cation release. This behaviour was particularly prominent for phosphate glass fibres with 0-2 mol % Fe_2O_3. This observed decrease in ion concentration in solution may indicate a precipitation process taking place between 24 to 96 h within the static degradation medium. This was confirmed by the presence of precipitates that were visually seen at the bottom of the glass vials holding the fibres during the degradation study. The decrease of Na^+ release with increasing Fe_2O_3 content can be attributed to two processes; the replacement of Na_2O with Fe_2O_3 with the associated reduction in the amount of Na^+ in the glass, and the increase in durability of the glass with increasing Fe_2O_3 content. Accordingly, as can be expected, the glass with no Fe_2O_3 showed the highest levels of Na^+ released. Intriguingly,

however all glass compositions contained 30 mol % CaO, there was a decrease in Ca^{2+} release with an increase in Fe_2O_3 content. This confirmed that the amount of Ca^{2+} released was affected by the degradation rate. In the same way, the highest Fe^{3+} released was observed for the glass with the lowest Fe_2O_3 content which may suggest that the release of Fe^{3+} was dictated by the glass degradation rather than the amount of Fe^{3+} available in the glass. In all compositions, both the amount and rate of Na^+, Ca^{2+} and Fe^{3+} ions released were higher for fibres pulled at 1600 $m.min^{-1}$ than for those pulled at 400 $m.min^{-1}$ and this was related to the surface area to volume ratio effect as shown in Table 4.6.

All anionic species release rates decreased with increasing Fe_2O_3 content; the highest release was observed for the cyclic $P_3O_9^{3-}$ metaphosphate anion when compared to the orthophosphate PO_4^{3-} and the linear $P_3O_{10}^{5-}$. This finding suggested that a relatively significant proportion of the $P_3O_9^{3-}$ anion was present in the original glass structure as reported for similar ternary-based phosphate glass systems (Ahmed *et al.*, 2004c). As was shown in the cation release, fibres with the greater surface area to volume ratio yielded greater rates of release. The release of these phosphate species into the surrounding medium could be confirmed by the reduction in pH that was observed over the degradation time. Since the dissolution of these species into the deionised water could form phosphoric acid, and this was also be found by Reis *et al.* (2001).

From the above, it was clear that both Na^+ and Ca^{2+} released at the same rates, and $P_3O_9^{3-}$ was released at the highest amount compared to the other anions species. This finding suggested that these three ions played a major part in forming the precipitate that was seen at the bottom of the glass vials. This could be confirmed by finding of Ahmed *et al.* (2004c) who performed an XRD study on these glass compositions, and their results indicated that sodium calcium phosphate [$NaCa(PO_3)_3$] constituted the

main phase of all glasses tested. At the same time there was no $P_2O_7^{4-}$ detected in the leached solution for iron containing glass fibres even though $NaFeP_2O_7$ was the dominant phase for the higher Fe_2O_3 content glass. This may be explained by the Yu *et al.* (1997b) model shown in Figure 4.36 where each P_2O_7 species was strongly bonded to two Fe^{3+} ions that masked the release of P_2O_7.

The morphological changes due to degradation studied with SEM suggested that the degradation process began with the formation of an outer hydrated gel layer. The cracks seen in on the surface of the fibre may be disintegration of this gel layer during the drying process for SEM preparation. This outer layer has also been observed by Choueka *et al.*, (1995) on the surface of the phosphate glass fibres. Moreover, Delahaye *et al.* (1998), Clement *et al.* (1999a,b), and Gao *et al.* (2004b) reported that dissolution of metaphosphate glass occurred with the formation of hydrated phosphate chains of several micrometers of thickness on the glass surface that separated in solution without hydrolysis. This was confirmed by solid state MAS-NMR study where the degraded glass sample maintained the same structure and composition of the bulk glass (Delahaye *et al.*, 1998). In literature, this layer was suggested to have a similar network structure to the parent glass except that the alkali and alkali earth ions had been replaced with hydrogen, plus one or more water molecule thus this structure was referred to as a hydrogen glass. Furthermore, this hydrogen glass undergoes localised hydrolysis and condensation over time to form a gel layer (Cacaina and Simon, 2003). Therefore, the reduction in pH of the medium during degradation may be accounted for by the hydrated phosphate chains dissociating into phosphoric acid.

By ageing over a longer period of time between 1 to 52 weeks, the precipitate formed due to the completely degrading fibres with 2 mol % Fe_2O_3 showed formation of tube like structure which was firstly observed by Knowles (2003) who found that the PGF

were able to form polycrystalline tubes when they degraded. However, with the relatively slow degrading fibres containing 5 mol % Fe_2O_3 showed this tube structure, but at relatively longer time (12-78 weeks) which may further support the finding that the fibres degradation rate inversely related to the amount of Fe_2O_3 in the glass. The mechanism of this tube formation is still not understood, and a further study will be required to help identify this mechanism. One suggested theory for this tube formation could be precipitation/reprecipitation process. This theory could be explained by separation of the hydrated layer that formed at the initial stage of degradation from the underlying core of the glass fibre. Eventually, the peeling of this layer into the surrounding medium occurred when it became totally hydrated. Dissociation of this separated layer into small species then occurred, and these small species started to build up in the surrounding medium. At a longer time period, when the medium became saturated with these species, their reprecipitation occurred around the core of the degrading fibres. In such case, the degrading fibres act as template for small species to build on. This theory could be employed for explaining the tube formation with 2 mol % Fe_2O_3 fibres. With 5 mol % Fe_2O_3 fibres, on the other hand, the mechanism seemed to be different since the fibres have a different morphology. It is more acceptable that the hydrated layer could not leach into the medium, but acts as a protective layer, while the fibres degrade internally from the core under the protective outer hydrated layer.

This iron containing phosphate glass fibres particularly those with 3 up to 5 mol % Fe_2O_3 could be potentially used as a 3-D scaffold for soft such as muscle, ligament and tendon and hard tissue engineering application such as bone. The glass fibres degradation rate was a decisive factor in determining the nature of cell-glass fibre composition interaction, and the more soluble glass fibres failed to support the viability of cells as observed by Bitar *et al.*, (2005). Also these glass fibres could be

potentially used in combination with either natural or synthetic polymers to provide the channel like structure within these polymers which may help the ingrowth of vascularisation and the diffusion of nutrient and waste through the scaffold.

4.5. Overall Discussion for the Phosphate-Based Glass Fibres

The potential use of phosphate glass fibres (PGF) as biomedical materials was investigated using two different quaternary glass systems. Two modifying oxides, CuO and Fe_2O_3 were incorporated into the highly soluble ternary glass system (in molar fraction) 50 P_2O_5-30 CaO-20 Na_2O developed for either antimicrobial or tissue engineering applications. These additional oxides were incorporated into the glass structure by partially substituting Na_2O. Fibres of different diameters were produced for each glass system from the melt by changing the setting of a custom made in house fibre rig. The effect of both composition and fibre diameter on thermal, structural properties, degradation and ion release both the cationic and anionic species was carried out.

Copper and iron are transition metals that can exist in more than one electronic configuration. Aside from the actual valence state of each ion, partial replacement of Na^+ by Cu^{2+} or Fe^{3+} produced an increase in density, thermal stability, and durability as measured by the degradation behaviours of glass fibres. This effect may be related to an increase in the cross-link density of the phosphate network together with the formation of the more water resistant Cu-O-P or Fe -O-P bonds compared to P-O-P bonds. However, Fe^{3+} had a more pronounced effect than Cu^{2+} on the above mentioned properties, the most striking the degradation rate of the fibres. The addition of Fe_2O_3 only up to 5 mol % produced a decrease in degradation rate by two orders of

magnitudes compared to the ternary formulation. Additionally, glasses with different degradation times ranging from several hours to weeks can be produced with incorporation of different amount of Fe_2O_3. As previously noted, under the given test conditions, copper containing glass system was completely degraded within several hours even when incorporated at 10 mol %. On the other hand, glasses with 0 and 1 mol % Fe_2O_3 completely degraded within several hours, 2 mol % Fe_2O_3 within a week, while those with more than 3 mol % remained for several weeks. This difference in behaviour of the two glass systems may reflect that when both Cu and Fe are incorporated in the glass, they have different roles, since Cu act only as network modifier while Fe can act as both network modifier and/or former. It was known the network former has strongest effect on the glass properties, e.g. Al^{+3}. The degradation rate followed an inverse linear relationship against CuO content, however, it followed inverse exponential behaviour against Fe_2O_3. Also, plotting the degradation rate against density for copper containing PGF followed an inverse linear relationship as shown in Figure 4.38; however, an inverse exponential relationship was observed for iron containing glass fibres as given in Figure 4.39. These findings reinforced the hypothesis that the role of both Cu and Fe is different.

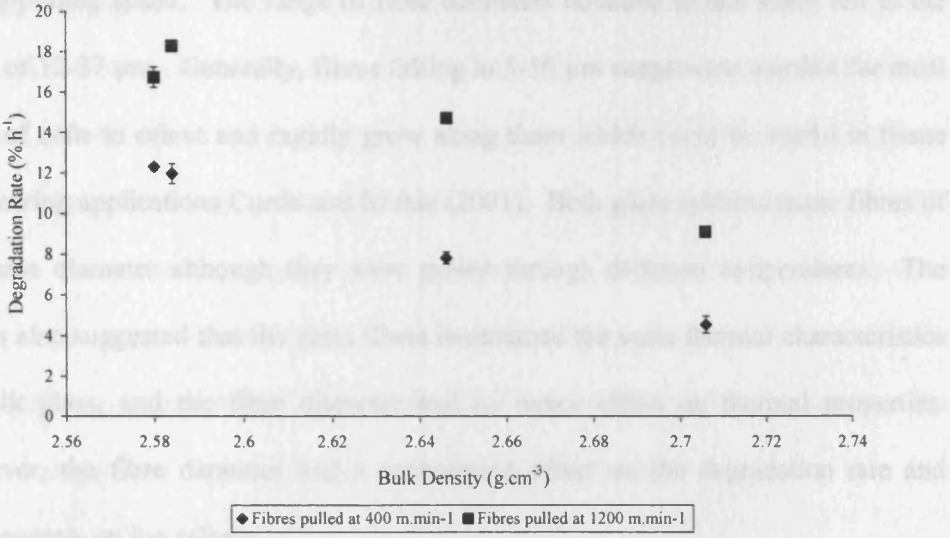

Figure 4.38: Degradation rate against bulk density of copper containing phosphate glass fibres.

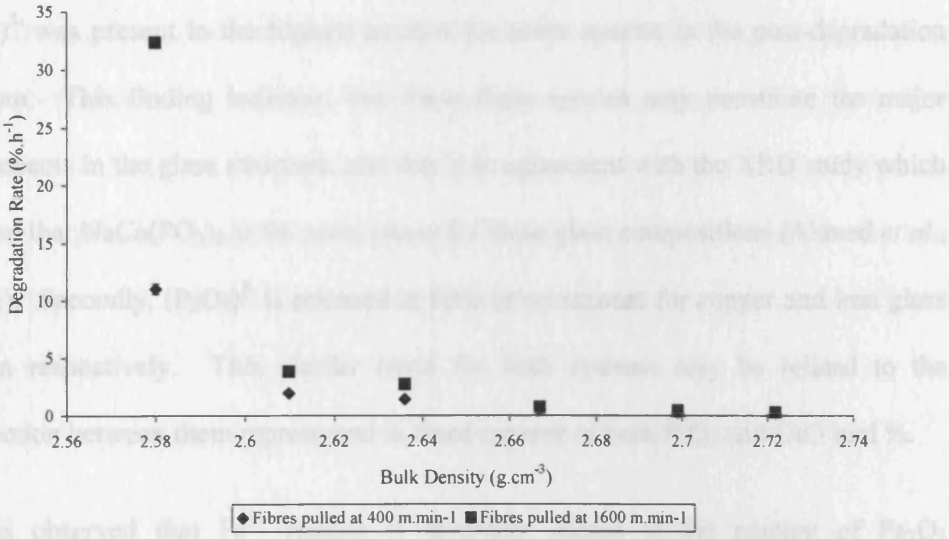

Figure 4.39: Degradation rate against bulk density of iron containing phosphate glass fibres.

Not all glasses make fibres, but in this study both glass systems were effectively pulled into fibres of different diameters within micrometer scale by controlling the drum speed. It was observed that there is an inverse relationship between fibre diameter and

the rig-pulling speed. The range of fibre diameters obtained in this study fell in the range of 12-37 μm. Generally, fibres falling in 5-50 μm range were suitable for most types of cells to orient and rapidly grow along them which could be useful in tissue engineering applications Curtis and Riehle (2001). Both glass systems made fibres of the same diameter although they were pulled through different temperatures. The results also suggested that the glass fibres maintained the same thermal characteristics of bulk glass, and the fibre diameter had no major effect on thermal properties. However, the fibre diameter had a pronounced effect on the degradation rate and consequently on ion release.

The ion release study showed two common features for both glass systems. Firstly, both Na^+ and Ca^{2+} released in the same amount for each glass compositions, also $(P_3O_9)^{3-}$ was present in the highest amount for anion species in the post-degradation medium. This finding indicates that these three species may constitute the major components in the glass structure, and this is in agreement with the XRD study which showed that $NaCa(PO_3)_3$ is the main phase for these glass compositions (Ahmed *et al.*, 2004c). Secondly, $(P_2O_7)^{4-}$ is released in little or no amount for copper and iron glass system respectively. This similar trend for both systems may be related to the connection between them represented in fixed amount of both P_2O_5 and CaO mol %.

It was observed that Fe^{3+} release is inversely related to the amount of Fe_2O_3 incorporated in the glass, where the glass with the lowest Fe_2O_3 content (1mol %) released the highest amount of Fe^{3+} compared to glass with the highest Fe_2O_3 (5 mol %). This was not the case with copper system, which can be considered as advantageous for the copper system that was proposed for antibacterial delivery use.

The antibacterial susceptibility against *S. epidermidis* showed that the addition of CuO into PGF was effective in reducing the number of bacteria attached to the fibres, which

was dose dependent. However, the fibre diameter had no significant effect except for the ternary PGF control. Therefore, the dominant effect was the composition with 10 mol % CuO were the most effective in preventing colonisation and reducing number of viable bacteria in the local environment. PGF with 10 mol % could be a promising for potential wound healing applications. Nevertheless, in general this glass system (within the range of tested compositions) is highly degradable, and further modification by introducing a higher amount of CuO would be needed, however the cytotoxicity issue of copper should be considered in this case.

Iron containing PGF seem to be promising substrate for potential tissue engineering applications such as muscle, ligament, tendon, and bone, particularly those with 3 up to 5 mol % Fe_2O_3. PGF containing 0 to 2 mol % Fe_2O_3 did not support cell growth more than week as observed by Bitar (2005), and this could be explained by the high degradation nature of these compositions. Moreover, upon degradation, these PGF form tube-like structure. In such case, they could be potentially used in combination with either natural or synthetic polymers to help the ingrowth of vascularisation and the diffusion of nutrient and waste through the scaffold, and also for cell transplantation.

Chapter 5

The Investigation of Plastic Compression of Collagen Gels for the Production of Dense Scaffolds

5.1. Introduction

This chapter investigated the mechanical and viscoelastic properties of reconstituted collagen gels under unconfined compression. This was performed by analysing the gels through quasi-static mechanical properties, dynamic mechanical analysis, and creep/recovery tests under different loading regimes. This was carried to investigate the mechanism of the plastic compression (PC) technique for preparation of tissue analogous implants based on collagen. Dense collagen scaffolds were produced by PC through a combination of compression and blotting actions, and characterised in term of weight loss, morphology, thermal, and tensile mechanical properties.

5.2. Experimental

5.2.1. Materials

5.2.1.1 **Raw Materials** (listed in Table 5.1)

Table 5.1: Raw materials used in collagen gel preparation.

Materials	**Supplier**
Rat Tail Collagen (Type I) Solution	First Link Ltd, UK.
Dulbecco's Modified Eagles Medium (x10 DMEM)	Sigma-Aldrich Co., UK.
Sodium Hydroxide (5 M NaOH)	BDH, UK.

5.2.1.2. Method of Gel Preparation

Collagen gels were prepared by neutralisation of 3 ml of sterile rate tail type I collagen (2.1 $mg.ml^{-1}$ protein in 0.6 % of acetic acid), 0.35 ml of 10 x concentration of Dulbecco's Modified Eagle's Medium (DMEM) with 5 M sodium hydroxide to initiate the temperature dependant gelation process during which the collagen solution assembled into linear filaments, which then aggregated to form fibrils. The neutralised collagen was left to set at 37 °C, in a 5 % CO_2 incubator for 30 minutes.

5.2.2. Methods of Characterisations

5.2.2.1. Investigations into Unconfined Compression of Collagen Gels

This study was carried out using a Dynamic Mechanical Analyzer (DMA-7e, Perkin-Elmer Instruments, USA).

5.2.2.1.1. Technique

The DMA-7e has been frequently used in materials science to characterize the mechanical and viscoelastic behaviour of materials (Nazhat *et al.*, 2000, 2001, 2004, Rich *et al.*, 2002, Bleach *et al.*, 2002, Blaker *et al.*, 2004). It is composed of four functional components: motor, detector, environmental, and measuring systems as shown in Figure 5.1.

The DMA-7e uses a linear force motor which can produce a downward force of 8500 mN and an upward force of 6500 mN. Dynamic force can be applied at frequencies from 0.01 to 51 Hz. The force is applied to the sample through the central core rod which is suspended in a magnetic field. The detector, a linear variable differential transducer (LVDT), measures the vertical deflection of the sample. The LVDT provides high sensitivity and repeatability for accurate measurements.

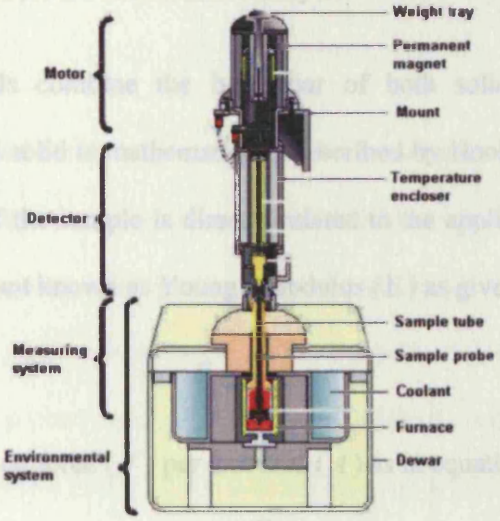

Figure 5.1: Cross section of dynamic mechanical analyzer (from DMA-7e, Perkin-Elmer manual).

The environmental system includes the purge gas, cooling device, and furnace, to allow the analysis of the material during cooling as well as during heating experiments. The measuring system holds a sample in place for testing with the DMA-7e and can accommodate a number of sample geometries and sizes. The systems used in this study were parallel plate and extension analysis measuring systems which are shown in Figure 5.2 a and b.

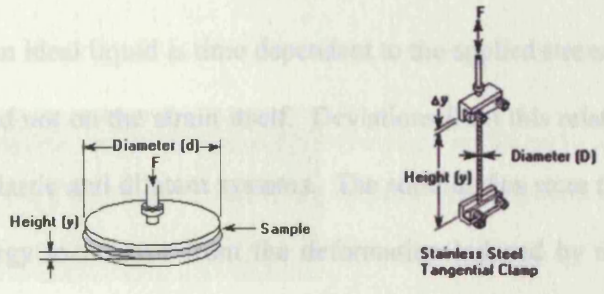

Figure 5.2: (a) The parallel plate and (b) extension analysis measuring system (from DMA-7e, Perkin-Elmer manual).

a) Theory of Dynamic Mechanical Analysis

Viscoelastic materials combine the behaviour of both solids and liquids. The behaviour of an ideal solid is mathematically described by Hooke's Law, which states that the strain (ε) of the sample is directly related to the applied stress (σ), and the proportionality constant known as Young's modulus (E) as given in equation (5.1).

$$E = \frac{\sigma}{\varepsilon} \tag{5.1}$$

Where σ is the applied force (F) per unit area (A) as in equation (5.2).

$$\sigma = \frac{F}{A} \tag{5.2}$$

However, ε is the change in dimension per unit dimension. The ideal solids will recover completely after the removal of the applied stress. Deviations from this relationship occur whenever the applied stress exceeds the elastic limit of the material i.e. irrecoverable sample deformation has occurred. However, for ideal liquids, Newton proposed that the applied stress is proportional to the rate of strain $\left[\frac{d\varepsilon}{dt}\right]$, the proportionality constant being referred to as viscosity (η) as in equation (5.3).

$$\eta = \frac{\sigma}{\left[\frac{d\varepsilon}{dt}\right]} \tag{5.3}$$

The response of an ideal liquid is time dependent to the applied stress i.e. dependant on the strain rate, and not on the strain itself. Deviations from this relationship in liquids occur in pseudoplastic and dilatant systems. The solid bodies store the applied energy and use this energy to recover from the deformation induced by the applied stress; whereas, the liquids dissipate the energy as heat and do not recover from the deformation. Viscoelastic materials combine both solid (elastic) and liquid (viscous)

properties, where the applied stress is proportional to the resultant strain and the strain rate.

In dynamic mechanical analysis (DMA), a sinusoidal stress or strain is applied to the sample and the mechanical response is measured as a function of oscillatory frequency, temperature, or time. For a Hookean solid, the maximum strain is observed at the same instance of the maximum stress. Conversely, a Newtonian liquid will exhibit a 90° phase lag to an applied stress. Viscoelastic materials will exhibit phase angles between the two extremes (Jones, 1999 and Krishnan *et al.*, 2004) as shown in Figure 5.3.

DMA measures the dynamic moduli ($E^{\backslash}$ and $E^{\backslash\backslash}$) and $\tan\delta$ as a function of time, where $E^{\backslash}$ is the elastic or storage modulus, $E^{\backslash\backslash}$ is the viscous or loss modulus, and $\tan\delta$ is the mechanical loss tangent or phase angle.

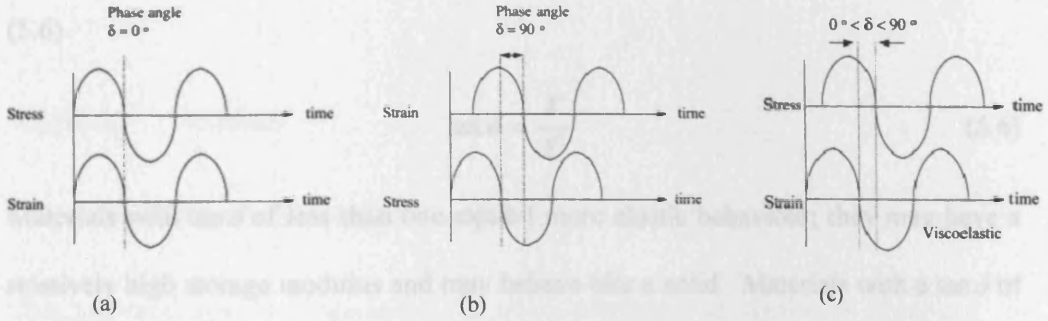

Figure 5.3: Material response (strain) following application of an oscillatory stress for (a) an ideal solid, (b) an ideal liquid, and (c) viscoelastic materials (from Jones, 1999).

The storage modulus, a measure of the energy stored within the material during deformation that will recover immediately after removal of load, reflects the solid like component of the viscoelastic material, and is calculated from equation (5.4).

$$E^{\backslash} = \frac{\sigma_o}{\varepsilon_o}\cos\delta \tag{5.4}$$

Where: σ_o is the dynamic stress amplitude, ε_o is the dynamic strain amplitude, and δ is the sample phase angle.

The loss modulus, a measure of the energy dissipated during deformation, reflects the liquid-like component, and it is calculated from equation (5.5).

$$E^{\backslash\backslash} = \frac{\sigma_o}{\varepsilon_o}\sin\delta \tag{5.5}$$

The phase angle, a measure of damping, gives an indication of state or phase of a material, and it describes the lag in time between stress and the strain sine waves. It also indicates relative importance of both viscous and elastic behaviours, and is calculated from the relationship between the loss and storage modulus as in equation (5.6).

$$\tan\delta = \frac{E^{\backslash\backslash}}{E^{\backslash}} \tag{5.6}$$

Materials with $\tan\delta$ of less than one exhibit more elastic behaviour; they may have a relatively high storage modulus and may behave like a solid. Materials with a $\tan\delta$ of more than one exhibit more viscous behaviour; they may have relatively high loss modulus, and behave more like a liquid.

b) Theory of Creep and Recovery Analysis

A common characteristic of viscoelastic systems is that the material continues to deform as a function of time; this phenomenon is referred to as creep. For the creep

and recovery test, an initial constant compressive stress is applied to the sample, and the resulting deformation is measured as a function of time. After this creep part, the compressive stress is removed and the recovery part commences; the response of the sample during recovery is also recorded. In viscoelastic materials, the instantaneous response to the applied stress corresponds to the elastic component, while the gradual deformation that follows is due to the viscous component within the material. When the stress is removed, the recovery response will be due to the elastic component, while the non-recoverable portion is due to the viscous portion as shown in Figure 5.4.

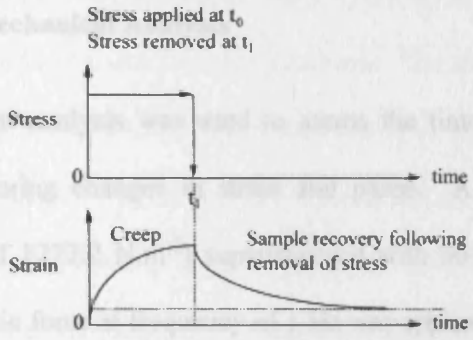

Figure 5.4: Typical creep response of viscoelastic solids (from Jones, 1999).

5.2.2.1.2. Methods

a) Quasi-Static Mechanical Analysis

This test was used to characterise the stress-dependant properties of materials. It applied a linearly increasing quasi-static stress to the sample, and the resultant deformation was recorded as a function of the applied stress. The test was conducted on ten repeat cylindrical-shaped specimens prepared by casting 700 µl of neutralized collagen suspensions into 12 mm diameter well plates (Perkin Elmer Life Sciences, UK), and set as previously described in Section 5.2.1.2. A DMA-7e with parallel plate measuring system was used for this study. Before starting the run, the system was

allowed to equilibrate at room temperature until the probe position became relatively stable. The sample height was measured before starting the test and the top plate diameter (10 mm) was used as the testing diameter. The effect of two loading rates on the response of the gels was investigated. An increasing static force from 10 to 1110 mN was applied to the sample at 100 and 500 $mN.min^{-1}$ (1273.2 and 6366 $N.m^{-2}.min^{-1}$ respectively). The stress-strain relationship was obtained, and the software (Pyris™ version 5 software, Perkin-Elmer, UK) also calculated the corresponding modulus of elasticity to be used as an indicator of the material stiffness or rigidity.

b) Dynamic Mechanical Analysis

Dynamic mechanical analysis was used to assess the time–dependant behaviour of materials by monitoring changes in strain and phase. A static force of 100 mN, (equivalent stress of 1273.2 $N.m^{-2}$) superimposed with 50 mN (equivalent stress of 636.6 $N.m^{-2}$) dynamic force at frequency of 1 Hz was applied to ten repeat cylindrical-shaped specimens as in Figure 5.5.

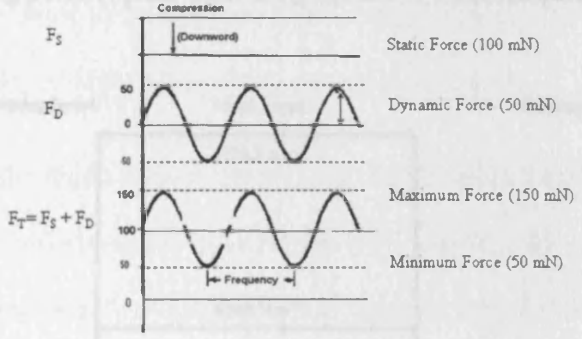

Figure 5.5: Diagrammatic model of the dynamic scan used for analysis of the dynamic properties of collagen gel. Where the total force is the sum of the static and dynamic force ($F_T=F_S+F_D$).

Specimens were tested using parallel plate measuring system at room temperature. The measured material properties were storage modulus (E'), loss modulus (E''), and mechanical loss tangent ($\tan\delta$) as a function of time, up to 15 minutes.

c) Creep and Recovery Analysis

This test was used to assess the time dependant behaviour of materials. Under a creep part of the experiment, a fixed stress was applied instantaneously to the sample and held constant for a given period of time, and the resultant strain was measured as a function of time. In the recovery part of the test, the static stress was instantaneously reduced, and the resultant strain was also measured. The design of the creep/recovery experiment is shown in Figure 5.6. Specimens were pre stressed under 12.7 $N.m^{-2}$ for 5 minutes to equilibrate. The stress was then increased to 25.5, 127.3, 636.6 and 1273.2 $N.m^{-2}$ (equivalent force of 2, 10, 50, and 100 mN) for 10 minutes (creep part). This was then followed by reducing the stress to 12.7 $N.m^{-2}$ for a further 10 minutes (recovery part). Ten repeat cylindrical-shaped specimens were tested under each loading stress using parallel plate measuring system at room temperature.

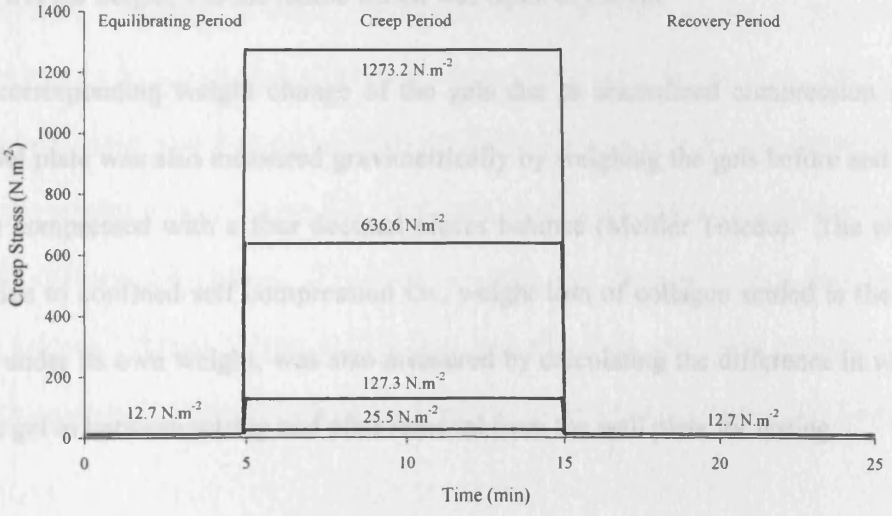

Figure 5.6: Stress regime applied during creep and recovery analysis.

5.2.2.1.3. *Statistical Analysis*

The linear regression analysis test was used to assess the effect of loading stress on strain. Student's *t*-test was used to asses the effect loading rate on gel stiffness. Significance was set at $p < 0.05$ for all comparisons using SPSS 12 package.

5.2.2.2. Plastic Compression to Produce Dense Collagen Constructs

5.2.2.2.1. *Analysis of Plastic Compression of Collagen Gels*

This test was carried out to study the changes in height of collagen gels as function of time when exposed to two different compressive stresses on ten repeat cylindrical-shaped specimens. These specimens were compressed for 5 minutes under stresses of 0.14 and 1.4 $kN.m^{-2}$ using the DMA-7e analyzer with the top plate diameter of 15 mm. The percentage height reduction due to sample compression was related to the starting nominal height of 6.2 mm which was calculated from equation (5.7).

$$V = \pi r^2 h \qquad (5.7)$$

Where: V is the volume of collagen gel which was equal to 0.7 cm^3, πr^2 is the surface area, h is the height, r is the radius which was equal to 0.6 cm.

The corresponding weight change of the gels due to unconfined compression using parallel plate was also measured gravimetrically by weighing the gels before and after being compressed with a four decimal places balance (Mettler Toledo). The weight loss due to confined self compression i.e., weight loss of collagen settled in the well plate under its own weight, was also measured by calculating the difference in weight of the gel in between setting and after removal from the well plate for testing.

5.2.2.2.2. *Application of the Plastic Compression Technique*

Collagen gel was prepared as described previously in Section 5.2.1.2., and after neutralization with NaOH, 2 ml of preset collagen solution was pipetted into a rectangular mould (Delrin® of the dimensions of 33 x 13 x 4 mm). A microscope glass slide formed the base of the mould for easy removal of collagen after setting, and was attached on both sides to the mould by a pair of clamps. Then the collagen solution was allowed to set at 37 °C, in CO_2 incubator for 30 minutes. Following setting and incubation, the gels were made free by running a sharp surgical blade along the edges of the gels just before removal from the mould. After removal from the mould, the gel of a nominal height of 4.6 mm was routinely compacted by a combination of compression and blotting using layers of meshes and paper sheets. A 165 μm thick stainless steel mesh of approximately 300 μm size and a layer of nylon mesh of approximately 50 μm mesh size were placed on a double layer of absorbent paper with the two stainless steel spacers of 300 μm thickness. The construct was placed between the spacers on the nylon mesh, covered with a second nylon mesh. A standard plastic compression (PC) method was used where a compressive stress of 1.4 $kN.m^{-2}$ was applied for 5 minutes at room temperature using a plate, giving a flat sheet of approximately 50 μm protected between two nylon meshes (Brown *et al.*, 2005). The compressed sheet was then rolled along its short axis to give a spirally assembled PC collagen construct as in Figure 5.7. This was used as the routine processing method for PC collagen preparation. The sample weight was recorded with a four decimal place balance (Mettler Toledo, UK) before and after they have been prepared into a spirally assembled collagen to determine weight loss due to compression and blotting.

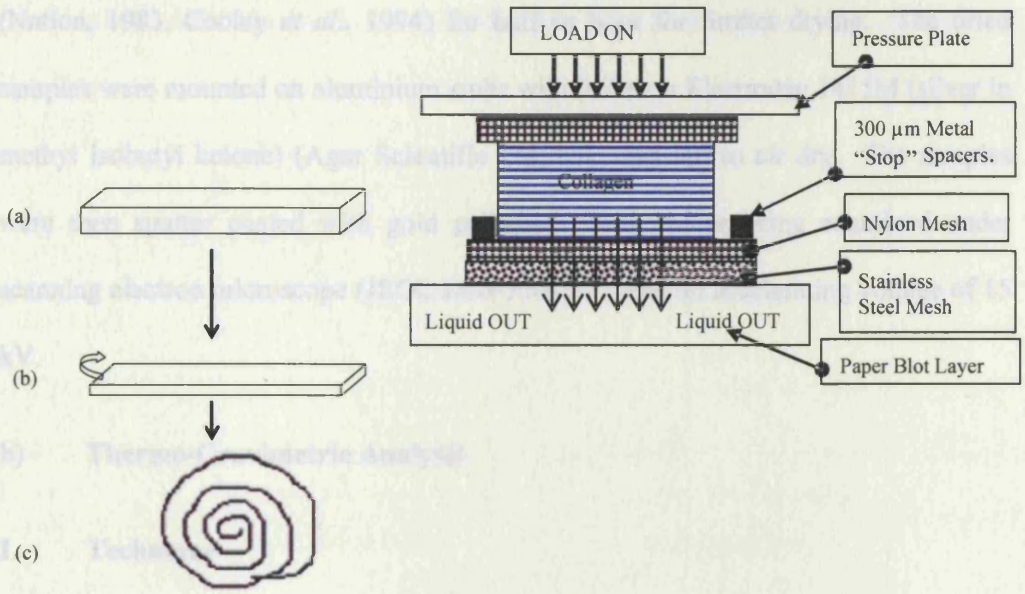

Figure 5.7: Diagrammatic representation of plastic compression technique for preparing collagen. (a) non-compressed gel (b) compressed sheet, and (c) a spirally assembled PC collagen (adapted from Brown *et al.*, 2005).

5.2.2.2.3. Characterisation of the Properties of PC Collagen

a) Scanning Electron Microscopy

The SEM of collagen was carried out to detect the changes in the microstructure as a result of the plastic compression processing technique. Samples for SEM were fixed in 4 % paraformaldehyde in 0.1 M sodium cacodylate buffer overnight at room temperature followed by washing in distilled water for 10 minutes. Afterwards, the samples were soaked for 1 hour in 1 % tannic acid (w/v) in 0.05 M sodium cacodylate for further fixation or stabilisation of collagen fibrils (Simionescu, and Simionescu, 1976, Wollweber *et al.*, 1981). The samples were then dehydrated in a series of graded ethanol of 70, 90, 96, and 100 %, respectively, and kept for half an hour in each concentration. Dehydrated samples were immersed in hexamethyldisilazane (HMDS)

(Nation, 1983, Cooley *et al.*, 1994) for half an hour for further drying. The dried samples were mounted on aluminium stubs with Acheson Electrodag 1415M (silver in methyl isobutyl ketone) (Agar Scientific Ltd, UK) and left to air dry. The samples were then sputter coated with gold palladium alloy before being examined under scanning electron microscope (JEOL JSM-5500LV) with an accelerating voltage of 15 kV.

b) Thermo-Gravimetric Analysis

I. Technique

In thermogravimetric analysis (TGA), changes in the weight of a known amount of material are monitored as a function of temperature or time, while it is purged with an inert gas. TGA can provide quantitative information resulting from any processes causing an obvious weight variation during controlled heating. For example, it was previously used by Wang *et al.* (2001) to verify the amount of hydroxyapatite (HA) in hydroxyapatite incorporated polysulfone composites. Shan *et al.* (2004) used TGA to evaluate the amount of collagen in collagen-g-PMMA/In_2O_3 nanocomposite, while Chang *et al.* (2002) used TGA to assess the amount of hydrated water and organic content in cross-linked HA/collagen nanocomposites. Moreover, TGA is a suitable technique to investigate the thermal stability of a polymer (Alexy *et al.*, 2003, Mano *et al.*, 2003), since the decomposition temperature represents the upper limit of the processing temperature. It also can be used to study the stoichiometry and kinetics of thermal decompositions helping in identification of the degradation mechanisms (Meenan *et al.*, 2000, Mano *et al.*, 2003).

Generally, two types of phenomena are shown on a TGA plot and are demonstrated in Figure 5.8. Weight loss (a), the most frequent phenomenon, is generally represented

by a downward shift in the plot, and weight gain (b) represented by an upward shift in the plot.

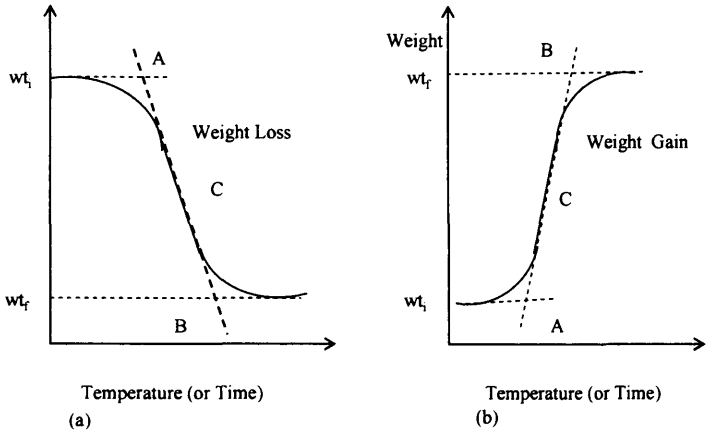

Figure 5.8: Diagrammatic representation of (a) weight loss and (b) weight gain during thermogravimetric run. Point A is the start of weight variation, B is the end of weight variation, and C is the inflexion point. wt_i is the initial while wt_f is the final weight (adapted from the DTA / TGA manual).

II. Method of analysis

Thermo-gravimetric analysis of the spirally assembled PC collagen was conducted using a Setaram Differential Thermal Analyser (DTA/TGA) to identify fluid content and therefore collagen concentration in PC collagen. The loss of sample weight during a linear increase in temperature was analysed at a uniform scanning rate of $20°C.min^{-1}$. The scanning sequence was ramped between 20 to 1000 °C. Samples of approximately 110 mg were put into a 400 µl platinum crucible. The test was carried out on five repeat specimens under air to provide both an oxidising atmosphere for the removal of organic component (collagen) and a flowing gas for the removal of fluid. A blank run was carried out with an empty platinum crucible to set the base line, and this was subtracted from the original data to correct any data obtained.

c) Mechanical Properties under Quasi-Static Uniaxial Tensile Testing

This test was carried out to identify the mechanical properties of PC collagen under tensile mode using the Perkin-Elmer DMA 7-e. The tests were carried out on the spirally assembled PC collagen (Figure 5.7 (c)) due to the difficulties with the gripping and dimension measurement of the thin sheet form post PC processing. The samples were mounted on the tangential clamp extension analysis measuring system (Figure 5.2 (b)), and the measurement was conducted at room temperature. To facilitate gripping of the samples during testing, the samples were clamped at each end using 2 mm strip of 165 µm thick steel mesh reinforced by cyanoacrylate adhesive. The diameter (approximately 1.75 mm) of each sample was measured with travelling microscope (Vernier Microscope). The initial applied load was 1 mN, and the specimen was tested in tension until failure at loading rate of 200 $mN.min^{-1}$. Constant sample hydration by application of DMEM was maintained during the test. From the stress-strain curve, the ultimate tensile strength, modulus of elasticity, and strain to break were calculated from 10 repeat specimens. Figure 5.9 shows the tensile test setup used for mechanical testing with the sample being clamped for testing.

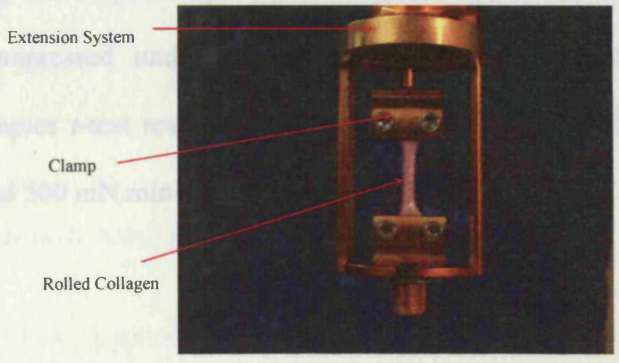

Figure 5.9: Photograph of the spirally assembled PC collagen being clamped for mechanical testing.

5.3. Results

5.3.1. Investigation into Unconfined Compression of Collagen Gels

5.3.1.1. Quasi-Static Mechanical Analysis

Figure 5.10 shows the unconfined compression behaviours of collagen gels, presented in terms of stress-strain and supplemented by modulus strain data. The stress-strain response was typical of a densification type behaviour of gels or polymers where the strain tended to initially undergo a rapid increase with stress. At high levels of strain greater than 90 %, the stress increases with relatively little increase in strain as the gels became more compressed. This was reflected in the modulus response where it showed a rapid increase at these latter stages. Prior to that point, the modulus showed an initial sharp increase, followed by a steady or near linear region. The results suggested that the gels became stiffer in response to the rapid loading of 500 $mN.min^{-1}$ than to slow loading of 100 $mN.min^{-1}$ as reflected by the higher modulus. In the linear region, the modulus value was approximately 6 and 8 $kN.m^{-2}$ under 100 and 500 $mN.min^{-1}$ loading rate respectively. Table 5.2 gives some of the results obtained for collagen gel compressed under unconfined condition under both loading rates. Independent Samples *t*-test revealed that there was a significant difference between 100 $mN.min^{-1}$ and 500 $mN.min^{-1}$ loading rate ($p = 0.002$).

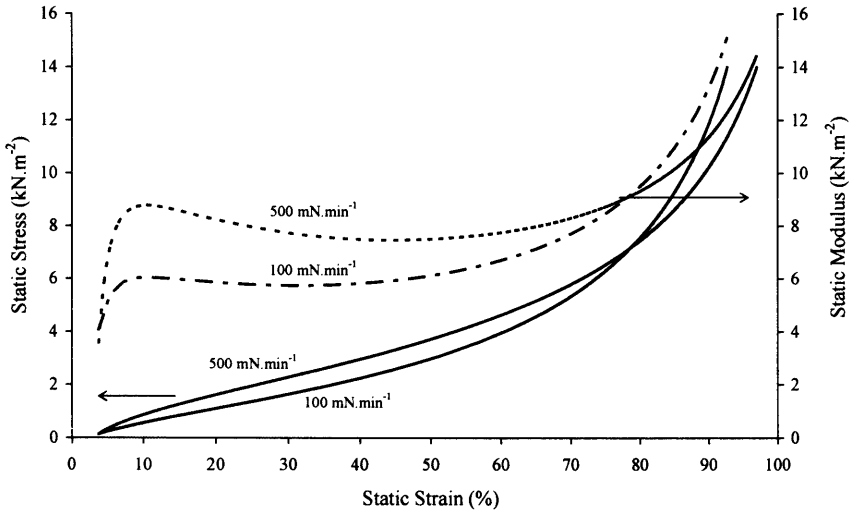

Figure 5.10: Unconfined compressive stress and modulus-strain curves for collagen gels.

Table 5.2: Strain and modulus for collagen gel under different unconfined compressive stresses.

Stress ($kN.m^{-2}$)	Strain %		Modulus ($kN.m^{-2}$)	
	100 $mN.min^{-1}$	**500 $mN.min^{-1}$**	**100 $mN.min^{-1}$**	**500 $mN.min^{-1}$**
0.5	9.3 ± 2.8	6.5 ± 1.3	6.0 ± 1.9	8.1 ± 1.5
1.1	20.9 ± 5.4	13.5 ± 2.0	5.8 ± 1.5	8.7 ± 1.3
1.7	30.0 ± 6.9	20.5 ± 2.9	5.8 ± 1.3	8.2 ± 1.2
2.3	40.6 ± 7.9	30.1 ± 3.9	5.8 ± 1.1	7.7 ± 1.1
3.1	50.8 ± 8.2	41.3 ± 4.7	6.1 ± 0.9	7.5 ± 0.9

5.3.1.2. Dynamic Mechanical Analysis

Figure 5.11 shows the storage, loss modulus, and tan δ values obtained from DMA tests carried out on the gels over a test period of 15 minutes. It can be seen that both moduli increased with time with storage modulus being higher than loss modulus, while tan δ remained relatively constant at approximately 0.25. The storage modulus

increased from 151.6 ± 10.2 up to 378.4 ± 39.7 kN.m^{-2}, and the loss modulus increased from 61.1 ± 7.7 up to 100.3 ± 20.8 kN.m^{-2} over 15 minutes. This apparent increase in elastic and viscous components was associated with the time dependent increase in the static strain from 5 ± 4.9 to 81.1 ± 4.7 % strain which in turn caused a decrease in the dynamic strain from 0.2 ± 0.1 to 0.1 ± 0.1 % as shown in Figure 5.12.

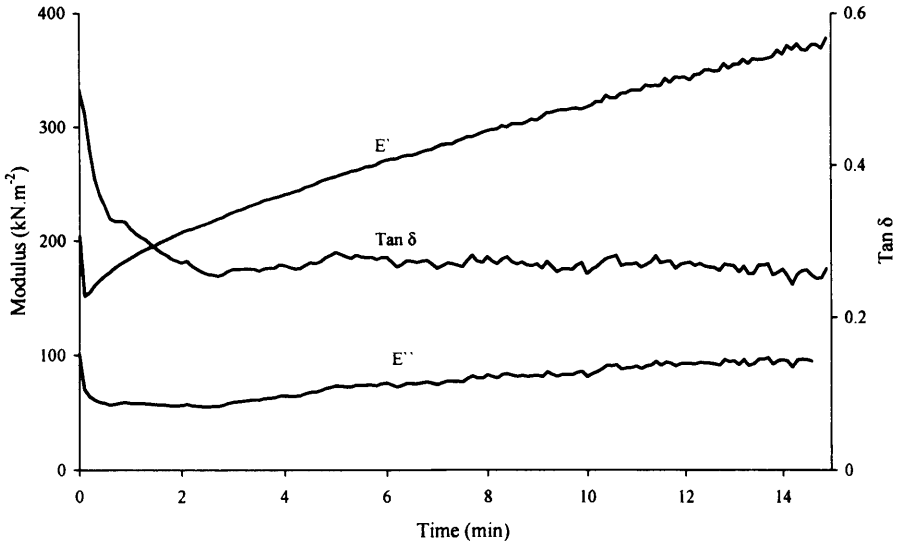

Figure 5.11: Storage modulus, loss modulus, and tan δ as a function of time obtained through unconfined compressive DMA of collagen gels.

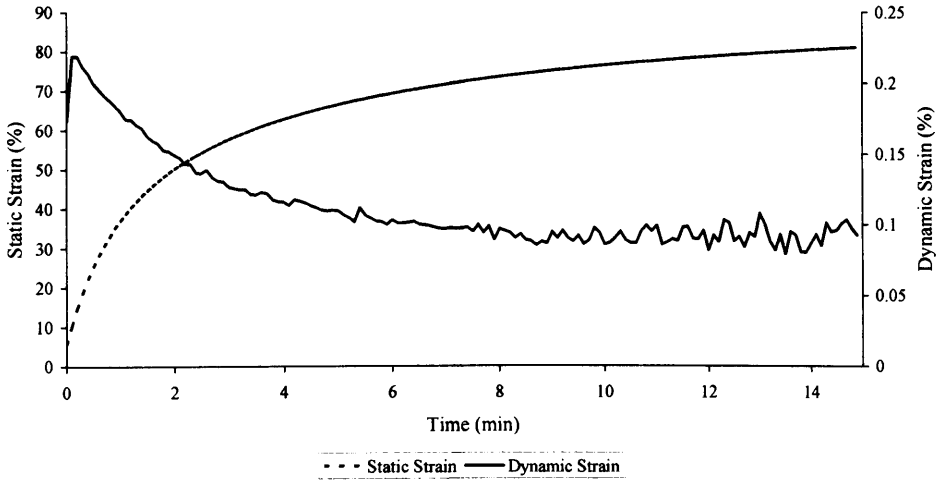

Figure 5.12: Static and dynamic strain as a function of time obtained through unconfined compressive DMA of collagen gels.

5.3.1.3. Creep and Recovery Analysis

A creep/recovery experiment was designed as described previously and demonstrated in Figure 5.6 to study the time dependant response of the collagen gels. After an equilibrating period, the creep part was designed to measure the strain response of the material to an applied stress, where this stress was varied by 2 orders of magnitude, whereas the recovery part was to measure the strain recovery after reducing this stress.

Figure 5.13 shows the creep and recovery data of collagen gels under different unconfined compressive creep stresses. Although all gels were set for 30 minutes, it was apparent that a load of 12.7 $N.m^{-2}$ during the equilibration phase resulted in varying strains. This may reflect the process of continuous self compression i.e., the gels undergoing compression under their own weight due to reorganisation of fibrils. Therefore, the normalisation of all creep curves to the equilibrating period was considered, as shown in Figure 5.14.

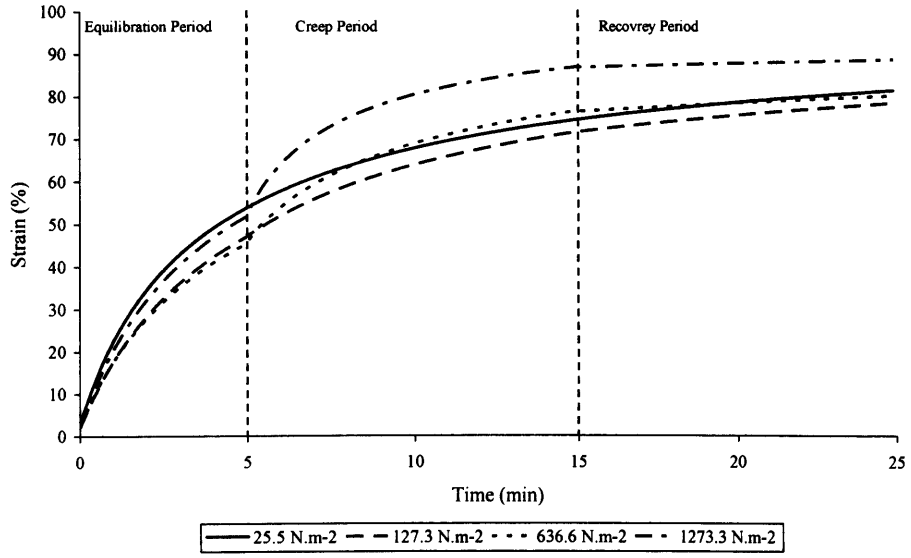

Figure 5.13: Raw creep and recovery data for collagen gel in response to different unconfined compressive stresses.

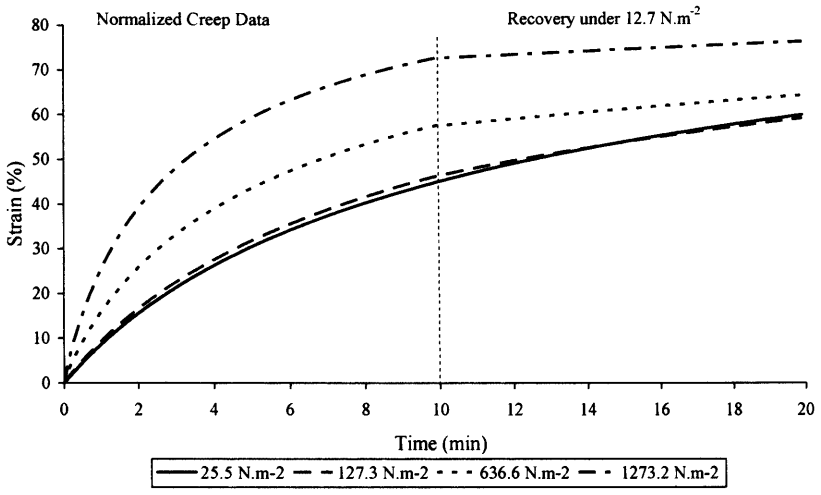

Figure 5.14: Normalised creep and recovery data for collagen gel in response to different unconfined compressive stresses.

From the normalised data, the creep increased with both time and stress. The statistical analysis showed a significant effect of the creep stress on the strain % at all time points ($p < 0.001$). In order to assess the effect of stress on the creep response of the gels, the strain rate was calculated through the slope of the initial creep part of the tests. Figure 5.15 shows that these initial strain rates were linearly related to the applied stress as would be expected for viscoelastic materials. After normalization of these data, therefore, both strain % and strain rate was dependant on the applied stress.

Upon reducing the load to 12.7 $N.m^{-2}$, an immediate recovery was present only at a higher stresses as shown in Figure 5.16, which is an expanded region to demonstrate the recovery zone for 1273.2 $N.m^{-2}$. However, it should be noted that this only resulted in 0.07 ± 0.02 % strain for 636.6 $N.m^{-2}$ and 0.12 ± 0.01 % for 1273.2 $N.m^{-2}$, while no recovery was observed under the lower stresses of 25.5 and 127.3 $N.m^{-2}$ as demonstrated by the negative strains recovery values as shown in Figure 5.17.

Moreover, beyond this recovery period of approximately 20 seconds, the gel constructs underwent further compression (creep) during this part of the test.

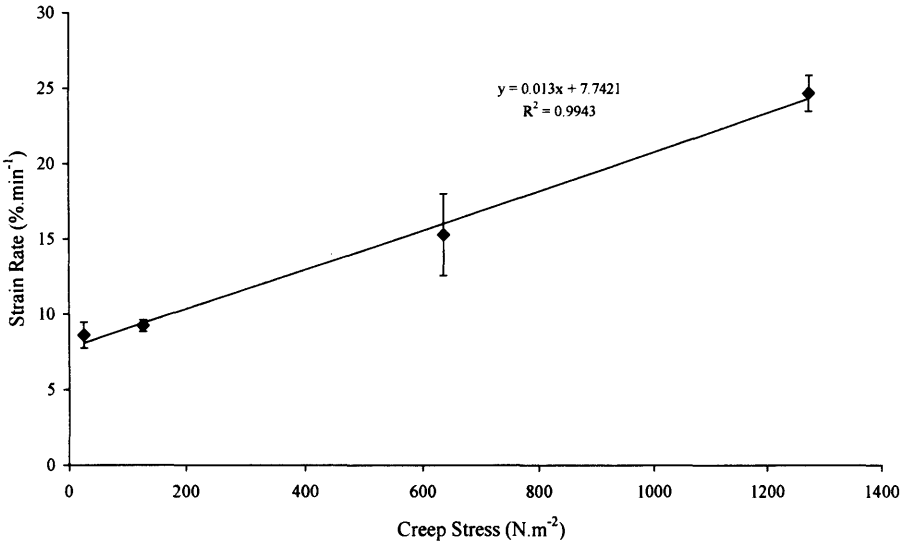

Figure 5.15: Strain rate as a function of the applied stress during the creep phase.

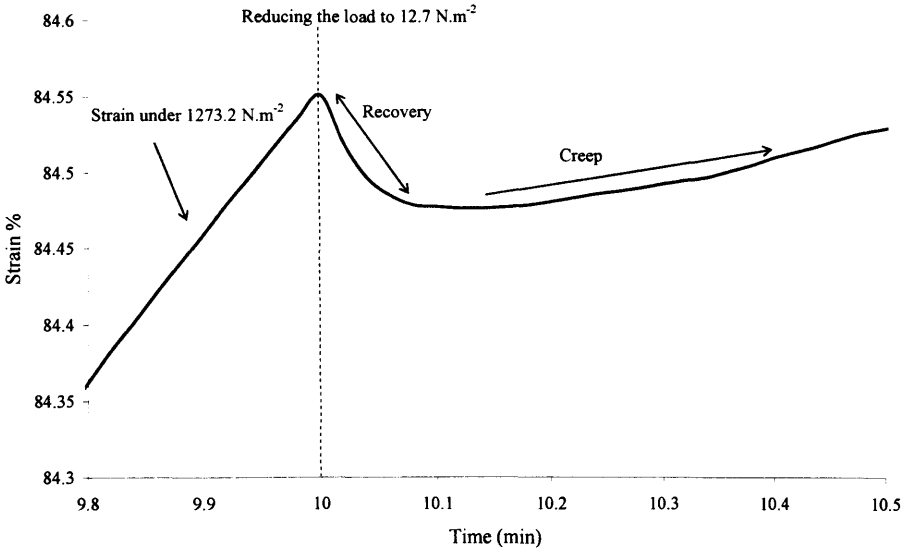

Figure 5.16: Expanded region of the creep and recovery data under creep stress of 1273.2 N.m^{-2}.

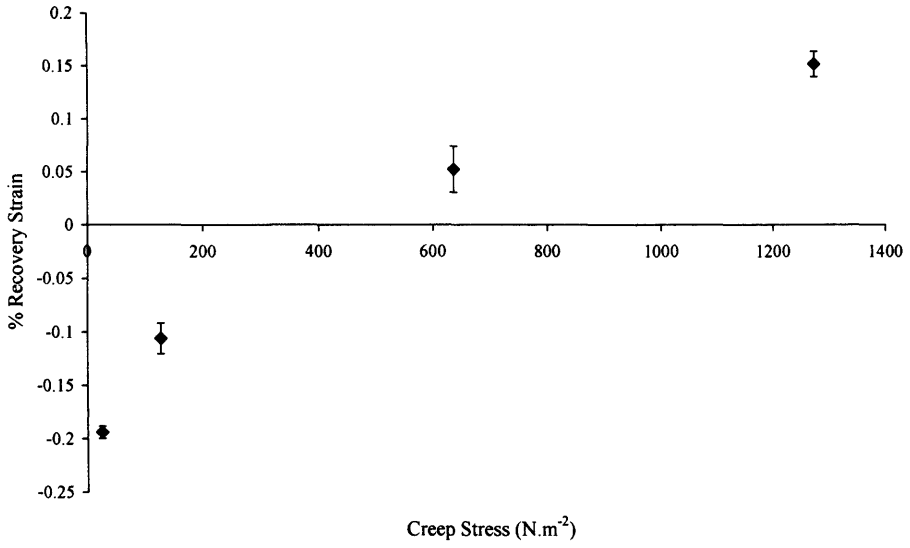

Figure 5.17: Percentage recovery under different unconfined compressive stresses after 10 min.

5.3.2. Plastic Compression to Produce Dense Collagen Constructs

5.3.2.1. Analysis of Plastic Compression of Collagen Gels

Figure 5.18 compares the real time change in height of collagen gels as a consequence of two different unconfined compressive stress levels; 0.14 and 1.4 $kN.m^{-2}$. The initial sample height as measured by the instrument was different under both stresses; gels loaded under 0.14 $kN.m^{-2}$ showed an initial height of 2.9 ± 0.29 mm which was higher than that recorded under 1.4 $kN.m^{-2}$ (1.3 ± 0.59 mm). These initial heights were also significantly lower than the nominal sample height of 6.2 mm as described in Section 5.2.2.2.1. These differences indicated that the gels responded differently to the two stresses. Under both stresses, the gels showed an instantaneous reduction in height that was followed by a more gradual decrease.

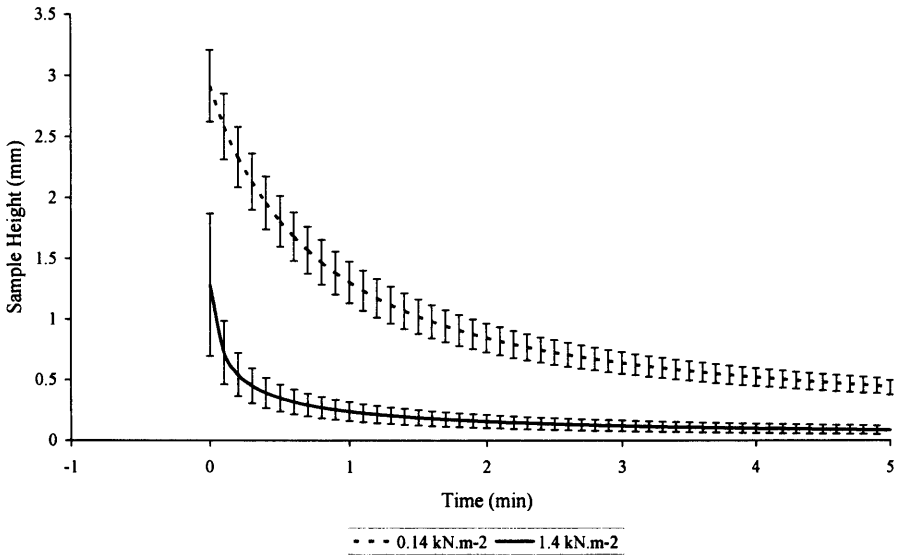

Figure 5.18: Sample height as a function of time comparing two stress levels of 0.14 and 1.4 kN.m^{-2} applied for 5 minutes, and illustrating the nature of plastic compression/compaction (PC) of collagen gels.

Figure 5.19 showed the % height reduction as a function of time related to the nominal height of 6.2 mm. The result showed both stresses achieved greater than 90 % shrinkage in height achieved in 5 minutes under both stresses. The height reduction was 93.1 ± 0.9 % under 0.14 which was significantly ($p < 0.0001$) different from 98.6 ± 0.6 % under 1.4 kN.m^{-2}. Therefore the magnitude of reduction in the gel thickness was dictated by the applied stress. The final gel thickness as measured by the technique was 430 ± 58 μm with 0.14 kN.m^{-2}, and 86 ± 35 μm was produced under 1.4 kN.m^{-2} as given in Table 5.3.

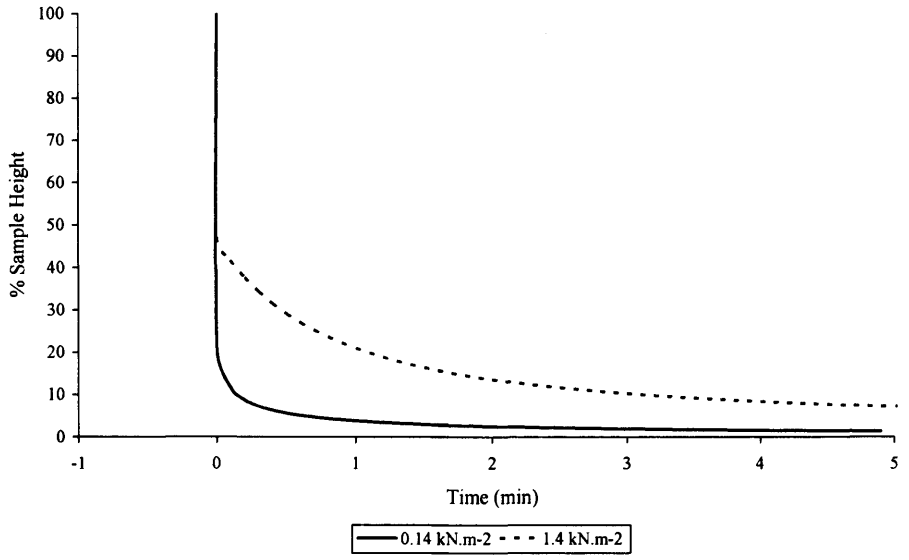

Figure 5.19: Sample height related to the theoretical height of 6.2 mm as a function of time comparing two stress levels of 0.14 and 1.4 kN.m^{-2} applied for 5 minutes.

The samples were also weighed before and after being compressed to determine the corresponding fluid loss due to the two compressive stresses. It was found that the percentage weight loss due to compression related to the applied stress, where it significantly (p = 0.0002) increased from 89.5 ± 2.0 % to 93.02 ± 1.3 % with 0.14 to 1.4 kN.m^{-2} respectively as given in Table 5.3. It was also observed that the collagen gel samples underwent weight loss by 24.6 ± 1.3 % under their own weight in a confined environment i.e. while stabilising within the well plate. This loss was due to confined self compression.

Table 5.3: Percentage weight loss through fluid expulsion, final height, and the percentage height reduction for the two stress levels compared to self compression.

	Confined Self Compression (control)	Unconfined PC 0.14 $kN.m^{-2}$ (5 minutes)	Unconfined PC 1.4 $kN.m^{-2}$ (5 minutes)
% Weight Loss (n=10)	24.6 ± 6.8	89.5 ± 2.0	93.02 ± 1.3
Final Height (μm) (n=10)	-	430 ± 58	86 ± 35
% Height Reduction as Measured by DMA (n=10)		84.4 ± 2.7	92.1 ± 3.9
% Height Reduction* (n=10)	-	93.1 ± 0.9	98.6 ± 0.6

* Using a nominal gel starting height of 6.2 mm.

5.3.2.2. Properties of Collagen Constructs Produced through Plastic Compression

5.3.2.2.1. Weight Loss due to Plastic Compression

Table 5.4 gives the percentage weight loss through the use of standard PC technique of 1.4 $kN.m^{-2}$ compressive stress for 5 minute in combination with blotting to prepare dense collagen gels.

Table 5.4: Percentage weight loss through fluid expulsion by combination of compression and blotting actions.

Materials (samples number)	Weight before compression (g)	Weight after rolling (g)	Final weight loss %
Collagen (n = 25)	1.65 ± 0.16	0.03 ± 0.01	98.16 ± 0.43

5.3.2.2.2. *Scanning Electron Microscopy*

Figure 5.20 shows the SEM micrographs of collagen gels before and after being processed through the plastic compression technique. Figure 5.20 (a) shows a micrograph of collagen gels in the x-y direction that consisted of a three-dimensional porous network of randomly oriented fibres with several nanometres in diameter and small interconnected voids were present between these fibrils. Expulsion of interstitial fluid from collagen matrix by plastic compression and probably due to dehydration effect of SEM preparation produced a matrix with a more dense structure than the original gel as shown in Figure 5.20 (b). The random three dimensional architecture of collagen gel was maintained throughout the processing method as can be inferred from SEM. From the cross-sectional view, the multiple layers (each of approximately 50-100 μm thickness) of the spirally assembled PC collagen were evidently in loose contact as evidenced by the presence of micro-spaces which could potentially be important for nutrient diffusion to the core of the construct Figure 5.20 (c and d). During sample preparation for cross sectional scanning, the cutting action by the scalpel blade obliterated some of these spaces, and this was an artefact due to sample preparation.

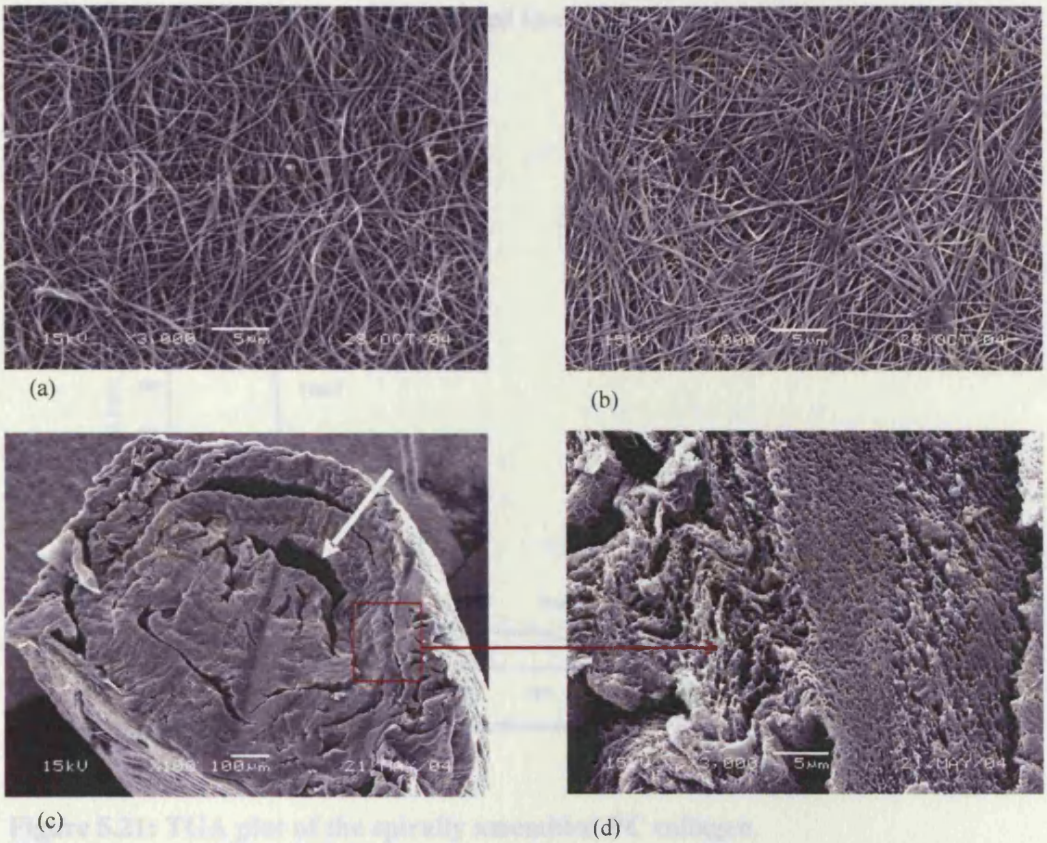

Figure 5.20: SEM of collagen through processing by PC technique (a) non-compressed collagen gels, (b) collagen sheet after plastic compression, (c, d) cross section of spirally assembled PC collagen. The white arrow refers to the presence of micro-spaces between different layers of the spiral construct.

5.3.2.2.3. Thermo-Gravimetric Analysis

Figure 5.21 shows the TGA plot of the spirally assembled PC collagen. It was clear that there were three distinct weight loss regions. The first broad region (I) was spread between 110 and 180 °C with an inflection point at 150 °C, the second weigh loss region (II) appeared between 280 and 390 °C with the inflection point at 330 °C, while the third region (III) was presented between 500 and 650 °C with the inflection point at 580 °C. The first region showed a sharp weight loss of approximately 85.44 ± 2.20 %,

while the second and third regions showed low weight losses of approximately 4.98 ± 1.08 and 3.47 ± 1.07 % respectively.

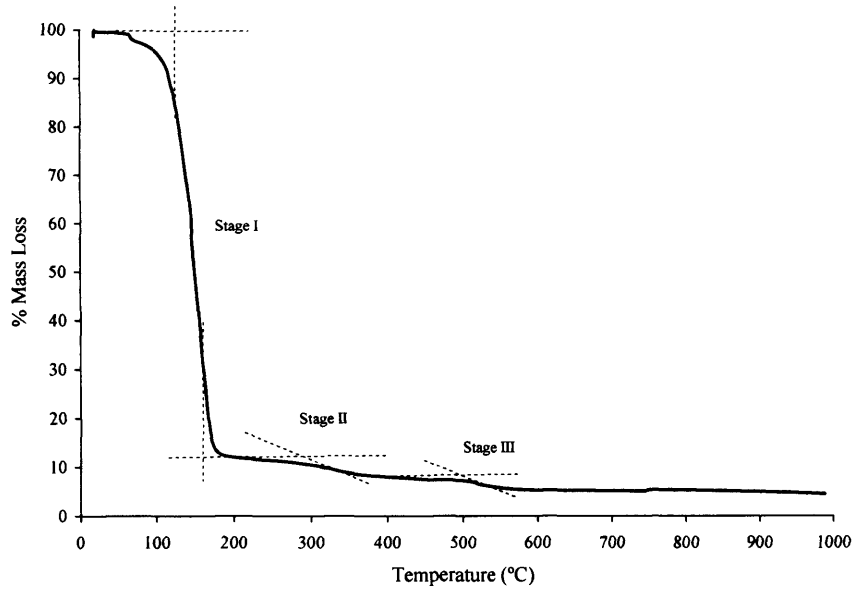

Figure 5.21: TGA plot of the spirally assembled PC collagen.

5.3.2.2.4. Mechanical Properties under Quasi-Static Uniaxial Tensile Testing

Figure 5.22 shows the typical stress and modulus-strain curve of the spirally assembled PC collagen. There were three main regions: firstly, a non linear stress-strain response in the low stress region (toe-in region) up to 12.8 ± 4 % strain; secondly, a linear region terminated by the yield point up to 47.3 ± 11.5 %, where the strain was related directly to the applied stress, and the modulus value was relatively constant around 1.3 ± 0.3 $MN.m^{-2}$; thirdly, a maximum breaking stress point, giving the ultimate strength of 0.6 ± 0.1 $MN.m^{-2}$, and over this region, the modulus dropped until the material failed at 55.0 ± 13.8 %.

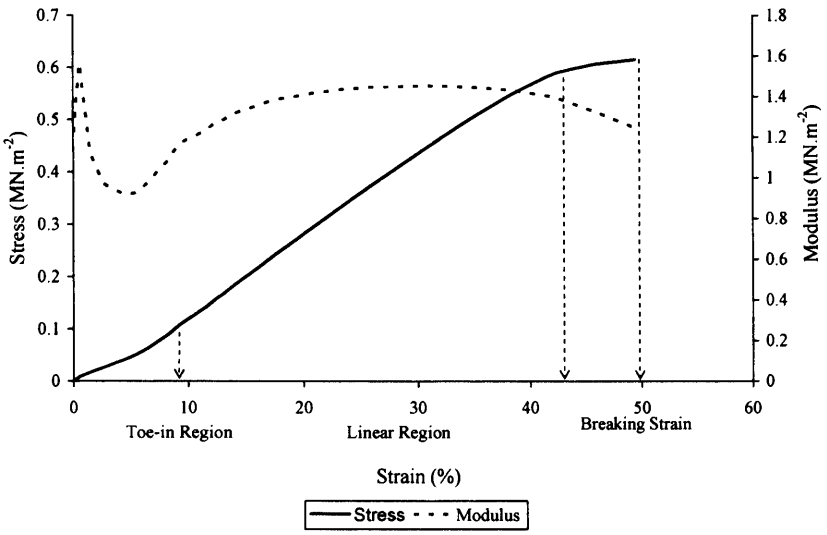

Figure 5.22: Typical tensile stress and modulus-strain curve for the spirally assembled PC collagen.

5.4. Discussion

This study investigated the mechanical and viscoelastic properties of collagen gels under unconfined compression to verify PC using quasi-static, dynamic and creep/recovery analysis, and the resultant deformation was measured as a function of stress and time. *In vitro* reconstituted type I collagen is biologically an excellent biomimetic material, but is mechanically very weak, it consists of randomly (isotropic) orientated fibrils within an excess of fluid generally greater than 99 %. (Knapp *et al.*, 1997). This liquid content is a result of the casting, rather than any inherent swelling property of the collagen. Its response to mechanical load can be dependent on factors such as the type of loading, time, frequency, the fluid content, and its interaction with the collagen fibrils.

The results from the quasi-static mechanical test showed that the stiffness of collagen gel significantly increased by increasing the loading rate from 100 to 500 $mN.min^{-1}$

which was an indicative of the viscoelastic nature of the gel. Prockop and Fertala (1998) related the viscoelasticity to the collagen fibrils structure. During fibrilogensis, collagen monomers assemble into fibrils through specific binding sites on collagen monomers. This assembling process resembles crystallisation in polymers, and some regions of the collagen fibrils are crystalline with solid like properties while the others are more flexible with liquid-like properties. In general, the reported values of the compressive modulus of collagen under confined compression by Sheu *et al.* (2001) was 4.23 $kN.m^{-2}$ which falls within the range of obtained in this study of between 6 to 8 $kN.m^{-2}$ obtained in the linear region at 100 and 500 $m.min^{-1}$ rates respectively.

The static modulus obtained in this study was two orders of magnitude lower than the storage modulus obtained through DMA where the E' increased from 151.6 ± 10.2 to 378.4 ± 39.7 $kN.m^{-2}$ over the time period of the experiment which could be due to the contribution of the rate-sensitive viscous part of collagen gels. This finding was also observed by Krishnan *et al.* (2004), who performed static and cyclic testing of collagen gels under tensile mode. The reported static modulus was 1.5 ± 0.01 $kN.m^{-2}$ and the dynamic modulus was 21.8 ± 0.2 $kN.m^{-2}$. The differences between the obtained modulus values in this study and those reported by Krishnan *et al.* (2004) may be due to the differences in the test conditions. During DMA, the observed increase in both storage and loss modulus with the time of the experiment can be explained by the observed time dependant significant increase in the static strain or otherwise creep behaviour of the gels. This increase in the static strain, associated with densification of the gels, produced a reduction in the dynamic strain and in turn an increase in both moduli. It can be inferred from the data that the magnitude of increase in both moduli was relatively the same as indicated by the constant tan δ value which remained constant.

From the un-normalised creep data, even though the gels had been compressed under the same equilibration conditions, the response was different suggesting that the gels underwent different levels of compression under their own weight. This could also be inferred from the relationship between the strain rate against creep stress, where the intercept was not zero, indicating that under no stress, the gels underwent creep under their own weight. Therefore, a study was carried out to detect the amount of self compression inferred by detecting the percentage of fluid loss from collagen gel samples under their own weight. It was observed that the gels showed 24.6 ± 6.8 % fluid loss under confined self compression (within the well plate) which would be expected to be higher under unconfined compression as observed by Brown *et al.*, (2005) where collagen gels lost 57 % fluid under un-confined self compression.

Normalisation of the creep data was considered so that the comparison between different creep stresses was made possible. From the normalised creep data, it was observed that not only the strain, but also the initial strain rate calculated from the slope on the initial part of the creep curve varied with the applied stress. This behaviour was suggestive of the viscoelastic nature of collagen gels with the viscous component seemed to predominate the gel behaviour as evidenced from the amount of both instantaneous strain and recovery that gels experienced. As evident from the recovery data, only a negligible immediate recovery of a maximum 0.2 % was observed suggesting the predominance of the visco-plastic deformation behaviour of these hyper-hydrated materials with an ability to undergo rapid plastic deformation.

Visco-plastic compressibility of collagen gel was used as the basis for the formation of tissue analogous 3-D collagen implants with improved tensile mechanical properties via a novel technique "plastic compression" based on the expulsion of fluid from collagen gel either by compression or combination of compression and blotting

actions. At the same time, structural features fabricated at the millimetre scale could be retained, but shrunk down to the meso-scale. Critically, this form of tissue fabrication is inherently cell-friendly and rapid i.e., taking minutes, as greater than 90 % fluid loss occurred within 5 minutes.

The percentage weight loss due to compression was 93.02 ± 1.3 compared to 98.16 ± 0.43 due to combination of compression and blotting action. This difference was attributed to the capillary action of the absorbent paper causing extra fluid loss. Plastic compression using a combination of compression and blotting actions was used as a standard to prepare 3-D PC collagen. Rolling of a PC collagen sheet along the short axis was attempted to produce the 3-D constructs and also due to the encountered difficulty in handling of the very thin collagen sheet. The weight loss, related to PC, was also associated with an increase in collagen density apparent from both SEM images and TGA. It was clearly seen that at 200 °C, the PC collagen lost 85.44 ± 2.20 % of its weight which can be attributed to fluid loss. This suggested that the remaining 15 % was made of collagen. The thickness of PC collagen sheet was 86 ± 35 μm as measured by the mechanical analysis whereas 98.6 ± 0.6 % reduction in thickness was produced by compressing the gel samples under 1.4 $kN.m^{-2}$ for 5 minutes.

Three zones of weight loss were observed from the TGA plot of PC collagen spirals. The first stage of transition was characterised by sharp weight loss, and observed between 110-180 °C could be related to loss of fluid. However, the second and the third stages, identified at 280-390 °C and 500-650 °C respectively, were characterised by significantly lower weight loss which could be due to equilibration and decomposition of collagen as highlighted in literature (Samouillan *et al.*, 1999 and 2003, Kumar *et al.*, 2003, and Shanmugasundaram *et al.*, 2004). Shanmugasundaram *et al.* (2004) concluded that the collagen source had an important impact on the

transition temperature, moreover, each collagen source had its characteristic amount of bound water content; consequently, the amount of weight loss during the first transition was different between sources.

Aside from the densification of collagen through PC, the improvement in mechanical properties was also considered as an advantage of this processing route, as collagen gels are an inherently fragile, weak material, and difficult to handle due to their low original concentration and lack of structure. PC collagen showed a quasi-static stress-strain curve characterised by the presence of toe-in region, linear region, and finally breaking. The stress-strain response was typical of network phase of the connective tissue (Lee *et al.*, 2001d, Puxkand *et al.*, 2002, Feng *et al.*, 2003b, Berglund *et al.*, 2003, Shields *et al.*, 2004, Berglund *et al.*, 2004, De Santis *et al.*, 2004) and hydrated gels (Chandran and Barocas 2004). Upon the tensile loading of the PC collagen, the stretching of randomly oriented collagen fibrils (Figure 5.23 (a)) occurred firstly as diagrammatically shown in Figure 5.23 (b) which was then followed by fibrils orientation in the direction of the applied load. The resistance of fibrils to further orientation gives the stiff or linear region in the stress strain curve, and gives an indication of the material stiffness. Finally, at further load applications beyond the yield point, sliding of these fibrils due to their disentanglement has been occurred as shown in Figure 5.23 (c). The similar findings were also observed by Feng *et al.* 2003a and Chandran and Barocas (2004).

The tensile strength and the modulus values obtained in this study was still higher than those for cellular construct obtained by Feng *et al.* (2003 a and b), Gravin *et al.* (2003), Seliktar *et al.* (2003), Devireddy *et al.* (2003), Berglund *et al.* (2004), and Neidert *et al.* (2004) as given previously in Table 2.2.

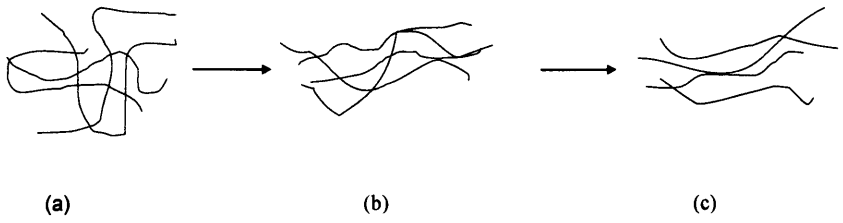

Figure 5.23: Diagrammatic representation of collagen fibrils under tensile loading (a) random orientation of collagen fibrils, (b) stretching of collagen fibrils, and (c) sliding of the collagen fibrils.

PC presents a novel method for producing 3-D meso-scale constructs, achieved in minutes, with controlled density and enhanced mechanical properties in a completely rapid, predictable manner depending on the applied load. PC involves the use of both unconfined compressive load and a capillary action by absorbent tissue to expel the interstitial fluid, responsible for gel weakness. The application of 1.4 KPa for 5 minutes produced significant fluid loss (approximately 98 %) and a reduction in the physical dimension from millimetre to micro-meter scale, but at the same time maintaining the same structural features. Once, the reconstituted collagen gel loses fluid, it can not return back after removal of the load. PC produced a collagen sheet of approximately less than 100 μm thickness compared to 4.6 mm initial nominal height indicating approximately 99 % reduction in height. This collagen sheet composed of approximately 15 % collagen and 85 % fluid (as measured here by TGA) compared to the original gel with fluid greater than 99 %. For conventional cell-based fabrication, Feng et *al.*, 2003a using collagen gel under tensile load, reaching a breaking strength of 0.16 $MN.m^2$ after 70 days in culture. Also the break stress reported by Garvin *et al.*, 2003 of the 7 day construct was 0.1 ± 0.01 and the modulus of 0.49 ± 0.24 $MN.m^{-2}$. However, these values still were substantially lower than the breaking strength of 0.6 $MN.m^{-2}$ and modulus of 1.3 $MN.m^{-2}$ obtained in this study using PC with no culture

period avoiding the problems of potential contamination and expenses of culture. Moreover, PC fabrication can therefore provide reproducible and controllable structure with improved tensile properties approaching those of some native tissues in a matter on minutes. However, the PC constructs still weaker than the strongest tissue such as tendon with 100 $MN.m^{-2}$. More interestingly that incorporating cells into collagen gels was always associated with shrinkage that depends on the cell type, density, and passage number. For example, type I collagen gels reduced in dimension by 85 % over 10 weeks in culture by incorporation of human fibroblasts at a density of 2.5 x 10^6/ construct. In another study conducted by Moriyama *et al.* (2001), human oral fibroblasts at a density of 10^5 cells/ml contracted collagen gel by about 58.5 % after one week of incubation. This shrinkage could be a limitation if the constructs were used as skin substitute, for example which could be avoided using PC collagen to start with as a template for cells to grow. Although the PC collagen sheets were difficult to handle, they could be potentially used as skin substitutes. The spirally assembled constructs, however, were convenient for handling, and testing and could be potentially used as a nerve and ligament regeneration template in form of tubes or rods.

Chapter 6

Development and Characterisation of 3-D Phosphate Glass Fibre Incorporated-PC Collagen Constructs

6.1. Introduction

This chapter reports on the application of plastic compression (PC) to incorporate unidirectional-phosphate-based glass fibres (PGF) into collagen for the production of both acellular and cellular constructs for potential muscle or tendon engineering applications. The effect of PGF incorporation was assessed morphologically and mechanically, and the efficacy of the PC processing route in controllably producing constructs based on these components was also confirmed through thermogravimetric analysis. Cellular constructs were also produced and assessed morphologically through confocal microscopy and live dead staining of primary human oral fibroblasts (HOF) seeded during processing.

6.2. Experimental

6.2.1. Materials

6.2.1.1. Raw Materials

6.2.1.1.1. Phosphate Glass Fibres

As highlighted in Chapter 4, glass fibres containing 3 mol % Fe_2O_3, pulled at 400 $m.min^{-1}$, and having diameters of 31.6 ± 6.5 μm were selected in this study as reinforcing agents.

6.2.1.1.2. Collagen

As in Chapter 5, rat tail type I collagen solution (First Link, UK Ltd, UK) was also used.

6.2.1.2. Method of Preparation

6.2.1.2.1. Production of Unidirectional Phosphate Glass Fibres

The unidirectional alignment of the glass fibres was carried out on the custom built fibre-rig shown previously in Figure 3.1, and described in Section 3.2.1.2.2. The drum rotates around an axis and move parallel to that axis, and the drum rotational and cross-head speeds control both vertical and horizontal movements respectively. The rotational speed organises the number of rotations per minute, hence the fibre diameter as shown previously in Figure 4.3. The cross-head speed, on the other hand, can be controlled by adjusting the frequency of a stepper motor, which in turn affects the horizontal movement speed of the drum. Therefore, the fibre number and spacing per surface area, and the weight % of fibres in the final scaffold can be controlled. It was hypothesised that increasing the cross-head speed will decrease the amount of PGF per specific distance provided that the same drum rotational speed was used.

An initial study was carried out to find the relationship between the frequency of the stepper motor and the drum cross-head speed. At different selected frequencies (10, 12.5, 20, 22.5, 25, 50 and 100 Hz), the horizontal movements (in cm) travelled by the drum in 60 seconds i.e. the drum cross-head speed in $cm.s^{-1}$ were measured at a fixed rotational speed of 400 $m.min^{-1}$ as shown in Figure 6.1. It was observed that the cross-head speed varied linearly with the frequency, following the approximate relation $y = 0.0028x$, where y was the cross-head speed, and x was the frequency of the stepper motor.

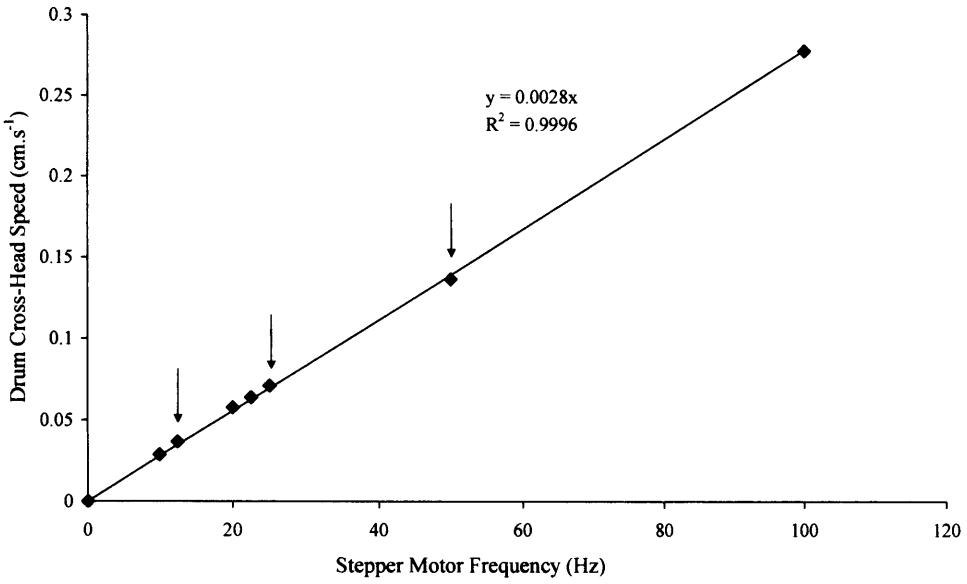

Figure 6.1: The relationship between the stepper motor frequency and the drum cross-head speed. The arrows showed the chosen frequencies for producing PGF with different quantities.

Three stepper motor frequencies (SMF) which were 50, 25, and 12.5 Hz were chosen to produce unidirectionally-aligned fibres with different amounts in an ascending order that was described as low, medium, and high. After aligning the fibres on the drum, they were stuck in place by an adhesive tape, and they became ready for use. From the obtained data, at frequency of 25 Hz and a rotational speed (RPM) of 400 m.min^{-1}, the total horizontal distance travelled by the drum per a minute (d_t) was equal to 4.3 cm. Then, the horizontal distance (in μm) travelled by the drum per single rotation (d_r) was calculated from equation (6.1).

$$d_r = \frac{d_t}{RPM} \tag{6.1}$$

Therefore, $d_r = \frac{4.3 \times 10 \times 1000}{400} = 107\,\mu m.$

Hence, in one rotation, a travel distance of 107 μm is achieved. As a result, the distance from one fibre to the next should be equal to d_r. Whilst the spacing between two fibres (S_f) was calculated from equation (6.2).

$$S_f = d_r - \phi \tag{6.2}$$

Where: ϕ was the fibre diameter.

Therefore, $S_f = 107 - 35 = 72$ μm as shown in Figure 6.2.

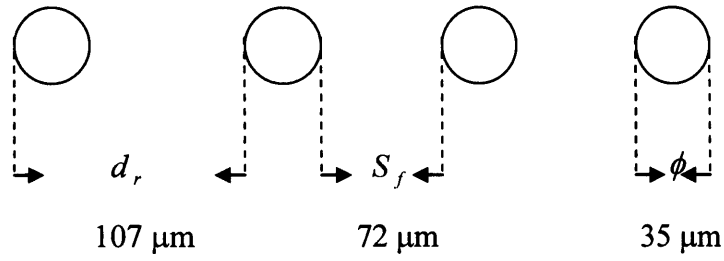

Figure 6.2: Diagrammatic representation of fibre spacing at 25 Hz frequency considering the fibre diameter of 35 μm.

The time (t) in seconds required to fill a distance of 3.3 cm (the mould length used for casting of collagen) was calculated from equation (6.3).

$$t = \frac{d}{s} \tag{6.3}$$

Where: d was the distance in cm, and s was the drum cross-head speed ($cm.s^{-1}$).

Therefore, $t = \frac{3.3}{0.071} = 46.4$ s.

The number of fibres (n) that should fill the mould was calculated from equation (6.4).

$$n = RPM \times t(\text{min}) \tag{6.4}$$

Therefore, $n = 400 \times \frac{46.4}{60} = 309$ fibres.

The same calculations were also applied at 25 and 50 Hz frequencies, taking into consideration the difference in the horizontal distance travelled by the drum, and they are given in Table 6.1.

Table 6.1: Theoretical time (t), number of fibres (n), and spacing between fibres (S_f), at different stepper motor frequencies and RPM of 400 m.min^{-1}, used to cover the surface area of the mould used for casting collagen.

Frequency (Hz)	t (s)	n	S_f (μm)
12.5	90	600	20
25	46	309	72
50	24	160	170

6.2.1.2.2. Preparation of Acellular PGF-PC Collagen Constructs

Adaptation of the PC method described previously in Section 5.2.2.2.2. was considered for preparation of PGF-PC collagen constructs. The unidirectionally-aligned fibres were placed on a microscope glass slide that formed the base of the Delrin® rectangular mould to give a construct with a nominal height of approximately 4.6 mm. The glass slide was clamped on both sides to the mould. Collagen gel was prepared as described in Section 5.2.1.2., and after neutralisation with NaOH, 2 ml of preset collagen solution was pipetted into the mould on the top of the glass fibres. Then collagen was allowed to set/stabilise in a 37 °C, CO_2 incubator for 30 min. Following setting, the construct was made free by running a sharp surgical blade along its edges just before removal from the mould. After removal from the mould, the construct was routinely compacted by a combination of compression and blotting using layers of meshes and paper sheets as diagrammatically shown in Figure 6.3.

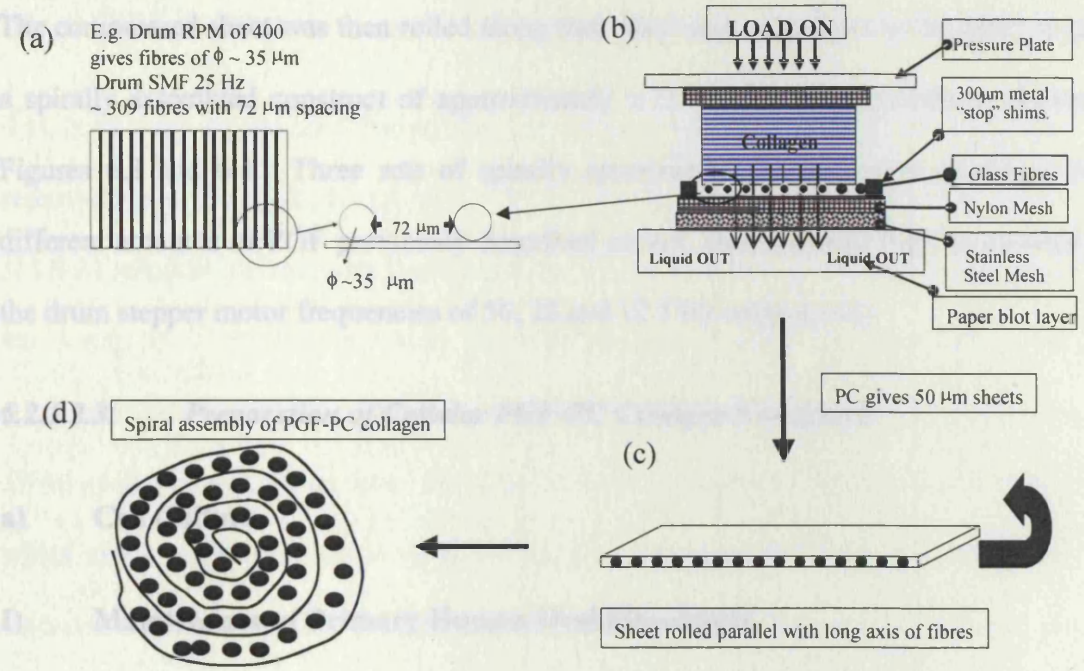

Figure 6.3: (a) Diagrammatic representation of glass fibre aligned at a drum SMF of 25 Hz showing the theoretical fibre number and spacing between two adjacent fibres, (b) diagram showing the routine PC processing used for producing of PGF-PC collagen with a standard stress of 1.4 kN.m^{-2} for 5 minutes at 37 °C, (c) PGF-PC collagen sheet (~50 μm thick), and (d) PGF-PC collagen spiral assembly (1.75 ± 0.25 mm diameter).

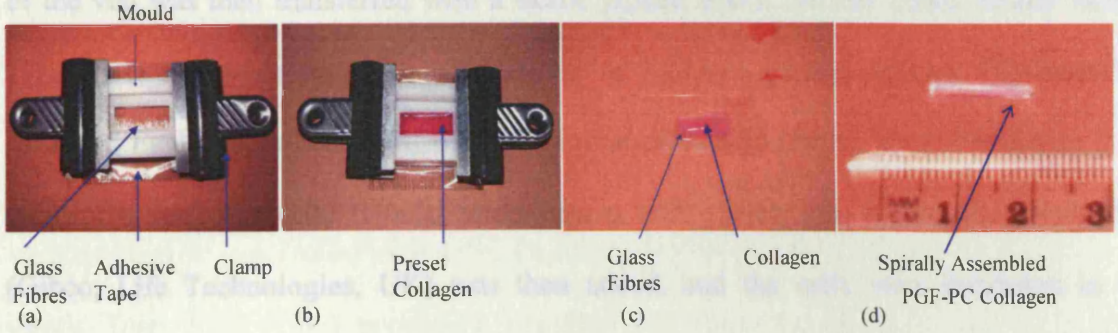

Figure 6.4: Photograph showing the different steps in preparation of the spirally assembled PGF-PC collagen (a) aligned PGF attached to the bottom of the mould, (b) collagen gel casted on the top of pre-aligned PGF, (c) PGF-collagen gel, and (d) PGF-PC collagen spiral.

The compressed sheet was then rolled along their short axis or parallel to the fibres to give a spirally assembled construct of approximately 1.75 ± 0.25 mm diameter as shown in Figures 6.3 and 6.4. Three sets of spirally assembled constructs were produced with different amounts of PGF previously described as low, medium, and high as dictated by the drum stepper motor frequencies of 50, 25 and 12.5 Hz respectively.

6.2.1.2.3. Preparation of Cellular PGF-PC Collagen Constructs

a) Cell Culture

I) Maintenance of Primary Human Oral Fibroblasts

HOF were obtained from the Eastman Dental Institute archive. These cells were in cryogenic storage and had been previously obtained from an explant culture from a gingival tissue mucosal biopsy after obtaining ethical approval. Frozen vials of HOF were retrieved from storage and defrosted in a 37 °C water bath. The exterior of the vial was wiped with a tissue soaked with 70 % ethanol to remove any contamination. The content of the vial was then transferred with a sterile pipette into a 150 cm^2 tissue culture flask (T_{150}) (BD Bio-Sciences, UK). Fifteen ml of standard growth medium [Dulbecco's Modified Eagle's Medium (DMEM), 10% Foetal calf serum (FCS), 1% L-Glutamine (L-Glut), 1% Penicillin (100 IU/ml)/ Streptomycin (100 µg/ml) and, 1% Amphotericin B] (Gibco, Life Technologies, UK) was then added, and the cells were incubated in a humidified incubator at 37 °C and 5 % CO_2. The growth medium was changed every three days.

II) Cell Subculture

The cells were trypsinized during the log phase of growth. The growth medium was removed from the flask; 10 ml of 0.5 % trypsin-0.02 % ethylene diamine triacetic acid (EDTA) solution (Gibco, Life Technologies, UK) was added, and the flask was incubated for 5 min at 37 °C during which the cells become rounded and detached. The cell suspension was gently triturated with a 10 ml pipette before being transferred into a sterile 50 ml graduated centrifuge tube. An aliquot of growth medium, approximately 10 ml, was added to the cell suspension to terminate the action of trypsin/EDTA. The cells were then collected by centrifugation at 1000 rpm for 5 min at room temperature; a balance weight was used when required. Once centrifuged, the supernatant was discarded, and the cell pellet was resuspended into 4 ml of standard growth medium for reseeding into 4 tissue culture flasks (T_{150}). Cells used for the experiments were collected from 15^{th} to 18^{th} passages.

III) Cell Counting

HOF were detached from the flasks, as described in cell subculture, and resuspended into growth medium. Then the cell number was determined using a haemocytometer, which is a thick glass slide with a central area designed as a counting platform for cells. Before the haemocytometer was loaded with cells, the cell clumps were dispersed by pipetting up and down. Then, 20 µl of cell suspension was transferred into a 1.5 ml micro-centrifuge tube and 20 µl of 0.4% trypan blue solution was added and homogenously mixed together. Trypan blue is metabolised by viable cells, and hence they will not stain blue, while dead cells will take up the stain and turn blue. About 10 µl of stained cell suspension was

transferred to the edge of each filling notch of the two counting chambers. A microscope was used to view the cells for counting.

IV) Cryopreservation of Cells

For preserving surplus cells to be used as required, HOF were detached from the flasks, as described in cell subculture, and the cell pellet having a cell density of $1x10^6$ cells/ml was prepared for freezing. The cell pellet was then resuspended in a freezing medium [90% of FCS and 10 % of dimethyl sulfoxide (DMSO) (Gibco, Life Technologies, UK). One ml aliquots were placed in cryovials that were labelled with the cell type/passage number and date of freezing. The cryovials were then placed in a cooled 'Mr. Frosty', a Styrofoam insulated container filled with isopropanol. The container was then transferred into a freezer at -80 °C with a cooling rate of -1 $°C.min^{-1}$ for 24 h. The cryovials was then preserved in liquid nitrogen (-196 °C) until needed.

b) Sterilization of Glass Fibres

Sheets of aligned glass fibres, produced as previously described in section 6.2.1.2.1, were sterilized by soaking in 70 % ethanol for 1 h. Sterilised PGF sheets were then washed, and preincubated in growth medium for 24 h for elimination of undesirable dissolution products (Blaker *et al.*, 2003, Clupper *et al.*, 2003). The sheets were then removed from medium, gently rinsed with fresh medium, and placed on a sterile glass slide that formed the bottom of the mould used for casting the gel.

c) Sterilization of the Casting Mould Setup

The Delrin® mould, glass slides, metal mesh, paper tissue, and the pressure plate were sterilised by autoclaving, and the nylon meshes were sterilized by soaking in 70 % ethanol

for 1 h and then washed with a sterile PBS. The clamps were sterilized by UV light for 1 h. All autoclaved materials were subjected to drying by holding at 60 °C temperature for 30 min.

d) Formation of the Constructs

For cellular constructs, HOF were mixed with the collagen solution immediately after neutralization, before setting and compaction, at a density of 3.3 x 10^5 cells.ml^{-1} collagen. PC was carried out as described above, and constructs with three different quantities of PGF and collagen alone were prepared in the form of compressed sheets and spirally assembled constructs. The seeded constructs were placed in 60 mm culture dishes with 10 ml of standard growth medium, and incubated in a humid atmosphere of 5 % CO_2 at 37 °C for up to 1 and 24 h.

6.2.2. Methods of Characterisation

6.2.2.1. Characterisation of Acellular PGF-PC Collagen Constructs

6.2.2.1.1. Morphological Characterisations

Scanning electron microscopy (SEM) and X-ray microtomography (XMT) were used to characterise the spirally assembled constructs morphologically in terms of structure and fibre alignment.

a) Scanning Electron Microscopy

Samples for SEM were prepared and viewed under scanning electron microscope (JEOL JSM-5500LV) with an accelerating voltage of 15-20 kV as previously described for collagen in Section 5.2.2.2.3.

b) X-Ray Microtomography

These were carried out in collaboration with Prof. Peter. D. Lee, Department of Materials, Imperial College London. Samples for XMT were cut to approximately 5 mm in length and inserted vertically into Perspex specimen holders designed for minimal X-ray attenuation and kept in standard growth medium during analysis. Prepared specimens were analysed using X-ray microtomography apparatus (Phoenix X-ray V|tome|Xs) using X-ray parameters of 80 kV and 80 μA. Projections were acquired at angular separations of 0.5°, resulting in a total of 720 transmission images. The magnification of the transmission images was approximately 115 giving a voxel resolution in the reconstructed images of 3.5 ± 0.1 μm. Reconstruction was performed using the commercially-available Sixtos software package.

6.2.2.1.2. Quantification of the PGF-PC Collagen Components

Two methods, thermo-gravimetric analysis (TGA) and ashing, were used for quantifying the individual components of the spirally assembled PGF-PC collagen with the three different weight % of PGF.

a) Thermo-gravimetric analysis

Thermo-gravimetric analysis of PGF-PC collagen with the three different weight % of PGF and their individual components, collagen and PGF, was determined using a Setaram Differential Thermal Analyser (DTA/TGA). The same method previously described in Section 5.2.2.2.3. for PC collagen was also employed. A plot of weight variation against temperature was obtained, showing the weight loss of the sample as the temperature increased, and this plot was used for calculating the weight % of different components of

the construct after the test completion. At least 5 repeat specimens were used for this test. The weight % of the residue ($wt_r\%$) was calculated from equation (6.1).

$$wt_r\% = \frac{(wt_i - wt_l)}{wt_i} * 100 \quad (6.1)$$

Where: wt_i was the initial weight of the sample, and

wt_l was the weight loss calculated from TGA plot.

b) Ashing

This test was used to verify the results obtained from TGA analysis; the weight of the same samples used for TGA before and after each run (final ashed content) was carried out to calculate the residual weight of each sample. The weight % of the residue was calculated from equation (6.2) (Vakiparta *et al.*, 2004).

$$wt_r\% = \frac{(wt_i - wt_f)}{wt_i} * 100 \quad (6.2)$$

Where, wt_f is the final weight of the sample.

6.2.2.1.3. Quasi-Static Uniaxial Tensile Testing

This test was carried out to identify the mechanical properties of the spirally assembled PGF-PC collagen of different weight % of PGF under tensile mode using the Perkin-Elmer DMA 7-e under the same conditions as previously described in Section 5.2.2.2.3. for PC collagen. The effect of the weight % of the PGF on the ultimate tensile strength, modulus of elasticity, and strain to break were calculated from at least 7 repeats from the stress-strain curve.

6.2.2.2. Characterisation of Cellular PGF-PC Collagen Constructs

6.2.2.2.1. Cell Viability using Live/Dead Staining and Confocal Microscopy

To assess the cell viability within the constructs, a live/ dead fluorescent stain was used and the samples viewed under confocal microscopy. This fluorescence-based staining was used to observe cell morphology and to differentiate between live and dead cells, where live cells stained with calcein acetoxymethyl ester (AM) (Molecular Probes, UK), and dead cells with propidium iodide (Sigma, UK) (Vijayasekaran *et al.*, 1998, Aizawa *et al.*, 2001, Aper *et al.*, 2004, Heywood *et al.*, 2004, Lu *et al.*, 2004).

a) Technique

Confocal microscopy offers two advantages over conventional optical microscopy including: (1) Elimination of out-of-focus information due to the presence of confocal aperture which eliminates all light coming from regions of the specimen above or below the plane of focus (Brigitte, 1998) as illustrated schematically in Figure 6.5.

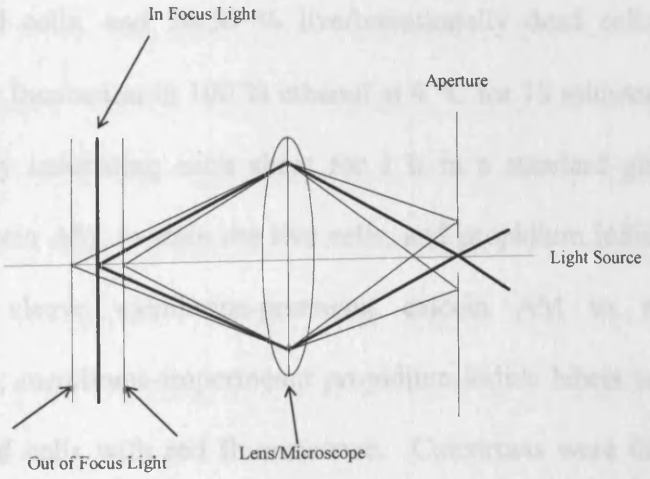

Figure 6.5: The principle of the confocal laser scanning microscope (Brigitte, 1998).

All in-focus information of each specimen point is recorded by a light-sensitive detector (photomultiplier) positioned behind the confocal aperture, and the analogue output signal is digitized and fed into a computer.

(2) The ability to collect serial sections throughout the whole specimen thickness with a proper control on the depth of field to be imaged. By moving the focal plane step by step through the depth of the specimen, a series of optical sections can be recorded. A composite projection image, or a volume rendered 3-D representation of the specimen can be generated from the stack of serial optical sections. This is particularly important for biological specimens where information from regions far-away from the plane of focus can obscure other images.

b) Method

I) Preliminary Experiment

A preliminary study was carried out to test the effectiveness of the live/dead staining method in assessing cell viability. This was conducted on a PC collagen sheet seeded with 100 % dead cells, and 50/50 % live/intentionally dead cells. The dead cells were sacrificed by incubation in 100 % ethanol at 4 °C for 15 minutes. Live/dead staining was conducted by incubating each sheet for 1 h in a standard growth medium containing 1μm/ml calcein AM, to stain the live cells, and propidium iodide, to stain the dead cells. Live cells cleave membrane-permeant calcein AM to yield cytoplasmic green fluorescence; membrane-impermeant propidium iodide labels nucleic acids of membrane compromised cells with red fluorescence. Constructs were then washed with dye-free Phosphate-buffered saline solution PBS (Invitrogen, UK) for 5 min. The

excitation/emission wavelength of calcein AM and propidium iodide is 495/515 nm and 536/617-636 nm respectively.

The assessment of cell viability in three dimensions was performed using confocal microscopy (Bio-Rad). In a typical scan, the sample was placed onto a bottom of 60 mm culture dish and sections of the sample were scanned using a 20X lens. The region of interest was 600 x 600 μm, x-y dimension, and the images were collected at 2. μm intervals through approximately 50 μm thickness of the compressed sheet and 4000 μm (nominal thickness) of gel in z-dimension (Z stacks) using Laser Sharp 2000 software. Excitation wavelengths for the fluorescent dyes for live and dead cells were provided at 488 nm from an argon laser and 543 nm from Green/HeNe laser respectively. Projection images were created by superimposing the z stack images that were captured throughout the construct thickness using ImageJ software. % Cell viability was calculated from 5 randomly chosen areas from each image.

II) Cell Viability up to 24 h

The effect of PC technique and PGF reinforcement on resident cell viability was assessed both immediately (1 h) and after 24 h construct incubation. Determination of cell viability was carried out at each stage of plastic compression, including sheet and spirally assembled constructs for both PC collagen and PGF-PC collagen, and compared to non compressed collagen as a control. The spirally assembled constructs were unrolled immediately before staining to ensure diffusion of the stains into the whole construct thickness.

6.2.2.3. *Statistical Analysis*

Student's *t* test was used to compare between the mean values of PGF obtained from TGA and ashing tests. Also it was used to compare between the mean of the % cell viability in constructs with different PGF contents compared to control immediately and after 24 hours incubation. However, for testing the effect of PGF weight % on mechanical properties, non-parametric Kruskall Wallis tests were performed, and Mann Whitney U test was used set the significance between pairs after adjusting *p* value for multiple testing using Bonferroni correction. The adjusted *p* value (*p*`) equals to *p* value multiplied by the number of testing. Differences were considered significant at 0.05 level. All the statistical analysis was carried out using SPSS 12.0.1 for Windows.

6.3. Results

6.3.1. Acellular PGF-PC Collagen Constructs

6.3.1.1. Morphological Characterisation

6.3.1.1.1. *Scanning Electron Microscopy*

Figure 6.6 shows typical SEM images of the cross-sectional view (a-d) and lateral view (e) of the spiral PGF-PC collagen prepared with low, medium, and high PGF content compared to PC collagen (f). It was apparent from the cross-sectional images that there was a clear difference in the amount of the glass fibres in each construct. As it was hypothesised, there was an increase in the amount of fibres incorporated in each construct by decreasing the drum cross-head speed.

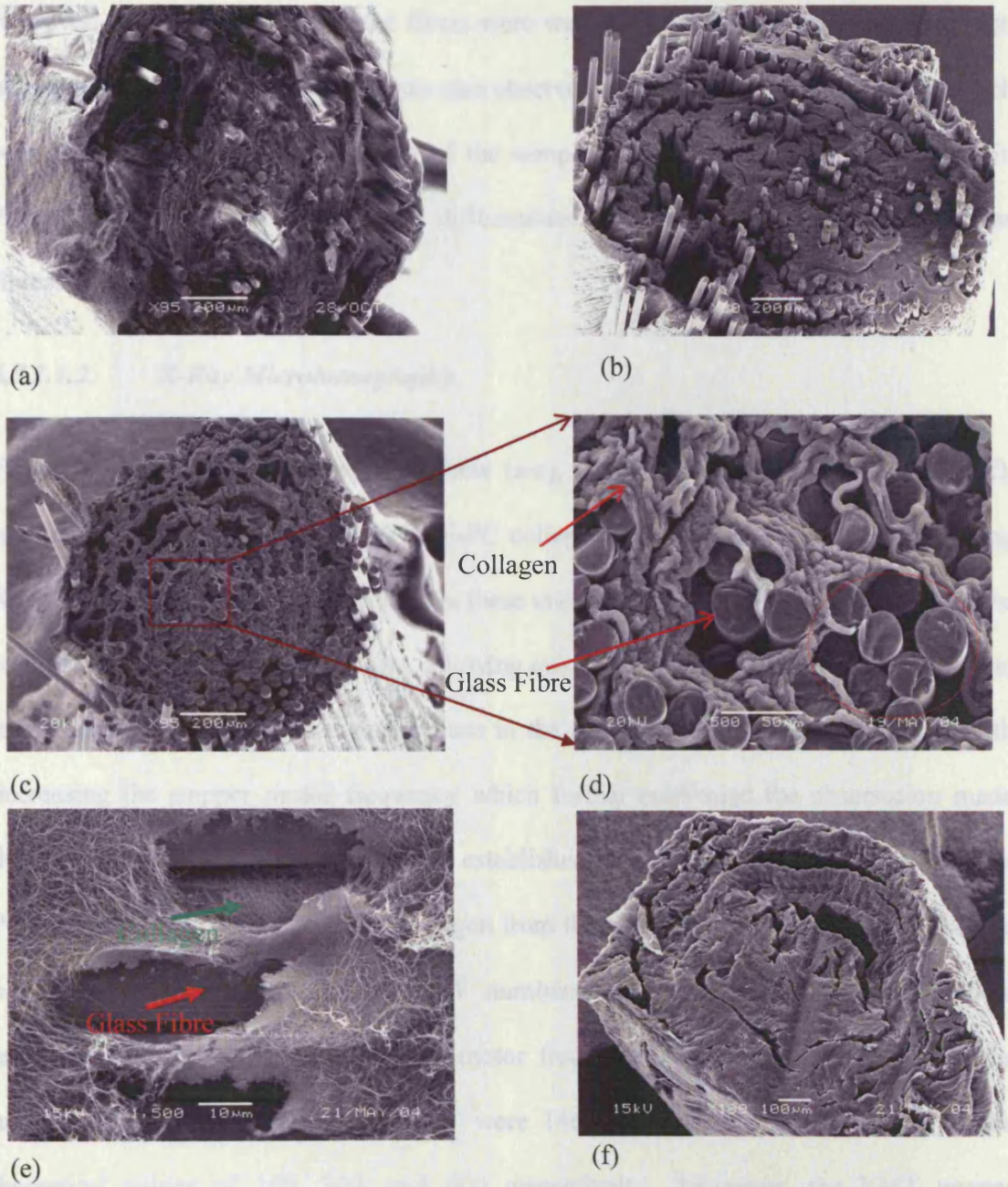

Figure 6.6: Scanning electron micrograph of cross-sectional view of the spirally assembled PGF-PC collagen with (a) low PGF generated at 50 Hz SMF, (b) medium PGF generated at 25 Hz SMF, (c) high PGF generated at 12.5 Hz SMF, and (d) high magnification of (c). The circle refers to the clustering of a group of fibres seen after processing, (e) lateral view of the spirally assembled PGF-PC collagen, and (f) PC collagen spiral.

However, it was also clear that the fibres were well distributed throughout the construct, although some clustering of fibres was also observed as shown in Figure 6.6 (d). A punch was made through the lateral aspect of the sample to show the internal structure as in Figure 6.6 (e) where it was easy to differentiate between collagen network and glass fibres.

6.3.1.1.2. X-Ray Microtomography

Figure 6.7 shows the cross-sectional view (a-c), and the three dimensional view (d-f), respectively of the three weight % PGF-PC collagen spiral constructs, as obtained using X-ray microtomography. The contrast in these micrographs was manipulated to render the collagen in the specimen transparent, allowing quantification of the PGF material. Again, it was apparent that there was an increase in the amount of PGF in each construct with decreasing the stepper motor frequency which further confirmed the observation made during SEM analysis. This was further established by manually counting the number of PGF in the three different PGF-PC collagen from the cross-sectional XMT images (Figure 6.7 (a-c)) which showed that the PGF numbers were comparable to the theoretical estimated numbers. At drum stepper motor frequencies of 50, 25, and 1.25 Hz, the numbers of PGF identified from XMT were 146, 303, and 571 corresponding to the theoretical values of 160, 309, and 600 respectively. Moreover, the XMT images demonstrated clear zones between separate sheets in the spirally assembled constructs. As in the SEM images, the clustering of PGF was also seen as in Figure 6.7 (f). The micrographs generated using XMT provided an excellent illustration of the degree of alignment of the PGF within the constructs, showing the fibres were generally well aligned with respect to each other. However, there was some evidence of fibres becoming

seriously misaligned, for example in Figure 6.7 (f). The misalignment may have been introduced during the cutting of the sample prior to XMT analysis.

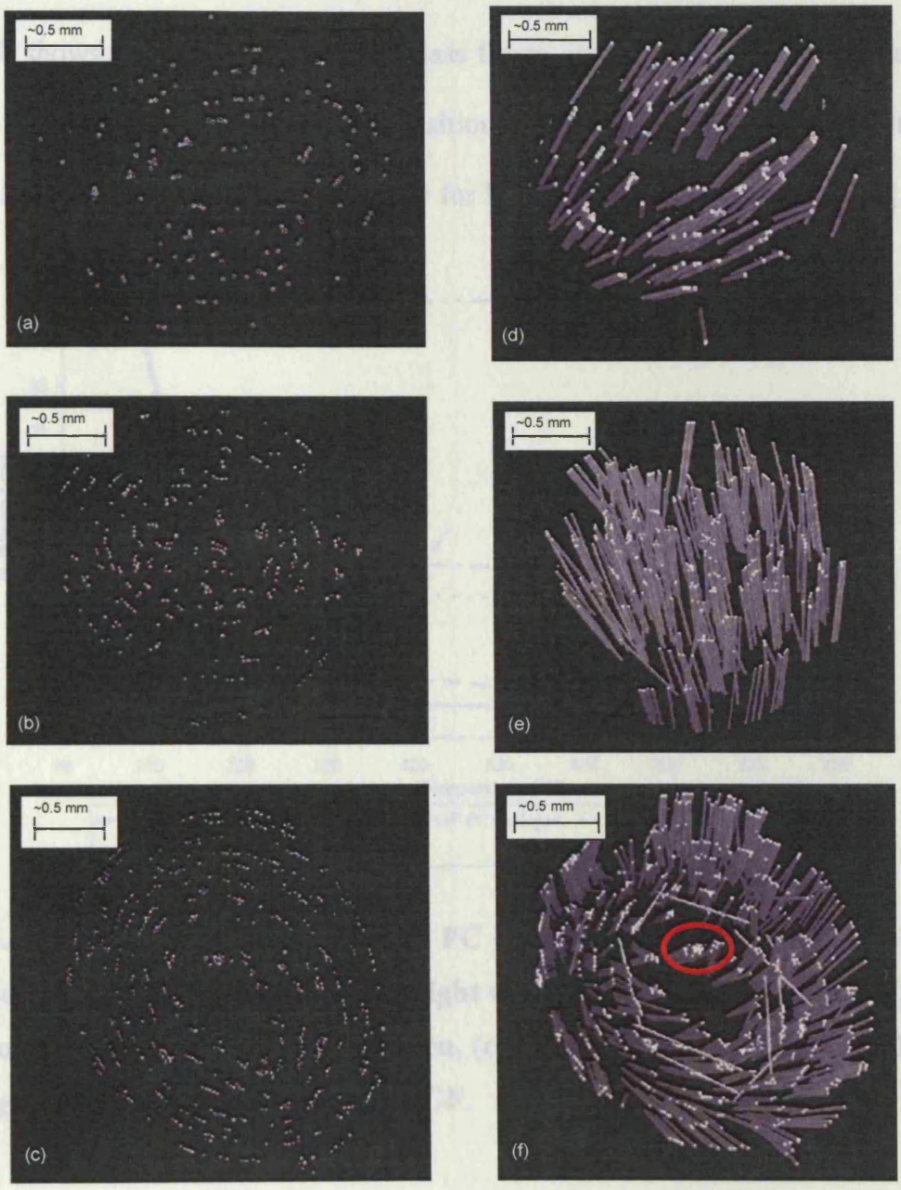

Figure 6.7: XMT of cross-sectional (a-c) and three dimensional views (d-f) of PGF-PC collagen with low (a & d), medium (b & e), and high PGF (c & f) respectively. The circle refers to the clustering of PGF seen after processing.

6.3.1.2. Quantification of PGF-PC Collagen Components

6.3.1.2.1. Thermo-Gravimetric Analysis

Figure 6.8 shows the TGA plots for the glass fibres, spirally assembled PC collagen, and PGF-PC collagen with the three compositions. PGF-PC collagen showed the same regions of weight loss identified previously for PC collagen shown in Figure 5.21.

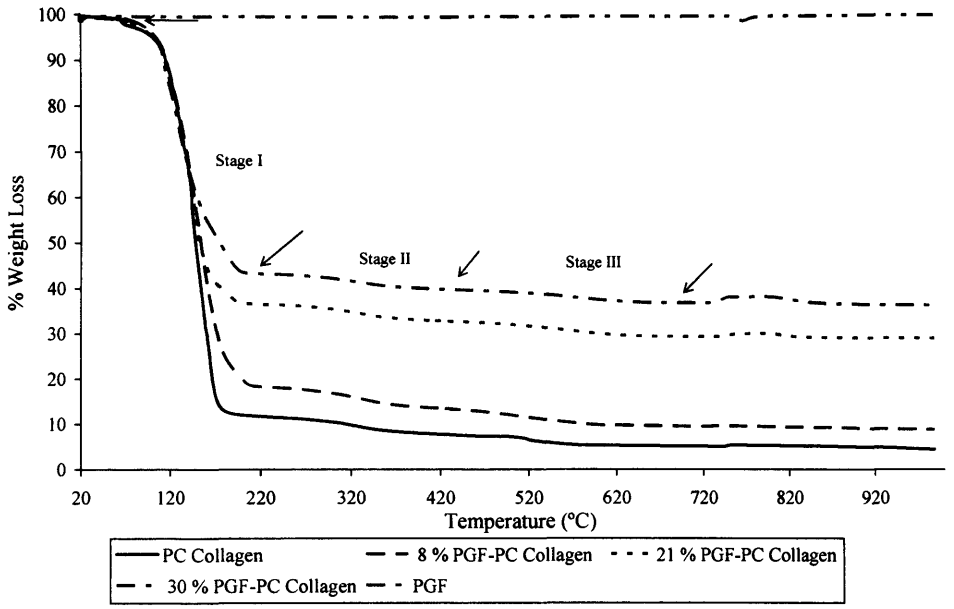

Figure 6.8: Thermo-gravimetric plot of PC collagen and PGF-PC collagen at three weight percentages. Three regions of weight variation were identified as I, II, and III. (a) PC collagen, (b) 8% PGF-PC collagen, (c) 21% PGF-PC collagen, (d) 30% PGF-PC collagen spiral assemblies, and (e) PGF.

Table 6.2 summarises the average % weight loss observed over these three regions identified in TGA plot.

Table 6.2: Summary of the average weight loss % of PGF-PC collagen with three different amounts of PGF and its individual components from TGA, and the % construct components calculated at 200 °C and from ashing.

Materials	Weight Loss (%)			Weight % Calculated at 200 °C			Ashing	
	First Stage (110-180 °C)	Second Stage (280-390 °C)	Third Stage (500-650 °C)	Fluid	Collagen	PGF	Weight Loss (%)	Weight Remaining (%)
Collagen (n=5)	85.4 ± 2.2	5.0 ± 1.1	3.5 ± 1.1	85.4 ± 2.2	14.6 ± 2.2	0	99.5 ± 0.2	0.5 ± 0.2
Low PGF (generated from 50 Hz SMF)-PC Collagen (n=5)	76.9 ± 6.8	4.8 ± 0.6	3.7 ± 0.4	77.0 ± 6.2	14.6 ± 2.2	8.4 ± 6.2	86.1 ± 3.2	13.9 ± 3.2
Medium PGF (generated from 25 Hz SMF)-PC Collagen (n=10)	65.1 ± 2.5	4.3 ± 0.6	3.4 ± 0.4	55.3 ± 6.3	14.6 ± 2.2	20.7 ± 2.4	76.5 ± 4.1	23.5 ± 4.1
High PGF (generated from 12.5 Hz SMF)-PC Collagen (n=10)	55.6 ± 5.8	3.3 ± 0.3	2.7 ± 0.3	64.7 ± 2.4	14.6 ± 2.2	30.1 ± 6.3	64.7 ± 6.6	35.3 ± 6.6

From this table, it was clear that the weight loss at both the second and third region was much smaller compared to the sharp weight loss during the first region, and that the average weight loss % significantly decreased by addition of PGF to collagen. Alternatively, the overall trend for the glass fibres alone shown in Figure 6.9 demonstrated a negligible weight loss of 0.38 ± 0.02 % over the studied temperature range. This weight variation was detected around 400-500 °C and 700-800 °C that correspond to the glass transition and melting temperature respectively as was previously observed through DTA in Section 4.3.2.2.2.

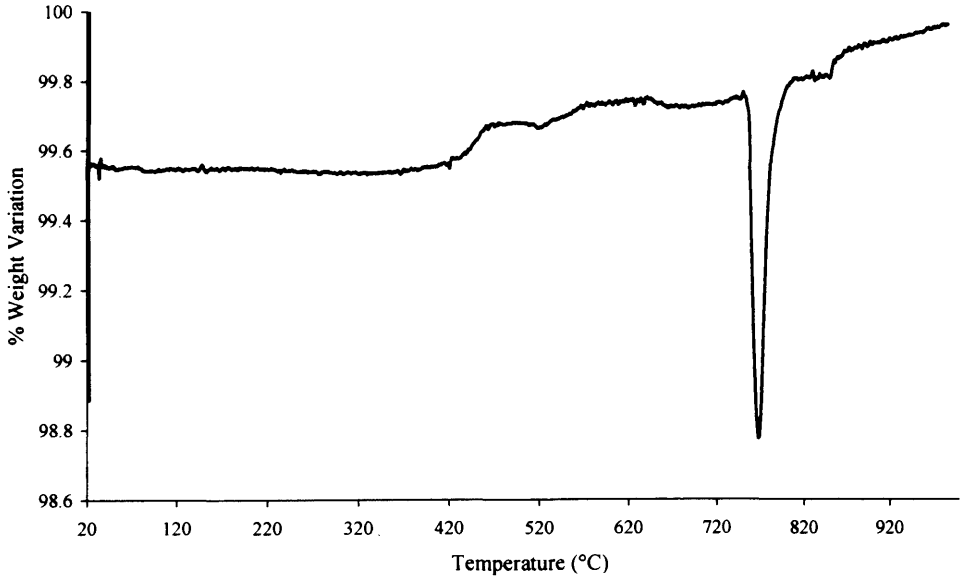

Figure 6.9: Thermo-gravimetric plot of phosphate glass fibres.

TGA was used as a quantitative technique to measure the weight % of various components of the construct. The calculations were considered at 200 °C where the fluid was completely eliminated; the results are also given in Table 6.2. There was a

significant increase in the weight % of the glass fibres with a decrease in the drum stepper motor frequency.

6.3.1.2.2. Ashing

Table 6.2 gives the final ashed weight % of the constructs, representing the glass fibre content. There was no statistically significant difference ($p > 0.05$) in the mean values obtained from both TGA and ashing methods. Collagen-only spiral constructs resulted in negligible residue by the end of the TGA run.

6.3.1.3. Quasi-Static Uniaxial Tensile Testing

Figure 6.10 shows the stress-strain curves obtained from quasi-static tensile testing of the spirally assembled PC collagen along with the three different weight % of PGF-PC collagen. Three regions were identified in the stress-strain analysis for PC collagen spirals, namely a toe-in region, a linear region, and a material failure region. The PC collagen constructs were significantly more compliant than PGF-PC collagen as shown by the tendency in the slope towards the x axis. By increasing the glass fibre content in the matrix, the construct became stiffer as the slopes shifted towards the y-axis, and exhibiting an increasingly brittle behaviour. The maximum strain for collagen only was 55.0 ± 13.8; which was significantly greater ($p < 0.05$) than that of PGF-PC construct that exhibited a small strain before failure ranging from 3.4 ± 1.2 to 7.7 ± 3.5 % for 30 and 8 wt % PGF-PC collagen construct respectively. Figure 6.11 shows the stress-strain superimposed with the modulus curve of 30 wt % of the spirally assembled PGF-PC collagen as an example to be studied in more detail.

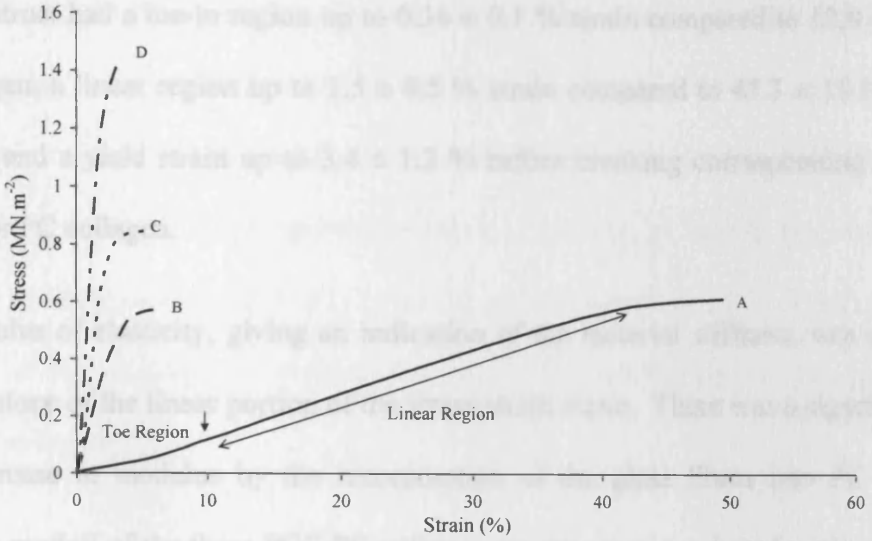

Figure 6.10: Stress-Strain curves obtained from quasi-static tensile testing of (a) PC collagen, (b) 8% PGF-PC collagen, (c) 21% PGF-PC collagen, and (d) 30% PGF-PC collagen spiral assemblies.

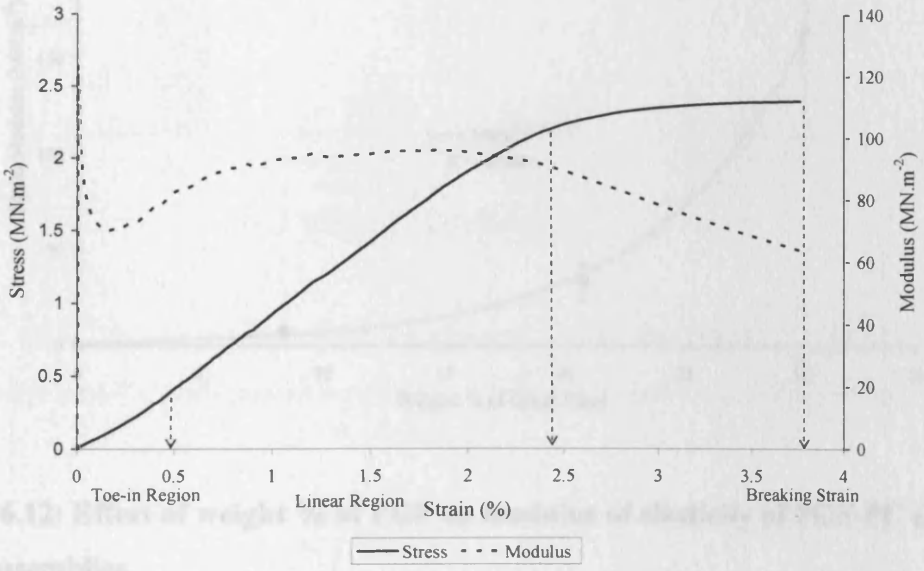

Figure 6.11: Stress-strain curve revealing the characteristic mechanical properties of 30 weight % PGF-incorporated collagen under tensile mode.

This construct had a toe-in region up to 0.36 ± 0.1 % strain compared to 12.8 ± 4 % for PC collagen, a linear region up to 1.5 ± 0.5 % strain compared to 47.3 ± 11.5 % of PC collagen, and a yield strain up to 3.4 ± 1.2 % before breaking corresponding to 55.0 ± 13.8 % for PC collagen.

The modulus of elasticity, giving an indication of the material stiffness, was calculated from the slope of the linear portion of the stress strain curve. There was a significant ($p < 0.05$) increase in modulus by the incorporation of the glass fibres into PC collagen. When the moduli of the three PGF-PC collagen constructs were plotted against the glass fibres weight % as shown in Figure 6.12, an exponential relationship was found.

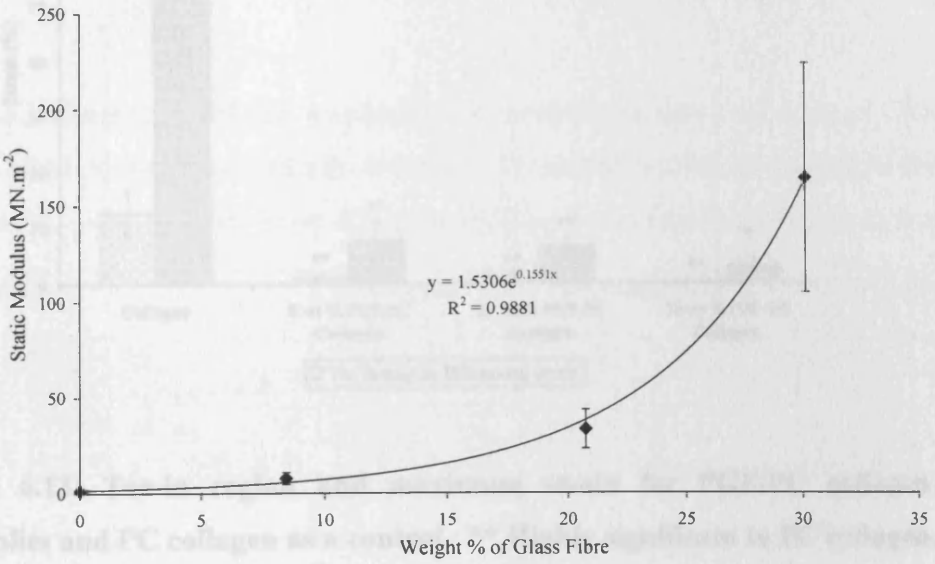

Figure 6.12: Effect of weight % of PGF on modulus of elasticity of PGF-PC collagen spiral assemblies.

The effect of glass fibre content on toe-in and breaking strain and the ultimate strength was presented in Figure 6.13 and 6.14 respectively. It was observed that there was a significant reduction in both strain components by the incorporation of the glass fibres. The ultimate tensile strength, corresponding to the stress at failure was significantly increased by incorporation of PGF. Table 6.3 gives a summery of the mean ± standard deviation of the various mechanical parameters of the spirally assembled collagen and PGF- PC collagen.

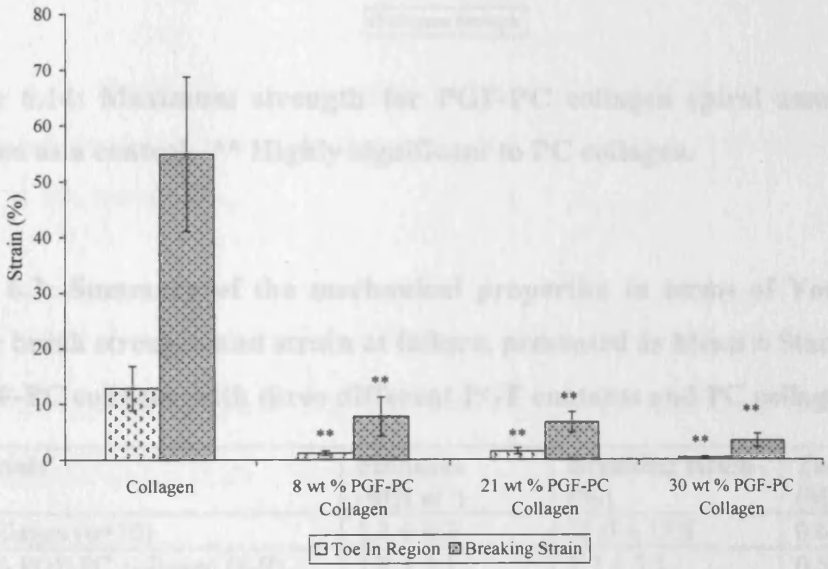

Figure 6.13: Toe-in region and maximum strain for PGF-PC collagen spiral assemblies and PC collagen as a control. ** Highly significant to PC collagen.

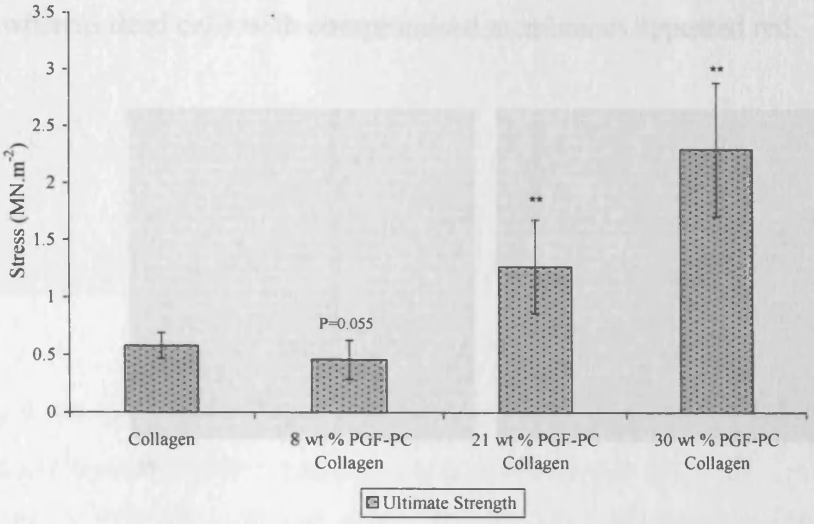

Figure 6.14: Maximum strength for PGF-PC collagen spiral assemblies and PC collagen as a control. ** Highly significant to PC collagen.

Table 6.3: Summary of the mechanical properties in terms of Young's Modulus, tensile break strength and strain at failure, presented as Mean ± Standard Deviation of PGF-PC collagen with three different PGF contents and PC collagen as a control.

Materials	Modulus ($MN.m^{-2}$)	Breaking strain (%)	Tensile strength ($MN.m^{-2}$)
PC collagen (n=10)	1.3 ± 0.3	55.0 ± 13.8	0.6 ± 0.1
8 wt % PGF-PC collagen (n-9)	7.8 ± 3.1	7.7 ± 3.5	0.5 ± 0.2
21 wt % PGF-PC collagen (n=9)	33.4 ± 10.2	6.7 ± 1.8	1.3 ± 0.4
30 wt % PGF-PC collagen (n=9)	164.9 ± 59.6	3.4 ± 1.2	2.3 ± 0.6

6.3.2. Cellular PGF-PC Collagen Constructs

6.3.2.1. Preliminary Experiment

Figure 6.15 shows confocal images of PC collagen sheet seeded with 100 % dead cells and 50/50 % live/dead cells. From these images, it was clear that the live/dead staining

was effective in differentiating between both cell states. The live cells fluoresce bright green, whereas dead cells with compromised membranes appeared red.

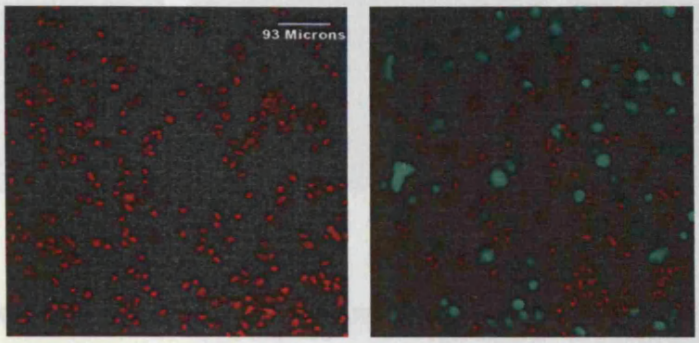

Figure 6.15: Confocal laser scanning micrographs of HOF immediately cultured (1 h) and entrapped within PC collagen sheet seeded with (a) 100 % dead cells, and (b) 50/50 % live/dead cells.

Also, the seeding of HOF within collagen solution before gelation entrapped these cells within the gel network, and they appeared to be well distributed throughout the final compressed collagen sheet. The obtained % of live cells in 50/50 % seeded samples was 43.2 ± 13.4 instead of the actual 50 % already seeded in the construct.

6.3.2.2. Cell Viability up to 24 h

The seeded constructs were analysed for the effect of both plastic compression and PGF inclusion on cell viability immediately (1 hour) after processing and after incubation for 24 h. Figure 6.16 shows the morphology of HOF seeded constructs with and without PGF incorporation at 21 wt %, used as an example. The cells showed a rounded morphology in both PC constructs with or without glass fibres. However, cell processes were only visible within non-compressed gels at the early time point of 1 h.

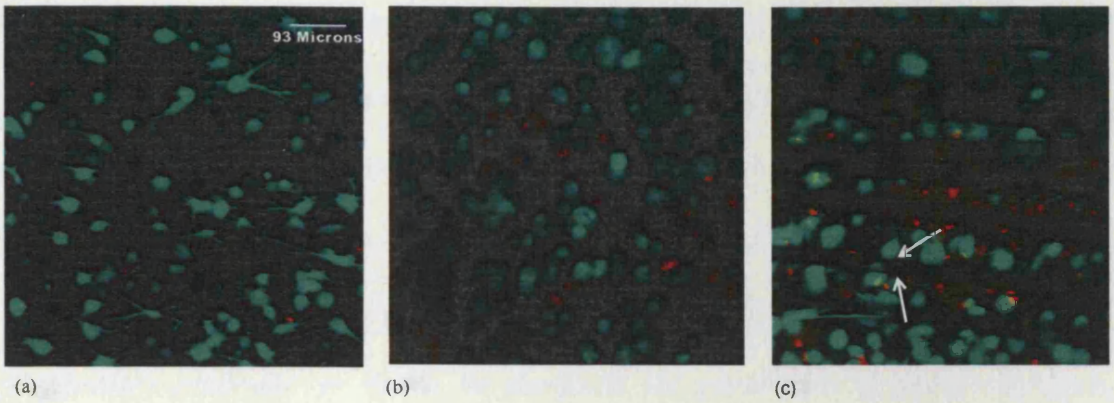

Figure 6.16: Confocal laser scanning micrographs of HOF immediately cultured (1 h) and entrapped within (a) non-compressed collagen gel, (b) PC collagen sheet, and (c) 21 wt % PGF-PC collagen sheet. The arrows indicate the edges of a glass fibre. Live cells are green, and dead cells are red.

The dead cells were clearly visible in PC constructs, PC collagen and 21 wt % PGF-PC collagen, compared to non-compressed collagen control. Moreover, there were some regions of focused cell death near the glass fibres. Figure 6.17 shows the morphology of HOF seeded constructs with and without PGF incorporation after 24 h in culture. After 24 h, the cells took on a tightly packed spindle shape appearances in three dimensions both in the PC collagen sheet and non-compressed collagen gels as shown in Figure 6.17 (a & b). HOF within PGF-PC collagen constructs also showed similar morphologies (Figure 6.16(c)) to those in PC collagen with no preference for either collagen matrix or glass fibres. Figure 6.18 shows a close up view of HOF cells aligned along a glass fibre after 24 h. Generally, the cells were abundant, and more closely connected to each other and to the substrate when compared to those in immediately (1 h) seeded constructs. On the other hand, within the PC spiral constructs shown in Figure 6.17 (d & e), the number of dead cells appeared to be higher than in the PC sheet forms.

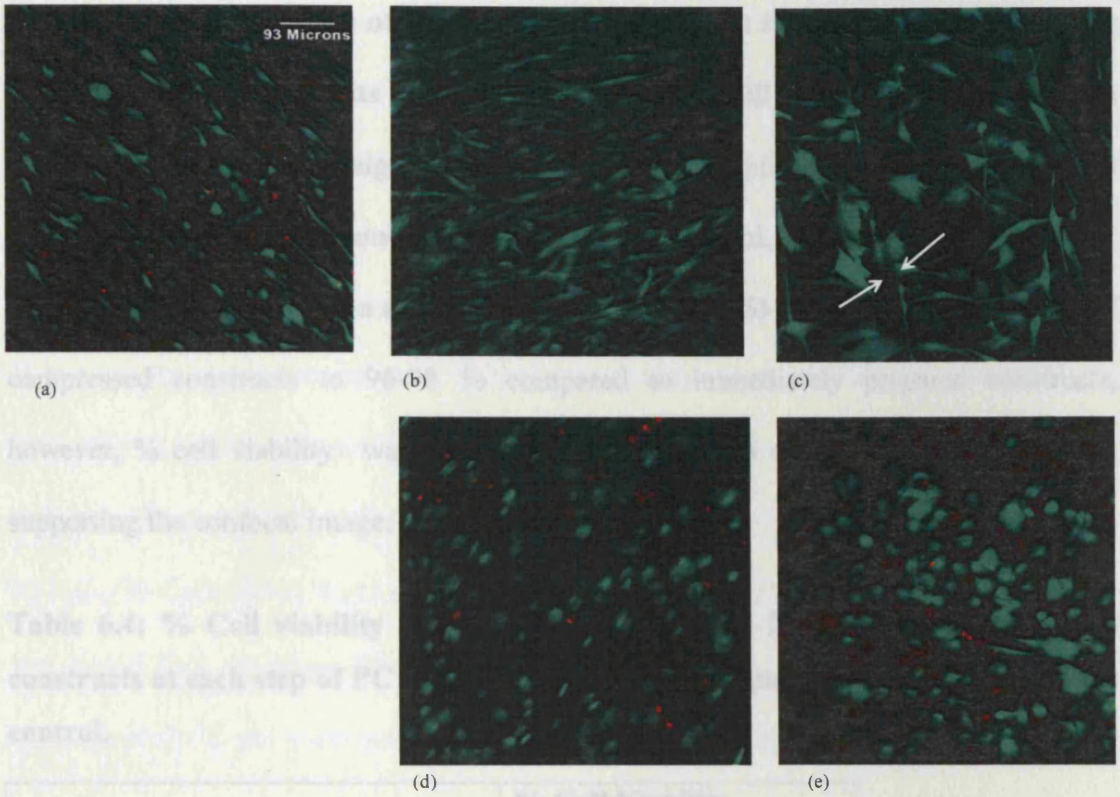

Figure 6.17: Confocal laser scanning micrograph after 24 h culture of HOF entrapped within (a) non-compressed collagen gel, (b) PC collagen sheet, (c) PC collagen spiral, (d) 21 wt % PGF-PC collagen sheet, and (e) 21 wt % PGF-PC collagen spiral construct. The arrows indicate the edges of a glass fibre. Live cells are green, and dead cells are red.

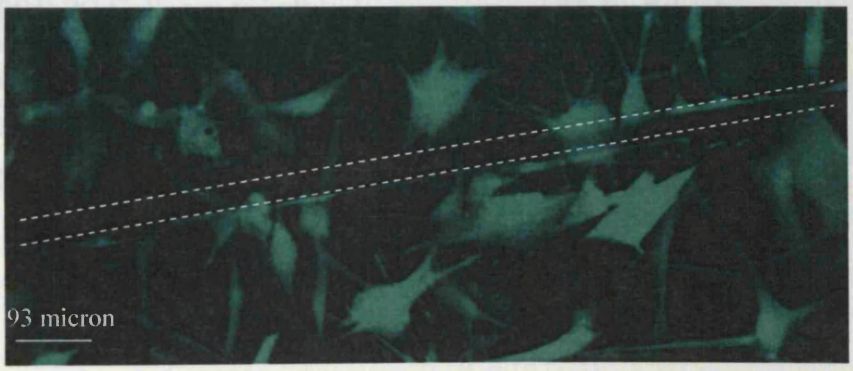

Figure 6.18: Closer view of HOF seeded in 21 wt % PGF-PC collagen sheet after 24 h demonstrating the attachment of cells showed no preference to either collagen or glass fibres (position indicated by the dashed lines).

Table 6.4 shows the change of cell viability of the resident fibroblasts due to PC with or without glass fibres was at its maximum only 20% across all types of constructs as given in Table 6.4. There was no significant difference ($p > 0.05$) in the immediate reduction in % cell viability between non-compressed collagen control, PC collagen, and PGF-PC collagen sheets. There was a significant increase (($p < 0.05$) in % cell viability at 24 h of compressed constructs to 96-98 % compared to immediately prepared constructs, however, % cell viability was significantly lower within spiral constructs after 24 h, supporting the confocal image.

Table 6.4: % Cell viability in immediately (1 h) and 24 h seeded PC produced constructs at each step of PC (sheet & spiral form) compared to non-compressed gel control.

Samples	% Cell Viability	
	Immediate	**24 h**
Non-compressed collagen	88.3 ± 8.3	85.9 ± 5.2
PC Collagen sheet	86.5 ± 7.7	100*
PC Collagen spiral	-	77.4 ± 7.7
8 wt % PGF-PC Collagen sheet	87.4 ± 9.5	98.4 ± 1.5
8 wt % PGF-PC Collagen spiral	-	83.8 ± 4.4
21 wt % PGF-PC Collagen sheet	80.4 ± 2.8	96 ± 2.3
21 wt % PGF-PC Collagen spiral	-	75.3 ± 8.4
30 wt % PGF-PC Collagen sheet	80 ± 5.3	100*
30 wt % PGF-PC Collagen spiral	-	79.7 ± 0.4

* No dead cells were detected in either PC-collagen-only or 30 % PGF-PC collagen sheets, probably due to the high cell density.

6.4. Discussion

In Chapter 5, the plastic compression technique was verified as a novel process for the rapid production of dense collagen matrices for potential use for tissue engineering application. The expulsion of fluid from hyper-hydrated collagen gels presented an

opportunity to prepare constructs with controlled meso-scale architecture and useful mechanical properties. This chapter applied the PC process to incorporate unidirectional-phosphate-based glass fibres into collagen constructs. This was carried out to further control the mechanical properties without compromising collagen biocompatibility, as phosphate-based glass contains ions which are naturally present in the body. These fibres also have the potential for tube formation as they degrade, therefore providing an intriguing possibility of capillary-like channels as demonstrated in Chapter 4 within the collagen. From a range of glass compositions based on the formulation (in mol fraction) 50 P_2O_5-30 CaO-(20-x) Na_2O-(x) Fe_2O_3, and fibre diameters ranging from 10 to 35 μm, it was found that the glass fibre compositions where $3 \leq x \leq 5$ having a diameter of approximately 35 μm were more durable than glasses with lower quantities of iron oxide, and of smaller diameters. Therefore, glass fibres containing 3 mol % Fe_2O_3 were selected to be used as reinforcing agents since this composition proved to be a compromise between highly degradable and relatively stable glass fibres. The application of PC to produce PGF-PC collagen was assessed by considering the repeatability of data obtained through morphological, thermal, and mechanical properties. The efficacy of this method for producing cellular PGF-PC constructs was also assessed by incorporation of HOF during the processing. HOF, being the predominant cells in subepithelial connective tissues and responsible for production of ECM and growth factors in these tissues (Gron *et al.*, 2002), were chosen to assess the effect of the processing for up to 24 h.

Morphological characterisation through SEM and XMT showed that the glass fibre content was significantly increased with a reduction in the drum cross-head speed; this finding was further confirmed by the data obtained from both TGA and ashing. This

indicated that changing the frequency of the fibre-rig stepper motor was an effective method of controlling the amount of the glass fibres within the final construct. It was evident that the glass fibres could be incorporated within the collagen matrix, and it proved be easy differentiated form the collagen network. The presence of clusters of glass fibres that were detected from SEM and XMT images can be attributed to several factors, such as the open air environment in which the fibres were pulled, and the hand-made processing of the constructs.

From the TGA results, the calculation of PGF content at 200 °C was considered to be more representative of the actual amount of PGF incorporated since the fluid was completely eliminated. This was also confirmed from the literature (Samouillan, 1999& 2003, Kumar, 2003, Shanmugasundaram, 2004). At 200 °C, the PC collagen lost 85 % water, and the remaining 15 % was collagen. By subtracting this collagen content, the PGF was 8, 21, and 30 wt % for fibres pulled at frequency of 50, 25, and 12.5 Hz respectively. Therefore, there was a significant increase in PGF wt % with a decrease in the fibre-rig stepper motor frequency. This was also confirmed by considering the final ashed weight % where there was no statistically significant difference ($p > 0.05$) in the mean values representing the glass fibre content obtained form both methods. Collagen-only spiral constructs resulted in a negligible residue by the end of the TGA run combining only the salt used for neutralisation of the collagen solution. PGF-PC collagen constructs underwent the same transitions as in PC collagen, suggesting that collagen was responsible for the thermal instability of the construct. On the other hand, the glass fibres were thermally stable over the same temperature range. Generally, the

transition observed between 110 and 650 °C for PGF-PC collagen correlated well to the range (70 to 800 °C) identified for HA-gelatin composites (Sivakumar and Rao, 2002).

The mechanical characterisation of the PGF-PC constructs showed a significant increase in both modulus and strength with the incorporation of the unidirectionally-aligned glass fibres into collagen. This was achieved in spite of the potential overestimation of the functional sample diameters caused by the imperfect contact or fluid pockets between construct sheets as suggested in SEM images, and the absence of any chemical interaction between collagen and glass fibres. The absence of chemical interaction was also observed during preparation since the glass fibres could be easily pulled away from the collagen matrix. This was expected, since no surface treatment or coupling agents were applied on the fibres during the setting of collagen. The mechanical properties observed for 21 wt % PGF- PC collagen construct were comparable with those previously reported by Dunn *et al.* (1997) for a resorbable composite of PLA and native collagen developed for the reconstruction of the anterior cruciate ligaments. Compared to PC collagen, the lower % deformation to break PGF-PC collagen was due to increasing the proportion of PGF, clearly reflecting the brittle behaviour of the glass fibre component. The observed reduction in toe-in region with the addition of glass fibres was expected since this region is a characteristic of viscoelastic materials. Since the break strength value of the PGF-PC constructs was significantly greater than that of PC collagen, once the glass fibres component underwent failure, the collagen failed immediately.

Two factors were evaluated throughout the viability study; firstly, the effect of the processing method, including compression and rolling, and secondly, the effect of

composition on cell behaviour by investigating the three different weight % of PGF. The cell viability was maintained at 86.5 ± 7.7 through plastically compressing collagen gels; and the viability was reduced down to 80 ± 5.3 by the incorporation of 30 weight % PGF. However, this difference was not statistically significant ($p > 0.05$) for both non-compressed and PC collagen; this finding suggested that the glass fibres had no deleterious effect on immediate cell viability. However, the focused cell death near the glass fibres was possibly due to the high stiffness of the fibres combined with the compressive and/or shears forces experienced during the rapid removal of fluid due to PC. The rounded cell morphology seen in immediately seeded constructs suggested that cells extend their processes and move through the denser PC constructs much more slowly than through hyper-hydrated non-compressed gels. Not surprisingly, the cells were denser in compressed constructs than in the non-compressed gels in parallel with the increased collagen density.

After 24 h, the results showed that PC collagen and PGF-PC collagen sheets demonstrated significantly higher cell viability, when compared to immediately seeded constructs suggesting that the cells were proliferating. The cells also showed a spread, spindle-shaped appearance, and they extended their cytoplasmic processes to attach to each other and to the surrounding matrix. This cell morphology was seen within all PC produced sheet constructs similar to the non-compressed collagen, which may suggest that the compression and PGF had no negative effect up to this time point. However, at 24 h, the % cell viability was significantly reduced within the spiral constructs compared to the non-compressed collagen control, and comparable PC produced sheets, probably due to hypoxia and perfusion limitations.

This chapter showed that the PC processing was successfully employed to produce cellular, dense, collagen matrices incorporating unidirectionally-aligned glass fibres. Changing the setting of the fibre-rig stepper motor was also effective in producing different weight % of PGF, and controlled fibre spacing as confirmed qualitatively by SEM and XMT, and quantitatively by TGA and ashing. The glass fibres significantly altered the tensile mechanical properties of PC collagen regardless of the absence of chemical interactions between these phases. This PGF-PC collagen could be potentially used for the engineering of skeletal muscles. The structure of muscle is made up of thousands of fibres often running all the way from origin to insertion, the fibres are bound together by connective tissue sheet which runs the blood vessels and nerves. Moreover, PGF showed biocompatibility to muscle cells and showed myotube formation (Ahmed et *al.*, 2004c). Hence it would be possible for the same construct to have fibres with different degradation rates, so that the highly degrading fibres could provide channels for the growth of blood vessels and nerve, and the relatively slower degrading fibres could allow for the alignment of cells to form myotubes thus mimicking the structure of muscle.

Chapter 7

Summary, Conclusions, and Further Work

7.1. Summary and Conclusions

Phosphate glasses are a unique class of materials that are degradable and biocompatible, and their degradation can be controlled by changing the glass chemistry. The potential use of phosphate glass fibres (PGF) as biomedical materials was investigated using two different quaternary glass systems. Two modifying oxides, CuO and Fe_2O_3 were incorporated into the highly soluble ternary glass system, based on 50 P_2O_5-30 CaO- 20 Na_2O composition, developed for either biomedical or tissue engineering applications. Glasses containing 50 mol % P_2O_5 ensured fibres were successfully produced for each glass system from the melt. These fibres were characterised in terms of thermal, structural properties, degradation, and ion release both the cationic and anionic species.

In the copper containing glass system, the results showed that the degradation of the glass fibres was linear over the first six hours, and the rate of degradation was substantially decreased as the CuO content increased. This reduction in the degradation rate was possibly due to increased cross-link density associated with P-O-Cu bonds, which also correlated with an increase in density and T_g. There was a further decrease in degradation with increasing fibre diameter. Both the amount and rate of copper ions released over the first six hours increased with increasing CuO content, as well as an increase in the surface area to volume ratio. Antimicrobial analysis showed that the copper ions released from the 10 mol % CuO PGF were the most effective in killing the opportunistic pathogen

Staphylococcus epidermidis. However, it was observed that the fibre diameters of copper containing glasses had no significant effect on the antimicrobial and thermal properties. Copper incorporated PGF, particularly those with 10 mol % CuO, could be prepared in a mesh form to be potentially used a wound dressing for the treatment of sever burns, leg ulcers, pressure sores, and infected surgical wounds. Moreover, it could be potentially used as sutures; however, the brittle nature of these materials may be a potential problem which can be controlled by a polymeric coating. Incorporation of these fibres into bone cement used for fixation of orthopaedic devices such as hip replacement devices could also be considered as another avenue for potential application.

In the iron containing glass system, the durability of phosphate glass was significantly increased with increasing Fe_2O_3 content as there were two orders of magnitude reduction in the rate of degradation by incorporating 5 mol % Fe_2O_3. This was related to the formation of more hydration resistant Fe-O-P bonds. This also correlated with the increase in both density and T_g. The ion release behaviour reflected the degradation behaviour of the glass. The degradation rate was also found to increase with decreasing fibre diameter due to the increased surface area to volume ratio. The durability of the glass was found to influence the cation and anion release behaviour as well as the pH change in the degradation medium. From the range of glass compositions and fibre diameters investigated, this study confirmed that glass fibres containing greater than 3 mol % iron oxide with a diameter of approximately 35 μm range would be more durable and more suitable for potential tissue engineering applications such as muscle, ligament, tendon, and bone. This is concurrent with the cell work carried out by Ahmed *et al.*, 2004c, and Bitar *et al.*, 2005. This study also found that the iron containing fibres formed tube-like structures when they degraded, therefore, they could be potentially used

in combination with either natural or synthetic polymers to help the ingrowth of vascularisation and the diffusion of nutrient and waste through the scaffold, and also for cell transplantation. However, the exact reasons for this tube formation are not currently understood, but it thought to be due to ordered precipitation associated with localised high ion concentration.

Both glass systems made fibres of the same diameter using the same pulling speed although they were pulled through different temperatures. Fe^{3+} had a stronger effect than Cu^{2+} on the tested properties, particularly the degradation rate of the fibres. This may reflect that both ions have different roles when they are incorporated into the glass structure, since Cu can act as network modifier while Fe can act as both network modifier and/or former. This was also confirmed by the finding that the degradation rate followed an inverse linear relationship against CuO content; whereas, it followed inverse exponential behaviour against Fe_2O_3. It was also noticed that Na^+, Ca^{2+}, and $(P_3O_9)^{3-}$ constituted the main components released from both glasses. This finding indicates that these three species may constitute the major components in the glass structure. On the other hand, it was observed that Fe^{3+} release is inversely related to the amount of Fe_2O_3, and this was not the case with the Cu^{2+} in the copper system.

Collagen gels are biologically excellent biomimetic materials; however, randomly oriented collagen fibrils with an excess of fluid (> 99 %) results in the gels being too weak to withstand manipulation or mechanical load. The plastic compression (PC) of native collagen gels is a novel method for the production of tissue analogous implants, and it achieves most of the demands for cell-independent tissue engineering. Key to this is the management of the aqueous component of the hyper-hydrated starting material. This

study undertook a number of mechanical tests to verify the mechanisms of PC in these gels through mechanical analyses under unconfined compression, and utilised this method for the production of unidirectional PGF incorporated collagen. These results indicated that the PC fabrication of tissue equivalent implants and biomaterials from very low density gels is clearly linked to polymer chemistry since the polymer here (collagen fibrils) have only weak inherent swelling potential at neutral pH. Unconfined compression of collagen gels expels fluid, which does not return on removal of the load: i.e. plastic compression. This presents a potentially ideal mechanism for controlling matrix density and mechanical properties. The potential scale of fluid displacement also means that the physical dimensions of constructs can be reduced by orders of magnitude. PC could be potentially used to engineer tissue-like constructs without cell action for connective tissue scaffolds construction as tubes, rods, or sheets.

The PC was successfully employed for the development of three dimensional constructs of cellular, dense, collagen matrices incorporating unidirectionally-aligned PGF. This was carried out for three main reasons; firstly, the versatility of PC in developing heterogeneous constructs, secondly, incorporation of PGF to further enhance the mechanical properties, and thirdly, to provide an intriguing possibility of channel formation. It was observed that the incorporation of fibres significantly increased the strength and stiffness of the constructs, but compromised the compliance regardless of the absence of chemical interactions between these phases. PC and PGF content did not significantly reduce cell viability compared to the non-compressed gel control. Moreover, the cell viability significantly increased after 24 h compared to immediately prepared constructs. PGF-PC collagen constructs, mimicking the morphology of the skeletal muscle, could be potentially used for engineering of these muscles.

7.2. Recommendation for Further Work

7.2.1. Copper Containing Phosphate Glass Fibres

- Possible incorporation of higher CuO/Na_2O ratio for production of glass fibres for long term antibacterial applications. However, the cytotoxicity issues of Cu should be considered to find compositions that encompass both properties.
- In depth antibacterial study to understand the precise mechanism responsible for the antibacterial effect of copper i.e., whether it is an actual antibacterial or anti-adhesiveness effect of copper ions in the glass fibres. This can be verified by viability study using flow cells or Constant Depth Film Fermenter (CDFF).

7.2.2. Iron Containing Phosphate Glass Fibres

- Investigating the glass fibre degradation in simulated body fluid and under dynamic environments to study the actual behaviour of fibre degradation. This may be different from the trend seen in deionised water; however, in such case, the ion release study may become complicated by the presence of the same ions at high levels than those released from fibres.
- A detailed study of the phenomena of tube formation through Energy dispersive X-Ray Analysis (EDAX), X-Ray Diffraction Analysis (XRD), Fourier Transform Infra-Red Spectroscopy (FTIR), and Raman Spectroscopy to see how these tubes formed, and are there any changes in composition while the fibres are degrading or any form of crystalline structure formation?.

7.2.3. PC Collagen

- Looking at the PC collagen construct at the meso-scale structural level by considering the collagen fibril diameter and pore size distribution, for example, by using atomic force microscopy, since these parameters may have an effect on cell viability particularly pore size distribution.
- Possible application of this processing method for other natural polymers particularly those containing high fluid contents such as; fibrin, fibronectin, and laminin.
- Studying the oxygen transportation and perfusion through PC spiral collagen as they may have an effect on cell viability particularly at the middle of the construct.

7.2.4. PGF-PC Collagen

- Further XMT studies for determination of the actual volume fractions of the glass fibres incorporated in each construct and relating to the mechanics of the constructs. More importantly, studying the mechanism of failure under tensile test through XMT.
- Possible use of coupling agents to introduce chemical bonding between collagen network and the glass fibres which may further enhance the mechanical properties for potential use in applications that require high tensile strength such as tendon.
- Long term viability and proliferation studies to look at the effect of composition to see if the fibre degradation will affect the cell behaviour. Also, studying the effect of incorporation of different cell densities on cell metabolism could be another point of interest.

- Studying the possibility of glass fibre tube formation within collagen after complete degradation of fibres by selecting a highly degradable fibre composition and low weight % incorporation.
- Possible incorporation of PGF into other polymers, synthetic or natural for potential channel formation which will help the diffusion of nutrient, gases, and waste and possibly therapeutic agents throughout the construct.
- Possible incorporation of copper containing PGF into PC collagen for the development of antimicrobial implants.

References

1. Ahmed, I., Lewis, M., Olsen, I., Knowles, J. C. 2004a. Phosphate glasses for tissue engineering: Part 1. Processing and characterisation of a ternary-based P_2O_5-CaO-Na_2O glass system. Biomaterials 25; 491-499.
2. Ahmed, I., Lewis, M., Olsen, I., Knowles, J. C. 2004b. Phosphate glasses for tissue engineering: Part 2. Processing and characterisation of a ternary-based P_2O_5-CaO-Na_2O glass fibre system. Biomaterials 25; 501-507.
3. Ahmed, I., Collins, C. A., Lewis, M., Olsen, I., Knowles, J. C. 2004c. Processing, characterisation and biocompatibility of iron-phosphate glass fibres for tissue engineering. Biomaterials 25; 3223-3232.
4. Ahmed, I., Lewis, M., Nazhat, S. N., Knowles, J. C. 2005. Quantification of anion and cation release from a range of ternary phosphate-based glasses with fixed 45 mol% P_2O_5. Journals of Biomaterials Applications 20; 65-80.
5. Aigner, T., Stove, J., 2003. Collagen-major component of the physiological cartilage matrix, major target of cartilage degeneration, major tool in cartilage repair. Advanced Drug Delivery Reviews 55; 1569-1593.
6. Aizawa, T., Kon, T., Einhorn, T. A., Gerstenfeld, L. C. 2001. Induction of apoptosis in chondrocytes by tumor necrosis factor-alpha. Journal of Orthopaedic Research 19; 785-796.
7. Alam, T. M., Tischendorf, B. C., Brow, R. K. 2005. High-speed ^1H MAS NMR investigations of the weathered surface of a phosphate glass. Solid State Nuclear Magnetic Resonance 27; 99-111.
8. Alexy, P., Bakos, D., Hanzelova, S., Kukolikova, L., Kupec, J., Charvatova, K., Chiellinin, E., Cinelli, P. 2003. Poly(vinyl alcohol)-collagen hydrolysate

thermoplastic blends: I. Experimental design optimisation and biodegradation behaviour. Polymer Testing 22; 801-809.

9. Aper, T., Teebken, E. O., Steinhoff, G., Haverich, A. 2004. Use of a fibrin preparation in the engineering of a vascular graft model. Eur. J. Endovasc. Surg. 28; 296-302.
10. Awad, H. A., Butler, D. L., Harris, M. T., Ibrahim, R. E., Wu. Y., Young, R. G., Kadiyala, S., Bovin, G. P. 2000. *In vitro* characterisation of mesenchymal stem cell-seeded collagen scaffolds for tendon repair: Effect of initial seeding density on contraction kinetics. J Biomed Mater Res. 51; 233-240.
11. Awad, H. A., Boivin, G. P. Dressler, M. R., Smith, F. N. L., Young, R. G., Butler, D. L. 2003. Repair of patellar tendon injuries using cell-collagen composite. Journal of Orthopaedic Research 21; 420-431.
12. Bae, B. S., Weinberg, M. C. 1991. Oxidation-reduction equilibrium in copper phosphate glass melted in air. J. Am. Ceram. Soc. 74(12); 3039-3045.
13. Beckett, D. R. 1976. The application of differential scanning Calorimetry to plastics processing and properties. Plastics and Rubber: Materials and Applications. 168-176.
14. Berglund, J. D., Mohseni M. M., Nerem, R. M., Sambanis, A. 2003. A biological hybrid model for collagen-based tissue engineered vascular constructs. Biomaterials 24; 1241-1254.
15. Berglund, J. D., Nerem, R. M., Sambanis, A. 2004. Incorporation of intact elastin scaffolds in tissue-engineered collagen-based vascular grafts. Tissue Engineering 10(9/10); 1526-1535.
16. Bitar, M., Salih, V., Mudera, V., Knowles, J. C., Lewis, M. 2004. Soluble phosphate glasses: *In vitro* studies using human cells of hard and soft tissue origin. Biomaterials 25; 2283-2292.

17. Bitar, M., Knowles, J. C., Salih, V. 2005. Soluble phosphate glass fibres for bone-ligament interface. Journal of Material Science: Materials in Medicine 16 (2005); 1131-1136.

18. Blaker, J. J., Gough, J. E., Maquet, V., Notingher, I., Boccaccini, A. R. 2003. *In vitro* evaluation of novel bioactive composites based on bioglass®-filled polylactide foams for bone tissue engineering scaffolds. J Biomed Mater Res. 67A; 1401-1411.

19. Blaker, J. J., Nazhat, S. N., Boccaccini, A. R. 2004. Development and characterisation of silver-doped bioactive glass-coated sutures for tissue engineering and wound healing applications. Biomaterials 25; 1319-1329.

20. Bleach, N. C., Nazhat, S. N., Tanner, K. E., Kellomaki, M., Tormala, P. 2002. Effect of filler content on mechanical and dynamic mechanical properties of particulate biphasic calcium phosphate-polylactide composites. Biomaterials 23; 1579-1585.

21. Boccaccini, A. R., Notingher, I. 2003. Bioresorbable and bioactive composite materials based on polylactide foams filled with and coated by bioglass® particles for tissue engineering applications. Journal of Material Science: Materials in Medicine 14; 443-450.

22. Bonassar, L. J., Vaccanti, C. A. 1998. Tissue engineering: the first decade and beyond. J Cell Biochem Suppls. 30(31); 297-303.

23. Bosetti, M., Cannas, M. 2005. The effect of bioactive glasses on bone marrow stromal cells differentiation. Biomaterials 26; 3873-3879.

24. Brigitte, M. G. 1998. Dentin permeability, adhesive penetration and interfacial stress. A confocal microscope study. Ph.D thesis, University of London.

25. Brow, R. K. 2000. Review: the structure of simple phosphate glasses. Journal of Non-Crystalline Solids 263 & 264; 1-28.

26. Brown, R. A., Wiseman, M., Chuo, C. B., Cheema, U., Nazhat, S. N. 2005. Ultra-rapid engineering of biomimetic tissues: A plastic compression fabrication process for nano-microstructures. Advanced Functional Materials 15; 1762-1770.

27. Bunker, B. C., Arnold, G. W., Wilder, J. A. 1984. Phosphate glass dissolution in aqueous solutions. Journal of Non-Crystalline Solids 64; 291-316.

28. Cacaina, D., Simon, S. 2003. Calcium influence on dissolution rates of potassium phosphate glasses. Journal of Optoelectronics and Advanced Materials 5(1); 191-194.

29. Cacou, C., Palmer, D., Lee, D. A., Bader, D. L., Shelton, J. C. 2000. A system for monitoring the response of uniaxial strain on cell seeded collagen gels. Medical Engineering & Physics 22; 327-333.

30. Cartmell, S. H., Dorthy, P. J., Rhodes, N. P., Hunt, J. A. 1998a. Haemocompatibility of controlled release glass. Journal of Material Science: Material in Medicine 9; 1-7.

31. Cartmell, S. H., Dorthy, P. J., Hunt, J. A., Healy, D. M., Gilchrist, T. 1998b. Soft tissue response to glycerol-suspended controlled-release glass particulate. Journal of Material Science: Material in Medicine 9; 773-777.

32. Celement, J., Manero, J. M., Planell, J. A., Avila, G., Martinez, S. 1999a. Analysis of the structural changes of a phosphate glass during its dissolution in simulated body fluid. Journal of Material Science: Material in Medicine 10; 729-732.

33. Clement, J., Torres, P., Gil, F. J., Planell, J. A., Terradas, R., Martinez, S. 1999b. Evaluation by Vickers indentation of fracture toughness of a phosphate biodegradable glass. Journal of Material Science: Material in Medicine 10; 437-441.

34. Ceruuti, M., Greenspan, D., Powers, K. 2005. Effect of pH and ionic strength on the reactivity of bioglass® 45S5. Biomaterials 26; 1665-1674.

35. Chahine, A., Et-tabirou, M., Pascal, J. L. 2004. FTIR and Raman spectra of the Na_2O-CuO-Bi_2O_3-P_2O_5 glasses. Material Letters 58; 2776-2780.

36. Chakradhar, R. P. S., Ramesh, K. P., Rao, J. L., Ramakrishna, J. 2003. Mixed alkali effect in borate glasses-electron paramagnetic resonance and optical absorption studies in Cu^{2+} doped x Na2O- (30-x) K_2O-70 B_2O_3 glasses. J. Phys.: Condens. Matter. 15; 1469-1486.

37. Chandran, P. L., Barocas, V. H. 2004. Microstructural mechanics of collagen gels in confined compression: Poroelasticity, viscoelasticity, and collapse. Transaction of the ASME 126; 152-166.

38. Chang, M. C., Ikoma, T., Kikuchi, M., Tanaka, J. 2002. The cross-linking effect of hydroxyapatite/collagen nanocomposites on a self-organization phenomenon. Journal of Material Science: Material in Medicine 13; 993-997.

39. Chapekar, M. S. 2000. Tissue engineering: challenges and opportunities. J Biomed Mater Res. 53(6): 617-620.

40. Charulatha, V., Rajaram, A. 2002. Influence of different crosslinking treatments on the physical properties of collagen membrane. Biomaterials 24; 759-767.

41. Chen, G., Sato, T., Ushida, T., Ocuhiai, N., Tateishi, T. 2004. Tissue engineering of cartilage using a hybrid scaffold of synthetic polymer and collagen. Tissue Engineering 10 (3/4); 323-330.

42. Choueka, J. Charvert, J. L., Alexander, H., Oh, Y. H., Joseph, G., Blumenthal, N. C., LaCourse, W. C. 1995. Effect of annealing temperature on the degradation of reinforcing fibres for absorbable implants. J Biomed Mater Res. 29; 1309-1315.

43. Chung, S. Y., Krivorov, N. P., Rausei, V., Thomas, L., Frantzen, M., Landsittel, D., Kang, Y. M., Chon, C. H., Ng, C. S., Fuchs, G. J. 2005. Bladder reconstitution with bone marrow derived stem cells seeded on small intestinal submucosa improves morphological and molecular composition. J Urol. 174 (1); 353-359.

44. Clupper, D. C., Gough, J. E., Hall, M. M., Clare A. G., La Course, W. C., Hench, L. L. *In vitro* bioactivity of S520 glass fibres and initial assessment of osteoblast attachment. 2003. J Biomed Mater Res. 67A; 285-294.

45. Clupper, D. C., Gough, J. E., Embanga, P. M., Notingher, I., Hench, L. L. 2004 Bioactive evaluation of 45S5 bioactive glass fibres and preliminary study of human osteoblast attachment. Journal of Material Science: Material in Medicine 15; 803-808.

46. Concas, G., Congiu, F., Muntoni, C., Pinna, G. 1995. Mössbauer spectroscopic investigation of iron in sodium phosphate glasses. J. Phys. Chem. Solids 56(6); 877-881.

47. Cooley, W. A., Scott, A. C., Simmons, M. M. 1994. The use of falcon cell culture inserts and hexamthyldisilazane for the study of small biological specimens by electron microscopy. Microscopy and Analysis 1; 23-25.

48. Corden, T., Jones, I. A., Rudd, C. D., Christian, P., Downes, S., McDougall, K. E. 2000. Physical and biocompatibility properties of poly-epsilon-caprolactone produced using in situ polymerization; a novel manufacturing technique for long fiber composite materials. Biomaterials 21; 713-724.

49. Cozar, O., Ardelean, I. 2003. Local structure and metal-metal interaction in some phosphate glasses. Journal of Optoelectronics and Advanced Materials 5 (1); 177-183.

50. Curless, C., Baclaski, J., Sachdev, R. 1996. Phosphate glass as a phosphate source in high cell density *Escherichia coli* fermentations. Biotechnol Prog. 12(1); 22-25.

51. Curtis, A., Riehle, M. 2001. Tissue engineering: The biophysical background. Phys. Med. Biol. 46; R47-R65.

52. Day, R. M., Boccaccini, A. R. 2005. Effect of particulate bioactive glasses on human macrophages and monocytes *in vitro*. J Biomed Mater Res. 73A (1); 73-79.

53. De Diego, M. A., Coleman, N. J., Hench, L. L. 2000. Tensile properties of bioactive fibers for tissue engineering applications. J Biomed Mater Res. 53; 199-203.

54. Delahaye, F., Montagne, L., Palavit, G., Touray, J. C., Baillif, P. 1998. Acid dissolution of sodium-calcium metaphosphate glasses. Journal of Non-Crystalline Solids 242; 25-32.

55. De Santis, R., Sarracino, F., Mollica, F., Netti, P.A., Ambrosio, L., Nicolais, L. 2004. Continuous fibre reinforced polymers as connective tissue replacement. Composites Science and Technology 64; 861-871.

56. Devireddy, R. V., Neidert, M. R., Bischof, J. C., Tranquillo, R. T. 2003. Cryopreservation of collagen-based tissue equivalents. I. Effect of freezing in the absence of cryoprotective agents. Tissue Engineering 9(6); 1089-1100.

57. Domingues, R. Z., Clark, A. E., Brennan, A. B. 2001. A sol-gel bioactive fibrous mesh. J Biomed Mater Res. 55; 468-474.

58. Drury, J. L., Mooney, D. J. 2003. Hydrogel for tissue engineering: scaffold design variables and applications. Biomaterials 24; 4337-3351.

59. Dunn, M. G., Bellincampi, L. D., Tria, A. J., Zawadsky, J. P. 1997. Preliminary development of a collagen-PLA composite for ACL reconstruction. J App Polym Sci. 63; 1423-1428.

60. Dvir-Ginzberg, M., Gamlieli-Bonshtein, I., Agbaria, R., Cohen, S. 2003. Liver tissue engineering within alginate scaffolds: Effects of cell-seeding density on hepatocytes viability, morphology, and function. Tissue Engineering 9(4); 757-766.

61. Enderle, J., Blanchard, S., Bronzino, J. 2000. Introduction to biomedical engineering. pp. 538. 1st edition, Academic Press.

62. Fang, X., Ray, C. S., Marasinghe, G. K., Day, D. E. 2000. Properties of mixed Na_2O and K_2O iron phosphate glasses. Journal of Non-Crystalline Solids 263&264; 292-298.

63. Feng, Z., Yamato, M., Akutsu, T., Nakamura, T., Okano, T., Umezu, M. 2003a. Investigation on the mechanical properties of contracted collagen gels as a scaffold for tissue engineering. J Artificial Organs 27(1); 84-91.

64. Feng, Z., Matsumoto, T., Nakamura, T. 2003b. Measurements of the mechanical properties of contracted collagen gels populated with rat fibroblasts or cardiomyocytes. J Artificial Organs 6; 192-196.

65. Fernandez, M., Mendez, J. A., Vazques, B., San Roman, J., Ginbera, M. P., Gil, F. J., Manero, J. M., Planell, J. A. 2002. Acrylic-phosphate glasses composites as self-curing controlled delivery systems of antibiotics. Journal of Material Science: Materials in Medicine 13; 1251-1257.

66. Ferraz, M. P., Feranandes, M. H., Trigo Cabral, A., Santos, J. D., Monteiro, F. J. 1999a. *In vitro* growth and differentiation of osteoblast-like human bone marrow cells on glass reinforced hydroxyapatite plasma-sprayed coating. J Mater Sci Mater Med. 10; 567-576.

67. Ferraz, M. P., Knowles, J. C., Olsen, I., Monteiro, F. J., Santos, J. D. 1999b. Flow cytometry analysis of effect of glass on response of osteosarcoma cells to plasma-sprayed hydroxyapatite / $CaO-P_2O_5$ coatings. J Biomed Mater Res. 47; 603-611.

68. Ferraz, M. P., Knowles, J. C., Olsen, I., Monteiro, F. J., Santos, J. D. 2000. Flow cytometry analysis of the effects of pre-immersion on the biocompatibility of glass reinforced hydroxyapatite plasma-sprayed coatings. Biomaterials 21; 813-820.

69. Franks, K., Abrahams. I., Knowles, J. C. 2000. Development of soluble glasses for biomedical use Part 1: *in vitro* solubility measurement. Journal of Material Science: Materials in Medicine 11; 609-614.

70. Franks, K. 2000. The structure and properties of soluble phosphate based glasses. PhD thesis, University of London.

71. Franks, K., Abrahams. I., Georgiou, G., Knowles, J. C. 2001. Investigation of thermal parameters and crystallisation in a ternary $CaO-Na_2O-P_2O_5$ based glass system. Biomaterials 22(5):497-501.

72. Franks, K., Salih, V., Knowles, J. C. 2002. The effect of MgO on the solubility behaviour and cell proliferation in a quaternary soluble phosphate based glass system. Journal of Material Science: Materials in Medicine 13; 549-556.

73. Friess, W. 1998. Collagen - biomaterial for drug delivery1. European Journal of Pharmaceutics and Biopharmaceutics 45(2); 113-136.

74. Fujioka, K., Maeda, M., Hojo, T., Sano, A. 1998. Protein release from collagen matrices. Advanced Drug Delivery Reviews 31:247-266.

75. Gabouev, A. I., Schultheiss, D., Mertsching, H., Koppe, M., Schlote, N., Wefer, J., Jonas, U., Stief, C. G. 2003. *In vitro* construction of urinary bladder

wall using porcine primary cells reseeded on acellularized bladder matrix and small intestinal submucosa. Int J Artif Organs 26 (10); 935-942.

76. Gage, J. P., Francis, M. J. O., Triffitt, J. T., Eds. The Collagens (Chapter 2). In: Collagen and dental matrices. Butterworth & Co. Ltd, 1989; pp 8-11.
77. Garvin, J., Jie, Q. I., Maloney, M., Banes, A. J. 2003. Novel system for engineering bioartificial tendons and application of mechanical load. Tissue Engineering 9 (5); 976-979.
78. Gao, H., Tan, T., Wang, D. 2004a. Effect of composition on the release kinetics of phosphate controlled release glasses in aqueous medium. Journal of Controlled Release 96; 21-28.
79. Gao, H., Tan T., Wang, D. 2004b. Dissolution mechanism and release kinetics of phosphate controlled release glasses in aqueous medium. Journal of Controlled Release 96; 29-36.
80. Geiger, M., Li, R.H., Friess, W. 2003. Collagen sponges for bone regeneration with rhBMP-2. Advanced Drug Delivery Reviews 55(12); 1613-1629.
81. Gelse, K., Poschl, E., Aigner, T. 2003. Collagens--structure, function, and biosynthesis. Advanced Drug Delivery Reviews 55(12); 1531-1546.
82. Gilchrist, T., Healy, D. M., Drake, C. 1991. Controlled silver-releasing polymers and their potential for urinary tract infection control. Biomaterials 12; 76-78.
83. Girton, T. S., Barocas, V. H., Tranquillo, R. T. 2002. Confined compression of a tissue-equivalent: collagen fibril and cell alignment in response to anisotropic strain. Transactions of the ASME 124; 568-575.
84. Götz, F. 2002. Staphylococcus and biofilms. Mol Microbiol. 43; 1367-78.

85. Gough, J. E., Christian, P., Scotchford, C. A., Rudd, C. D., Jones, I. A. 2002. Synthesis, degradation, and *in vitro* cell responses of sodium phosphate glasses for craniofacial bone repair. J Biomed Mater Res. 59(3); 481-489.

86. Gough, J. E., Christian, P., Scotchford, C. A., Jones, I. A. 2003. Long-term craniofacial osteoblast culture on a sodium phosphate and a calcium/sodium phosphate glass. J Biomed Mater Res. 66A; 233-240.

87. Gough, J. E, Nottingher, I., Hench, L. L. 2004a. Osteoblast attachment and mineralized nodule formation on rough and smooth 45S5 bioactive glass monotiths. J Biomed Mater Res. 66A; 640-650.

88. Gough, J. E., Jones, I. A., Hench, L. L. 2004b. Nodule formation and mineralization of human primary osteoblasts cultured on a porous bioactive glass scaffold. Biomaterials 25; 2039-2046.

89. Greaves, G. N., Smith, W., Giulotto, E., Pantos, E. 1997. Local structure, microstructure and glass properties. Journal of Non-Crystalline Solids 222; 13-24.

90. Griffith, L. G., Naughton, G. 2002. Tissue engineering-current challenges and expanding opportunites. Science 295; 1009-1014.

91. Gron, B., Stoltez, K., Andersson, A., Dabellsteen, E. 2002. Oral fibroblasts produce more HGF and KGF than skin fibroblasts in response to co-culture with keratinocytes. APMIS 110; 892-898.

92. Gu, W. Y., Yao, H., Huang, C. Y., Cheung, H. S. 2003. New insight into deformation-dependent hydraulic permeability of gels and cartilage, and dynamic behaviour of agarose gels in confined compression. Journal of Biomechanics 36(4); 593-598.

93. Hardingham, T., Tew, S., Murdoch, A. 2002. Tissue engineering: chondrocytes and cartilage. Arthritis Res. 4(suppl 3); S63-S68.

94. Harimoto, M., Yamato, M., Hirose, M., Takahashi, C., Isoi, Y., Kikuchi, A., Okano, T. 2002. Novel approach for achieving double-layered cell sheets co-culture: Overlaying endothelial cell sheets onto monolayer hepatocytes utilizing temperature-responsive culture dishes. J Biomed Mater Res. 62(3); 464-470.

95. Hassen, A., Saidi, N., Cherif, M., and Boudabous, A. 1998. Resistance of environmental bacteria to heavy metals. Bioresource and Technology 64; 7-15.

96. Hatcher, B. M., Seegert, C. A., Brennan, A. B. 2003. Polyvinylpyrrolidone modified bioactive glass fibres as tissue constructs: *in vitro* mesenchymal stem cell response. J Biomed Mater Res. 66A; 840-849.

97. Hench, L. L., Anderson, O. Bioactive glasses. An introduction to bioceramics. Editors. Hench, L. L., Wilson, J. 1993. World Scientific. Singapore. pp 41.

98. Heywood, H. K., Sembi, P. K., Lee, D. A., Bader, D. L. 2004. Cellular utilisation determines viability and matrix distribution profiles in chondrocytes-seeded alginate constructs. Tissue Engineering 10(9/10); 1467-1479.

99. Hillmann, G., Steinkamp-Zucht, A., Geurtsen, W., Gross, G., Hoffmann, A. 2002. Culture of primary human gingival fibroblasts on biodegradable membranes. Biomaterials 23; 1461-1469.

100. Ho, H-O., Tasi, T., Liu, C., M., Sheu, M. T. 2002. Influence of cosolvents and in situ forming hydroxyapatite on the mechanical characterisation of collagen films. J Biomed Mater Res. 62 (1); 22-29.

101. Ho, H-O., Tsai, Y. T., Chen, R. N., Ke, W. T., Lin, Y. T., Lin, Y. K., et al. 2003. Viscoelastic characterizations of acellular dermal matrix (ADM) preparations for using as injectable implants. Controlled Release Society 30th Annual Meeting Proceedings 153.

102. Hoppe, U. A structural model for phosphate glasses. 1996. Journal of Non-Crystalline Solids 195; 138-147.

103. Hoppe, U., Walter, G., Kranold, R., Stachel, D. 2000 Structural specifics of phosphate glasses probed by diffraction methods: a review. Journal of Non-Crystalline Solids 263&264; 29-47.

104. Hunter, C. J., Imler, S. M., Malaviya, P., Nerem, R. M., Levenston, M. E. 2002. Mechanical compression alters gene expression and extracellular matrix synthesis by chondrocytes cultured in collagen I gels. Biomaterial 23; 1249-1259.

105. Hutmacher, D.W. 2000. Scaffolds in tissue engineering bone and cartilage. Biomaterials 21(24); 2529-2543.

106. Imaizumi, F., Asahina, I., Moriyama, T., Ishii, M., Omura, K. 2004. Cultured mucosal cell sheet with a double layer of keratinocytes and fibroblasts on a collagen membrane. Tissue Engineering 5/6 (10); 657-665.

107. Itoh H, Aso Y, Furuse M, Noishiki Y, Miyata T. 2001a. A honeycomb collagen carrier for cell culture as a tissue engineering scaffold. Artificial Organs 25(3); 213-217.

108. Itoh, S., Kikuchi, M., Takakuda, K., Koyama, Y., Matsumoto, H. N., Ichinose, S., Tanaka, J., Kawauchi, T., Shinomiya, K. 2001b. The biocompatibility and osteoconductive activity of a novel hydroxyapatite/collagen composite biomaterial, and its function as a carrier of rhBMP-2. J Biomed Mater Res. 54; 445-453.

109. Itoh, S., Kikuchi, M., Koyama, Y., Takakuda, K., Shinomiya, K., Tanaka, J. 2002a. Development of an artificial vertebral body using a novel biomaterial, hydroxyapatite/collagen composite. Biomaterials 23; 3919-3926.

110. Itoh, S., Takakuda, K., Kawabata, S., Aso, Y., Kasai, K., Itoh, H. Shinomiya, K. 2002b. Evaluation of cross-linking procedures of collagen tubes used in peripheral nerve repair. Biomaterials 23(23); 4475-4481.

111. Itoch, M., Hiraoka, Y., Kataoka, K., Huh, N. H., Tabata, Y., Okochi, H. 2004. Novel collagen sponge reinforced with polyglycolic acid fibre produces robust, normal hair in murine hair reconstitution model. Tissue Engineering 10(5/6); 818-824.

112. Jayaraman, M., Subramaian, M. V. 2002. Preparation and characterization of two new composites: collagen-brushite and collagen octa-calcium phosphate. Med Sci Monit. 8(11); BR481-487.

113. Jones, D. S. 1999. Dynamic mechanical analysis of polymeric system of pharmaceutical and biomedical significance. International Journal of Pharmaceutics 179; 167-178.

114. Khattak, G. D., Mekki, A., Wenger, L. E. 2004. Local structure and redox state of copper in tellurite glasses. Journal of Non-Crystalline Solids 337; 174-181.

115. Kikuchi, M., Itoh, S., Ichinose, S., Shinomiya, K., Tanaka, J. 2001. Self-organization mechanism in a bone-like hydroxyapatite/collagen nanocomposite synthesized *in vitro* and its biological reaction *in vivo*. Biomaterials 22; 1705-1711.

116. Kikuchi, M., Ikoma, T., Itoh, S., Matsumoto, H. N., Koyama, Y., Takakuda, K., Shinomiya, K., Tanaka, J. 2004. Biomimetic synthesis of bone-like nanocomposites using the self-organization mechanism of hydroxyapatite and collagen. Composite Science and Technology 64; 819-825.

117. Kirkpatrick, R. J., Brow, R. K. 1995. Nuclear magnetic resonance investigation of the structures of phosphate and phosphate-containing glasses: a review. Solid State Nuclear Magnetic Resonance 5; 9-21.

118. Knapp, D. M., Barocas, V. H., Moon, A. G., Yoo, K., Petzold, L. R., Tranquillo, R. T. 1997. Rheology of reconstituted type I collagen gel in confined compression. The society of Rheology 41(5); 971-993.

119. Knowles, J. C., Bonfield, W. 1993. Development of a glass reinforced hydroxyapatite with enhanced mechanical properties. The effect of glass composition on mechanical properties and its relationship to phase changes. J Biomed Mater Res. 27; 1591-1598.

120. Knowles, J. C., Rehaman, I., Bonfield, W. 1994. Spectroscopic and crystallographic analysis of the solution kinetics of a range of soluble phosphate based bioactive glasses. Bioceramics 7; 85-90.

121. Knowles, J. C., Franks, K., Abrahams. I., 2001. Investigation of the solubility and ion release in the glass system K_2O-Na_2O-CaO-P_2O_5. Biomaterials 22; 3091-3096.

122. Knowles, J. C. 2003. Phosphate based glasses for biomedical applications. J Mater Chem., 13; 2395-2401.

123. Kokubo, T., Kim, H. M., Kawashita, M., Nakamura, T. 2004. Bioactive metals: preparation and properties. Journal of Material Science: Materials in Medicine 15; 99-107.

124. Koob, T. J., Willis, T. A., Hernandez, D. J. 2001a. Biocompatibility of NDGA-polymerized collagen fibres. I. Evaluation of cytotoxicity with tendon fibroblasts *in vitro*. J Biomed Mater Res. 56; 31-39.

125. Koob, T., Willis, T. A., Qiu, Y. S., Hernandez, D. J. 2001b. Biocompatibility of NDGA-polymerized collagen fibres. II. Attachment, proliferation, and migration of tendon fibroblasts. J Biomed Mater Res. 56; 40-48.

126. Koob, T. J., Hernandez, D. J. 2002. Material properties of polymerized NDGA-collagen composite fibres: development of biologically based tendon constructs. Biomaterials 23; 203-212.

127. Krishnan, L., Weiss, J. A., Wessman, M. D., Hoying, J. B. 2004. Design and application of a test system for viscoelastic characterisation of collagen gels. Tissue Engineering 10(1/2); 241-252.

128. Kumar, T. R., Shanmugasundaram, N., Babu, M. 2003, Biocompatible collagen scaffolds from a human amniotic membrane: physicochemical and *in vitro* culture characteristics. J Bimater. Sci. Polymer Edn. 14 (7); 689-706.

129. Kurkjian, C. R. 2000. Mechanical properties of phosphate glasses. Journal of Non-Crystalline Solids 263&264; 207-212.

130. Langer, R. 1997. Tissue engineering: A new field and its challenges. Pharmaceutical Research 14(7); 840-841.

131. Langer, R. 2000. Biomaterials in drug delivery and tissue engineering: One laboratory's experience. Acc Chem Res. 33; 94-101.

132. Lee S. J., Lee, J. H., Lee, H. B. 1999a. Interaction of fibroblasts cells onto fibres with different diameter. Korea Polymer Journal 7(2); 102-107.

133. Lee, S. J. Shim, K. B., Auh, K. H., Knott, P. 1999b. Activation energy of crystal growth in PbTiO3 glass using differential thermal analysis. Journal of Non-Crystalline Solids 248; 127-136.

134. Lee, C. H., Singla, A., Lee, Y. 2001a. Biomedical applications of collagen. International Journal of Pharmaceutics 221(1-2); 1-22.

135. Lee, J-E., Park, J-C., Kim, J-G., Suh, H. 2001b. Preparation of collagen modified hyaluronan microparticles as antibiotic carrier. Yonsei Medical Journal 42(3); 291-298.

136. Lee, C. R. Grodzinsky, A. J. Spector, M. 2001c.The effect of cross-linking of collagen-glycosaminoglycan scaffolds on compressive stiffness, chondrocytes-mediated contraction, proliferation and biosynthesis. Biomaterials 22; 3145-3154.

137. Lee, J-E., Park, J-C., Hwang, Y-S., Kim, J-K., Kim, J-G., Suh, H. 2001d. Characterisation of UV-irradiated dense/porous collagen membranes: morphology, enzymatic degradation, and mechanical properties. Yonsei Medical Journal 42(2); 172-179.

138. Lee, C. R., Grodzinsky, A. J., Spector, M. 2003. Modulation of the contractile and biosynthetic activity of chondrocytes seeded in collagen-glycosaminoglycan matrices. Tissue Engineering 9(1); 27-36.

139. Letic-Gavrilovic, A., Piattelli, A., Abe, K. 2003. Nerve growth factor β (NGF β) delivery via a collagen/hydroxyapatite (Col/HAp) composite and its effect on new bone ingrowth. Journal of Material Science: Material in Medicine 14; 95-102.

140. Li, W-J., Tuli, R., Okafor, C., Derfoul, A., Danielson, K. G., Hall, D. J., Tuan, R. S. 2005. A three-dimensional nanofibrous scaffold for cartilage tissue engineering using human mesenchymal stem cells. Biomaterials 26; 599-609.

141. Lin, S. T., Krebs, S. L., Kadiyala, S., Leong, K. W., LaCourse, W. C., Kumar, B. 1994. Development of bioabsorbable glass fibres. Biomaterials 15(13); 1057-1061.

142. Lockyer, M. W. C., Holland, D., Howes, A. P., Dupree, R. 1995. Magnetic-angle spinning nuclear magnetic resonance study of the structure of some PbO-Al_2O_3-P_2O_5 glasses. Solid State Nuclear Resonance 5; 23-34.

143. Lopes, M. A., Knowles, J. C., Santo, J. D., Monterio, F. J., Olsen, I. 2000. Direct and indirect effect of P_2O_5 glass reinforced-hydroxyapatite composites on the growth and function of osteoblast-like cells. Biomaterials 21; 1165-1172.

144. Lu, Q., Ganesan, K., Simionscu, D. T., Vyavahare, N. R. 2004. Novel porous aortic elastin and collagen scaffolds for tissue engineering. Biomaterials 25; 5227-5237.

145. Mahmood, J., Takita, H., Ojima, Y., Kobayashi, M., Kohgo, T., Kuboki, Y. 2001. Geometric effect of matrix upon cell differentiation: BMP-induced osteogensis using a new Bioglass with a feasible structure. J. Biochem. 129; 163-171.

146. Mano, J. F., Koniarova, D., Reis, R. L. 2003. Thermal stability of thermoplastic starch/synthetic polymer blends with potential biomedical applicability. Journal of Material Science: Material in Medicine 14; 127-135.

147. Marasinghe, G. K., Karabulut, M., Ray, C. S., Day, D. E., Shumsky, M. G., Yelon, W. B., Booth, C. H., Allen, P. G., Shuh, D. K. 1997. Structural features of iron phosphate glasses. Journal of Non-Crystalline Solids 222; 144-152.

148. Marasinghe, G. K., Karabulut, M., Ray, C. S., Day, D. E., Shuh, D. K., Allen, P. G., Saboungi, M. L., Grimsditch, M., Haeffner, D. 2000. Properties and structure of vitrified iron phosphate nuclear wasteforms. Journal of Non-Crystalline Solids 263&264; 146-154.

149. Marcolongo, M., Ducheyne, P., LaCourse, W. C. 1997. Surface reaction layer formation *in vitro* on a bioactive glass fibre/polymeric composite. J Biomed Mater Res. 37; 440-448.

150. Marcolongo, M., Ducheyne, P., Garino, J., Schepers, E. 1998. Bioactive glass fibre/polymeric composites bond to bone tissue. J Biomed Mater Res. 39; 161-170.

151. Marler, J. J., Upton, J., Langer, R., Vacanti, J. P. 1998. Transplantation of cells in matrices for tissue regeneration. Advanced Drug Delivery Reviews 33(1-2); 165-182.

152. Meenan, B. J., McClorey, C., Akay, M. 2000. Thermal analysis studies of poly (etheretherketone) /hydroxyapatite biocomposite mixtures. Journal of Material Science: Material in Medicine 11; 481-489.

153. Melankovic, A. M., Gajovic, A., Santic A., Day, D. E. 2001. Structure of sodium phosphate glasses containing Al_2O_3 and / or Fe_2O_3. Part I. Journal of Non-Crystalline Solids 289; 204-213.

154. Mesko, M. G., Day, D. E. 1999. Immobilization of spent nuclear fuel in iron phosphate glass. Journal of Nuclear Materials 273; 27-36.

155. Metwalli, E., Karabulut, M., Sidebottom, D. L., Morsi, M. M., Brow, R. K. 2004. Properties and structure of copper ultraphosphate glasses. Journal of Non-Crystalline Solids 344; 128-134.

156. Milberg, M. E., Daly, M. C. 1963. Structure of oriented sodium metaphosphate glass fibres. The Journal of Chemical Physics 39(11); 2966-2973.

157. Minuth, W. W., Sittinger, M., Kloth, S. 1997. Tissue engineering: Generation of differentiated artificial tissues for biomedical applications. Cell and Tissue Research 291(1); 1-11.

158. Moriyama, T., Asahina, I., Ishii, M., Oda, M., Ishii, Y., Enomoto, S. 2001. Development of composite cultured oral mucosa utilizing collagen sponge matrix and contracted collagen gel: A preliminary study for clinical applications. Tissue Engineering 7(4); 415-427.

159. Mooney, D. J., Mazzoni, C. L., Breuer, C., McNamara, K., Hern, D., Vacanti, J. P., Langer, R. 1996. Stabilized polyglycolic acid fibre-based tubes for tissue engineering. Biomaterials 17; 115-124.

160. Murgatroyd, J. B. 1948. The delayed elastic effect in glass fibres and the constitution of glass in fibre form. Journal of the Society of Glass Technology 32; 291-300.

161. Mulligan, A. M., Wilson, M., Knowles, J. C. 2003a. The effect of increasing copper content in phosphate-based glasses on biofilms of *Streptococcus Sanguis*. Biomaterials 24(10); 1797-1807.

162. Mulligan, A.M., Wilson, M., Knowles, J. C. 2003b. Effect of increasing silver content in phosphate-based glasses on biofilms of *Streptococcus Sangius*. J Biomed Mater Res. 67A; 401-412.

163. Navarro, M., Valle. S. D., Martinez, S., Zeppetelli, S., Ambrosio, L., Planell, J. A., Ginebra, M. P. 2004. New macroporous calcium phosphate glass ceramic for guided bone regeneration. Biomaterials 25; 4233-4241.

164. Navarro, M., Ginebra, M. P., Planell, J. A., Zeppetelli, S., Ambrosio, L. 2004. Development and cell response of a new biodegradable composite scaffold for guided bone regeneration. Journal of Material Science: Materials in Medicine 15; 419-422.

165. Nasseri, B. A., Pomerantseva, I., Kaazempur-Mofrad, M. R., Sutherland, F. W. H., Perry, T., Ochoa, E., Thompson, C. A., Mayer, J. E., Oesterle, S. N.,

Vacanti, J. P. 2003. Dynamic rotational seeding and cell culture system for vascular tube formation. Tissue Engineering 9(12); 291-299.

166. Nation, J. L. 1983. A new method using hexamthyldisilazane for preparation of soft insect tissues for scanning electron microscopy. Florida Agricultural Experimental Station Journal 58(6); 347-350.

167. Nazhat, S. N., Joseph, R., Wang, R., Smith, R., Tanner, K. E., Bonfield, W. 2000. Dynamic mechanical characterisation of hydroxyapatite reinforced polyethylene: effect of particle size. Journal of Material Science Material in Medicine 11; 621-628.

168. Nazhat, S. N., Parker, S., Patel, M. P., Braden, M. 2001. Isoprene-styrene copolymer elastomer and tetrahydrofurfuryl methacrylate mixtures for soft prosthetic applications. Biomaterials 22; 2411-1416.

169. Nazhat, S. N., Parker, S., Braden, M. 2004. Silica-filled elastomer/methacrylate system as soft liners. J. Biomater., Sci., Polymer Edn. 15 (6); 727-739.

170. Neidert, M. R., Devireddy, R. V., Tranquillo, R. T., Bischof, J. C.2004. Cryopreservation of collagen-based tissue equivalents. II. Improved freezing in the presence of cryoprotective agents. Tissue Engineering 10(1/2); 23-32.

171. Newman S, Cloitre M, Allain C, Forgacs G, Beysens D.1997. Viscosity and elasticity during collagen assembly *in vitro*: Relevance to matrix-driven translocation. Biopolymers 41; 337-347.

172. O'brien, F. J., Harely, B. A., Yannas, I. V., Cibson, L. J. 2005. The effect of pore size on cell adhesion in collagen-GAG scaffolds. Biomaterials 26; 433-441.

173. O'connor, S. M., Stenger, D. A., Shaffer, K. M., Wu Ma. 2001. Survival and neurite outgrowth of rat cortical neurons in three-dimensional agarose and collagen gel matrices. Neuroscience Letters 304; 198-193.

174. Ochi, M., Uchio, Y., Tobita, M., Kuirwaka, M. 2001. Current concept in tissue engineering technique for repair of cartilage defect. Artificial Organs 25(3); 172-179.

175. O'Grady, J. E., Bordon, D. M. 2003. Global regulatory registration requirements for collagen-based combination products: points to consider. Advanced Drug Delivery Reviews 55; 1699-1721.

176. Orifice, R. L., Hench, L. L., Clark, A. E., Brennan, A. B., 2001. Novel sol-gel bioactive fibres. J Biomed Mater Res. 55; 460-467.

177. O'sullivan, T. N., Smith, J. D., Thomas, J. D., Drake, C. 1991. Copper molluscicides for control of Schistosomiasis. 2. Copper phosphate controlled release glass. 1991. Environ. Sci. Technol. 25; 1088-1091.

178. Pachence, J. 1996. Collagen-based device for soft tissue repair. J Biomed Mater Res., (Appl. Biomater.) 33; 35-40.

179. Park, S-N., Park, J-C., Kim, H. O., Song, M. J., Suh, H. 2002. Characterisation of porous collagen/hyaluronic acid scaffold modified by 1-ethyl-3-(3-dimethylaminopropyl) carbodiimide cross-linking. Biomaterials 23; 1205-1212.

180. Parsons, A. J., Burling, L.D., Rudd, C. D., Scotchford, C. A., Walker, G. S. 2004a. The effect of production regime and crucible materials on the thermal properties of sodium phosphate glasses produced from salts. J Biomed Mater Res. Part B: Appl Biomater. 71B; 22-92.

181. Parsons, A. J., Evans, M., Rudd, C. D., Scotchford, C. A. 2004b. Synthesis and degradation of sodium iron phosphate glasses and their *in vitro* cell response. J Biomed Mater Res. 71A; 283-291.

182. Pederson, A. W., Ruberti, J. W., Messersmith, P. B. 2003. Thermal assembly of a biomimetic mineral/collagen composite. Biomaterials 24 (26); 4881-4890.

183. Prabhakar, R. L., Brocchini, S., Knowles, J. C. 2005. Effect of glass composition on the degradation properties and ion release characteristics of phosphate glass-polycaprolactone composites. Biomaterials 26; 2209-2218.

184. Prockop, D. J., Fertala, A. 1998. The collagen fibril: the almost crystalline structure. Journal of Structural Biology 122; 111-118.

185. Puxkand, R., Zizak, I., Paris, O., Keckes, J., Tesch, W., Bernstorff, S., Purslow, P., Fratzl, P. 2002. Viscoelastic properties of collagen: synchrotron radiation investigations and structural model. Phil. Trans. R. Soc. Lond. B 357; 191-197.

186. Ray, C. A., Fang, X., Karabulut, G. K., Day, D. E. 1999. Effect of melting temperature and time on iron valence and crystallisation of iron phosphate glasses. Journal of Non-Crystalline Solids 249; 1-16.

187. Reis, S. T., Karabulut, M., Day, D. E. 2001. Chemical durability and structure of zinc-iron phosphate glasses. Journal of Non-Crystalline Solids 292; 150-157.

188. Rich, J., Tuominen, J., Kylma, J., Seppala, J., Nazhat, S. N., Tanner, K. E. 2002. Lactic acid based PEU/HA and PEU/BCP composites: Dynamic mechanical characterisation of hydrolysis. J Biomed Mater Res. 63; 346-353.

189. Richardson, M. J. 1976. Quantitative interpretation of DSC results. Plastics and Rubber: Materials and Applications. 867-901.

190. Rinehart, J. D., Taylor, T. D., Tian, Y., Latour[Jr1], R. A. 1999. Real-time dissolution measurement of sized and unsized calcium phosphate glass fibres, J. Biomed. Mater. Res. (Appl. Biomater.) 48 (6); 833-840.

191. Rodrigues, C. V. M., Serricella, P., Linhares, A.B. R., Guerdes, R. M., Borojevic, R., Rossi, M. A., Duarte, M. E. L., Farina, M. 2003. Characterization of a bovine collagen-hydroxyapatite composite scaffold for bone tissue engineering. Biomaterials 24 (27); 4987-4997.

192. Rose, F. R. A. J., Oreffo, R. O. C. 2002. Bone tissue engineering: Hops vs hype. Biochemical and Biophysical Research Communications 292(1); 1-7.

193. Rosenblatt, J., Devereux, B., Wallace, D. G. 1994. Injectable collagen as a pH-sensitive hydrogel. Biomaterials 15(12); 985-995.

194. Roether, J. A., Gough, J. E., Boccaccini, A. R., Hench, L. L., Maquet, V., Jerome, R. 2002. Novel bioresorbable and bioactive composites based on bioactive glass and polylactide foams for bone tissue engineering. Journal of Material Science: Materials in Medicine 13; 1207-1214.

195. Ruszczak, Z., Friess, W. 2003. Collagen as a carrier for on-site delivery of antibacterial drugs. Advanced Drug Delivery Reviews 55(12); 1679-1698.

196. Ruszczak, Z. 2003. Effect of collagen matrices on dermal wound healing. Advanced Drug Delivery Reviews 55(12); 1595-1611.

197. Saadeh, P. B., Khosla, R. K., Mehrara, B. J., Steinbrech, D. S., McCormick, S. A. DeDover, D. P., Longaker, M. T. 2001. Repair of a critical size defect in the rat mandible using allogenic type I collagen. The Journal of Craniofacial Surgery 12(6); 573-579.

198. Sales, B. C., Boatner, L. A., Ramey, J. O. 2000. Chromatographic studies of the structures of amorphous phosphates: a review. Journal of Non-Crystalline Solids 263&264; 155-166.

199. Salih, V., Franks, K., James, M., Hastings, G. W., Knowles, J. C. 2000. Development of soluble glasses for biomedical use. Part 2: The biological response of human osteoblast cell lines to phosphate-based soluble glasses. Journal of Material Science: Materials in Medicine 11; 615-620.

200. Samouillan, V., Dandurand-Lods, J., Lamure, A., Lacabanne, G., Gerosa, G., Venturini, A., Casarotto, D., Gherardini, L., Spina, M. 1999. Thermal analysis characterisation of aortic tissue for cardiac valve bioprostheses. J Biomed Mater Res. 46; 531-538.

201. Samouillan, V., Dandurand, J., Lacabanne, C., Thoma, R. J., Adam, A., Moore, M. 2003. Comparison of chemical treatments on the chain dynamics and thermal stability of bovine pericardium collagen. J Biomed Mater Res. 64A; 330-338.

202. Sano, A., Maeda, M., Nagahara, S., Ochiya, T., Honma, K., Itoh, H. et al. 2003. Atelocollagen for protein and gene delivery. Advanced Drug Delivery Reviews 55(12); 1651-1677.

203. Saravanapavan, P., Jones, J. R., Pryce, R. S., Hench, L. L. 2003. Bioactivity of gel-glass powders in the $CaO-SiO_2$-system: A comparison with ternary ($CaO-P_2O_5-SiO_2$) and quaternary glasses ($SiO_2-CaO-P_2O_5-Na_2O$). J Biomed Mater Res. 66; 110-119.

204. Sawhney, R. K., Howard, J. 2002. Slow local movements of collagen fibers by fibroblasts drive the rapid global self-organization of collagen gels. The Journal of Cell Biology 157(6); 1083-1091.

205. Schlapp, M., Friess, W. 2003. Collagen/ PLGA microparticle composites for local controlled delivery of gentamicin. J Pharm Sci. 92; 2145-2151.

206. Schlegel, A. K., Mohler, H., Busch, F., Mehl, A. 1997. Preclinical and clinical studies of a collagen membrane (Bio-Gide®). Biomaterials 18(7); 535-538.

207. Schmelzeisen, R., Schimming, R., Sittinger, M. 2003. Making bone: Implant insertion into tissue-engineered bone for maxillary sinus floor augmentation-a preliminary report. Journal of Cranio-Maxillofacial Surgery 31; 34-39.

208. Schneider, J., Oliveira, S. L., Nunes, L. A. O., Bonk, F., Panepucci, H. 2005. Short-range structure and cation bonding in calcium-aluminium metaphosphate glasses. Inorg Chem. 44; 423-430.

209. Seliktar, D., Nerem, R. M., Galls, Z. S. 2003. Mechanical strain-stimulated remodeling of tissue-engineered blood vessel constructs. Tissue Engineering 9(4); 657-666.

210. Sethi, K. K., Yannas, I. V., Mudera, V., Eastwood, M., Mcfarland, C., Brown, R. A. 2002. Evidence for sequential utilization of Fibronectin, vitronectin, and collagen during fibroblast-mediated collagen contraction. Wound Rep Reg. 10; 397-408.

211. Shah, R, Sinanan, A. C. M., Knowles, J. C., Hunt, N. P., Lewis, M. P. 2005. Craniofacial muscle engineering using a 3-dimensional glass fibre construct, Biomaterials 26; 1497-1505.

212. Shan, Y., Zhou, Y., Cao, Y., Xu, Q., Ju, H., Wu, Z. 2004. Preparation and infrared emissivity study of collagen-g-PMMA/In_2O_3 nanocomposite. Materials Letters 58; 1655-1660.

213. Shanmugasundaram, N., Ravilumar, T., Babu, M. 2004. Comparative physico-chemical and *in vitro* properties of fibrillated collagen scaffolds from different sources. Journal of Biomaterials Applications 18; 247-264.

214. Sheu, M. T., Hung, J-C., Yeh, G-C., Ho, H-O. 2001. Characterization of collagen gel solutions and collagen matrices for cell culture. Biomaterials 22; 1713-1719.

215. Shi, Y., Vesely, I. 2003. Fabrication of mitral valve chordae by directed collagen gel shrinkage. Tissue Engineering 9(6); 1233-1242.

216. Shields, K. J., Beckman, M. J., Bowlin, G. L., Wayne, J. S. 2004. Mechanical properties and cellular proliferation of electrospun collagen type II*. Tissue Engineering 10(9/10); 1510-1517.

217. Shih, P. Y., Yung, S.W., Chin, T. S. 1998. Thermal and corrosion behaviour of P_2O_5-Na_2O-CuO glasses. Journal of Non-Crystalline Solids 224; 143-152.

218. Shih, P. Y., Chin, T. S. 1999. Effect of redox state of copper on the properties of P_2O_5-Na_2O-CuO glasses. Materials Chemistry and Physics 60; 50-57.

219. Shih, P. Y., Yung, S. W., Chin, T. S. 1999. FTIR and XPS studies of P_2O_5-Na_2O-CuO glasses. Journal of Non-Crystalline Solids 244; 211-222.

220. Shin, M., Yoshimoto, H., Vacanti, J. P. 2004. *In vitro* bone tissue engineering using mesenchymal stem cells on a novel electrospun nanofibrous scaffold. Tissue engineering 10 (1/2): 33-41.

221. Shinoka, T. 2002. Tissue engineered heart valves: Autologous cell seeding on biodegradable polymer scaffold. Artificial Organs 26(5); 402-406.

222. Silver, F. H., Garg, A. K. Collagen: 1997. Characterisation, processing, and medical applications. In: Domb A. J., Kost J., Wiseman, D. M. editors. Handbook of biodegradable polymers. Amsterdam: Harwood Academic Publishers, p. 319-346.

223. Simionescu, N., Simionescu, M. 1967. Galloylglucoses of low molecular weight as mordant in electron microscopy. The Journal of Cell Biology 70; 608-621.

224. Sittinger, M., Bujia, J., Rotter, N., Reitze, D., Minuth, W. W., Burmester, G. R. 1996. Tissue engineering and autologous transplant formation: Practical approaches with resorbable biomaterials and new cell culture techniques. Biomaterials 17 (3); 237-242.

225. Sivakumar, M., Rao, P. 2002. Preparation, characterization, and *in vitro* release of gentamicin from coralline hydroxyapatite-gelatin composite microspheres. J Biomaterials 23; 3175-3181.

226. Steer, D. L., Nigam, S. K. 2004. Developmental approaches to kidney tissue engineering. American Journal of Physiology-Renal Physiology 286(1); F1-F7.

227. Telfer, S. B., Illingworth, D. V., Anderson, P. J. B., Zervas, G., Carlos, G. 1985. Effect of soluble-glass boluses on the copper, cobalt and selenium status of sheep. Biochemical Society Transactions 13; 529-529.

228. Tuan, T-L., Song, A., Chang, S., Younai, S., Nimni, M. E. 1996. *In vitro* fibroplasias: Matrix contraction, cell growth, and collagen production of fibroblasts cultured in fibrin gels. Experimental Cell Research 223; 127-134.

229. Ueda, M., Tohnai, I., Nakai, H. 2001. Tissue engineering research in oral implant surgery. Artificial Organs 25(3); 164-171.

230. Uo, M., mizuno, M., Kuboki, Y., Makishima, A., Watari, F. 1998. Properties and cytotoxicity of water soluble Na_2O-CaO-P_2O_5 glasses. Biomaterials 19; 2277-2284.

231. Usha, R., Ramasami, T. 1999. Influence of hydrogen bond, hydrophobic and electrovalent salt linkage on the transition temperature, enthalpy and activation energy in rat tail tendon (RTT) collagen fibre. Thermochimica Acta 338; 17-25.

232. Vakiparta, M., Yli-Urpo, A., Vallittu, P. K. 2004. Flexural properties of glass reinforced composite with multiphase biopolymer matrix. Journal of Material Science Material in Medicine 15; 7-11.

233. Vallbacka, J. J. Nobrega, J. N., Sefton, M. V. 2001. Tissue engineering as a platform for controlled release of therapeutic agents: implantation of the microencapsulated dopamine producing cells in the brain of the rats. Journal of Controlled Release 72; 93-100.

234. Van Wazer, J. R., Holst, K. A. 1950a. Structure and properties of condensed phosphates. I. Some general considerations about phosphoric acids. Journal of American Chemical Society. 72; 639-643.

235. Van Wazer, J. R. 1950b. Structure and properties of the condensed phosphates. II. A theory of the molecular structure of sodium phosphate glasses. Journal of American Chemical Society. 72; 644-646.

236. Varshneya, A. K. Fundamentals of inorganic glasses. 1994. Elsevier Science, USA.pp1.

237. Veilleux, N. H., Yannas, I. V., Spector, M. 2004. Effect of passage number and collagen type on the proliferative, biosynthetic, and contractile activity of adult canine articular chondrocytes in type I and II collagen-glycosaminoglycan matrices *in vitro*. Tissue Engineering 10 (1/2); 119-127.

238. Vijayasekaran, S., Fitton, J. H., Hicks, C. R., Chirila, T. V., Crawford, G. J., Constable, I. J. 1998. Cell viability and inflammatory response in hydrogel sponges implanted in the rabbit cornea. Biomaterials 19; 2255-2267.

239. Vinholis, A. H. C., De-Figueiredo, L. C., Junior, E. M. Marcantonio, R. A. C., Salvador, S. L. S., Goissis, G. 2001. Subgingival utilization of a 1% chlorhexidine collagen gel for the treatment of periodontal pockets. A clinical and microbiological study. Braz Dent J. 12(3); 209-213.

240. Walgenbach, K-J., Voigt, M., Riabikhin, A. W., Andree, C., Schaefer, D. J., Stark, G. B. 2001. Tissue engineering in plastic reconstructive surgery. The Anatomical Record 263(4); 372-378.

241. Wallace, K. E., Hill, R. G., Pembroke, J. T., Brown, C. J., Hatton, P. V. 1999. Influence of sodium oxide content on bioactive glass properties. Journal of Material Science: Materials in Medicine; 10(12); 697-701.

242. Walter, G., Hoppe, U., Baade, T., Kranold, R., Stachel, D. 1997. Intermediate range order in MeO- P_2O_5 glasses. Journal of Non-Crystalline Solids 217; 299-307.

243. Walter, G., Vogel, J., Hoppe, U., Hartmann, P. 2001. The structure of CaO-Na_2O-MgO-P_2O_5 invert glass. Journal of Non-Crystalline Solids 296; 212-223.

244. Wang, M., Yue, C. Y., Chua, B. 2001. Production and evaluation of hydroxyapatite reinforced polysulfone for tissue replacement. Journal of Material Science Material in Medicine 12; 821-826.

245. Wang, X., Du, Y., Fan, L., Liu, H., Hu, Y. 2005. Chitosan-metal complexes as antimicrobial agent: Synthesis, characterisation and structure-activity study. Polymer Bulletin 55; 105-113.

246. William, D. F. 1987. Advanced applications for materials implanted within the human body. Materials Science and Technology 3; 797-806.

247. Wollweber, L., Stracke, R., Gothe, U., 1981. The use of a simple method to avoid cell shrinkage during SEM preparation. Journal of Microscopy 121; 185-189.

248. Wolter, J. R., Meyer, R. F. 1984. Sessile macrophages forming clear endothelium-like membrane on inside of successful keratoprosthesis. Trans Am Ophthalmol Soc. 82; 187-202.

249. Yamauchi, K., Takeuchi, N., Kurimoto, A., Tanabe, T. 2001. Films of collagen cross linked by S-S bonds: preparation and characterisation. Biomaterials 22; 855-863.

250. Yamauchi, K., Goda, T., Takeuchi, N., Einaga, H., Tanabe, T. 2004. Preparation of collagen/calcium phosphate multilayer sheet using enzymatic mineralization. Biomaterials 25; 5481-5489.

251. Young, C. S., Terada, S., Vacanti, J. P., Honda, M., Bartlett, J. D., Yelick, P. C. 2002. Tissue engineering of complex tooth structures on biodegradable polymer scaffolds. J Dent Res. 81(10); 695-700.

252. Yu, H. S., Grynpas, M., Kandel, R. A. 1997a. Composition of cartilagenous tissue with mineralized and non-mineralized zones formed *in vitro*. Biomaterials18 (21); 1425-1431.

253. Yu, X., Day, D. E., Long, G. J., Brow, R. K. 1997 b. Properties and structure of sodium-iron phosphate glasses. Journal of Non-Crystalline Solids 215; 21-31.

254. Zachariasen, W. H. 1932. The atomic arrangement in glass. American Chemical Society. 54(3); 3841-3851.

255. Zhang, R., Ma, P. X. 2004. Biomimetic polymer/apatite composite scaffolds for mineralized tissue engineering. Macromol. Biosci. 4; 100-111.

Appendices

Appendix I. List of Conference Proceedings and Abstracts

1. Abou Neel E.A., Ahmed I., Nazhat S. N., Knowles J. C. DSC as a rapid test method for determining T_g of phosphate-based glass fibres. Proceedings of the 1st Annual Biomaterials Workshop, Cranfield University. Shrivenham, March 2003.

2. Abou Neel E. A., Ahmed I., Pratten J., Nazhat S. N., Knowles J. C.. Characterisation of a novel antimicrobial releasing glass fibre. Proceeding of the 3rd Annual Conference, University of Brighton. July 2004.

3. Abou Neel E. A., Knowles J. C., Brown R. A., Nazhat S. N. Mechanical and viscoelastic characterisation of collagen gel demonstrating the engineering of tissue through ultra-rapid plastic compression. Conference: The Joint Meeting of the "Tissue Engineering Society International" and the "European Tissue Engineering Society" from 10th to 13 October, Lausanne, Switzerland, 2004.

4. Abou Neel E.A., Hope C., Kershaw C.M, Lee P.D., Brown R.A., Knowles J.C., Nazhat S. N. Plastic compression as an ultra rapid preparation of cellular phosphate glass fibre/collagen constructs. Oral presentation at the 19th European Society for Biomaterials Meeting, at Sorrento, Italy, during September 11th to 15th 2005.

5. Brown R.A., Cheema U., Chuo C.B., Abou Neel E.A., Knowles J.C., Nazhat S.N.. Ultra-rapid fabrication of tissues and scaffolds: fabrication of complex, biomimetic

meso-structure. 8th Annual Meeting of 'Tissue Engineering Society', Shanghai International Convention Centre, Shanghai, China. October 22nd-25th, 2005.

6. Abou Neel E. A., Knowles J. C., Brown R. A., Nazhat S. N. Development of 3D phosphate glass fibre-plastic compressed collagen constructs for tissue engineering. Oral presentation at "A Forecast of the Future for Biomaterials". Professor Larry L Hench Symposium. Imperial College London, September 29-30, 2005.

Appendix II. List of Publications

1. Abou Neel E. A., Ahmed I., Pratten J., Nazhat S. N., Knowles J. C. 2005. Characterisation of antibacterial copper releasing degradable phosphate glass fibres. Biomaterials 26; 2247-2254.

2. Abou Neel E. A., Ahmed I., Blaker J. J., Bismarck A., Boccaccini A. R., Lewis M. P., Nazhat S. N., Knowles J. C. 2005. Effect of iron on the surface, degradation and ion release properties of phosphate-based glass fibres. Acta Biomaterialia 1; 553-563.

3. Salih V., Mordan N., Abou Neel E. A., Armitage D. V., Jones F. H., Knowles J. C., Nazhat S. N., Vargas-Coronado R., Cauich-Rodriguez J. V. 2006. Surface characterisation of various bone cements prepared with functionalised methacrylates/bioactive ceramics in relation to HOB behaviour. Acta Biomaterialia (in press).